

[REDACTED]

# A Reproduced Copy

OF

[REDACTED]

CLASSIFICATION CHANGE

~~CONFIDENTIAL~~  
UNCLASSIFIED

By authority of  
Changed by *L. Shirley*

~~CONFIDENTIAL~~

E.O. 11652

Date 1-17-74

Reproduced for NASA

by the

Scientific and Technical Information Facility

This material contains information affecting the national defense of the United States within the meaning of the espionage laws, Title 18, U.S.C. Sections 793 and 794, the transmission or revelation of which in any manner to an unauthorized person is prohibited by law.

207p

N-112372  
3.2  
9



Code 2

NASA CR 5394

MH Aero Report 1300-TR1

FINAL REPORT

ADVANCED CONTROL SYSTEM  
FOR THE SATURN V CONFIGURATION  
(U)

Contract No. NAS8-5069

27 November 1963

HONEYWELL *Aeronautical Division*

LIBRARY COPY

FEB 1964  
LANGLEY RESEARCH CENTER  
LIBRARY, NASA  
LANGLEY STATION  
HAMPSHIRE, VIRGINIA



~~CONFIDENTIAL~~

MH Aero Report 1300-TR1

27 November 1963

FINAL REPORT

ADVANCED CONTROL SYSTEM  
FOR THE SATURN V CONFIGURATION  
(U)

Contract No. NAS8-5069

Prepared for:

George C. Marshall Space Flight Center, National Aeronautics  
and Space Administration, Huntsville, Alabama

Prepared by:

- R. Hendrick
- C. Wandrey
- S. Hummel
- R. Sackett

Approved by:

*R. J. Kell*  
 \_\_\_\_\_  
 R. J. Kell  
 Assistant Project Engineer

*J. K. Olson*  
 \_\_\_\_\_  
 J. K. Olson  
 Section Head  
 Advanced Flight Systems

*L. K. Bishop*  
 \_\_\_\_\_  
 L. K. Bishop  
 Sr. Program Administrator

DOWN LOADED AT 4 YEAR INTERVALS.  
 DECLASSIFIED AFTER 12 YEARS  
 DATE 03-20-10

NOTICE

This document contains information affecting the National Defense of  
 the United States within the meaning of the Espionage Laws, Title 18,  
 U. S. C., Sections 793 and 794, the transmission or the revelation of its  
 contents in any manner to an unauthorized person is prohibited by law.

Minneapolis-Honeywell Regulator Company  
 Aeronautical Division  
 Minneapolis, Minnesota

~~CONFIDENTIAL~~

## FOREWORD

This document comprises the final report on a Saturn V control system study program conducted by the Minneapolis-Honeywell Aeronautical Division for the NASA Marshall Space Flight Center at Huntsville under NASA Contract NAS8-5069. Work under this contract began in August 1962 and was concluded in November 1963. (U)



13944

ABSTRACT

A

A study was conducted to develop advanced techniques capable of controlling the Saturn V booster. The control system designed during the study utilizes a Honeywell-developed gyro blender to obtain favorable structural bending pickup from the combined acceleration, rate, and position feedback sensors. A nonlinear filtering technique (sample-hold filter) developed by the Marshall Space Flight Center was investigated during the program. The final system configuration, however, utilizes a high-order linear filter to decouple the control system from the structural modes.

encl

(U)

Author

CONTENTS

		Page
SECTION I	INTRODUCTION	1
SECTION II	CONCLUSIONS AND RECOMMENDATIONS	2
	Conclusions	2
	Recommendations	3
	Comparison of Blender System and Conventional Linear System	3
	Addition of Adaptive Phase/Gain Control	4
SECTION III	SUMMARY	5
SECTION IV	BASIC CONTROL SYSTEM CONFIGURATION	7
	Feedback Design Considerations	7
	Accelerometer Prefilter	7
	Accelerometer Location	14
	Feedback Gains and Dynamic Characteristics	15
	Rate Gyro Locations	15
	Summary of Final Control System Parameters	16
	Bending Filter Design	17
	Bending Filter Requirements	17
	Preliminary Bending Filter Designs	20
	Final Filter Design	21
SECTION V	BLENDER DESIGN AND OPERATION	28
	General Concept	28
	Practical Applications	29
	Phase Stabilization	30
	Recommended Blender Design Approach	34
	Analytical Results	37
	Sample Calculation	41
	Calculation Procedure	42
	Blender Breadboard	43
SECTION VI	SYSTEM EVALUATION	46
	Nominal Operation	46
	Analog Tolerance Studies	47
	Individual Component Tolerances	47
	Tolerance Combinations	63
	Computer Procedure for Tolerance Runs	68
	Analog Adaptability Studies	94

CONTENTS

	Page
SECTION VII	
SAMPLE-HOLD FILTER ANALYSIS AND BREADBOARD EVALUATION	98
Analysis	98
Concept of the Sample-Hold Filter	98
Block Diagram and Theory of Operation	100
Analysis of the Sample-Hold Filter	102
Breadboard Evaluation and Modifications	120
SECTION VIII	
DESIGN DIFFICULTIES ENCOUNTERED	121
Instability Caused by Blender	121
First Mode Gain Stability	124
Z-Plane Analysis	125
Variable Rate Investigation	125
Constant Rate Investigation	127
Recommendations for Conducting Future Studies	129
REFERENCES	131
APPENDIX A	GLOSSARY
APPENDIX B	SATURN V EQUATIONS OF MOTION
APPENDIX C	COORDINATE SYSTEMS
APPENDIX D	FREE-FREE BENDING MODE DATA
APPENDIX E	SYSTEM PARAMETER VALUES (Revision 5)
APPENDIX F	MOTION AND CONTROL EQUATIONS MATRIX AND COEFFICIENTS
APPENDIX G	ANALOG COMPUTER WIRING DIAGRAMS
APPENDIX H	ANALOG SIMULATION POTENTIOMETER SETTINGS
APPENDIX J	SYNTHETIC WIND SHEAR PROFILES

ILLUSTRATIONS

Figure	Page
1 Final Saturn V Gyro Blender Control System Diagram	8
2 Gyro Blender Breadboard Cabinet - Front Panel	9
3 Gyro Blender Breadboard - Top View	10
4 Preliminary Saturn V Control System Diagram	11
5 Slosh Damping Ratio versus $K_{Rcrit}$	13
6 Acceleration Gain ( $K_A$ ) Schedule	15
7 Rate Gain ( $K_R$ ) Schedule	16
8 Bending Filter Phase and Gain Requirements	18
9 Filter A Frequency Response Compared to Requirements	22
10 Nominal Seven-Stage Filter Frequency Response Compared to Requirements	23
11 Theoretical Filter B Frequency Response Compared to Requirements	25
12 Mechanization Method for Filter B	26
13 Actual Filter B Frequency Response Compared to Requirements	27
14 Basic Gyro Blender Concept Diagram	28
15 Examples of Possible First Bending Mode Root Locus Plots	31
16 Effect of Blender Position upon Critical Gain	36
17 Blender Block Diagram	38
18 Blender Simplified Block Diagram	38
19 Blender Breadboard Block Diagram	44
20-24 Analog Computer Runs - Nominal Operation	48-52
25-34 Open-Loop Frequency Response Plots - Nominal Operation	53-62
35-45 Analog Computer Runs - Tolerance Conditions	79-89
46-49 Open-Loop Frequency Response Plots - Tolerance Conditions	90-93
50 Sample-Hold Filter, Simplified Input-Output Relationship	100
51 Sample-Hold Filter Block Diagram	101
52 Sample-Hold Filter with Sine-Wave Input	103
53 Sample-Hold Filter Phase Relationships	103
54 Sample-Hold Filter Frequency Response for Single-Frequency Input, No Inhibit	106

ILLUSTRATIONS

Figure		Page
55	Sample-Hold Filter Frequency Response for Single-Frequency Input Only	107
56	Sample-Hold Filter Frequency Response of Low-Frequency Output to Low-Frequency Input, with Constant High-Frequency Sampling	111
57	Sample-Hold Filter Composite Frequency Response	111
58	Sample-Hold Filter Frequency Response for Single-Frequency Input, No Inhibit	113
59	Sample-Hold Filter Frequency Response for Single-Frequency Input Only	113
60	Sample-Hold Filter Frequency Response of Low-Frequency Output to Low-Frequency Input, with Constant High-Frequency Sampling	114
61	Sample-Hold Filter Composite Frequency Response	114
62	Sample-Hold Filter Composite Frequency Response with Sampling Delay of 0.01 Per Cent of the Period of the Inhibit Frequency	116
63	Sample-Hold Filter Frequency Response for Single-Frequency Input, No Inhibit	116
64	Sample-Hold Filter Frequency Response for Single-Frequency Input Only	117
65	Sample-Hold Filter Frequency Response of Low-Frequency Output to Low-Frequency Input, with Constant-High Frequency Sampling	117
66	Sample-Hold Filter Composite Frequency Response	118
67	Composite Frequency Response for First-Order Lag Plus Sample-Hold Filter with High-Frequency Input to Cause Constant Sampling	119
68	Sample-Hold Filter Composite Frequency Response with Sampling Delay of 0.01 Per Cent of the Period of the Inhibit Frequency	119
69	Frequency Response Results for Engine Angle Disturbances in a System Containing Rigid Body with Second-Order Model, Tail-Wag-Dog Zeros, and First Bending Mode at Maximum Dynamic Pressure	122
70	Sample-Hold Filter Representation	126
71	Simplified Vehicle in a Closed-Loop Configuration	127
72	Root-Locus of System of Figure 71	128

TABLES

Table		Page
1	Final Control System Nominal Parametric Values	17
2	Gain and Phase Margins of Slosh and First Bending Modes - Nominal System	46
3	Direction of Change of Each Mode Shape Parameter to Increase Effective Bending Pickup	66
4	Parameter Tolerance Values Designated by Sets and Groups	69
5	Tolerance Combinations used in Analog Computer Tolerance Study	70
6-10	Tolerance Study Results	72-76
11	Gain and Phase Margins for Four Tolerance Combinations	78
12	First Mode Tolerance Combinations used in Analog Computer Adaptability Tests	95
13	Results of Adaptability Studies, First Mode Variations with Other Parameters - Nominal	96
14	Results of Adaptability Studies, First Mode Variations with All Other Parameters Set to Tolerance Combination No. 12	96

## SECTION I INTRODUCTION

The Saturn booster presents control problems which strain the capabilities of conventional autopilots. In this booster, low structural bending frequencies approach the control system frequencies. These bending frequencies and mode shapes are difficult to predict or to determine experimentally. Large fuel sloshing masses couple with the bending modes to create further problems. Limited control forces, a need to withstand large wind shears, and high dynamic pressures further complicate the problem. (U)

The primary purpose of the study undertaken by Honeywell for the NASA Marshall Space Flight Center (MSFC) was to develop advanced techniques capable of controlling the Saturn V booster. The following goals were fulfilled:

- A gyro blender was developed and incorporated into a workable breadboard model.
- A control system for the vehicle first stage was developed utilizing the gyro blender to phase-stabilize the first bending mode and a conventional linear filter to stabilize the second and higher modes.
- The MSFC sample-and-hold filter was examined analytically and experimentally. A valid technique for analysis of this filter was developed.
- An analog computer study utilizing the blender breadboard was conducted at five different flight times ( $t = 0, 40, 79, 120,$  and  $153$  seconds). The computer study demonstrated that adequate system performance is obtained (all vehicle bending and slosh modes included) using realistic tolerance conditions with both pitch command and large wind shear inputs.
- Simplified open-loop blender calculation procedures were developed. These will be useful in designing future blender hardware. (C)

SECTION II  
CONCLUSIONS AND RECOMMENDATIONS

CONCLUSIONS

The gyro blender control system developed during this study successfully controlled the Saturn V vehicle with the first four bending modes (0.5 per cent modal damping) even with the worst tolerance combination examined. Analog computer adaptability studies showed that a blender designed to phase-stabilize the first bending mode retains a large portion of the adaptive capability possessed by gain-stabilized gyro blender systems. The blender is capable of stabilizing the nominal system for first mode slope and deflection variations of at least 400 per cent. (C)

The design of a blender which gain-stabilizes the first bending mode is not feasible at this time because:

1. Band-pass amplifier gains under changing environmental conditions cannot be held to the 0.5 to 1 per cent tolerances demanded with the present state of the art.
2. Phase measuring and changing devices capable of less than the 22 arc-minutes of resolution required for proper operation are not available at the present time. (C)

The blender is very tolerant of basic changes in the control system design. The only significant parameters which require optimization are blender imbalance (ratio between the two band-pass amplifier gains) and integrator gain. (C)



The MSFC sample-and-hold filter cannot be used effectively for launch vehicle filter applications, although it might be suitable for other applications. While this filter has slightly greater attenuation at some frequencies than a comparable linear second-order filter, the relatively small increase did not justify the increase in complexity for this particular application. (C)

The use of acceleration feedback in the system requires careful location of the accelerometer and filtering of the feedback signal to stabilize the low-frequency wash modes. (C)

## RECOMMENDATIONS

This study program revealed the need for two areas of investigation that were not within the scope of the present contract:

- Performance and stability comparison of the gyro blender system and a conventional linear system.
- Adaptability increases obtainable by adding some adaptive phase and/or gain ratio control to the blender concept. (U)

These studies could be conducted by analog computer simulation without the use of breadboard circuitry. (U)

### Comparison of Blender System and Conventional Linear System

The present study was concerned with developing the gyro blender concept as fully as possible for this application; therefore, there was no opportunity to compare the performance and stability of the final design with an entirely different approach. Comparison with a conventional linear system is essential in ascertaining the true worth of the blender concept. (U)

Addition of Adaptive Phase/Gain Control

The phase stability of the current system depends upon the vicissitudes of both vehicle and control system dynamic characteristics. If an additional adaptive device were developed which could change the phase relationships of the blended signals, phase stability would be assured, thereby increasing system adaptability. A separate control system for automatically controlling this ratio is therefore another recommended study area. (U)

SECTION III  
SUMMARY

The control system designed during this study utilizes

- A Honeywell-developed gyro blender to obtain favorable structural bending pickup from the combined acceleration, rate, and position feedback sensors.
- A high-order linear filter to decouple the control system from the structural modes. (C)

A nonlinear sample-hold filter developed by MSFC was investigated as part of the program. (U)

Feedback and bending filter design considerations leading to definition of the basic control system configuration are discussed in Section IV. Section V describes the basic gyro blender concept, the recommended design approach, and the blender breadboard. The system is evaluated in Section VI. Analog tolerance and adaptability studies are described and results are given. In Section VII the sample-hold filter furnished by MSFC is analyzed and evaluated. Section VIII describes some of the difficulties encountered and approaches tried and discontinued. (U)

Analytical data and equations of motion for this study were obtained from the MSFC document, "A Model Vehicle for Adaptive Control Studies" (Reference 1). The equations of motion, nomenclature, parameter values, analog computer schematics, and related data applicable to this study are given in the appendices. (U)

The control system analysis considered only the portion of flight from launch to first stage burnout. Five flight times were chosen for the point stability (small perturbation) analysis:

- 0 seconds
- 40 seconds
- 79 seconds
- 120 seconds
- 153 seconds

(C)

Step inputs in commanded pitch attitude were used as standard forcing functions for analog computer studies. Straight-line approximations (two breakpoints) to the synthetic wind shear profile data supplied by MSFC were also used as inputs at 40, 79, and 120 seconds. Definition of the wind shear profiles used was obtained from MSFC Memorandum M-Aero-G-10-62 dated 22 May 1962 (Reference 2). (C)

Fuel slosh data used was based upon cylindrical baffled tanks. Linear slosh damping factors were assumed. (C)

## SECTION IV BASIC CONTROL SYSTEM CONFIGURATION

The final Saturn V gyro blender control system (shown in Figure 1) uses attitude, attitude rate, and acceleration feedback signals. The attitude and acceleration signals are passed through separate lag time constants ( $T_I$  and  $T_A$  respectively) and separate gains ( $K_P$  and  $K_A$  respectively) before being summed. This signal sum is then added to both the forward and aft rate gyro signals to obtain  $\phi_{FF}$  and  $\phi_{FA}$  as shown in Figure 1. The signals  $\phi_{FA}$  and  $\phi_{FF}$  are then fed to blender attenuators  $K$  and  $1-K$  before being summed and then attenuated by the basic inner-loop rate gain  $K_R$ . (C)

The blender logic also receives the signals from the  $K$  and  $1-K$  attenuators and automatically varies  $K$  until the desired balance between the two signals is obtained. An attenuator,  $U$ , is used to alter the imbalance between the two band-pass amplifiers, thereby providing a means of changing the equilibrium value of  $K$  for a given set of conditions. Two views of the blender breadboard mechanization of this configuration are shown in Figures 2 and 3. (C)

### FEEDBACK DESIGN CONSIDERATIONS

#### Accelerometer Prefilter

The preliminary control system (shown in Figure 4) combined the acceleration and attitude signals after they passed through their respective gains and then lagged this total signal through a second-order filter common to both. A common filter was used for mechanization simplicity since it was known that the attitude and acceleration signals would each require 90 degrees of phase shift (at the first mode bending frequency) to bring them into the correct phase relationship with the rate signals. The need for two separate filters was not apparent until slosh stability problems were encountered. It was then theorized that heavy slosh coupling was being introduced by the accelerometer signals, thereby aggravating the stability situation. (C)

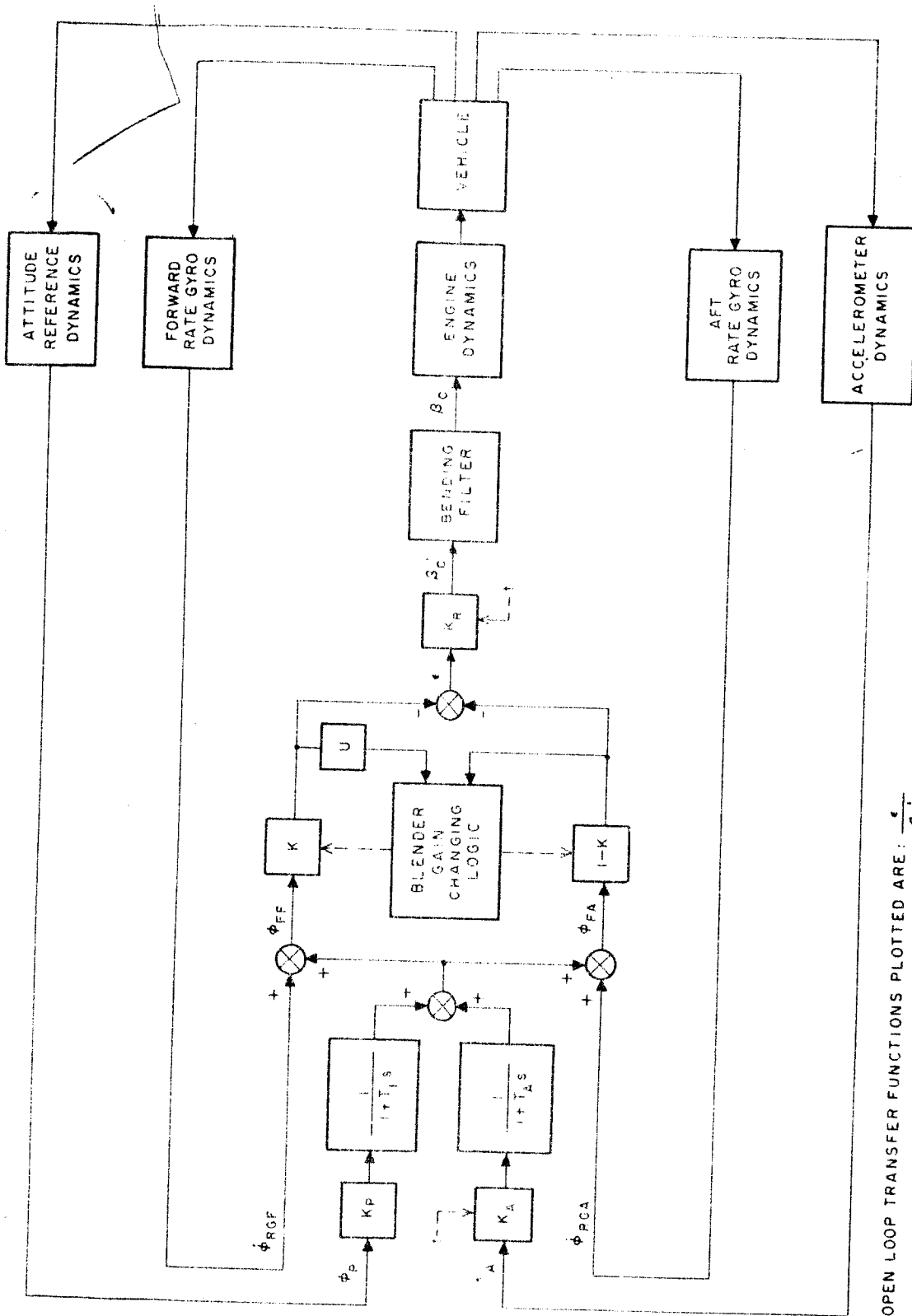


Figure 1. Final Saturn V Gyro Blender Control System Diagram

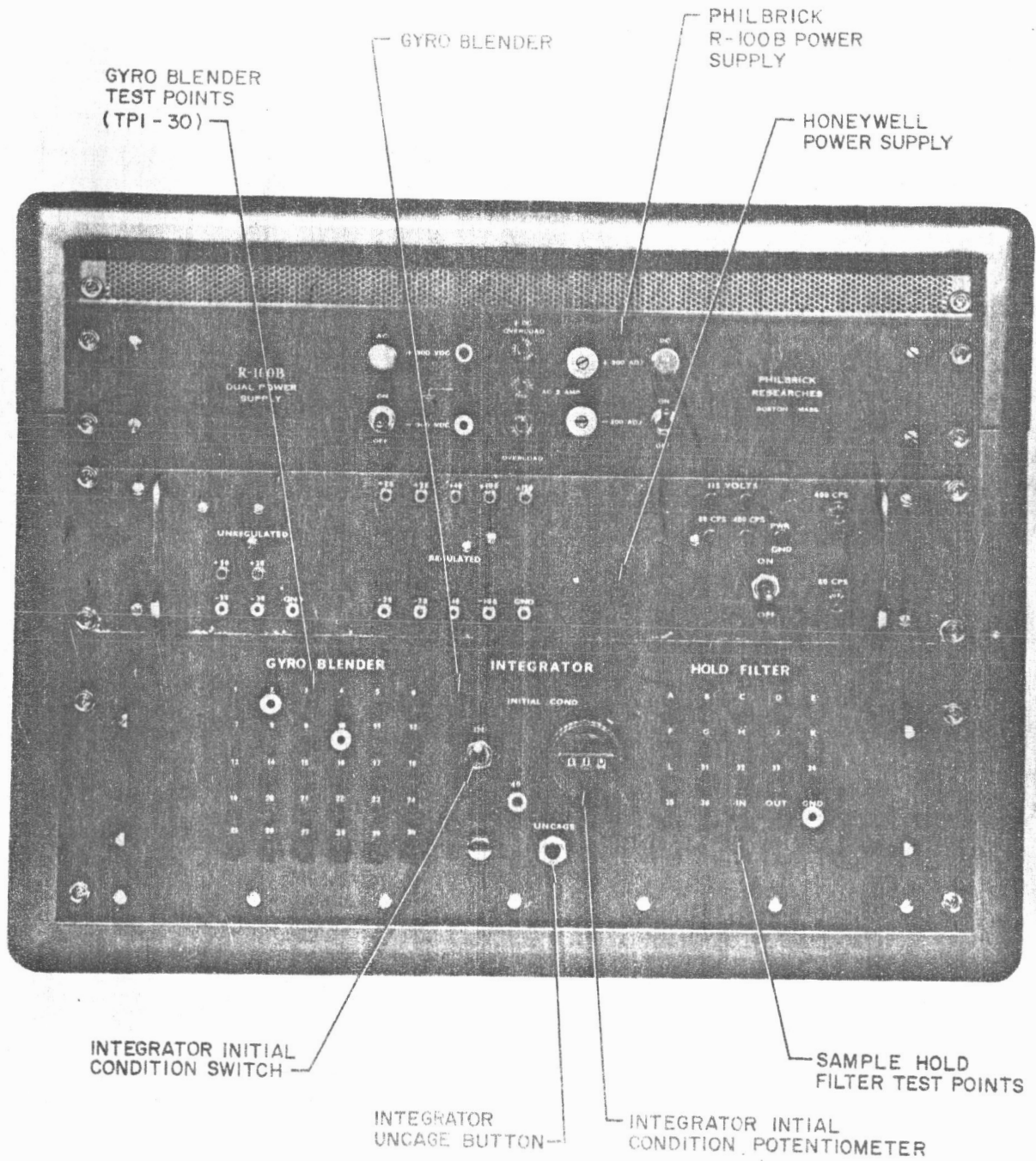


Figure 2. Gyro Blender Breadboard Cabinet - Front Panel

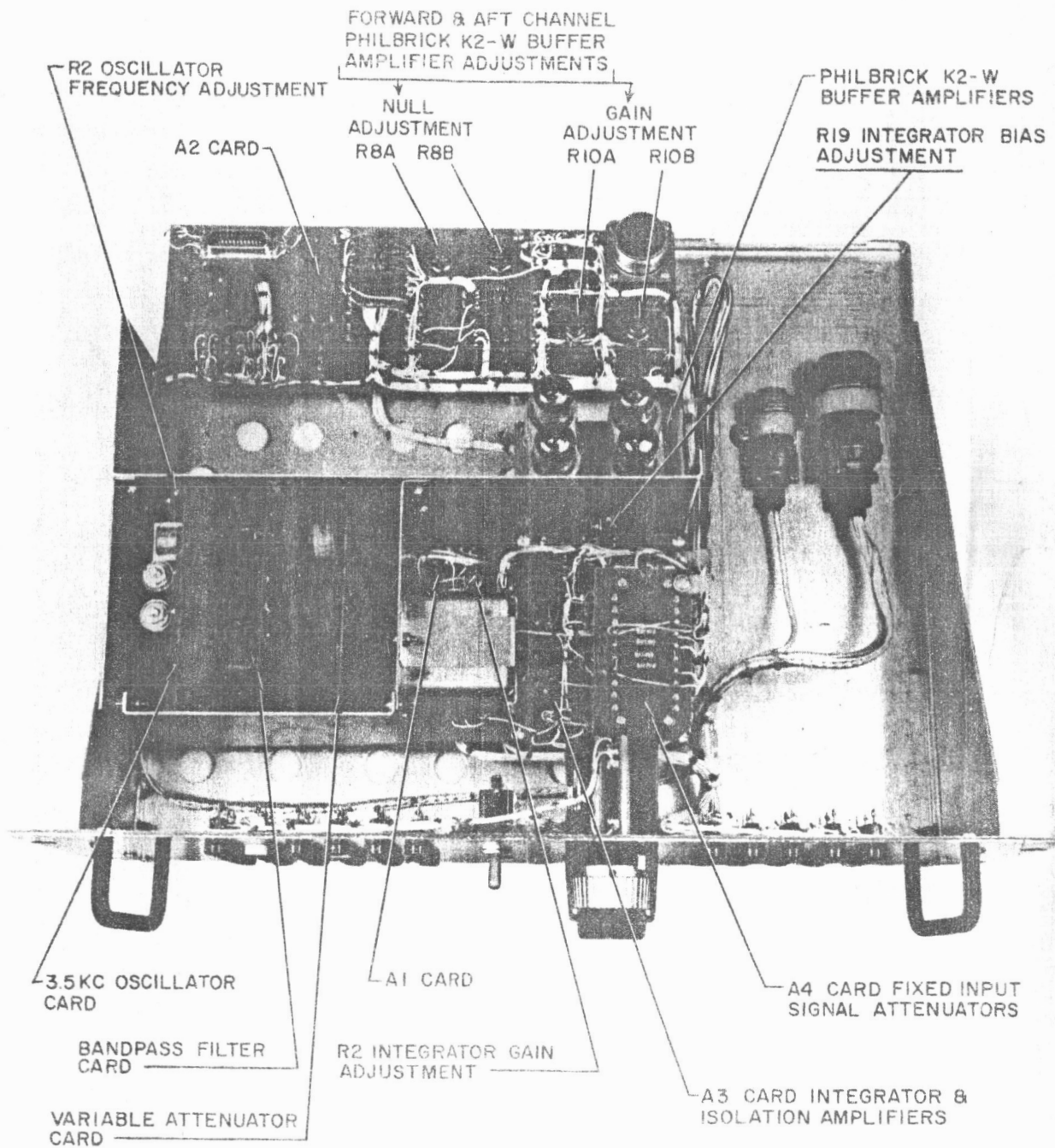


Figure 3. Gyro Blender Breadboard - Top View



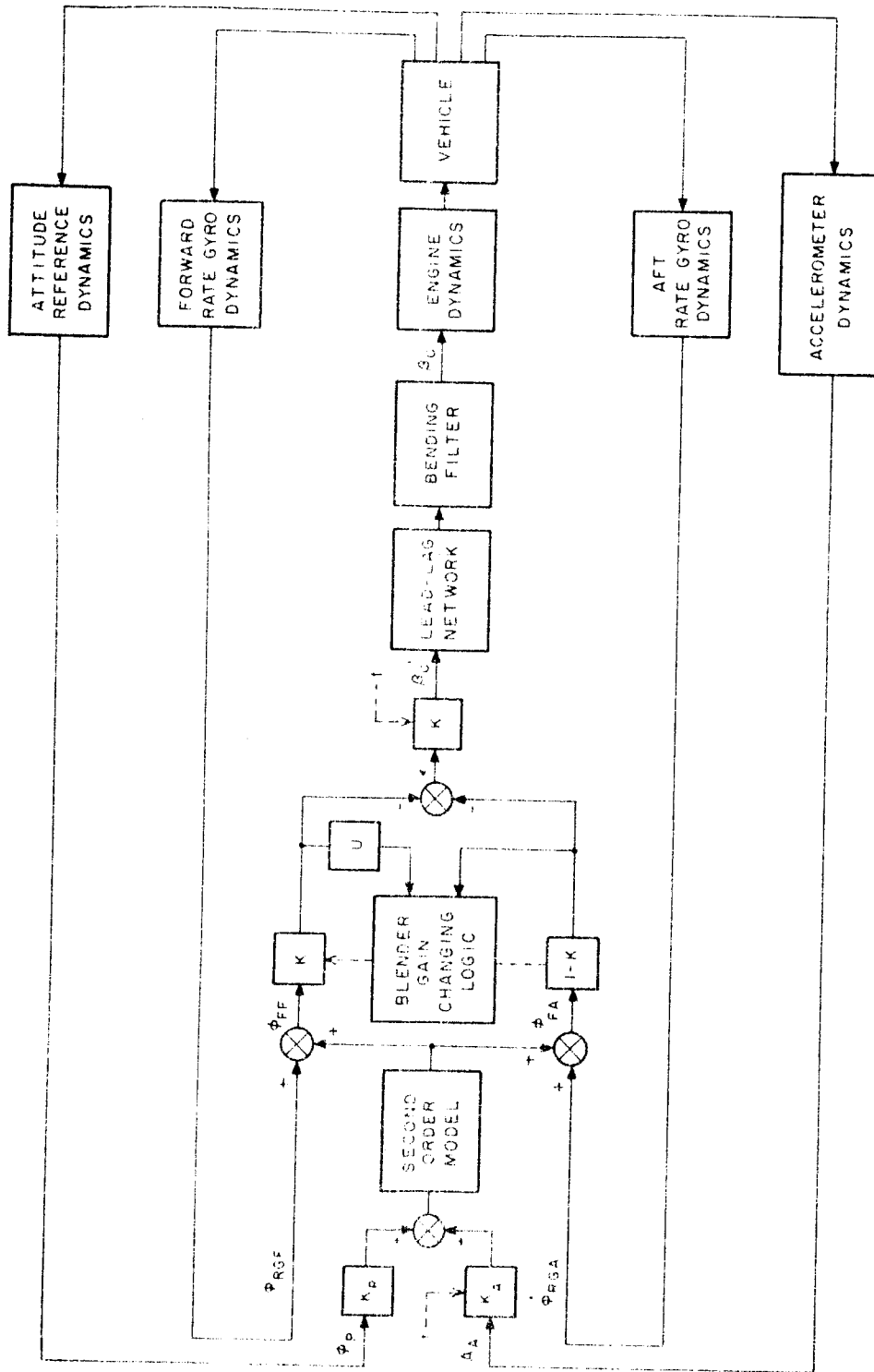


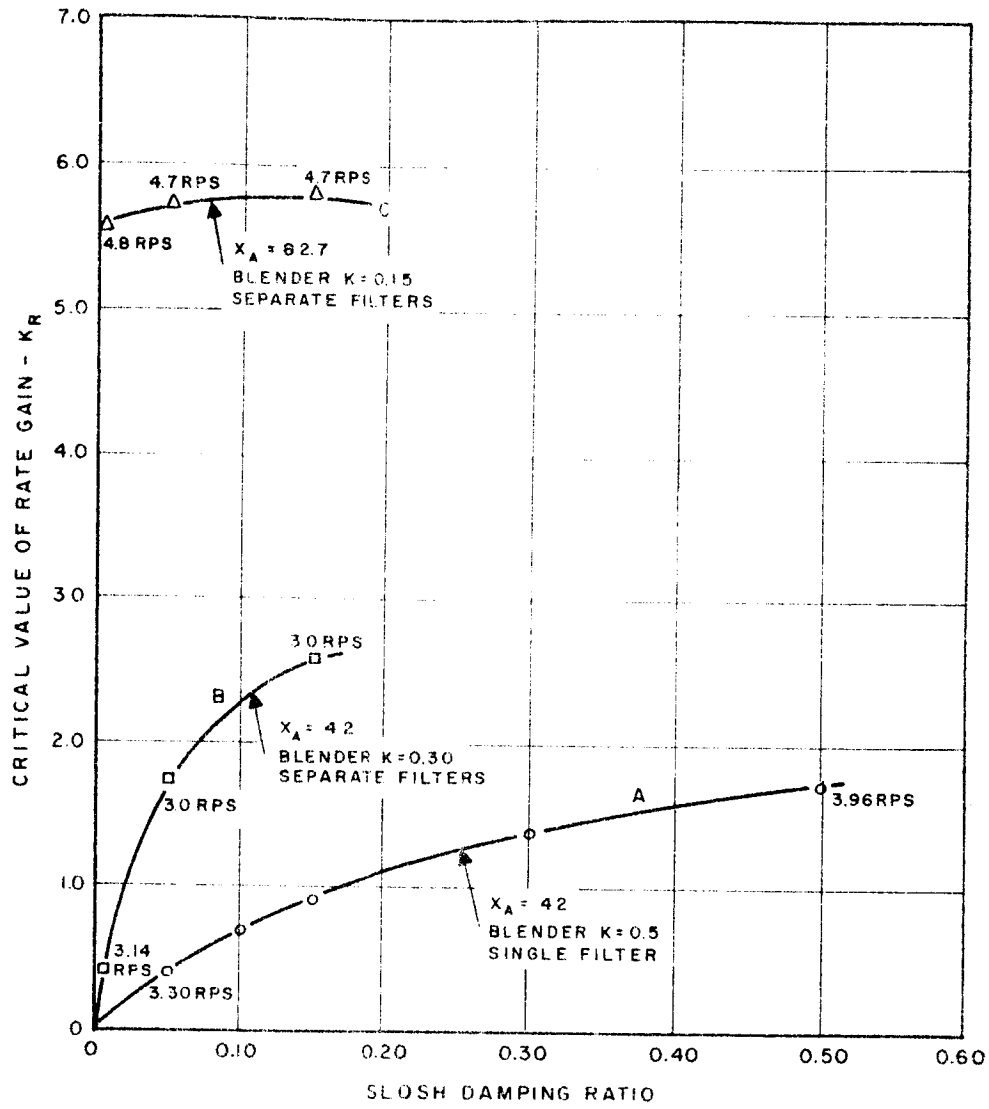
Figure 4. Preliminary Saturn V Control System Diagram

Subsequent investigation indicated that when the lag on the acceleration signal was approximately two seconds, a significant improvement could be obtained in the critical gain required for a given slosh damping ratio. This improvement can be seen by comparing curves A and B of Figure 5, which is a plot of slosh damping ratio versus the critical rate gain  $K_R$ . Curve A represents the results obtained with the preliminary system (Figure 4) while curve B was obtained using separate lags on the attitude and acceleration signals. Although the two-second lag aided slosh stability when included in the acceleration signal, a very small lag (0.2 second) was required in the attitude signal to maintain rigid-body response. This was the main reason for using separate filters in the final system. (C)

The revised system was satisfactory until the first bending mode was included in the simulation. The blender then had difficulty in operating properly because of an unfavorable phase lag at the first bending frequency which resulted in a limit cycle type of operation at the first mode frequency. Removal of the forward loop lead-lag network corrected the blender problems. This lead-lag was originally included in the system to help blender operation; therefore, its removal can be considered a reduction in system complexity. However, removal of the lead-lag reduced rigid-body damping at low values of  $K_R$ . The damping could have been increased in two ways:

1. Increase the operating range of  $K_R$ .
2. Move the accelerometer forward. (C)

Increasing  $K_R$  was undesirable since it would increase the attenuation requirements on the higher mode bending filter. Moving the accelerometer forward lowers the frequency of the model zeros. However, the basic locus is changed in such a way that, for a given gain, the rigid-body damping is increased appreciably with little loss in frequency compared to results obtained with the original accelerometer location. In addition to providing better rigid-body response, the second solution had another important advantage. The open-loop



- A ○ - PRELIMINARY CONTROL SYSTEM FILTER =  $\frac{1+0.130s}{(1+0.333s)^2}$ , LEAD LAG =  $\frac{1+0.5s}{1+0.1s}$ ,  
 $K_A = 0.050, K_P = 0.90, X_A = 42 M$ , BLENDER FIXED AT  $K = 0.5$
- B □ - SPLIT FILTER CONTROL SYSTEM - NO LEAD LAG  
 $K_A = 0.050, K_P = 1.5, X_A = 42, T_I = 0.30, T_A = 2.0$ , BLENDER FIXED AT  $K = 0.30$
- C △ - SAME AS ABOVE, BUT  $X_A = 82.7$  AND BLENDER GAIN FIXED AT  $K = 0.15$

NOTE:  
 VEHICLE RIGID BODY, TAIL-WAGS-DOG, FIRST BENDING MODE  
 AND ALL SLOSH MODES AT  $t = 79$  SECONDS

Figure 5. SLOSH Damping Ratio versus  $K_{R_{crit}}$

phase angle of the system around the slosh frequency was decreased considerably by relocating the accelerometer, resulting in a significant increase in slosh stability. The amount of this improvement can be seen in Figure 5 where curve C represents the results obtained with the accelerometer located at  $X_A = 82.7$  meters. (C)

### Accelerometer Location

The final choice of accelerometer location was based on the following considerations:

1. Magnitude of bending pickup
2. Slosh mode stability
3. Rigid-body response (C)

Only accelerometer locations ( $X_A$ ) between 61 (top of the second-stage fuel tank) and 85 meters were considered feasible. Positions beyond 85 meters were unacceptable because all bending mode pickups were excessively high. These high pickups would cause not only higher mode attenuation difficulties but, in addition, if the first mode acceleration pickup became too large, it would destroy the blender adaptive action. (C)

An  $X_A$  position of 64 meters was selected because the third mode bending pickup was at a minimum and the second mode pickup was not changing significantly over this range. The slosh stability at this  $X_A$  was reduced slightly because a slosh damping ratio of 0.005 was no longer satisfactory. However, slosh damping ratios of 0.03 to 0.06 were still usable. The rigid-body response at this  $X_A$  was of higher frequency but lower damping ratio than at more forward locations, but this was considered a desirable trade-off. The nominal rigid-body frequency with this accelerometer location was always greater than the minimum of 0.1 cps specified by MSFC. (C)

Feedback Gains and Dynamic Characteristics

The accelerometer gain ( $K_A$ ) schedule determined by previous rigid-body studies was satisfactory with the revised control system configuration. This schedule of  $K_A$  versus flight time is shown in Figure 6. The acceleration lag ( $T_A$ ) of 2.0 seconds was determined by analog computer studies with synthetic wind shear disturbance inputs at the  $t = 79$  flight time. A 2.0-second time constant was the maximum value that could be used and still be within the maximum  $\alpha q$  limit ( $35,800 \text{ kg-deg/m}^2$ ) under all tolerance conditions. (C)

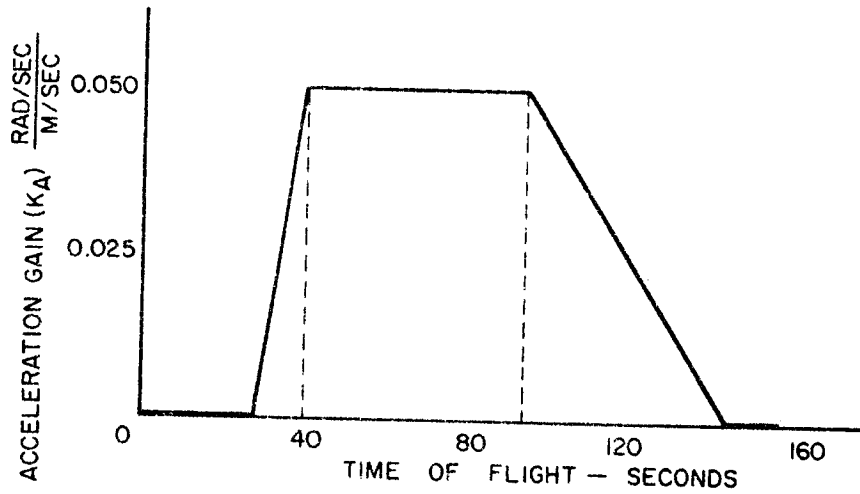


Figure 6. Acceleration Gain ( $K_A$ ) Schedule

Rate Gyro Locations

The forward rate gyro location was examined using the same guidelines used to select the accelerometer location. The original location of 85.3 meters was completely satisfactory in all respects as well as being conveniently located in the guidance package. (C)

The aft rate gyro location was selected to be 5 meters primarily because this was the only satisfactory location available which had the desired bending slope sign. (C)

Approximate values of attitude gain ( $K_P$ ) and attitude time constant ( $T_1$ ) were first calculated analytically and then optimized on an analog computer. The optimization goal was to obtain the highest rigid-body frequency with the largest damping ratio. Nominal values of  $K_P = 0.90$  (deg/sec)/deg and  $T_1 = 0.20$  second were selected from this study. (C)

The rate gain schedule shown in Figure 7 consists of a constant  $K_R$  of 0.8 deg/deg/sec until  $t = 130$  seconds, at which time  $K_R$  is reduced to 0.4. This nominal schedule could be selected only after the final configuration, including the bending filter, had been determined because the specific values of  $K_R$  depended upon the value of  $K_{Rcrit}$ . The value of  $K_{Rcrit}$  was understandably sensitive to the phase lags introduced by the bending filter and slosh modes. (C)

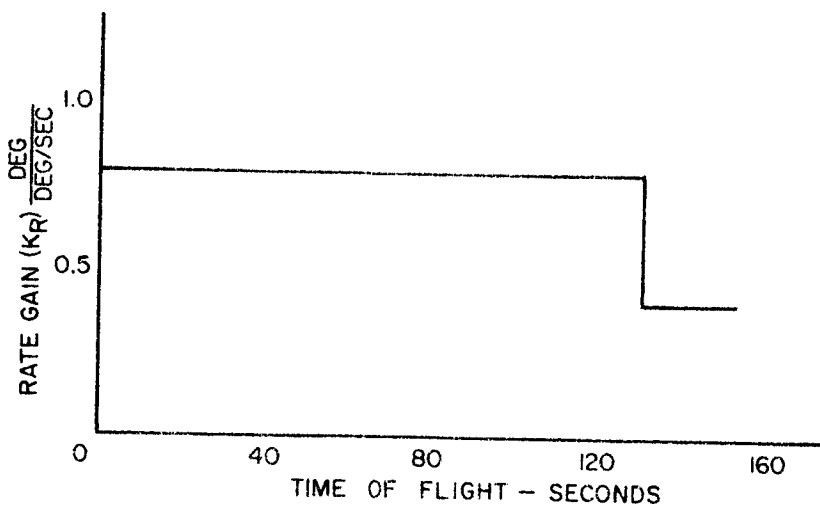


Figure 7. Rate Gain ( $K_R$ ) Schedule

Summary of Final Control System Parameters

The gains, dynamics, and sensor locations selected for the Saturn V control system configuration shown in Figure 1 are summarized in Table 1. (C)

Table 1. Final Control System Nominal Parametric Values

Parameter	Nominal Value Selected	Units
Acceleration Gain, $K_A$	See schedule in Figure 6	$\frac{\text{rad/sec}}{\text{m/sec}^2}$
Attitude Gain, $K_P$	0.90	$\frac{\text{deg/sec}}{\text{deg}}$
Rate Gain, $K_R$	See schedule in Figure 7	$\frac{\text{deg}}{\text{deg/sec}}$
Acceleration Lag, $T_A$	2.0	seconds
Attitude Lag, $T_I$	0.2	seconds
Accelerometer Location, $X_A$	64	meters
Aft Rate Gyro Location, $X_{RGA}$	5.0	meters
Forward Rate Gyro Location, $X_{RGF}$	85.3	meters

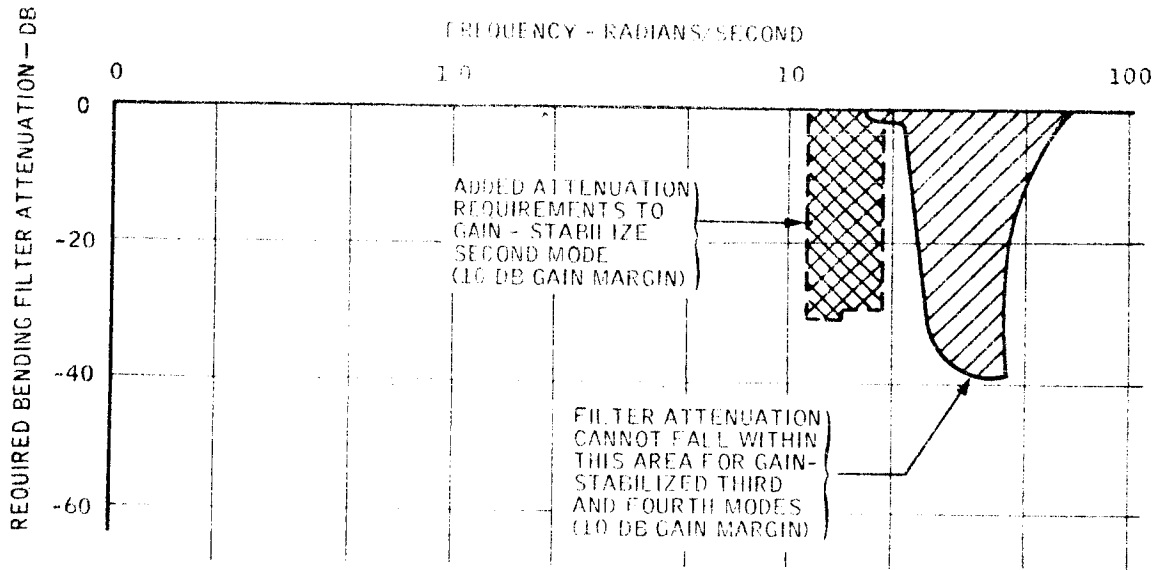
(C)

## BENDING FILTER DESIGN

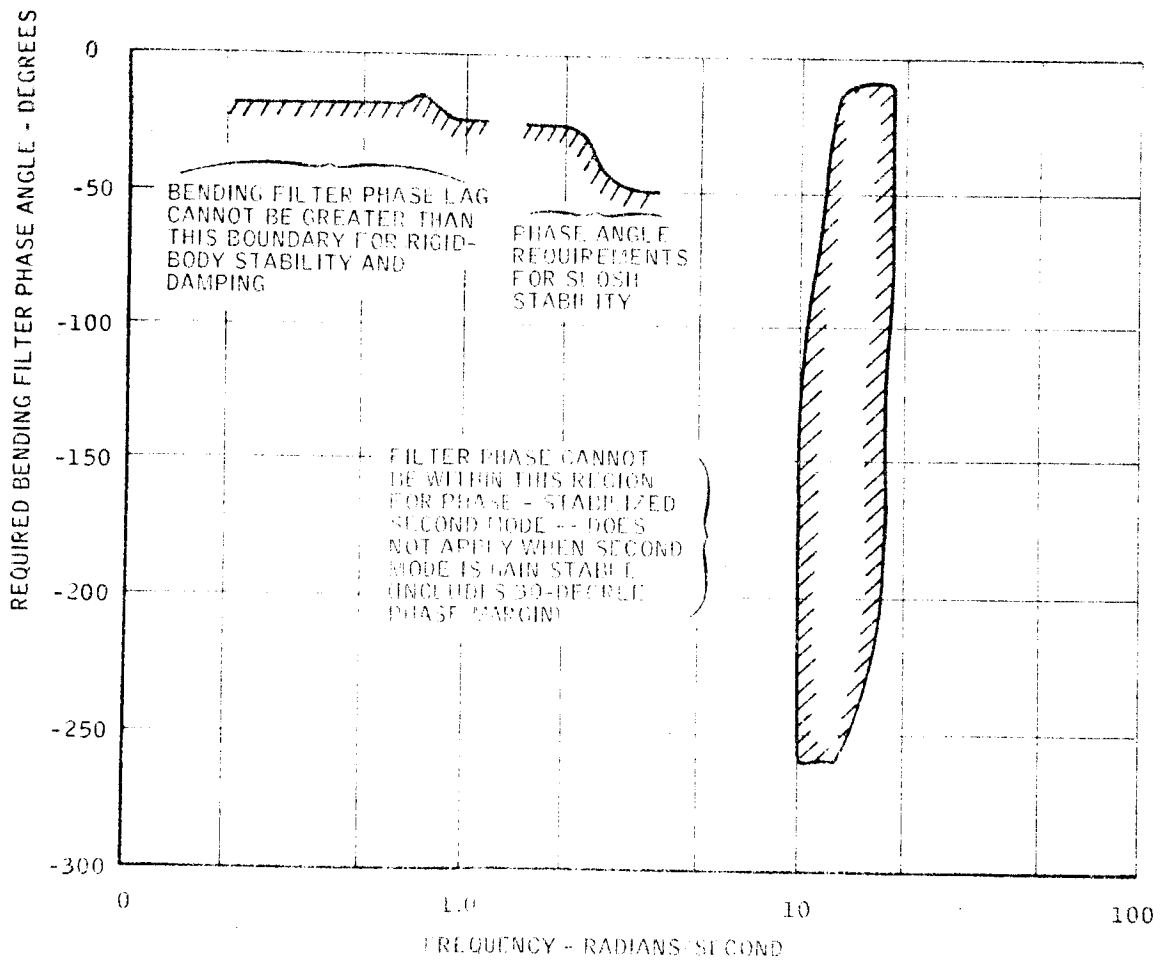
### Bending Filter Requirements

The phase and gain requirements of the bending filter needed to stabilize the second and higher bending modes were tabulated for all flight times and tolerance conditions. Suitable phase and gain margins were added to these requirements, and the results were plotted as shown in Figure 8. (U)

Tentative filter designs were evaluated on the plot shown in Figure 8. If a filter could pass these requirements, there seemed to be little chance of failure on the analog tolerance studies. (U)



(a) Attenuation



(b) Phase

Figure 8. Bending Filter Phase and Gain Requirements



Three areas are of concern in determining the filter requirements:

1. Rigid-body response
2. Slosh stability
3. Bending stability

These criteria were used to establish the bending filter requirements for each of the areas discussed below. (U)

Rigid-Body Response -- It was assumed that the lowest acceptable rigid-body damping ratio is  $\zeta = 0.10$  (74 per cent overshoot). The phase margin required to obtain this damping ratio, 12.8 degrees, is therefore the minimum acceptable phase margin. The phase margins for all flight times were obtained from frequency response plots made using the complete system except for the bending filter. The differences between these and the minimum acceptable phase margin are the phase shifts that can be contributed by the bending filter at each zero-decibel crossover frequency. This information is plotted in Figure 8(b) in the frequency range of 0.2 to 1.0 radian per second. (C)

Slosh Stability -- The minimum acceptable phase margin for the slosh modes under tolerance conditions was assumed to be 10 degrees. A minimum closed-loop slosh damping ratio of slightly less than 0.1 would be obtained under these conditions. The allowable bending filter lags at the slosh frequencies were computed and plotted in the same manner described above for rigid-body response, but in the frequency range of 1.5 to 4.0 radians per second. (C)

Bending Stability -- Filter requirements at the bending frequencies differ depending on whether the second bending mode is phase- or gain-stabilized. Rigid-body and slosh tolerances remain the same in either case. (C)

The phase margin ranges for the second bending mode for two cases -- without attenuation and with 10 decibels of attenuation -- were computed for all flight

times with  $\pm 10$  per cent frequency variations. An additional phase margin of 30 degrees was added to each value and plotted on Figure 8(b). Only the values obtained with no attenuation were plotted because the differences were negligible. (C)

In addition to phase-stabilizing the second bending mode, the bending filter must gain-stabilize the third and fourth bending modes. The attenuation requirements were determined by adding 10 decibels to the peak values indicated on the frequency response plot. The attenuation requirements were tabulated for all flight conditions with  $\pm 10$  per cent frequency variations. The boundary determined from these requirements is shown on Figure 8(a). (C)

The unacceptable phase region is quite large, and staying within the acceptable region requires either a very rapid phase drop (210 degrees in a little more than an octave) or a phase lead. The first method is extremely difficult to accomplish because of the rapid phase shift, and the latter is impractical because of its basic incompatibility with higher mode attenuation requirements. Therefore, it was decided to abandon the phase-stabilized approach in favor of gain-stabilizing the second mode. (C)

The attenuation requirements for the gain-stabilized second mode were determined in the same manner described above for the third and fourth modes. The additional boundary for these requirements is indicated in Figure 8(a). (C)

#### Preliminary Bending Filter Designs

The bending filter used in the final system configuration evolved as the filter requirements became more clearly defined. For the nominal system a filter designated "filter A" was tried. Filter A consisted of two second-order lag networks in series, each with  $\zeta = 0.5$  and  $\omega = 10$  radians per second. This filter had the advantage of simplicity; however, it was inadequate for stability

when vehicle and filter tolerances were included. The frequency response plot of filter A is shown superimposed upon the gain and phase requirements in Figure 9. It can be seen that this filter is not adequate for phase-or gain-stabilizing the second bending mode if adequate rigid-body performance is to be maintained. Figure 9 indicates the desirability of gain-stabilizing the second mode because of the stringent requirements for phase stability of this mode. (C)

A possible filter consisting of seven sharp notches in series was also considered. This filter could be mechanized using seven operational amplifiers. The frequency response of a filter with the transfer function

$$\frac{e_{out}}{e_{in}} = \prod_{n=0}^6 \frac{[s^2 + 0.05 \omega_o (1.25)^n s + (1.25)^{2n} (\omega_o)^2]}{[s^2 + \omega_o (1.25)^n s + (1.25)^{2n} (\omega_o)^2]}$$

is shown superimposed upon the gain and phase requirements in Figure 10. (C)

This filter gain-stabilizes the second bending mode, but it is marginal for slosh stability and requires that filter tolerances be tight. (C)

### Final Filter Design

Another filter was designed which has improved phase characteristics at low frequencies and which can be mechanized using four stages of passive RC circuits and two active stages. This filter, hereafter designated "filter B", was used in the final system configuration. The nominal transfer function of filter B is given below: (C)

$$\frac{e_{out}}{e_{in}} = \frac{(s^2 + 144)(s^2 + 1764)(s + 1.45)(s + 18.4)(s^2 + 6.84s + 324)(s^2 + 12.16s + 1024)(365)(s + 8.05)}{(s^2 + 48s + 144)(s^2 + 168s + 1764)(s^2 + 2.66s + 49)(s^2 + 68.4s + 324)(s^2 + 121.6s + 1024)(s^2 + 200s + 1600)}$$

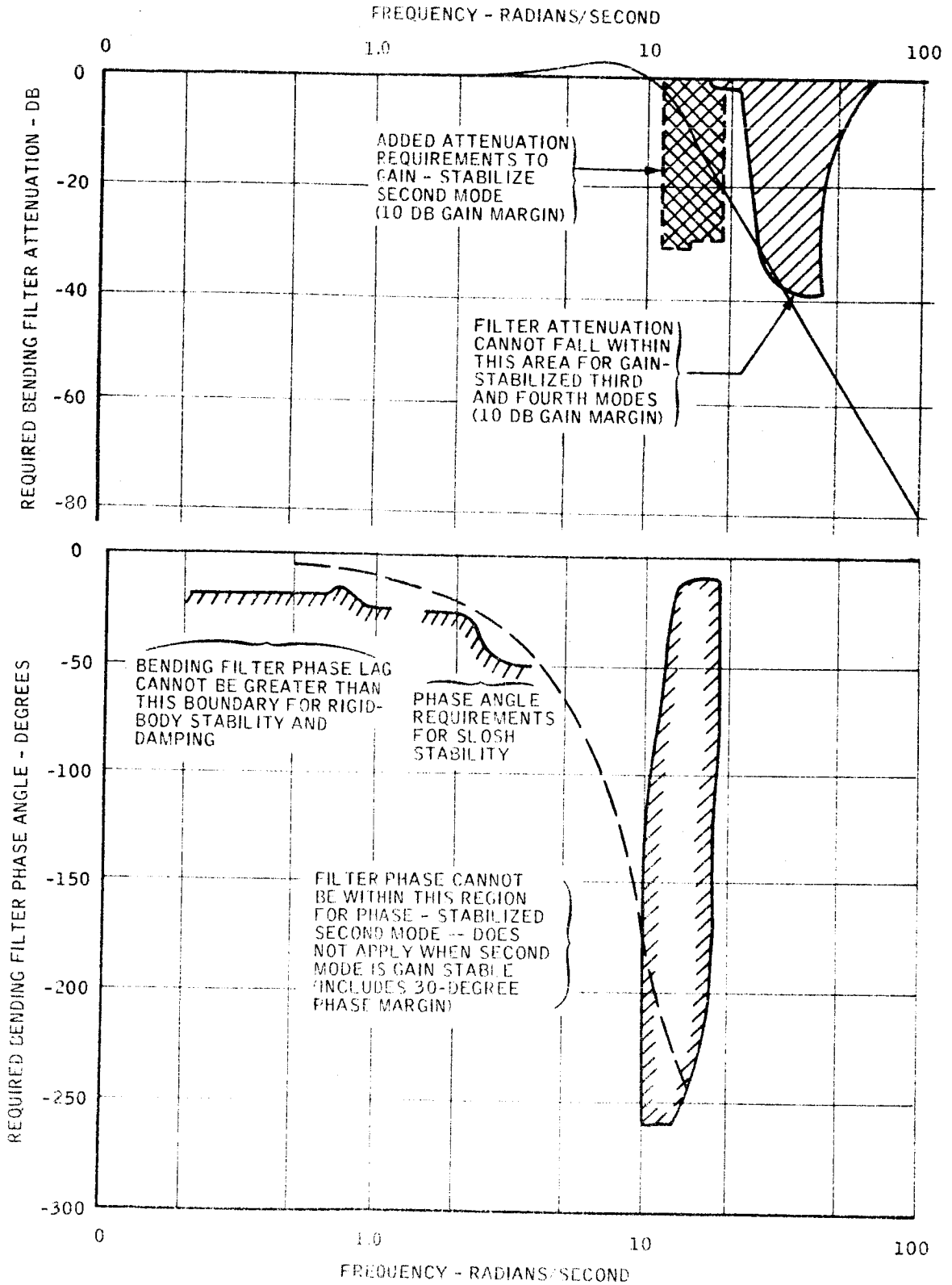


Figure 9. Filter A Frequency Response Compared to Requirements

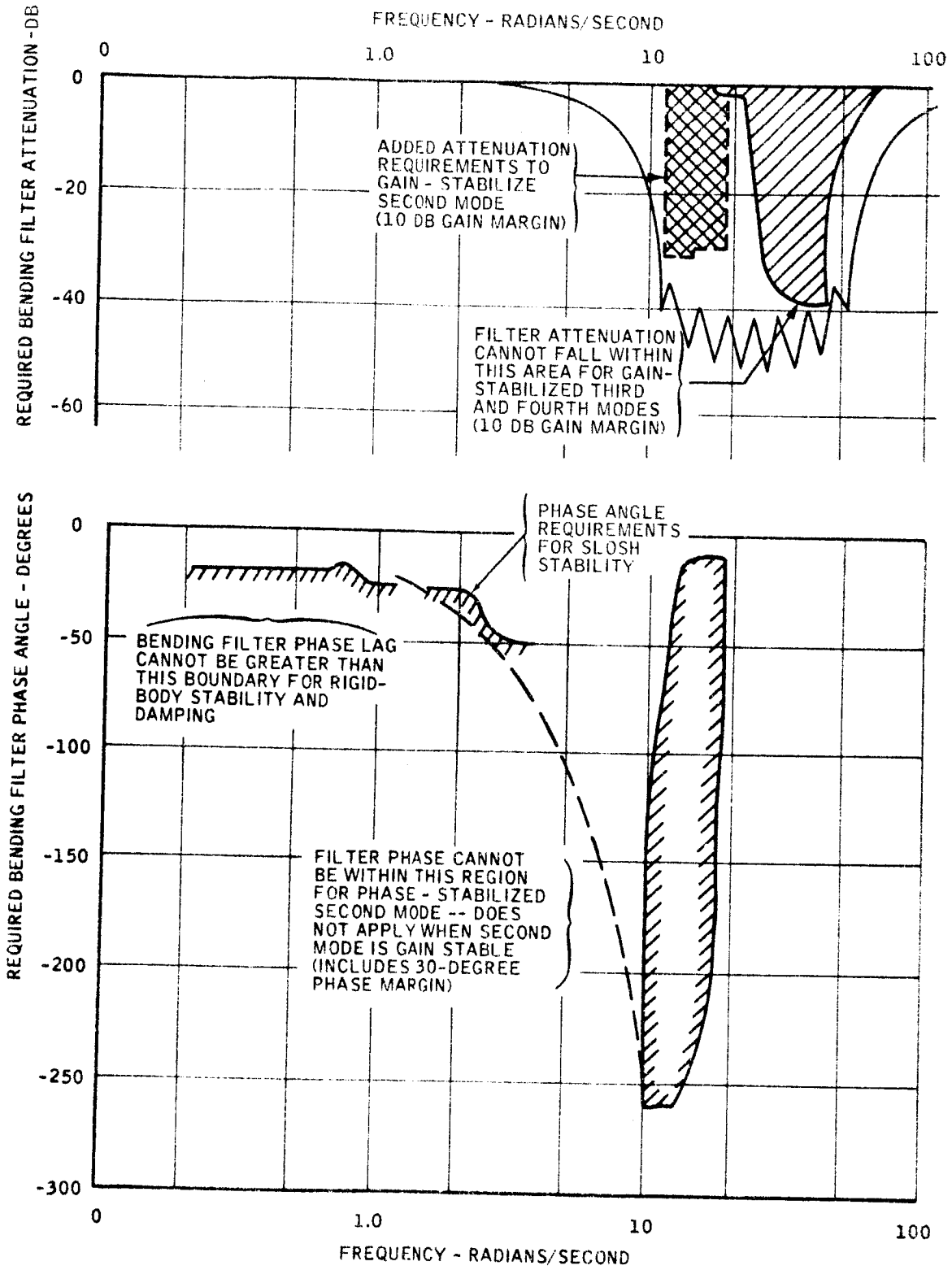


Figure 10. Nominal Seven-Stage Filter Frequency Response Compared to Requirements

A frequency response plot of this transfer function is superimposed upon the gain and phase requirements in Figure 11. Filter B can theoretically gain-stabilize the second and higher bending modes. This filter is not as sensitive to component tolerance variations as the previously mentioned active filter. A mechanization method for filter B is given in Figure 12. (C)

For the analog computer tolerance study, the tolerance on resistors was assumed negligible compared with capacitor tolerances. A tolerance of  $\pm 10$  per cent was used for capacitors. The worst conditions occurred when all capacitors were high or all low, giving a  $\pm 10$  per cent shift in frequencies. No attempt was made to "tune" the filter to compensate for loading effects, etc. Consequently, the filter mechanized on the analog computer had somewhat degraded phase characteristics compared with the theoretical filter. This can be seen from the experimentally determined frequency response plot superimposed on the gain and phase requirements in Figure 13. (C)

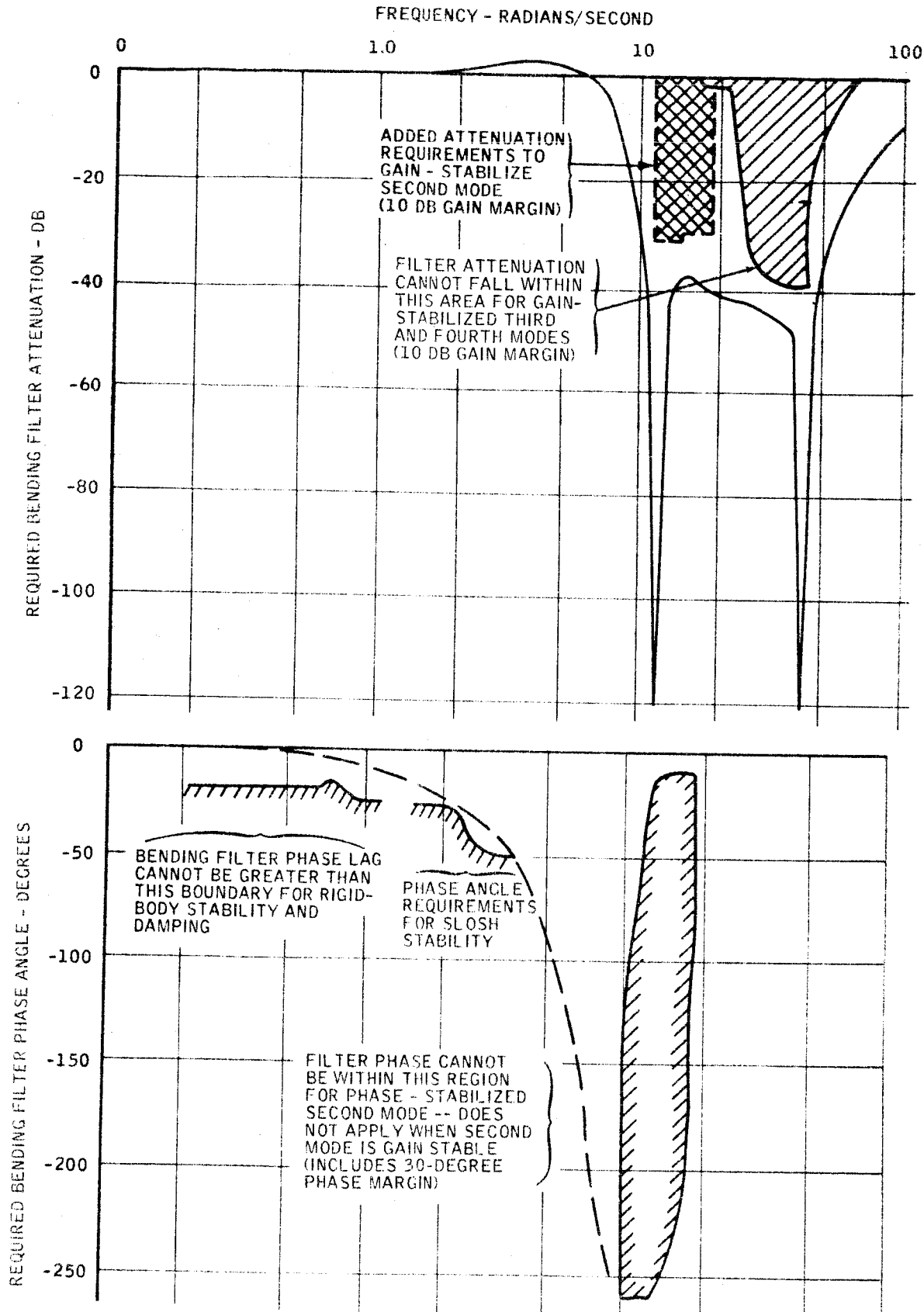


Figure 11. Theoretical Filter B Frequency Response Compared to Requirements





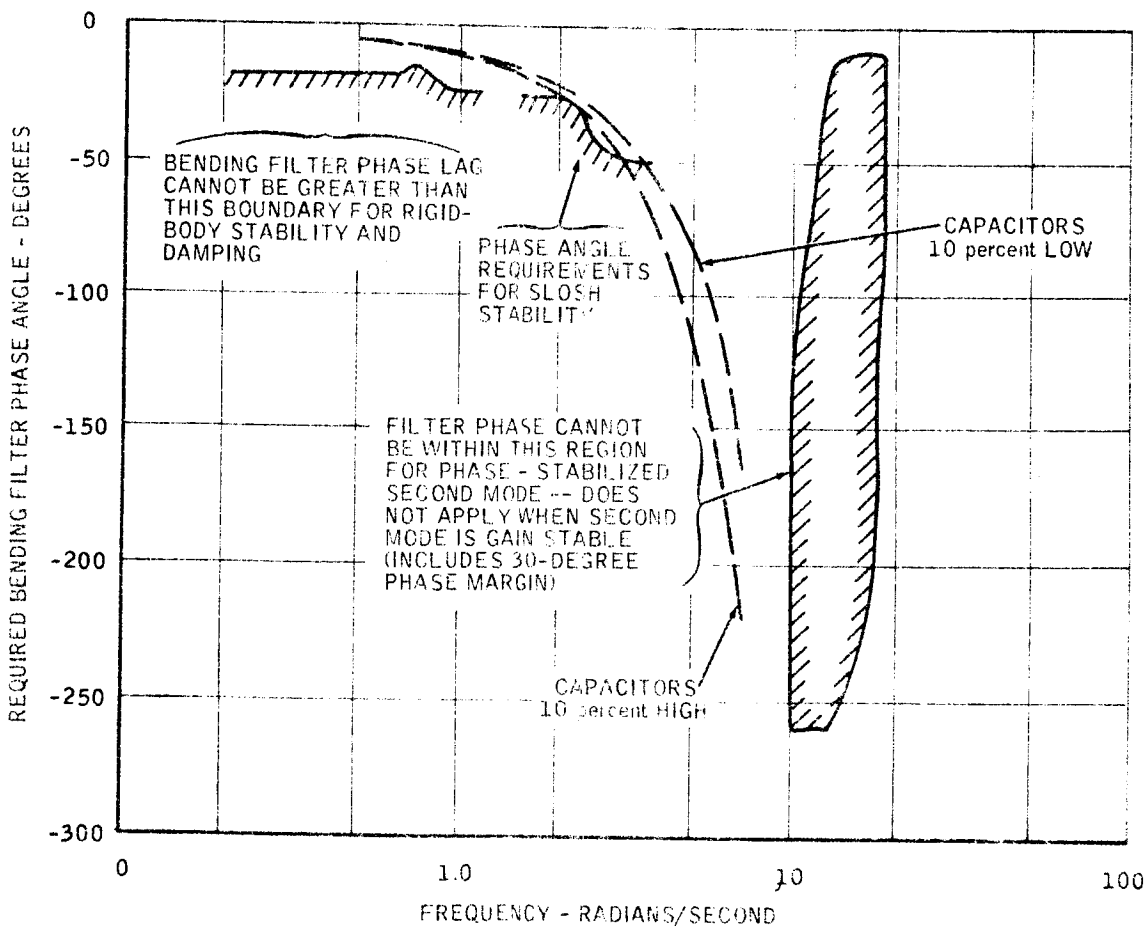
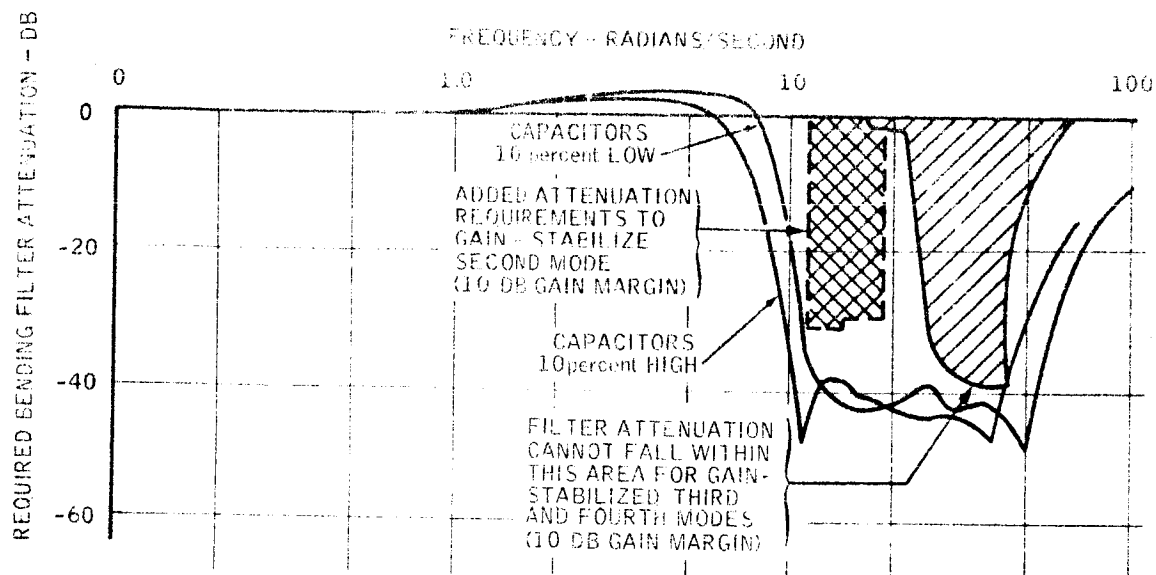


Figure 12. Actual Filter B Frequency Response Compared to Requirements

SECTION V  
BLENDER DESIGN AND OPERATION

GENERAL CONCEPT

In the basic gyro blender concept, the outputs of two rate gyros, one placed aft and the other forward of the first bending mode antinode, are attenuated and summed before being used as the control system rate signal. A block diagram of this basic system is shown in Figure 14. The attenuators are adaptively adjusted until the opposing first mode bending signals (opposing because of opposite slopes) are equal in magnitude and therefore cancel each other. (C)

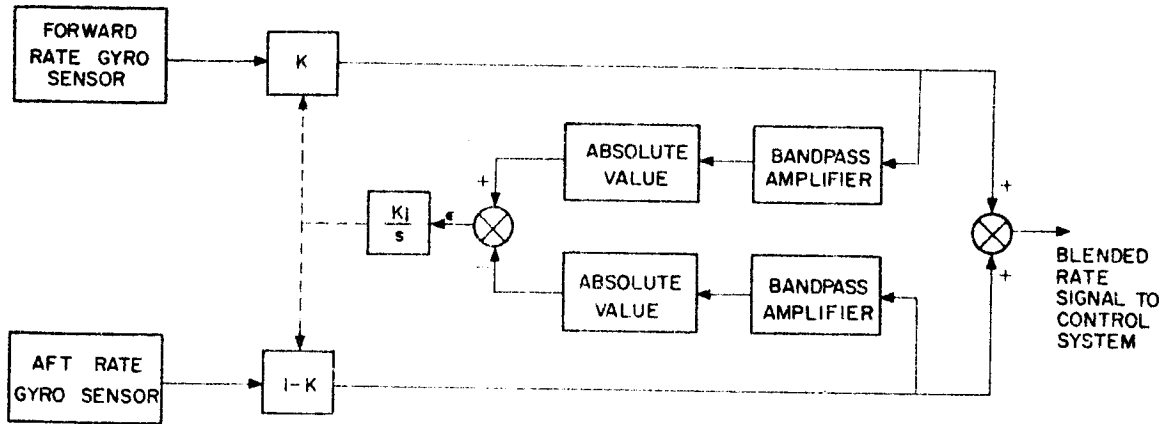


Figure 14. Basic Gyro Blender Concept Diagram

If the attenuation of one gyro signal is represented by  $K$  and the other by  $1-K$ , it can be seen that signals common to both channels (rigid body in this case) will not be affected in any way by this attenuation-summing procedure. (C)

The adaptive attenuation adjustment is obtained by comparing the magnitude of the first mode bending pickups from each gyro (after the K and 1-K attenuations) and adjusting the value of K until these signals are equal. (C)

To isolate the first bending mode signals from the other system frequencies, the outputs of K and 1-K are put through bandpass amplifiers with center frequencies equal to the first bending mode frequency. The comparison of magnitude only is ensured by the use of absolute value circuits following the bandpass filters. The error signal ( $\epsilon$ ) resulting from the subtraction of these two bending signal magnitudes is integrated, and its output is used to set the variable attenuators. (C)

### Practical Applications

The blender concept described above can theoretically remove all first mode bending content from the feedback signal if the only feedbacks are from the two rate gyros. Attitude and acceleration feedbacks were desired on the Saturn V vehicle, but unfortunately these signals are both 90 degrees out of phase with the rate signals and, therefore, apparently could not be cancelled out when summed with the rate signals. One solution to this problem is the use of lag networks on both the acceleration and attitude feedbacks. These lags were designed to give approximately 90 degrees of phase shift at the first bending mode frequency, thus bringing these signals into phase alignment with the rate gyros and enabling the first mode bending components of all feedback signals to be self-canceling. (C)

A blender system design relying on exact bending component cancellation proved unsatisfactory because of the potentially unstable situation obtained when exact phase alignment was not possible because of tolerances and other system variables. (The phase and amplitude tolerances required are discussed further in Section VIII.) A considerable amount of beneficial adaptive action could be retained, however, even if some bending pickup were allowed to enter the control system;

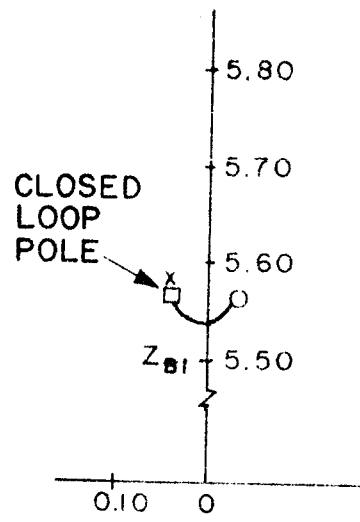
but stability problems are possible if the system is not analyzed thoroughly with conventional servomechanism techniques and analog computer studies. These studies are similar to those required for a linear system development, the only difference being that the adaptive action must be verified for the maximum range of expected parameter variations. (C)

This study program has shown that the blender is very tolerant to basic system changes; e. g., blender imbalance and integrator gain are the only system parameters that require optimization for extensive system changes. This is illustrated by the fact that the basic breadboard circuit design was initiated before any system work had been started. The only information required at that time was the range of first bending mode frequencies, and these were used to determine the desired center frequency of the bandpass amplifiers. The only changes required throughout the program were to the blender imbalance and the integrator gain. Determining the correct values of these two parameters for any given system is a relatively straightforward procedure explained later in this section. (C)

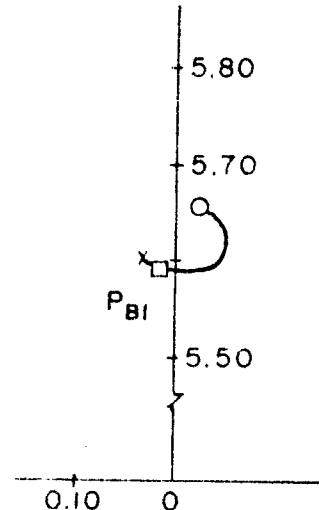
#### Phase Stabilization

If the bending components had all been exactly opposite in phase, therefore allowing the first mode signals to the control system to be completely attenuated (first mode zeros directly on top of first mode poles), it would have been feasible to consider gain stabilizing the first bending mode. This implies that even though the first mode zeros do not completely cancel the first mode poles, they are so close that the closed-loop roots at the maximum expected system gain cannot cross the  $j\omega$  axis regardless of phase field changes around this dipole. This can be more clearly seen in Figure 15. (C)

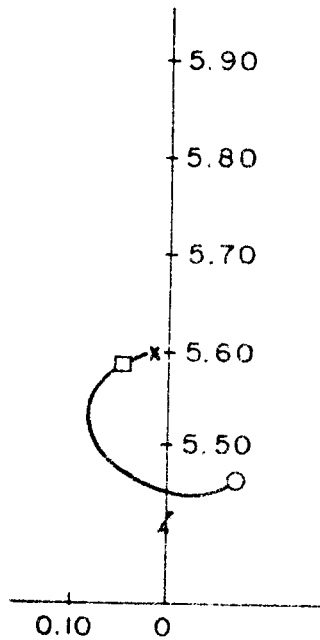
In Figure 15(a), the first mode bending dipoles are not completely cancelled, yet they are both phase and gain stable because the first mode zeros are very close to the pole and in a position that results in a favorable root locus. In



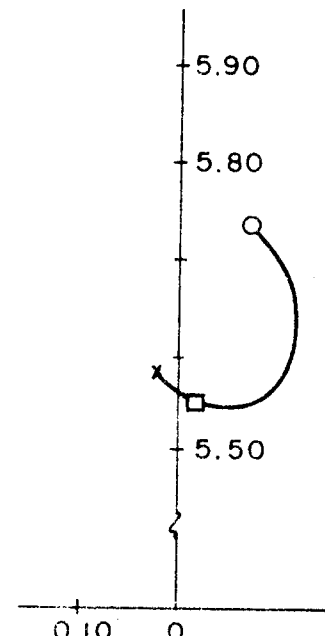
(a)  
GAIN AND  
PHASE STABLE



(b)  
GAIN STABLE



(c)  
PHASE STABLE



(d)  
UNSTABLE

Figure 15. Examples of Possible First Bending Mode Root Locus Plots

Figure 15(b), these zeros are still the same distance from the poles, but their position now results in an undesirable locus. The system is still stable, however, because the closed-loop poles could not travel very far on this small locus and therefore did not get into the right half plane. Figure 15(c) presents the same general case, except that now the distance between the poles and zeros has increased. The system remains stable because the zeros produce a desirable locus. However, if these zeros are placed above the poles, as shown in Figure 15(d), the locus heads toward the right half-plane; the closed-loop poles are now unstable because they travel farther on a larger locus for a given gain. This situation is aggravated in the Saturn 5 for two reasons:

1. The first mode frequency is so low that for a given bending damping ratio ( $\zeta_B$ ) the poles are not far from the  $j\omega$  axis; e. g., with a bending frequency of 5.0 radians per second and  $\zeta_B = 0.005$ , the bending poles are  $(0.005)(5) = 0.025$  radian per second from the  $j\omega$  axis, while poles with a bending frequency of 20 radians per second and the same damping are  $(0.005)(20) = 0.10$  radian per second from the  $j\omega$  axis.
2. In addition to being closer to the  $j\omega$  axis, the low-frequency first mode indicates that this mode will be attenuated less by the system dynamics than would be the case at a higher frequency. This means that the closed-loop poles will travel further along a given locus, making it more difficult to ensure gain stability. (C)

Because the basic root locus in the immediately vicinity of the dipoles is very predictable, the maximum possible distance between the poles and zeros for gain stability can be estimated quite accurately. For the present system at  $t = 79$ , this distance is 0.06 radian per second. This maximum distance should not vary much with the type of control system used because the locus in the immediate vicinity of a dipole varies directly with the distance between the pole and zero for a constant phase field. (C)

An important system design guide can be determined from the preceding analysis: If a pair of zeros can be consistently placed within 0.06 radian per second of the first bending poles under all conditions of tolerance and change, a very good gain-stable system with wide tolerances to bending variations can be designed. If, however, this cannot be guaranteed, a miss by as little as 0.10 radian per second could result in an unstable system, as illustrated in Figure 15(d). This accuracy requirement is not limited to the gyro blender concept; it will be an important consideration in any system attempting to cancel first mode poles. (C)

The present gyro blender cannot maintain the first mode zeros to these tolerances without the addition of an adaptive phase-changing device and very close tolerances on the gain difference between the two bandpass amplifiers. The specific phase and gain requirements are discussed in a later section. Fortunately, the gyro blender concept does not have to rely on exact cancellation to retain its adaptability to changes in bending characteristics. All that is required is to keep the zeros in a position that results in a phase-stable mode, such as shown on Figure 15(c), under all tolerances and changing conditions. (C)

A phase-stable mode is defined here as a mode which has a specific phase and gain margin. This differs from the frequently used definition in which the mode, by virtue of its phase, is stable for all values of gain and thus does not have a gain margin. The differences in these definitions is illustrated in Figure 15(c). In this root locus, the closed-loop root can become unstable in two ways:

1. System gain increase.
2. Phase change at the mode frequency sufficient to rotate the locus. (U)

This example illustrates the definition used in this report. The alternate definition would be illustrated if the zero shown was moved from the right to the left half plane. With this configuration the closed-loop root would be stable at any gain and could be made unstable only by phase changes. (U)

## RECOMMENDED BLENDER DESIGN APPROACH

The blender design difficulties encountered led to the formulation of a design procedure that can be used in other phase-stabilized blender applications. This recommended design approach is presented in the following paragraphs. (C)

The stability of a phase-stabilized mode is, by definition, dependent on the phase angle of the complete control system at the particular modal frequency. The phase angle at the first mode frequency is strongly influenced by the basic control system configuration and the sensor locations. The design procedure necessary to ensure satisfactory blender operation is as follows:

1. Design the control system to fulfill all dynamic requirements, such as rigid-body response, slosh stability, and bending mode (second and higher modes) attenuation, without considering any of the first bending mode effects. This procedure should be identical to conventional methods of linear system design. The only special considerations required are:
  - a. Any signals that are to be added to the rate gyro signals for blending must be examined to determine if their magnitude at the first mode frequency is greater than the magnitude of the rate gyro signal opposing the additional signal. If the added signal is greater than its opposing rate signal, bending cancellation will be impossible because the signals no longer have opposite signs.
  - b. The rate signal for the control system must come from two rate gyros placed in convenient locations on both sides of the first mode antinode. The signals are combined in the same manner as in the actual blender; however, the blender position should be considered fixed at 0.5. This assumption introduces some error into the attenuation requirements of the higher bending modes because the effective slopes of the higher modes are dependent on the blender position and will



vary if the equilibrium gain selected by the blender logic is not close to 0.5. This restriction is not felt to be serious because the higher bending mode attenuation requirements can be revised if the actual blender position is significantly different from this estimate. (C)

2. Using the basic system developed in (1) above but now including the first bending mode effects, the values of blender imbalance ( $U$ ) and integration gain ( $K_i$ ) can be determined:
  - a. To aid in determining the desired blender imbalance, the stability boundaries of  $K_{R_{crit}}$  versus blender position are determined at each flight condition. These boundaries may be determined by analytical methods or by the use of an analog computer simulation.

Typical stability boundaries obtained in this study are shown in Figure 16. Also indicated in this figure are the equilibrium gains obtained for various blender imbalances. A desired equilibrium gain can easily be determined for each flight condition and a compromise equilibrium gain, which is satisfactory at all flight conditions, can be established.

Once the desired equilibrium gain has been established, it is relatively simple to determine experimentally a blender imbalance that will give this position on an analog computer.

- b. Integrator gain is selected on the basis of the ability to recover from an initially unstable blender position. The extreme blender positions ( $K = 1$  and  $K = 0$ ) are usually used in this type of investigation. It was found that if the blender system had the ability to recover from unstable conditions, attitude command step inputs (up to 1.5 degrees) were also handled satisfactorily. (C)

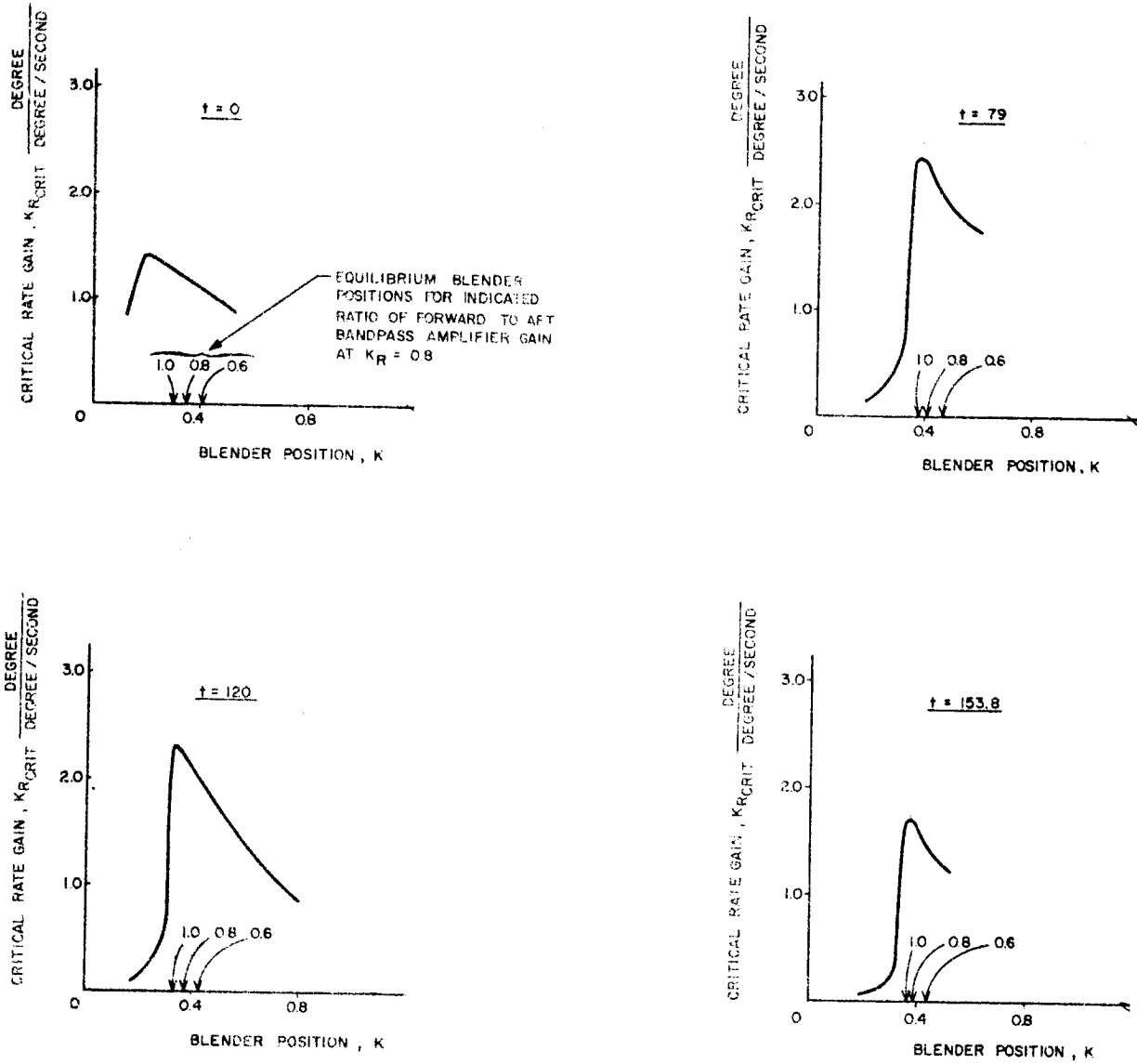


Figure 16. Effect of Blender Position Upon Critical Gain

### Analytical Results

The preceding discussion indicates that considerable experimental work is required to determine the blender parameters needed for satisfactory closed-loop operation. No analytical methods for determining the stability of the system as a function of blender parameters are presently available. The ease and dependability of the analog computer methods for solving this nonlinear problem have made large-scale analytical efforts unnecessary. During this study, however, some analytical work has been done with the blender considered as an open-loop component. The results are very useful in the hardware design of the blender and will allow the initial design to be much closer to a final configuration than has previously been possible. (U)

In the following discussion, a basic time constant for the blender loop is derived. The steady-state blender error resulting from substitution of a first-order lag approximation for the integrator is then discussed and compared with test results. (U)

The blender loop of concern is shown in Figure 17. The sinusoidal signals  $\phi_{FF}$  and  $\phi_{FA}$  have frequencies equal to the bandpass amplifier center frequency. Because of this single-frequency input characteristic, the loop can be analyzed as if it were a d-c loop. The bandpass amplifier characteristics can now be neglected if it is remembered that  $B_1$  and  $B_2$  are the bandpass amplifier gains at the input signal frequency. (U)

The absolute value circuits act as rectifiers; therefore, the peak-to-peak sinusoidal input values must be multiplied by  $2/\pi$  to obtain the average value. The simplified block diagram is now as shown in Figure 18. The equations for this system are

$$\epsilon = \left[ \phi_{FF} K B_1 - \phi_{FA} (1 - K) B_2 \right] \frac{2}{\pi} \quad (1)$$

$$K = \frac{K_i}{s} \epsilon \quad (2)$$

(C)

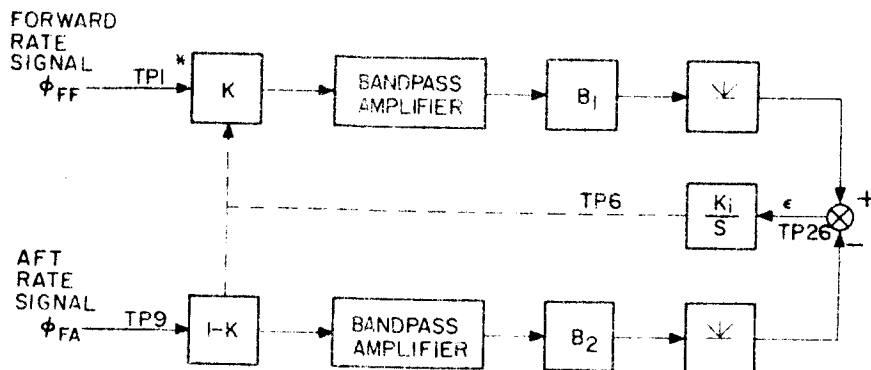
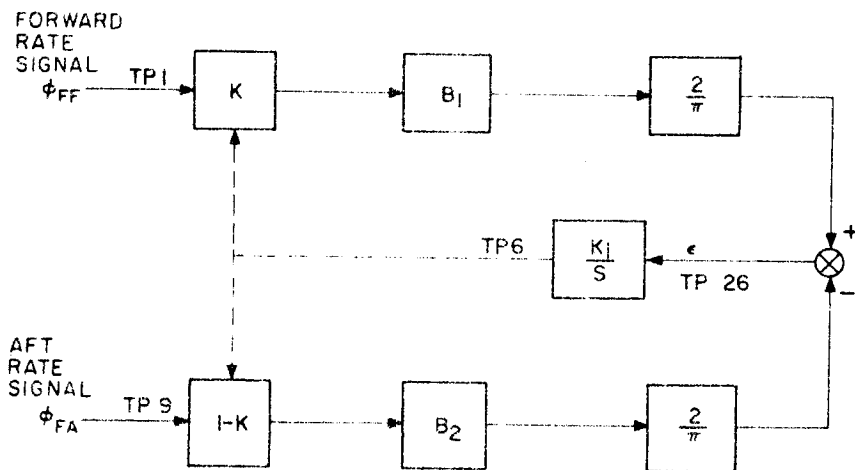


Figure 17. Blender Block Diagram



\* TEST POINTS (TP) ARE THOSE SHOWN ON HONEYWELL DRAWING SK83608, SIGNAL CIRCUITS, GYRO BLENDER BREADBOARD

Figure 18. Blender Simplified Block Diagram

Since the gyro blender positions itself (determines an equilibrium value of K) as a function of the ratio between  $\phi_{FF}$  and  $\phi_{FA}$ , the desired transfer function of this system is,

$$\frac{K}{\phi_{FF}/\phi_{FA}}(s) = f(s, K_i, B_1, B_2)$$

Combining Equations (1) and (2),

$$K = \frac{2K_i}{\pi s} \left[ \phi_{FF} K B_1 - \phi_{FA} (1 - K) B_2 \right]$$

$$K \left[ \phi_{FF} B_1 + \phi_{FA} B_2 - \frac{\pi s}{2K_i} \right] = \phi_{FA} B_2$$

$$\frac{K}{\phi_{FA}}(s) = \frac{\phi_{FF} B_2}{\phi_{FF} B_1 + \phi_{FA} B_2 - \frac{\pi s}{2K_i}} = \frac{\frac{\phi_{FF} B_2}{\phi_{FF} B_1 + \phi_{FA} B_2}}{1 - \frac{\pi s}{2K_i (\phi_{FF} B_1 + \phi_{FA} B_2)}} \quad (3)$$

Equation (3) is the desired transfer function from which both steady-state error and the approximate time response characteristics of the gain-changer action can be determined. The time response to a step change in the ratio  $\phi_{FA}/\phi_{FF}$  has a characteristic time constant of

$$\tau_K = - \frac{\pi}{2K_i (\phi_{FF} B_1 + \phi_{FA} B_2)}$$

Notice that  $K_i$  or  $B_1$  and  $B_2$  must be negative or the system will be unstable. (U)

The steady-state error obtained with the system represented in Equation (3) is zero because a pure integrator is used. (U)

The steady-state error obtained when a first-order lag is used instead of an ideal integrator can be found through the use of Equation (3) with  $T_B/1+T_B s$  substituted for  $1/s$ :

$$\frac{\frac{K}{\phi_{FA}}(s)}{\phi_{FF}} = \frac{\frac{\phi_{FF} B_2}{\phi_{FF} B_1 + \phi_{FA} B_2}}{1 - \frac{(\pi/T_B) + \pi s}{2 K_i (\phi_{FF} B_1 + \phi_{FA} B_2)}} \quad (4)$$

The per cent steady-state error can be found from the following equation:

$$\% \text{ Steady-State Error} = 100\% \left[ 1 - \frac{1}{1 - \frac{\pi}{2 T_B K_i (\phi_{FF} B_1 + \phi_{FA} B_2)}} \right] \quad (5)$$

To obtain meaningful answers, the coefficients used in the foregoing equations must be obtained with care. The following procedures and units should be used:

Input Signals  $\phi_{FA}$  and  $\phi_{FF}$  -- Unitless values are obtained by dividing the peak-to-peak voltage of both input signals by the value of the largest. Thus one signal will always have a value of 1.0 and the other will be some fraction of it. The peak-to-peak voltage used as the normalizing factor is included in gains  $B_1$  and  $B_2$ . (U)

Bandpass Amplifier Gains  $B_1$  and  $B_2$  -- The bandpass amplifier gains must be calculated at the input signal frequency and have units of volts per volt. For use in these equations the gains must include the normalizing factor used in finding  $\phi_{FF}$  and  $\phi_{FA}$  in addition to the conventionally calculated system gains. (U)

Integrator Gain ( $K_i$ ) -- Integrator gain must be calculated in terms of gain units (attenuator gain  $K$ ) per volt. If a first-order lag is used instead of an integrator, the equivalent value of  $K_i$  must be calculated from the lag transfer function. (U)

### Sample Calculation

The values used in this sample calculation were taken directly from the bread-board blender circuit before any bandpass amplifier imbalance modifications were made ( $B_1 = B_2$ ). (U)

#### Input Signals:

Forward channel	30 volts peak to peak* at 5.4 rad/sec
Aft channel	30 volts peak to peak at 5.4 rad/sec

#### Bandpass Amplifier Gains:

Forward channel	TP1 to TP26**	-0.08 v/v at 5.4 rad/sec
Aft channel	TP9 to TP26	-0.08 v/v at 5.4 rad/sec

#### Integrator Gain:

The integrator is represented by the following first-order lag. The gain indicated is from TP26 to TP6.

$$\frac{e_{out}}{e_{in}} = \frac{37.5}{1 + 60 s} \text{ gain units/volt}$$

---

\* This corresponds to a rate gyro output of 3 degrees per second peak to peak.

\*\* See Figure 18.

Calculation Procedure

$$\phi_{FF} = \frac{30 \text{ v}}{30 \text{ v}} = 1.0 \quad \text{and} \quad \phi_{FA} = \frac{30 \text{ v}}{30 \text{ v}} = 1.0$$

The normalizing factor used in the following calculations of  $B_1$  and  $B_2$  is therefore 30.

$$B_1 = [-0.08 \text{ v/v}][30] = -2.4 \text{ v/v}$$

$$B_2 = [-0.08 \text{ v/v}][30] = -2.4 \text{ v/v}$$

The ideal integrator  $K_i/s$  was replaced by the first-order lag  $K_i T_B / (1 + T_B s)$  so the equivalent value of  $K_i$  must be calculated by dividing the first-order lag gain by the lag time constant. Thus

$$K_i = \frac{37.5}{60} = 0.625 \frac{\text{gain units}}{\text{volt}}$$

The effective time constant of this system's equilibrium gain response to a step change in  $\phi_{FF}/\phi_{FA}$  is then

$$\tau_K = \frac{3.14}{(2)(0.625) [(1)(-2.4) + (1)(-2.4)]} = 0.524 \text{ second}$$

This time constant agrees closely with the experimental value of 0.51 second obtained in a "blender only" breadboard test procedure. (U)

The steady-state error is calculated as follows:

$$\text{Steady-State Error} = 100\% \left[ 1 - \frac{1}{1 - \frac{3.14}{60(2)(0.625) [(1)(-2.4) + (1)(-2.4)]}} \right]$$

$$= 0.83\% \text{ (with 30-volt peak-to-peak input signals)}$$

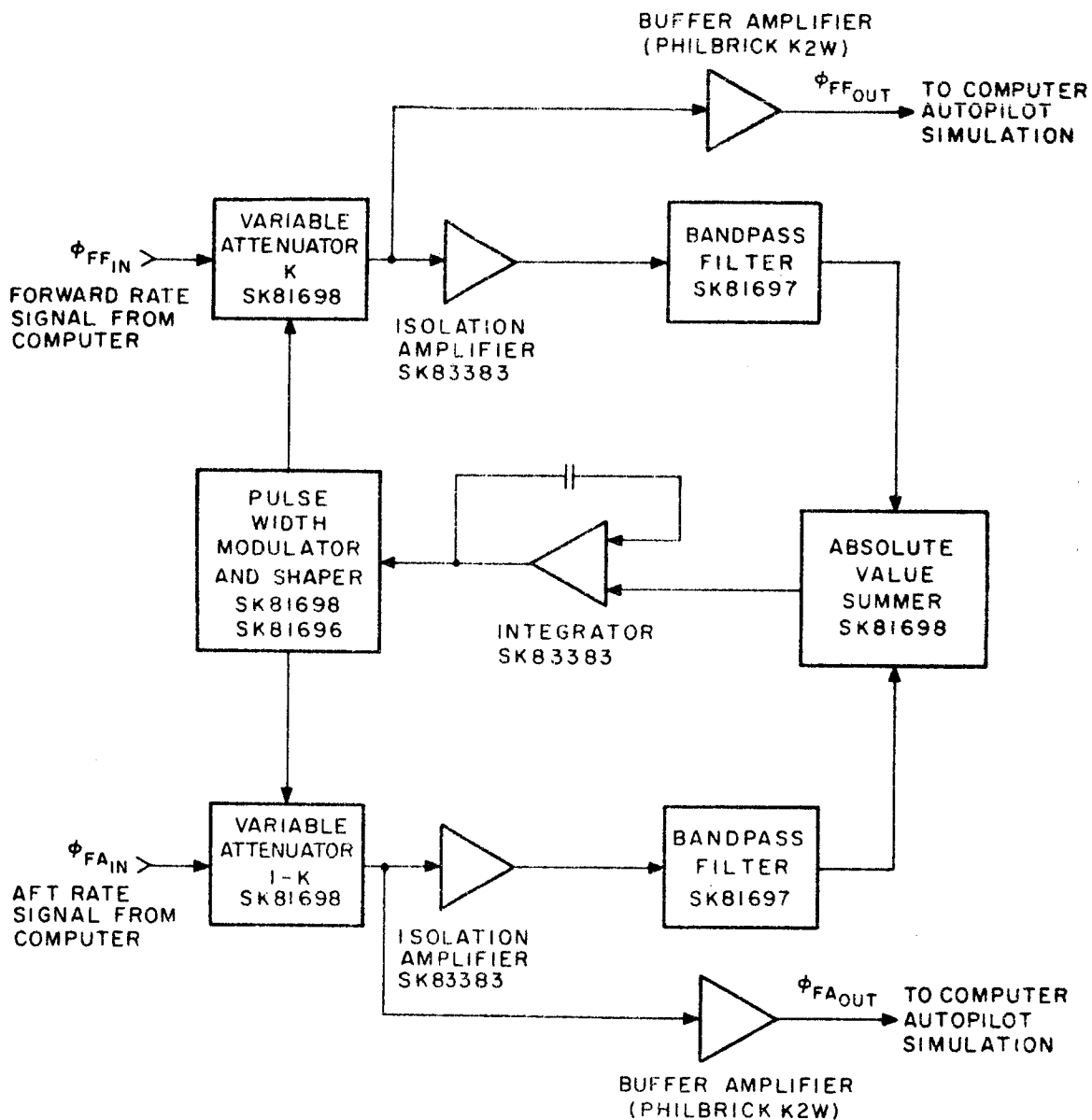


A specific comparison with the actual steady-state error was not made because of the difficulties involved in accurately measuring this quantity. (U)

## BLENDER BREADBOARD

A block diagram of the blender breadboard is shown in Figure 19. Drawing numbers for each functional portion of the blender are shown on the diagram. Two primary factors have influenced the design philosophy of the breadboard: (1) It has been designed for compatibility with an analog computer for simulation studies. (2) The design utilizes flightworthy components. Some of the features of the blender that have resulted from this two-sided approach are:

- The unit has been designed to accept input signal levels of  $\pm 100$  volts without saturation or component damage.
- The integrator cage and uncage relay is controlled by a 28-volt d-c signal from the analog computer for simplicity of operator control and synchronization of all integrator relays. A panel-mounted switch is used to uncage the integrator manually.
- A panel-mounted potentiometer and switch are used to set the integrator initial condition.
- The breadboard is a self-contained unit with all necessary power supplies located in the cabinet.
- Numerous test points are located on the front panel for ease in troubleshooting or signal monitoring without opening the cabinet.
- Blender parameters (such as loop gain and bandpass filtering) can be readily modified if desired for study purposes. Provision has been made for inclusion of analog computer networks in the blender loop.



NOTES:

1. RECOMMENDED INPUT SIGNAL SCALE FACTOR:  
100 VOLTS = 10 DEGREES PER SECOND

$$2. \frac{\phi_{FFOUT}}{\phi_{FFIN}} = \frac{0.4K}{1+0.0022s}, \quad \frac{\phi_{FAOUT}}{\phi_{FAIN}} = \frac{0.4(1-K)}{1+0.0022s}$$

Figure 19. Blender Breadboard Block Diagram

- The breadboard utilizes card assembly, printed circuit, and welded module techniques that have been developed and proven on other programs.
- Solid-state transistorized and magnetic amplifier circuits are used throughout the blender loop to provide a reliable and flightworthy design. (U)

A detailed operation manual for the breadboard blender has been published as a separate document (Reference 3). This manual includes checkout and calibration procedures as well as schematic diagrams and an explanation of system operation. (U)

SECTION VI  
SYSTEM EVALUATION

NOMINAL OPERATION

Analog computer traces showing responses to step attitude commands and synthetic wind shear profile disturbances are given in Figures 20 through 24 for the nominal system with filter B at the five standard flight times. Corresponding frequency response and root-locus plots are shown in Figures 25 through 34. These plots are for the system transfer function  $\epsilon/\beta_c$  as shown in Figure 1. The frequency response plots show that the second, third, and fourth bending modes have been gain-stabilized with a gain margin varying from 20 to 60 decibels. (C)

The gain and phase margins at the slosh and first bending mode frequencies for the nominal system are given in Table 2. It was necessary to increase the slosh damping ratio to 0.06 to meet the tolerance requirements, and the nominal system reflects this increased slosh damping ratio. The gain and phase margins of the first bending mode at  $t = 79$  and 120 seconds are barely adequate. However, the value of 0.005 used for structural damping ratios has probably been too conservative, especially for the first mode. Nominal gain and phase margins of the slosh modes are adequate. (C)

Table 2. Gain and Phase Margins of Slosh and First Bending Modes - Nominal System

Flight Time (sec)	Fuel Slosh		First Bending Mode	
	Gain Margin (db)	Phase Margin (deg)	Gain Margin (db)	Phase Margin (deg)
0	7.0	29	18.0	55
40	5.5	47	12.0	45
79	3.0	42	2.0	10
120	4.5	33	1.5	15
153	9.0	31	16.0	100

(C)

## ANALOG TOLERANCE STUDIES

Tolerance studies were made on a computer to verify the acceptability of the final system configuration. Tolerance combinations were chosen to include worst possible conditions while limiting the total number of analog runs to a realistic number. The tolerance combinations used and the reasons for their selection are given below. (C)

### Individual Component Tolerances

The following vehicle and component tolerances are considered typical and form the basis for the tolerance combinations:

a. Vehicle

1. Rigid body: Aerodynamic moment coefficient  $C_1$  and control moment  $C_2$ ,  $\pm 20$  per cent.
2. Body bending:

Bending frequencies for all modes	$\pm 10$ per cent
First mode slopes and deflections	$\pm 20$ per cent
All other bending mode slopes and deflections	$\pm 30$ per cent
3. Slosh: Slosh mode frequencies,  $\pm 10$  per cent. (C)

VEHICLE AND SYSTEM TOLERANCES:  
NOMINAL

$K_R = 0.80 \text{ DEG/DEG/SEC}$   
 $K_A = 0 \text{ DEG/SEC/M/SEC}^2$   
 $K_P = 0.90 \text{ DEG/SEC/DEG}$   
 $T_I = 0.20 \text{ SEC}$   
 $T_A = 2.00 \text{ SEC}$

SLOSH  $\tau = 0.060$   
BENDING  $\tau = 0.005$   
BENDING FILTER - B  
 $X_A = 64 \text{ m}$   
 $X_{RGF} = 85.3 \text{ m}$   
 $X_{RGA} = 5.0 \text{ m}$

BLENDER BREADBOARD  
INTEGRATOR OUTPUT  
(VOLTS)

(16 volts represents a  
blender position K of  
approximately 1.0)

VW  
WIND GUST INPUT  
(METERS/SEC)

$\alpha$   
VEHICLE  
ANGLE OF ATTACK  
(DEGREES)

$\beta_R$   
ENGINE  
DEFLECTION ANGLE  
(DEGREES)

$\dot{\theta}_{CG}$   
PITCH RATE  
(DEG/SEC)

$\theta_{CG}$   
PITCH ATTITUDE  
(DEGREES)

$\ddot{\theta}_R$   
ACCELERATION  
NORMAL TO VEHICLE  
(METERS/SEC<sup>2</sup>)

$\ddot{z}_{CG}$   
ACCELERATION ALONG  
REFERENCE AXIS  
(METERS/SEC<sup>2</sup>)

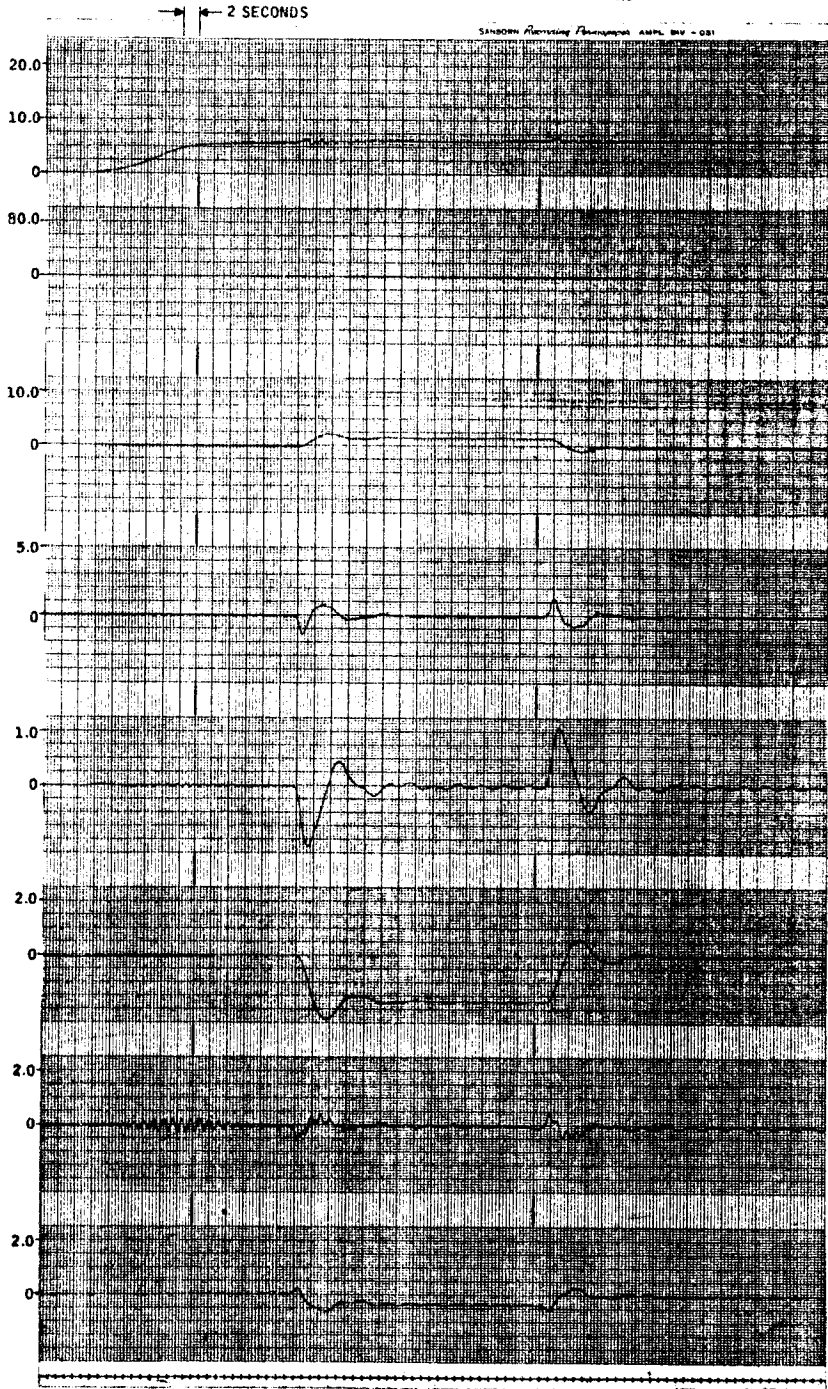


Figure 20. Analog Computer Run 1 (t = 0 seconds)

VEHICLE AND SYSTEM TOLERANCES:  
NOMINAL

$K_R = 0.80 \text{ DEG/DEG/SEC}$   
 $K_A = 0.05 \text{ DEG/SEC/M/SEC}^2$   
 $K_D = 0.90 \text{ DEG/SEC/DEG}$   
 $T_I = 0.20 \text{ SEC}$   
 $T_A = 2.00 \text{ SEC}$

SLOSH  $\tau = 0.060$   
BENDING  $\tau = 0.005$   
BENDING FILTER = B  
 $X_A = 64 \text{ m}$   
 $X_{RGF} = 85.3 \text{ m}$   
 $X_{RGA} = 5.0 \text{ m}$

BLENDER BREADBOARD  
INTEGRATOR OUTPUT  
(VOLTS)

(16 volts represents a  
blender position K of  
approximately 1.0)

WV  
WIND GUST INPUT  
(METERS/SEC)

$\alpha$   
VEHICLE  
ANGLE OF ATTACK  
(DEGREES)

$\beta_R$   
ENGINE  
DEFLECTION ANGLE  
(DEGREES)

$\dot{\phi}_{CG}$   
PITCH RATE  
(DEG/SEC)

$\phi_{CG}$   
PITCH ATTITUDE  
(DEGREES)

$\ddot{z}_R$   
ACCELERATION  
NORMAL TO VEHICLE  
(METERS/SEC<sup>2</sup>)

$\ddot{z}_{CG}$   
ACCELERATION ALONG  
REFERENCE AXIS  
(METERS/SEC<sup>2</sup>)

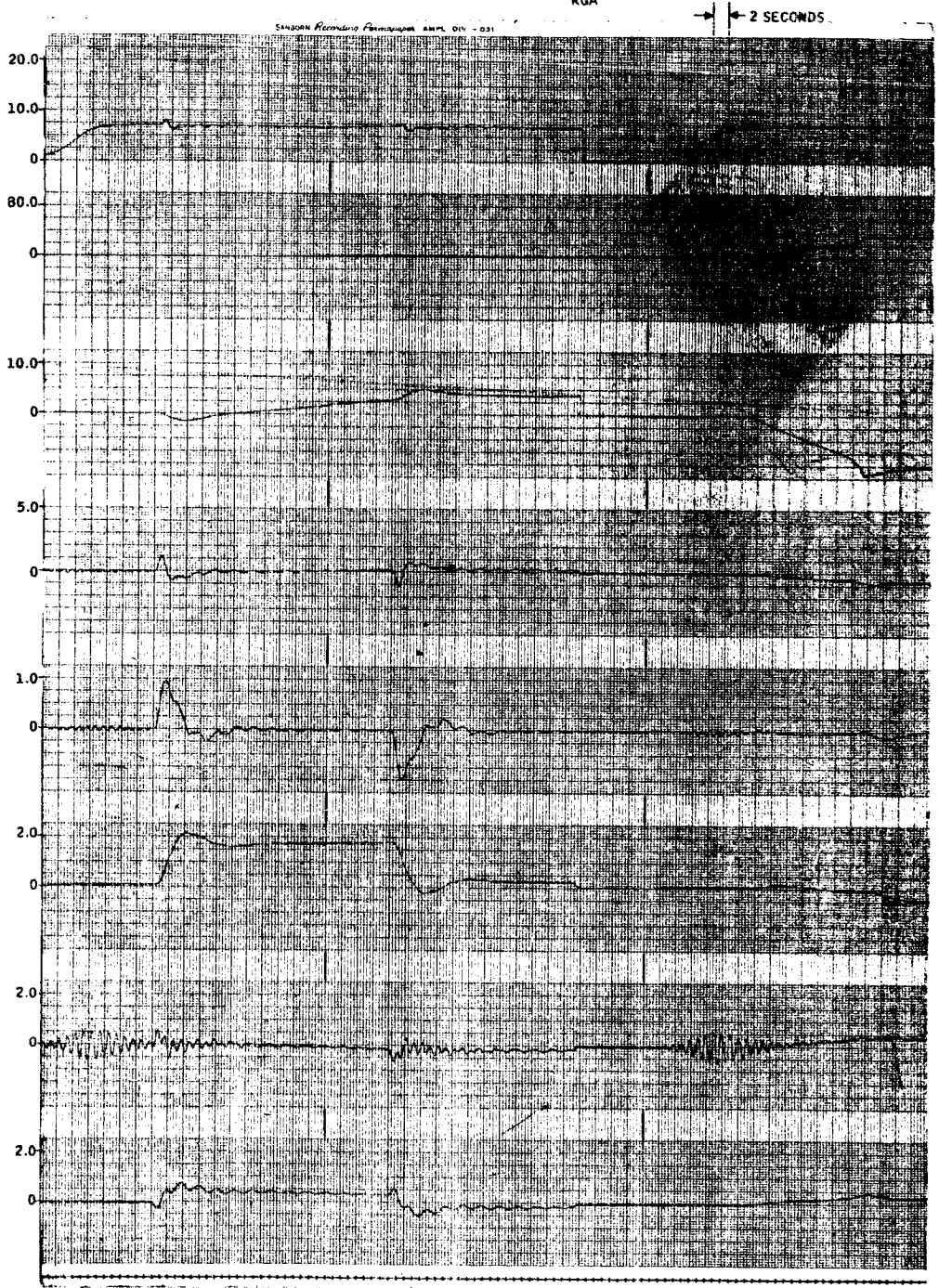


Figure 21. Analog Computer Run 1 (t = 40 seconds)

VEHICLE AND SYSTEM TOLERANCES:  
NOMINAL

$K_R = 0.80 \text{ DEG/DEG/SEC}$   
 $K_A = 0.05 \text{ DEG/SEC/M/SEC}^2$   
 $K_P = 0.90 \text{ DEG/SEC/DEG}$   
 $T_I = 0.20 \text{ SEC}$   
 $T_A = 2.00 \text{ SEC}$

SLOSH  $\zeta = 0.060$   
BENDING  $\zeta = 0.005$   
BENDING FILTER = B  
 $X_A = 64 \text{ m}$   
 $X_{RGF} = 85.3 \text{ m}$   
 $X_{RGA} = 5.0 \text{ m}$

← 2 SECONDS

BLENDER BREADBOARD  
INTEGRATOR OUTPUT  
(VOLTS)

(1.6 volts represents a  
blender position K of  
approximately 1.0)

VW  
WIND GUST INPUT  
(METERS/SEC)

$\alpha$   
VEHICLE  
ANGLE OF ATTACK  
(DEGREES)

$\beta_R$   
ENGINE  
DEFLECTION ANGLE  
(DEGREES)

$\dot{\alpha}_{CG}$   
PITCH RATE  
(DEG/SEC)

$\alpha_{CG}$   
PITCH ATTITUDE  
(DEGREES)

$\ddot{r}$   
ACCELERATION  
NORMAL TO VEHICLE  
(METERS/SEC<sup>2</sup>)

$\ddot{z}_{CG}$   
ACCELERATION ALONG  
REFERENCE AXIS  
(METERS/SEC<sup>2</sup>)

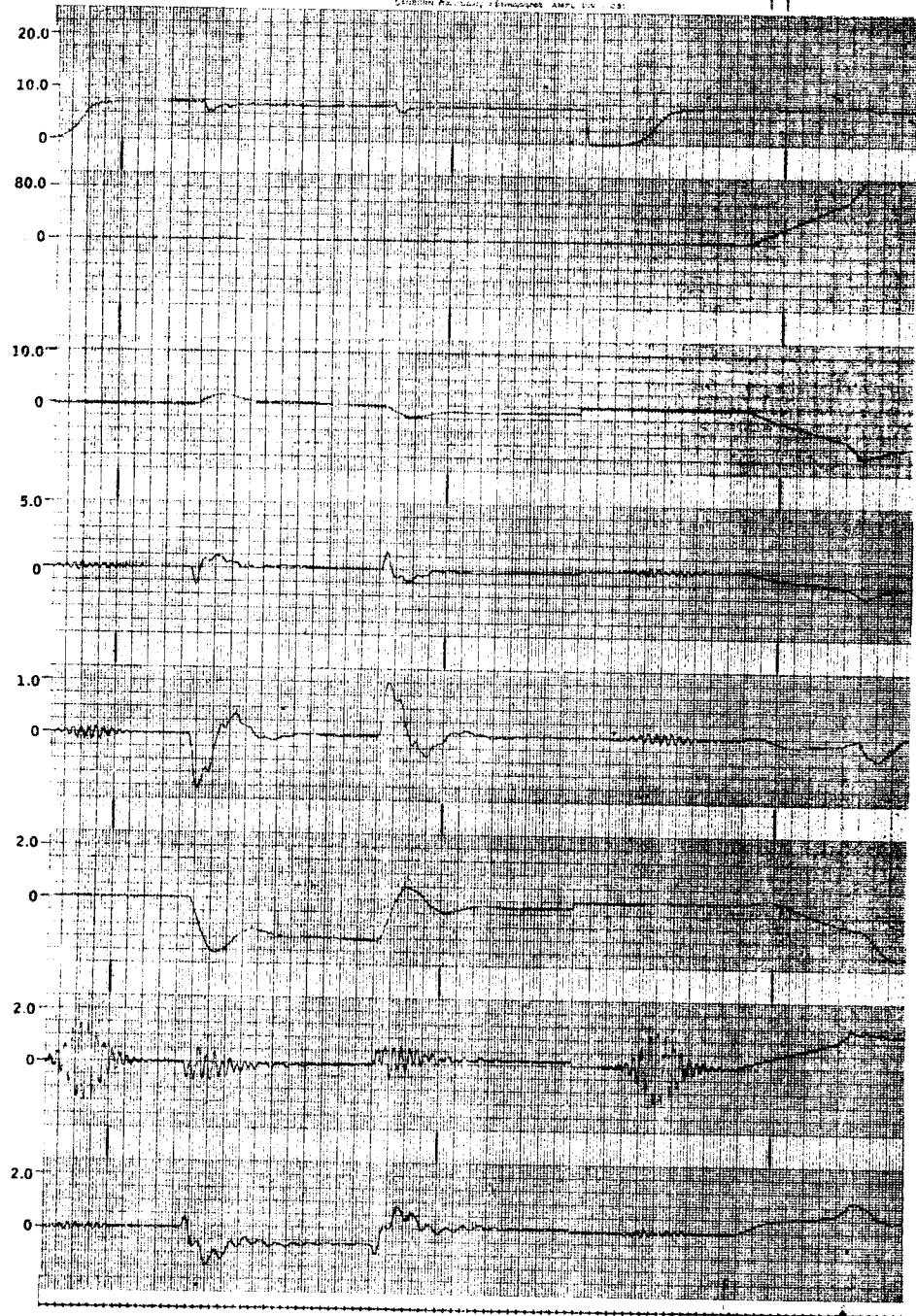


Figure 22. Analog Computer Run 1 (t = 79 seconds)



VEHICLE AND SYSTEM TOLERANCES:  
NOMINAL

$K_R = 0.80 \text{ DEG/DEG/SEC}$   
 $K_A = 0.20 \text{ DEG/SEC/M/SEC}^2$   
 $K_P = 0.90 \text{ DEG/SEC/DEG}$   
 $T_1 = 0.20 \text{ SEC}$   
 $T_A = 2.00 \text{ SEC}$

SLOSH  $\zeta = 0.060$   
 BENDING  $\zeta = 0.005$   
 BENDING FILTER = B  
 $X_A = 64 \text{ m}$   
 $X_{RGF} = 85.3 \text{ m}$   
 $X_{RGA} = 5.0 \text{ m}$

BLENDER BREADBOARD  
INTEGRATOR OUTPUT  
(VOLTS)

(1.6 volts represents a  
blender position K of  
approximately 1.0)

VW  
WIND GUST INPUT  
(METERS/SEC)

$\alpha$   
VEHICLE  
ANGLE OF ATTACK  
(DEGREES)

$\beta_R$   
ENGINE  
DEFLECTION ANGLE  
(DEGREES)

$\dot{\phi}_{CG}$   
PITCH RATE  
(DEG/SEC)

$\phi_{CG}$   
PITCH ATTITUDE  
(DEGREES)

$\ddot{z}_R$   
ACCELERATION  
NORMAL TO VEHICLE  
(METERS/SEC<sup>2</sup>)

$\ddot{z}_{CG}$   
ACCELERATION ALONG  
REFERENCE AXIS  
(METERS/SEC<sup>2</sup>)

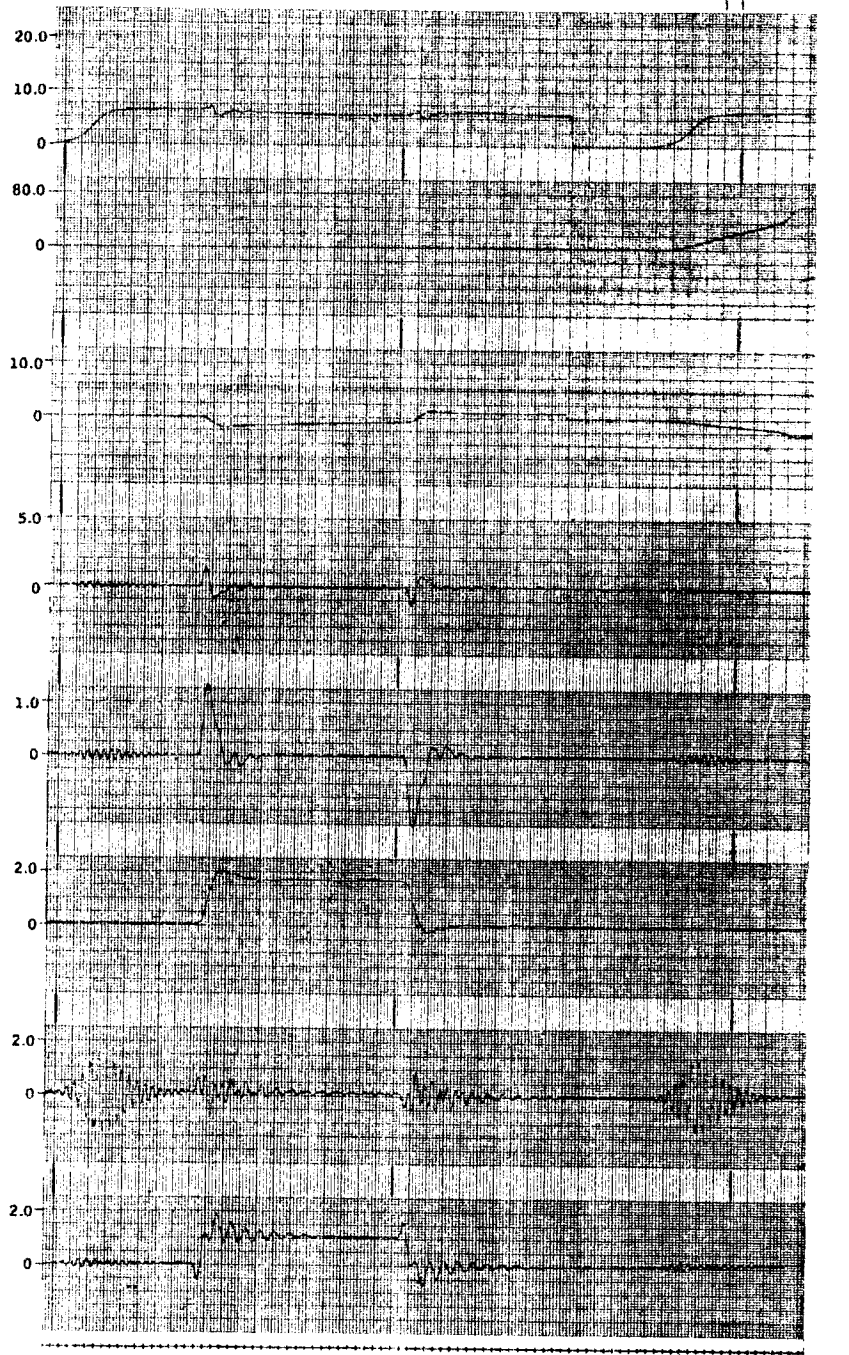


Figure 23. Analog Computer Run 1 (t = 120 seconds)

VEHICLE AND SYSTEM TOLERANCES:  
NOMINAL

$K_R = 0.40 \text{ DEG/DEG/SEC}$

$K_A = 0.05 \text{ DEG/SEC/M/SEC}^2$

$K_V = 0.90 \text{ DEG/SEC/DEG}$

$T_1 = 0.20 \text{ SEC}$

$T_A = 2.00 \text{ SEC}$

$\text{SLOPE } \epsilon = 0.060$

$\text{BENDING } \epsilon = 0.005$

$\text{BENDING FILTER} = B$

$X_A = 64 \text{ m}$

$X_{RGF} = 85.3 \text{ m}$

$X_{RGA} = 5.0 \text{ m}$

BLENDER BREADBOARD  
INTEGRATOR OUTPUT  
(VOLTS)

(16 volts represents a  
blender position  $K$  of  
approximately 1.0)

VW  
WIND GUST INPUT  
(METERS/SEC)

$\alpha$   
VEHICLE  
ANGLE OF ATTACK  
(DEGREES)

$\beta_R$   
ENGINE  
DEFLECTION ANGLE  
(DEGREES)

$\dot{\phi}_{CG}$   
PITCH RATE  
(DEG/SEC)

$\phi_{CG}$   
PITCH ATTITUDE  
(DEGREES)

$\ddot{t}_R$   
ACCELERATION  
NORMAL TO VEHICLE  
(METERS/SEC<sup>2</sup>)

$\ddot{z}_{CG}$   
ACCELERATION ALONG  
REFERENCE AXIS  
(METERS/SEC<sup>2</sup>)

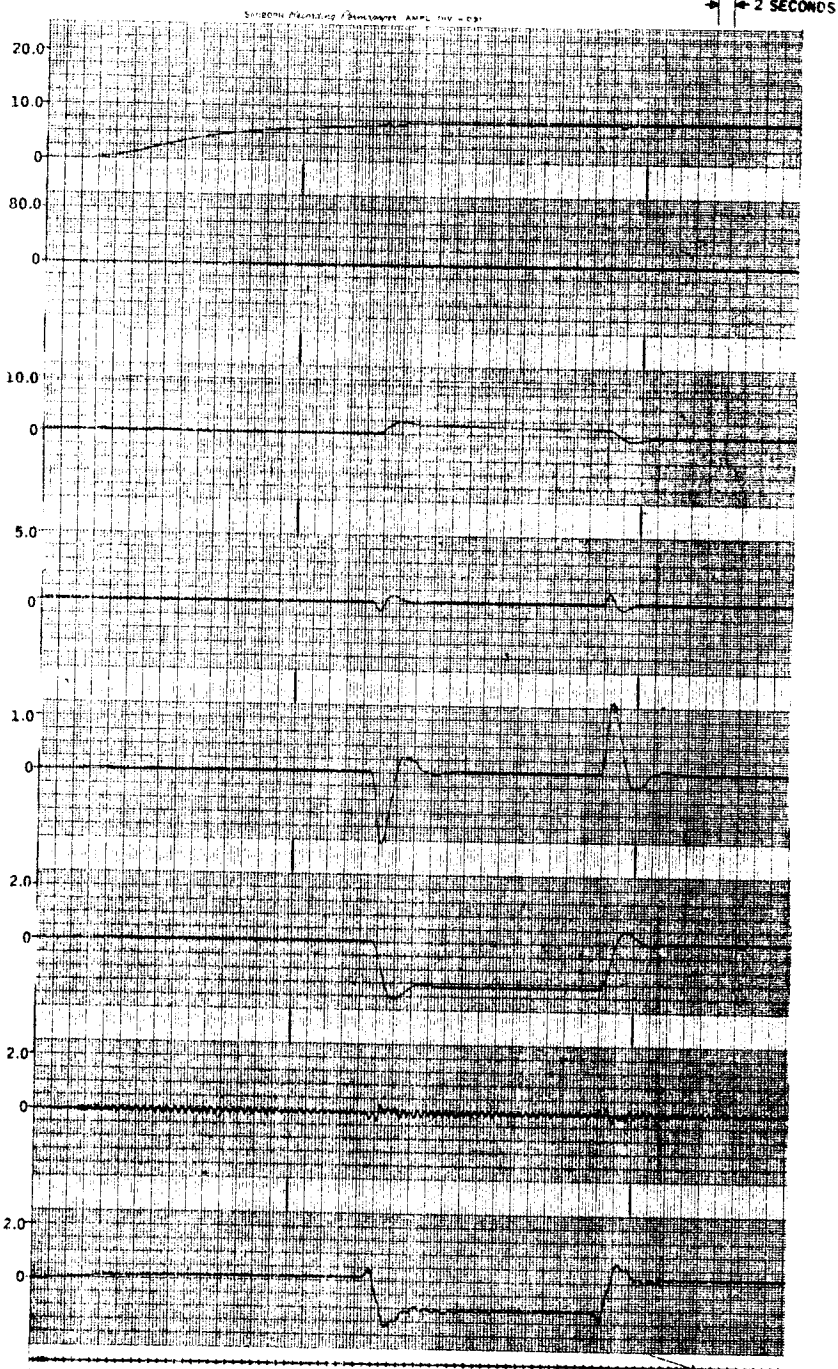


Figure 24. Analog Computer Run 1 (t = 153 seconds)

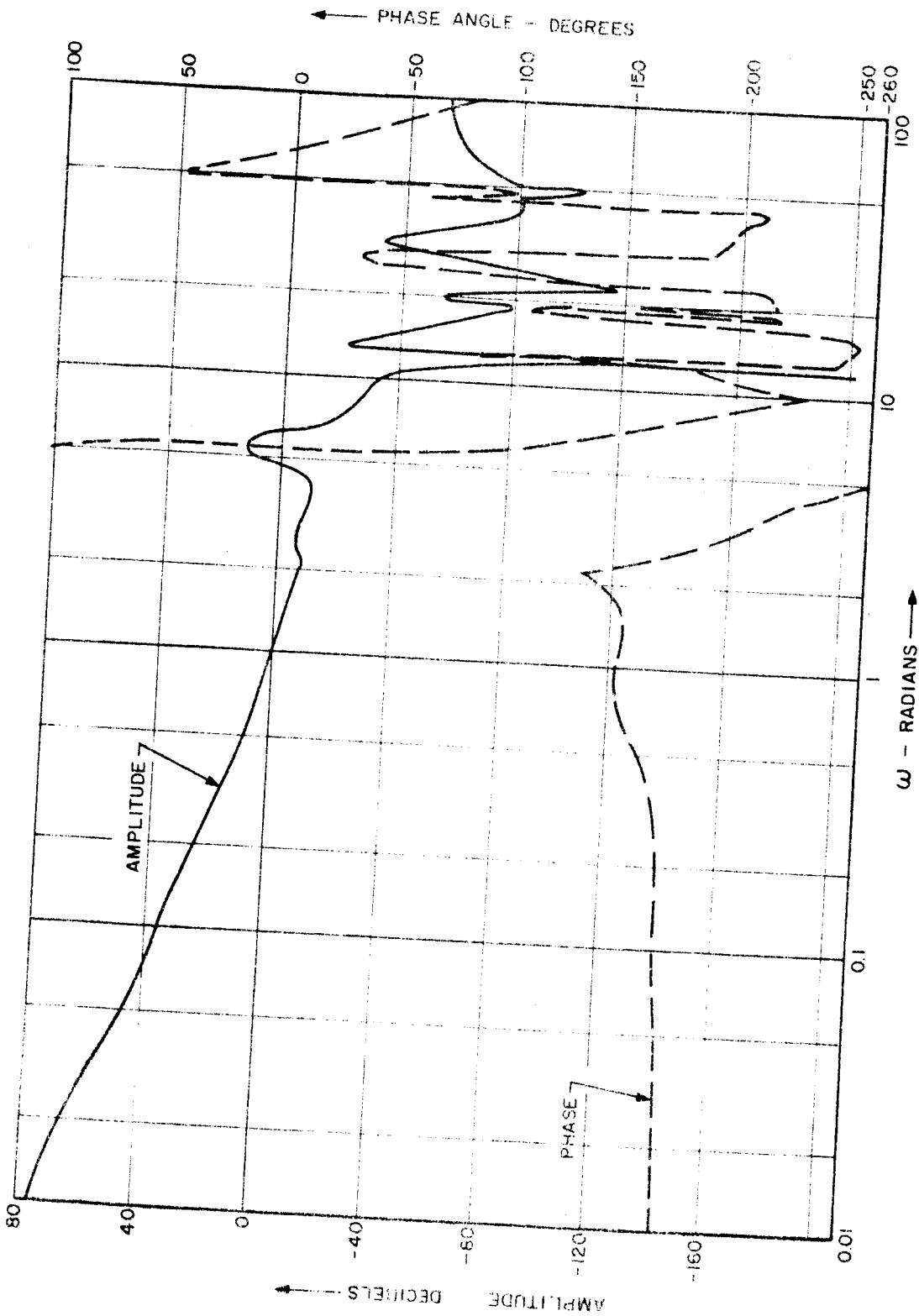


Figure 25. Open-Loop Frequency Response, Nominal System with Filter B ( $t = 0$ )

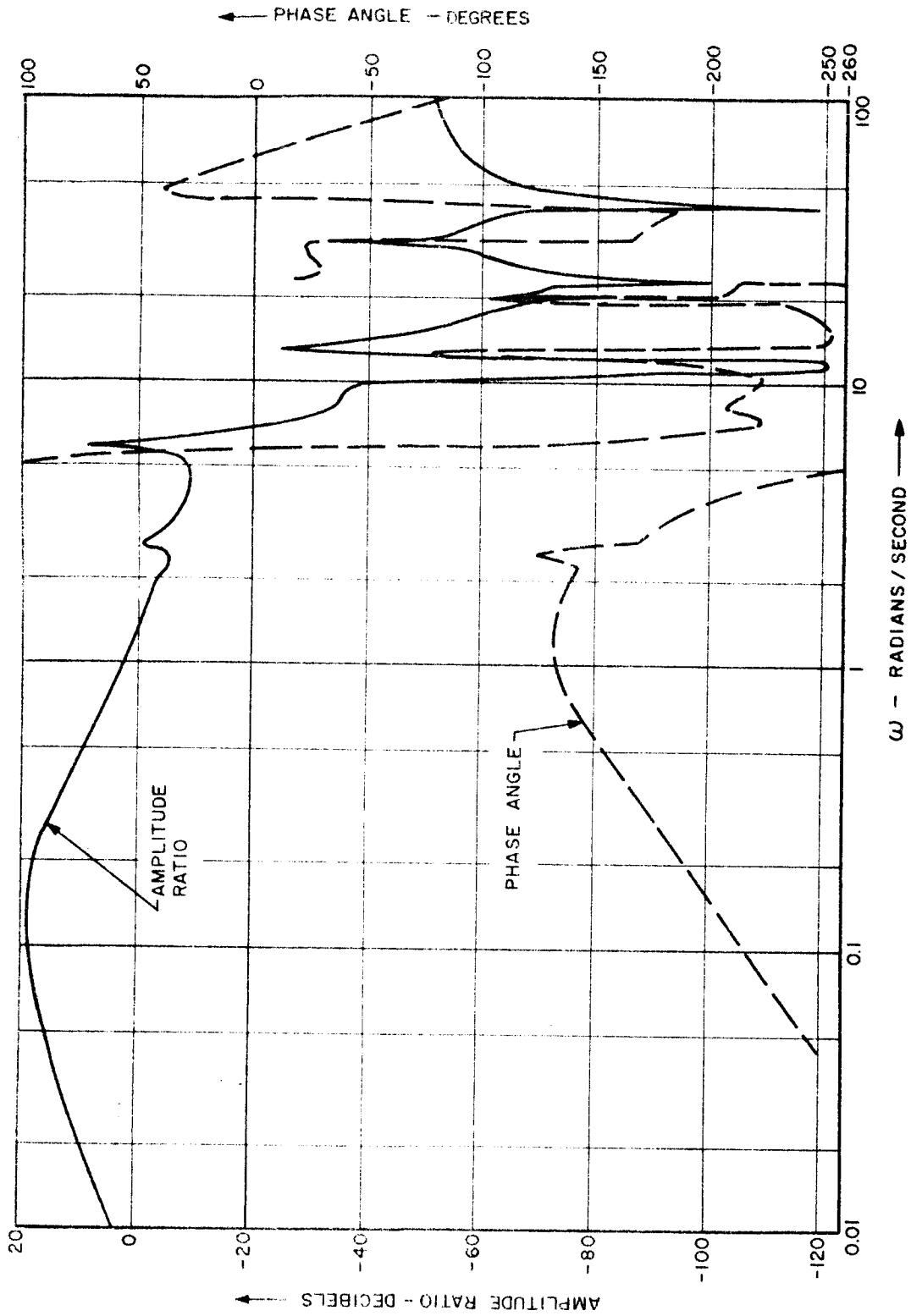


Figure 26. Open-Loop Frequency Response, Nominal System with Filter B ( $t = 40$ )

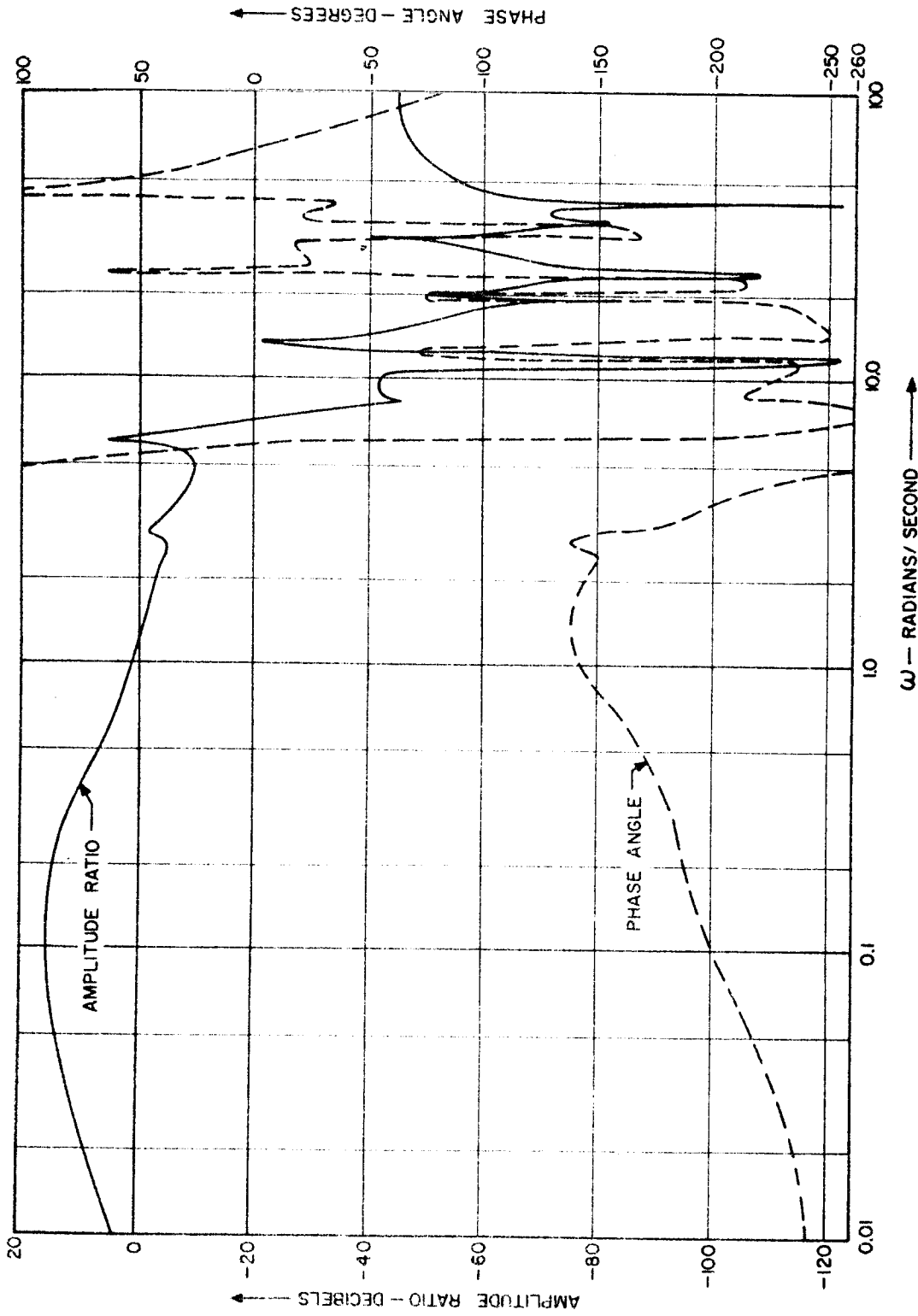


Figure 27. Open-Loop Frequency Response, Nominal System with Filter B ( $t = 79$ )

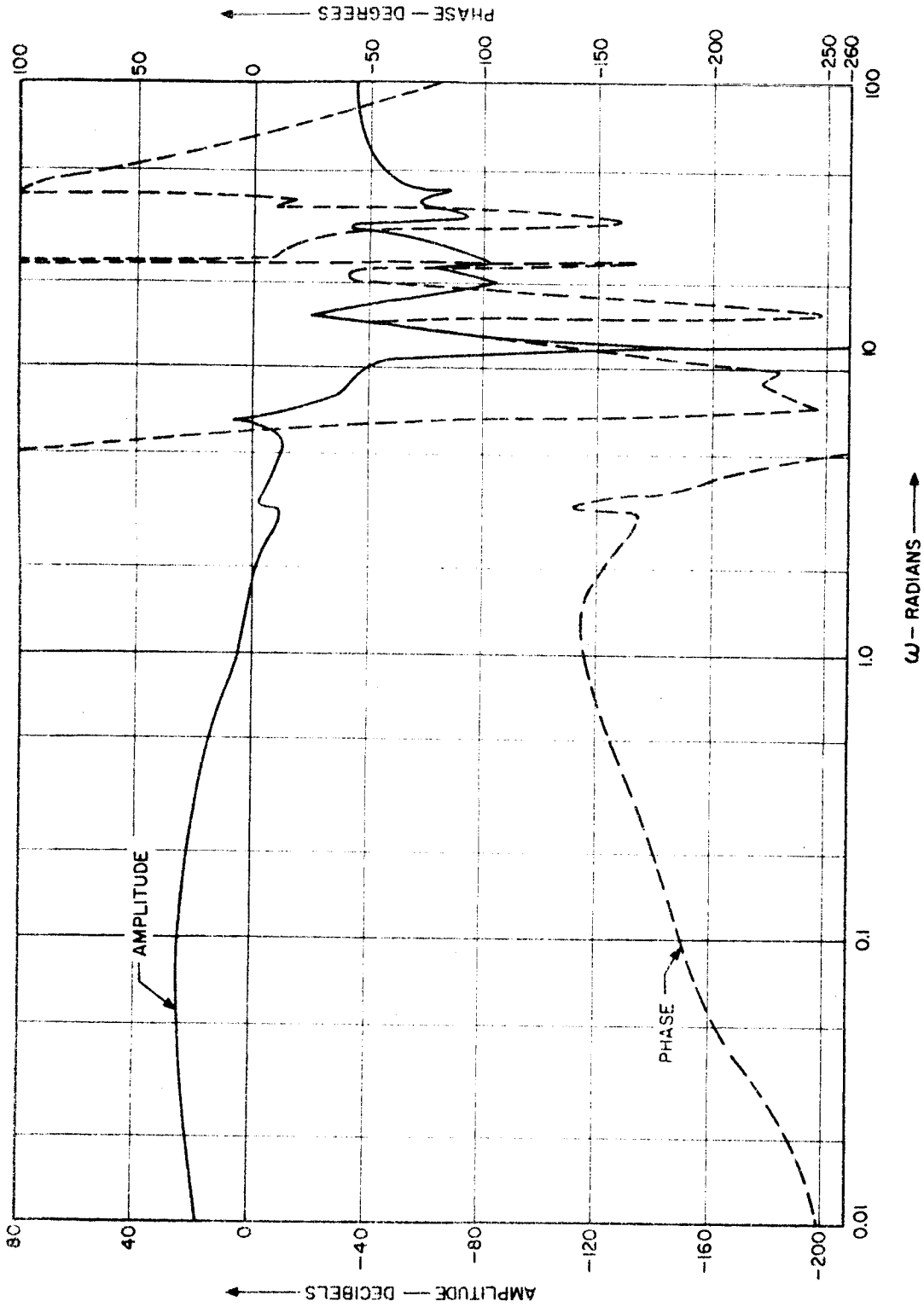


Figure 28. Open-Loop Frequency Response, Nominal System with Filter B ( $t = 120$ )

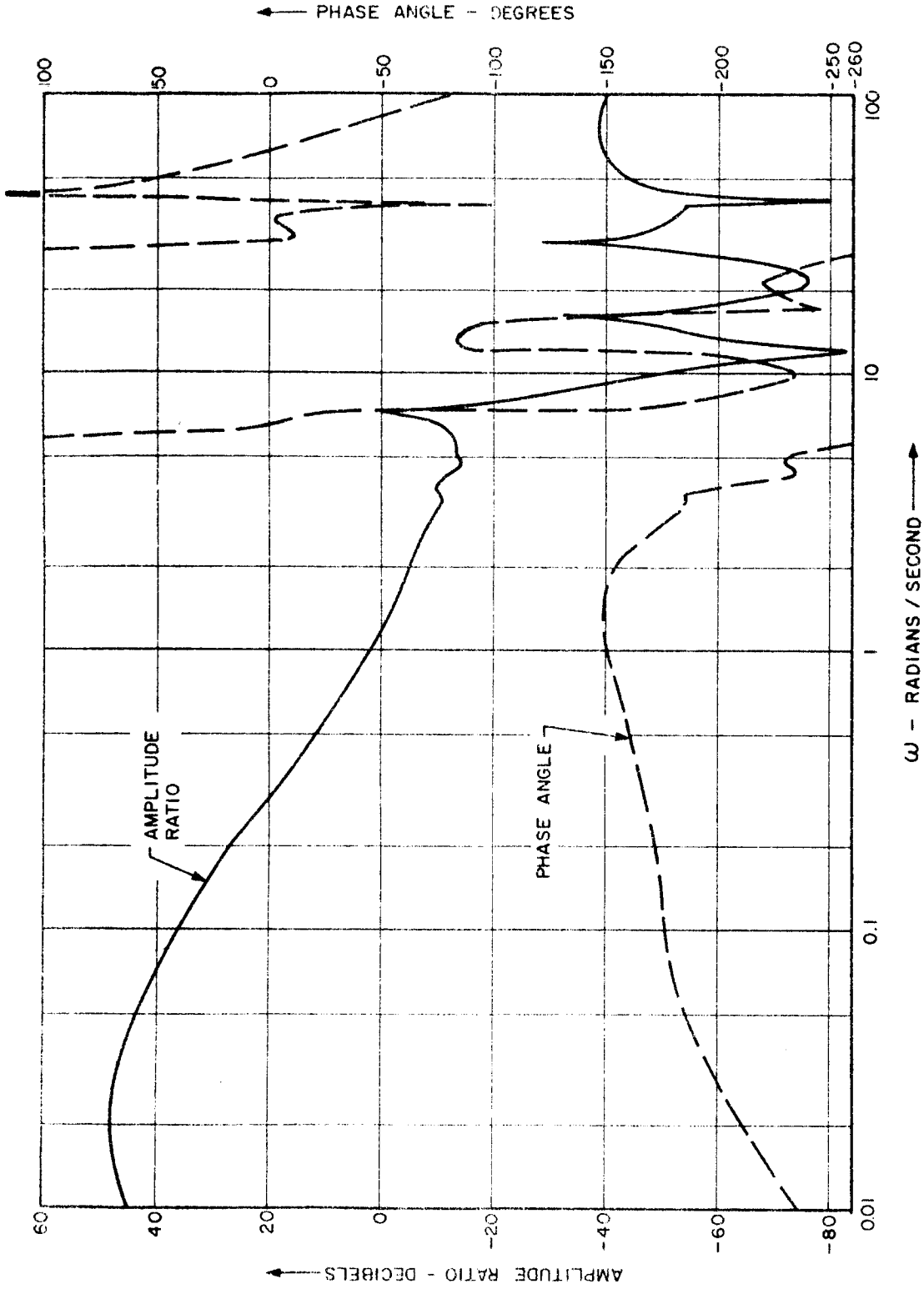


Figure 29. Open-Loop Frequency Response, Nominal System with Filter B ( $t = 153$ )

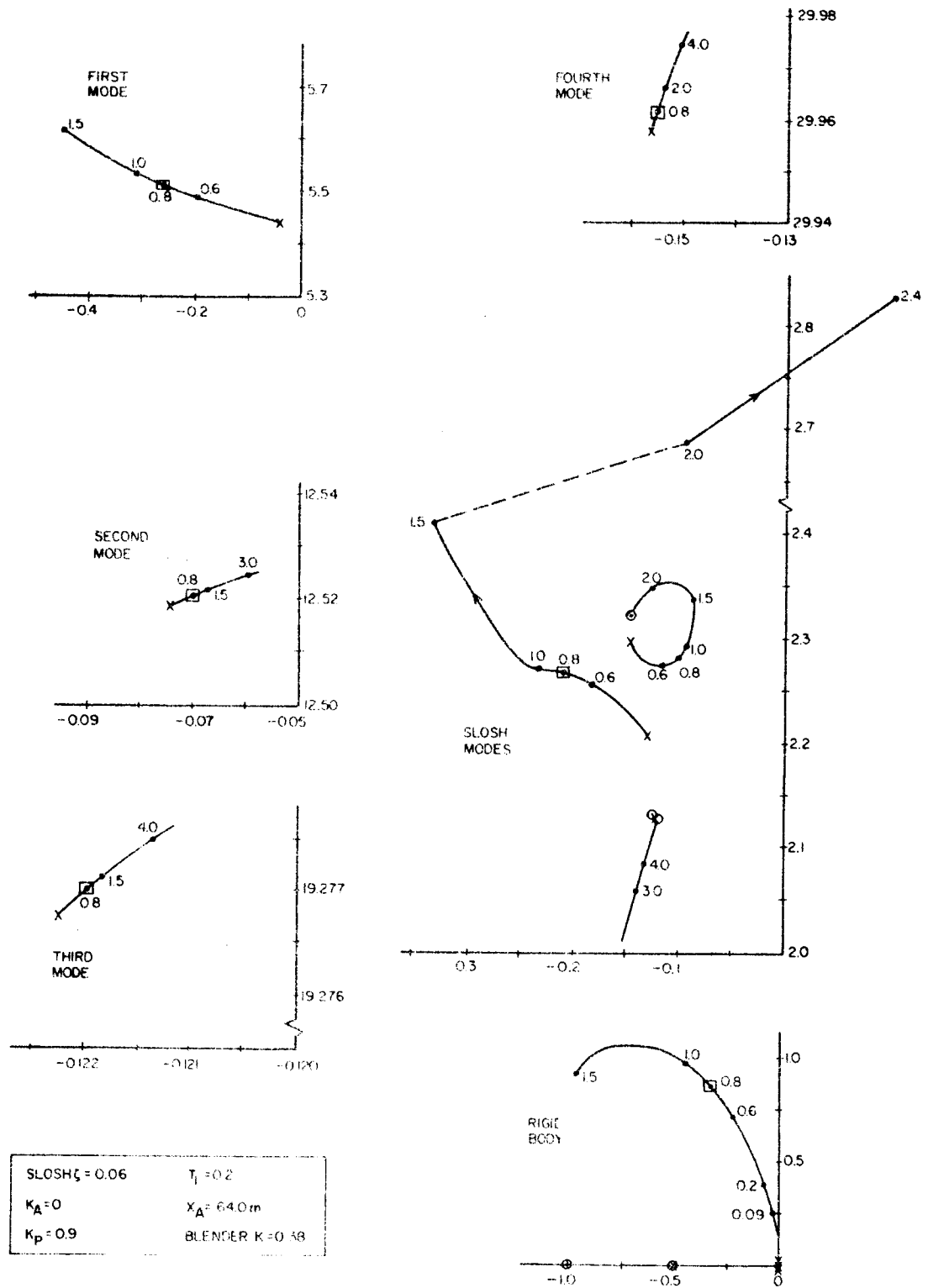


Figure 30. Root-Locus Plot, Nominal System with Filter B ( $t = 0$ )



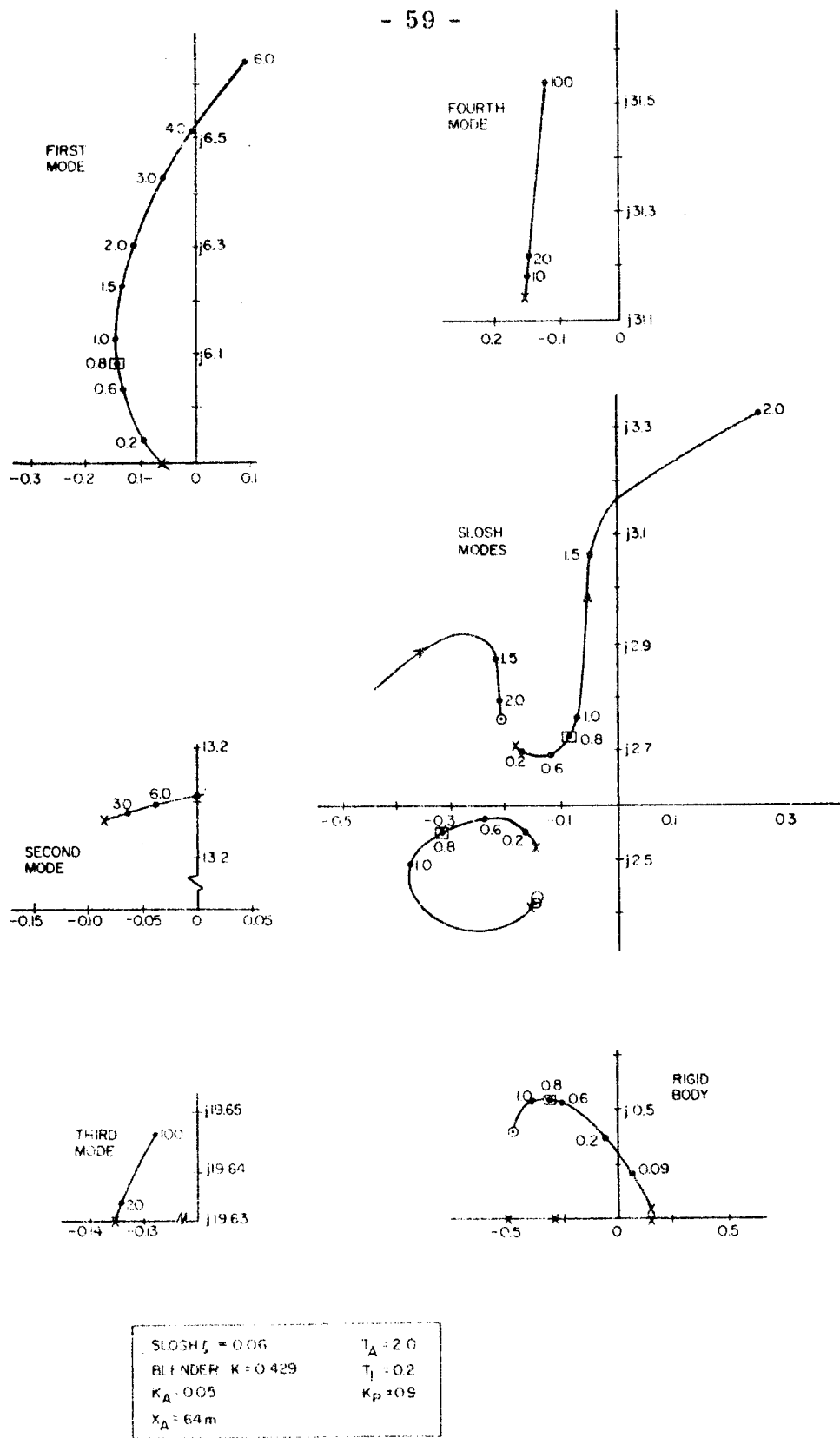


Figure 31. Root-Locus Plot, Nominal System with Filter B (t = 40)

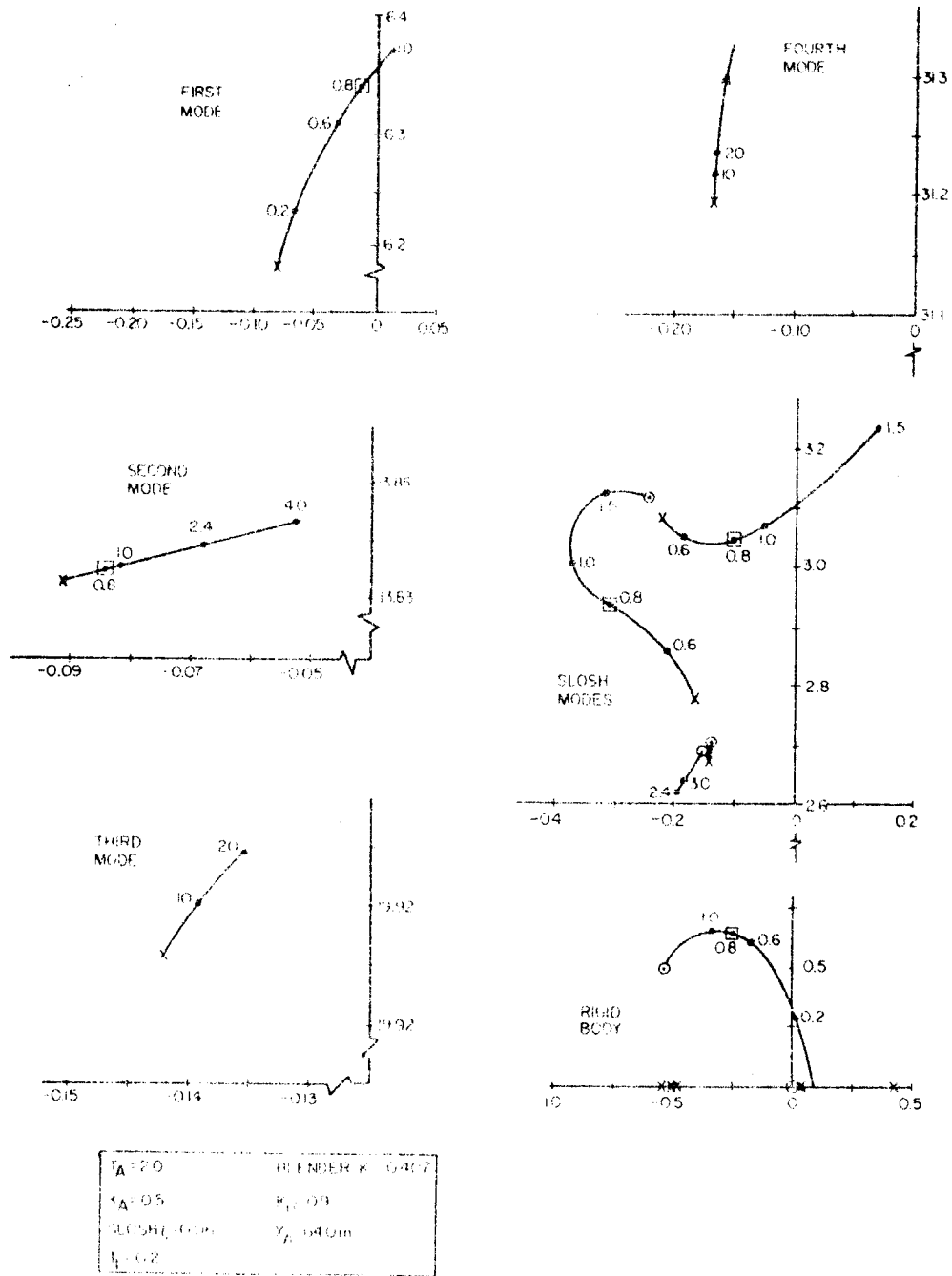


Figure 32. Root-Locus Plot, Nominal System with Filter B (t = 79)

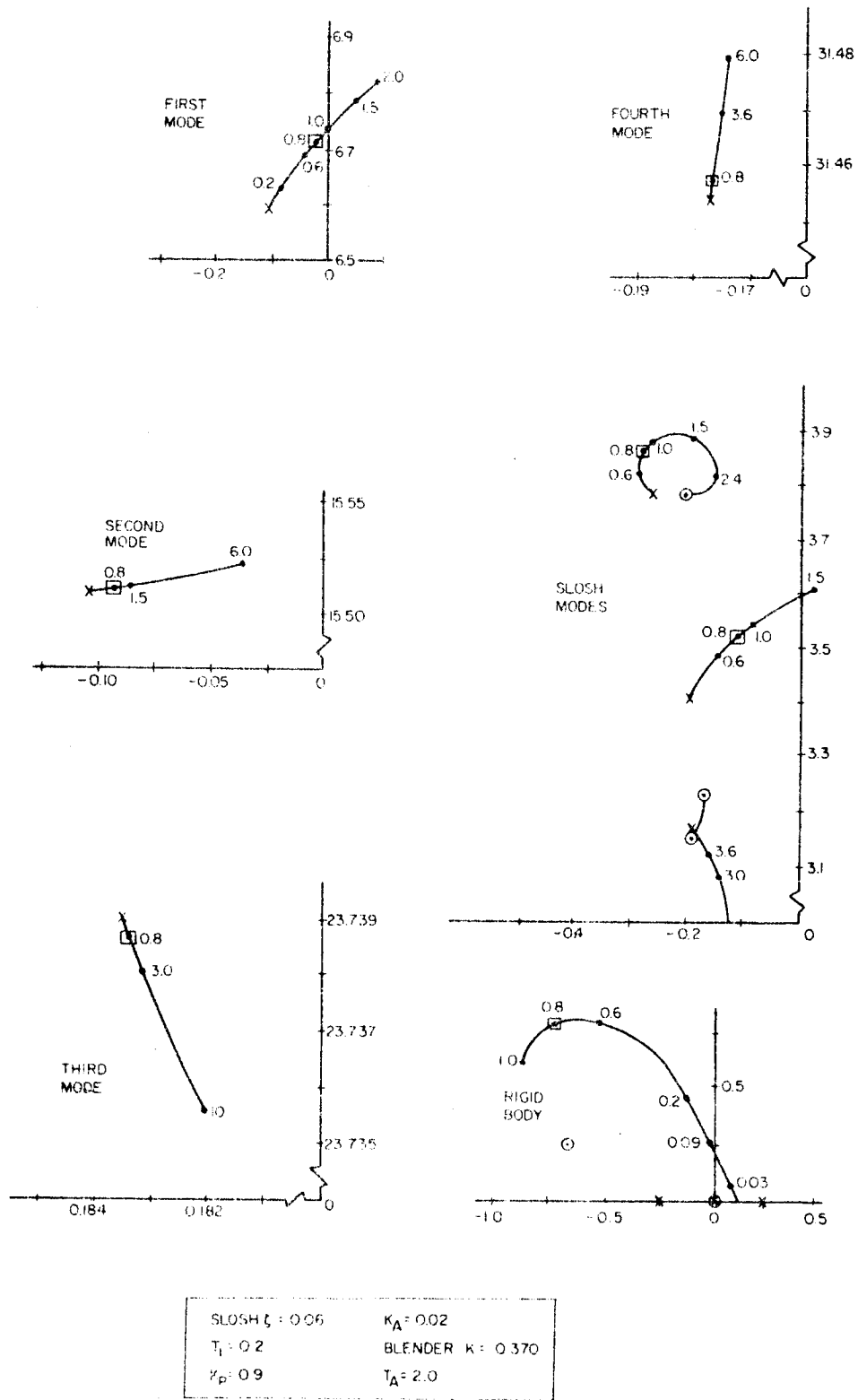


Figure 33. Root-Locus Plot, Nominal System with Filter B ( $t = 120$ )

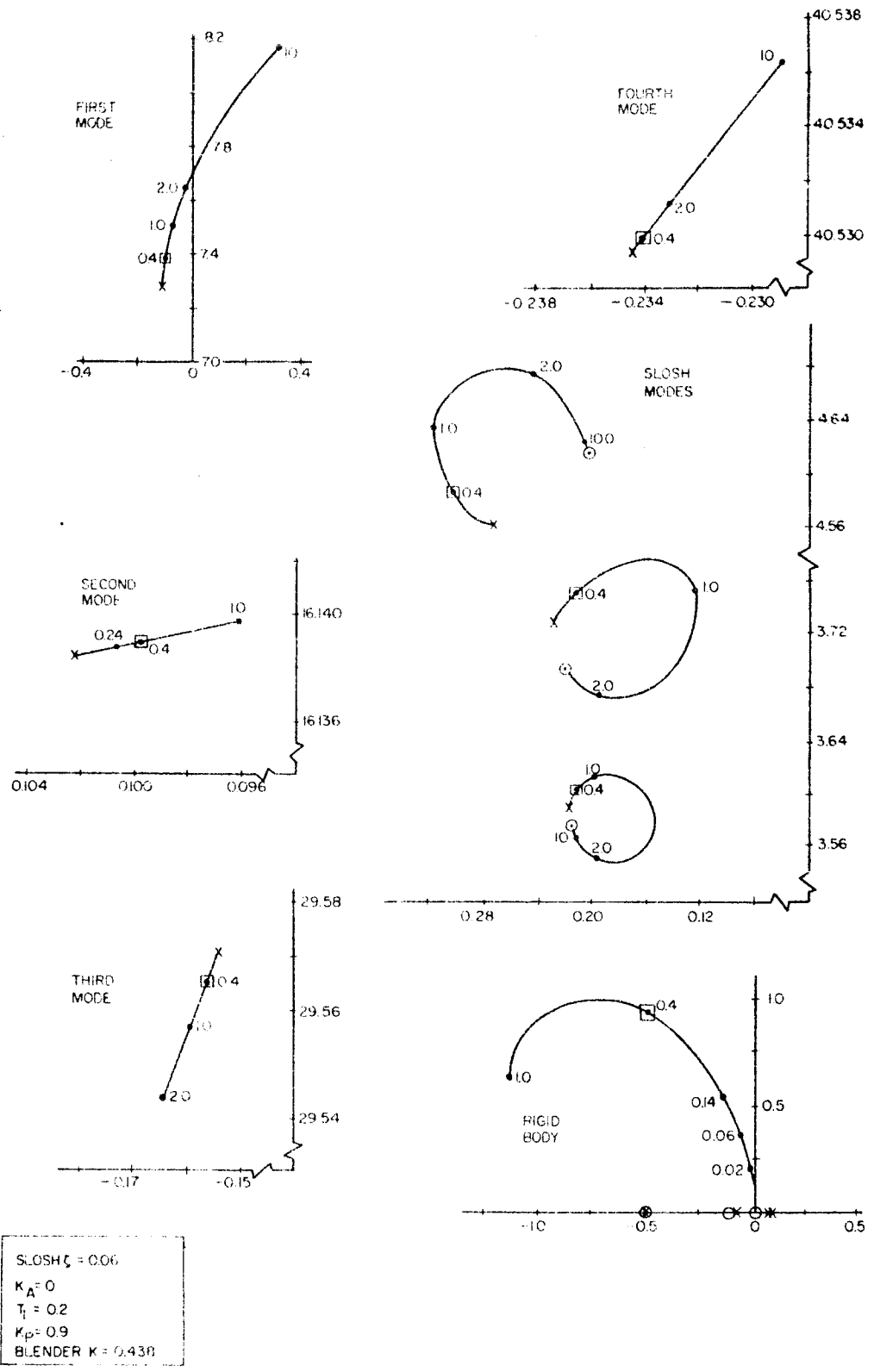


Figure 34. Root-Locus Plot, Nominal System with Filter B ( $t = 153$ )

b. Control System

1. Rate gyros:

Frequency,  $\pm 17$  per cent

Damping ratio,  $+50$  per cent

2. Accelerometer:

Frequency,  $\pm 17$  per cent

Damping Ratio,  $\pm 50$  per cent

3. Attitude and acceleration feedback lags:  $T_A$  and  $T_1$ ,  $\pm 10$  per cent

4. System gains:  $K_A$ ,  $K_P$ ,  $K_R$ ,  $K_I$ ,  $\pm 10$  per cent

5. Bending filter:

Frequency,  $\pm 10$  per cent

6. Blender imbalance,  $\pm 10$  per cent (C)

Tolerance Combinations

The number of tolerance combinations tested was limited by the amount of analog running considered feasible at each flight condition. This limit was estimated to be approximately 60 to 70 runs per flight condition. (C)

All the tolerances listed in the previous subsection were divided into six groups. Each group contains a set of tolerances that could be logically combined to form either a worst-best or a high-low situation. (C)

The six groups are discussed below. Reasons for selecting the particular tolerance combination within each group are given. (C)

Group 1, Rigid-Body Tolerances -- The worst combination of the rigid-body parameters  $C_1$  and  $C_2$  is a high  $C_1$  together with a low  $C_2$ . Wind shears cause more than normal disturbances because of the high  $C_1$ , and the control system has less than normal authority because of the reduced  $C_2$ . The opposite situation (low  $C_1$  and high  $C_2$ ) has good gust response but reduces the available high-frequency gain margin. (C)

The following combinations were tested:

Set A:  $C_1$  increased by 20 per cent and  $C_2$  decreased by 20 per cent.

Set B:  $C_1$  decreased by 20 per cent and  $C_2$  increased by 20 per cent. (C)

Group 2, Bending and Slosh Mode Tolerances -- The number of parameters involved in the bending and sloshing dynamics require that a careful analysis be made of the potential effects of the various combinations to ensure consideration of the most critical cases within a limited number of tolerance runs. This analysis has been performed for the specific system configuration under study using the following "ground rules":

1. The frequencies of all four bending modes were simultaneously decreased. The philosophy behind this is that the major variation in frequencies will result from a source common to all the modes. (C)
2. The variations in sloshing parameters will affect only the stability of the slosh modes themselves. Hence these combinations of sloshing and bending tolerances which aggravate sloshing stability to the greatest extent should be employed. For the particular system under study, these combinations are achieved by simultaneously increasing all sloshing frequencies and decreasing all bending frequencies, or vice versa. It is assumed that the nominal slosh masses and damping ratios have been set at values which reflect the pessimistic extremes of their respective tolerance bands; thus frequencies are the only sloshing parameters varied. (C)

3. The worst-case stability condition for a given bending mode results from the highest effective net pickup associated with that mode, regardless of the mode shape tolerances applied to the other bending modes. This assumption implies that the residues of all modes are sufficiently small to avoid significant phase and gain influences on neighboring modes. Actually, since the first, second, and third modes of the subject system have their zeros at frequencies below the respective pole frequencies, a high pickup on a lower mode increases the gain at a higher mode. Consequently, increasing all modal pickups simultaneously reflects a worse case situation for the gain-stabilized third and fourth modes. Determination of the maximum effective pickup for each mode requires examination of the magnitude and sign of the input from each sensor, along with the blender position. Hence the total pickup for a given mode will depend on the slopes and deflection of the first mode affecting blender position as well as the shape of the specific mode in question. The results of this examination are summarized in Table 3. (C)

The results given in Table 3 are valid at all flight conditions for all modes except the third, which requires a reversed first mode situation at flight times of 0, 40, and 79 seconds. At these isolated flight conditions, however, the residue of the third mode is so small that the mode itself is not a significant stability threat. Hence to avoid doubling the total number of tolerance runs, the conditions defined by the table were applied to all tolerance runs. (C)

In accordance with the above results and assumptions, the bending and sloshing tolerance group was studied in two combinations:

- Set A: All bending frequencies increased, all bending pickup increased, and all slosh frequencies decreased.
- Set B: All bending frequencies decreased, all bending pickup increased, and all slosh frequencies increased. (C)

Table 3. Direction of Change of Each Mode Shape Parameter to Increase Effective Bending Pickup

Bending Parameter	First Mode	Second Mode	Third Mode	Fourth Mode
$Y'_{1RGA}$	Increase	Increase	Increase	Increase
$Y'_{1RGF}$	Decrease	Decrease	Decrease	Decrease
$Y'_{1A}$	Increase	Increase	Increase	Increase
$Y'_{2RGA}$		Increase		
$Y'_{2RGF}$		Increase		
$Y'_{2A}$		Decrease		
$Y'_{3RGA}$			Increase	
$Y'_{3RGF}$			Increase	
$Y'_{3A}$			Decrease	
$Y'_{4RGA}$				Decrease
$Y'_{4RGF}$				Increase
$Y'_{4A}$				Decrease

(C)

Group 3. Control System Gains -- Maximum values of angle of attack ( $\alpha$ ) are obtained when  $K_R$  and  $K_A$  are low and when  $K_P$  is high. Conversely, the high-frequency bending stability is less when all three gains are high. (C)

The gyro blender integrator gain ( $K_i$ ) can also be considered in this group. One of the most important criteria used in selecting the nominal  $K_i$  was the blender position transient response from an initially unstable setting. If the blender is too fast the system becomes oscillatory and, in extreme cases, unstable. The speed at which the blender positions itself is proportional to the rate of divergence of the unstable system and the value of  $K_i$ . (C)



Since the rate of divergence for the initially unstable system is greater for large values of  $K_R$ , the worst tolerance condition will occur when  $K_i$  is increased along with  $K_R$ . (C)

The following combinations of gains were tested:

Set A: All gains high.

Set B: All gains low except  $K_P$ , which remains high. (C)

Group 4, Control System Dynamics -- The tolerances included in this group are those which have a direct effect on the phase alignment of the blender input signals. This group includes all control system dynamics except the bending filter, which is examined separately. (C)

Two tolerance combinations were investigated. The worst case (Set A) occurs when combined attitude and acceleration signals are furthest from alignment with the rate gyro signals:

Set A:

- (1) Forward rate gyro natural frequency high and damping ratio low.
- (2) Aft rate gyro natural frequency low and damping ratio high.
- (3)  $T_1$  and  $T_A$  low.
- (4) Accelerometer natural frequency high and damping ratio low.

Set B: Tolerances opposite to Set A were run to confirm the selection of Set A as the worst case. (C)

Group 5, Bending Filter -- The over-all notch width of the bending filter has been designed to provide sufficient attenuation for second and higher modes if the nominal filter frequency shifts  $\pm 10$  per cent. Over-all notch depth is sufficient so that changes in damping ratio of the individual notches are less critical than frequency shifts. The worst case occurs when the frequency is 10 per cent low since this causes increased phase lag at the rigid body and slosh frequencies. Conversely the best condition occurs when the frequency is 10 per cent high. (C)

Set A: Frequency 10 per cent low.

Set B: Frequency 10 per cent high. (C)

Group 6, Blender Imbalance -- The plus and minus variation assumed for the blender imbalance is obtained from the following sources:

1. Bandpass filter center frequency mismatch.
2. Absolute value circuit gain mismatch.
3. Bandpass filter attenuation mismatch. (C)

Table 4 lists the specific percentage changes for the individual items changed in each group. (C)

#### Computer Procedure for Tolerance Runs

The analog computer tolerance study used combinations of the six groups and the two sets within each group. A list of the exact combinations run is given in Table 5. Twenty-seven runs were made for each flight condition, for a total of 135 runs. The following procedure was used for each run:

1. A step attitude command was used to establish the blender equilibrium position, rigid-body frequency and damping, and maximum engine angle. (U)

Table 4. Parameter Tolerance Values Designated by Sets and Groups

Group	Set A High and/or Worst Value (per cent)	Set B Low and/or Best Value (per cent)
Group 1 - Rigid Body Aerodynamic moment coefficient, $C_1$ Control moment coefficient, $C_2$	+20 -20	-20 +20
Group 2 - Bending and Slosh All bending frequencies All slosh frequencies Bending mode slopes and deflections: $Y_{1RGA}^1$ $Y_{1RGF}^1$ $Y_{1A}$ $Y_{2RGA}^1$ $Y_{2RGF}^1$ $Y_{2A}$ $Y_{3RGA}^1$ $Y_{3RGF}^1$ $Y_{3A}$ $Y_{4RGA}^1$ $Y_{4RGF}^1$ $Y_{4A}$	-10 +10 +20 +30 +30 -30 +30 +30 -30 -30 +30 -30	+10 -10 +20 +30 +30 -30 +30 +30 -30 -30 +30 -30
Group 3 - Control System Gains Rate gain, $K_R$ Attitude gain $K_P$ Acceleration gain, $K_A$ Blender integrator gain, $K_i$	+10 +10 +10 +10	-10 +10 -10 -10
Group 4 - Control System Dynamics Forward rate gyro frequency Forward rate gyro damping ratio Aft rate gyro frequency Aft rate gyro damping ratio Accelerometer frequency Accelerometer damping ratio Attitude lag $T_1$ Acceleration lag $T_A$	+17 -50 -17 +50 +17 -50 -10 -10	-17 +50 +17 -50 -17 +50 +10 +10
Group 5 - Bending Filter Bending filter frequency	-10	+10
Group 6 - Blender Imbalance	+10	-10

Table 5. Tolerance Combinations Used in Analog Computer Tolerance Study

Analog Computer Run No.	Tolerance Group*					
	1	2	3	4	5	6
1	Nominal Conditions					
2	A	A	A	A	A	A
3	A	A	B	A	A	A
4	B	A	A	A	A	A
5	B	A	A	A	A	B
6	B	A	A	B	A	A
7	A	A	B	B	A	A
8	A	A	A	B	A	A
9	A	B	A	B	A	A
10	A	B	B	B	A	A
11	B	B	A	B	A	A
12	B	B	A	A	A	A
13	A	B	B	A	A	A
14	A	B	A	A	A	A
15	A	B	A	A	B	A
16	A	B	B	A	B	A
17	B	B	A	A	B	A
18	B	B	A	B	B	A
19	A	B	B	B	B	A
20	A	B	A	B	B	A
21	A	A	A	B	B	A
22	A	A	B	B	B	A
23	B	A	A	B	B	A
24	B	A	A	A	B	A
25	B	A	A	A	B	B
26	A	A	B	A	B	A
27	A	A	A	A	B	A

\*See Table 4 for contents of groups and sets.

2. The blender was preset to an unstable position so that it would move approximately to its equilibrium position with no input before the synthetic wind shear profile input was introduced. The maximum angle of attack due to this input was observed. (U)

The following parameters were tabulated for each run and are given in Table 6:

1. Maximum angle of attack for the synthetic wind shear input,  $\alpha$  maximum.
2. Maximum engine angle,  $\beta_R$  maximum.
3. Basic rigid-body frequency and damping for attitude commands.
4. Blender equilibrium position, K.
5. Frequency and approximate damping ratio of slosh oscillations (for the most lightly damped tolerance cases only). (U)

The results contained in Tables 6 through 10 can be summarized as follows:

Rigid-body response -- The rigid-body response was satisfactory. The worst-case damping ratio was  $\zeta = 0.142$ . This occurred for Run 22,  $t = 79$  seconds.

Angle of attack -- The maximum angle of attack at  $t = 79$  seconds for the wind shear profile reached but did not exceed the permissible limit of 9.8 degrees. At other flight times the permissible limits were not reached.

Engine angle  $\beta_R$  -- The maximum engine angle reached was 1.8 degrees, which occurred at  $t = 0$  for several runs. This was much less than the permissible limit of 5 degrees. (C)

Table 6. Tolerance Study Results (t = 0 seconds)

Computer Run Number	$\beta_R$ Maximum, Degrees	Blender Equilibrium Position, K	$\omega$ Rigid Body radians/second	$\zeta$ Rigid Body
2	1.80	0.43	0.97	0.24
3	1.53	0.43	0.7	0.25
4*	1.80	0.43	1.09	0.325
5†	1.80	0.465	1.09	0.31
6	1.66	0.45	1.03	0.29
7*	1.50	0.465	0.75	0.22
8	1.80	0.43	0.97	0.25
9	1.76	0.43	0.83	0.26
10	1.50	0.43	0.78	0.23
11	1.36	0.42	0.97	0.34
12	1.80	0.42	0.97	0.36
13	1.50	0.42	0.75	0.23
14	1.80	0.42	0.87	0.26
15	1.80	0.42	0.83	0.29
16	1.44	0.42	0.75	0.26
17	1.78	0.415	0.83	0.35
18	1.62	0.40	0.88	0.35
19	1.40	0.42	0.70	0.23
20	1.50	0.42	0.78	0.26
21	1.62	0.43	0.87	0.25
22	1.38	0.42	0.68	0.23
23	1.60	0.42	1.04	0.31
24	1.60	0.42	1.09	0.31
25	1.60	0.465	1.04	0.31
26	1.45	0.425	0.75	0.23
27	1.76	0.43	0.87	0.26

\* Analog computer trace included

Run 4 - Figure 33

Run 7 - Figure 34

† Lightly Damped Stosh Oscillations

<u>Frequency</u> (radians/second)	<u>Damping</u> Ratio
2.4	0.039

Table 7. Tolerance Study Results (t = 40 seconds)

Computer Run Number	$\beta_R$ Maximum, Degrees	$\theta$ Maximum, Degrees (wind gust input)	Blender Equilibrium Position, K	$\omega$ Rigid Body radians/second	$\zeta$ Rigid Body
2	1.6	11.3	0.5	0.65	0.31
3	1.4	11.5	0.48	0.63	0.21
4†	1.6	11.5	0.48	0.75	0.41
5†	1.6	11.5	0.47	0.7	0.41
6	1.4	11.7	0.47	0.7	0.48
7*	1.3	11.5	0.47	0.6	0.24
8	1.6	11.4	0.5	0.68	0.36
9	1.6	11.4	0.5	0.68	0.36
10†	1.35	11.5	0.47	0.65	0.24
11*	1.25	11.7	0.48	0.63	0.405
12	1.6	11.5	0.51	0.78	0.41
13	1.42	11.5	0.46	0.65	0.21
14	1.6	11.5	0.5	0.7	0.34
15	1.6	11.5	0.51	0.7	0.36
16	1.4	11.5	0.49	0.6	0.21
17	1.42	11.8	0.51	0.78	0.43
18	1.44	11.5	0.5	0.83	0.43
19	1.25	11.5	0.45	0.58	0.21
20	1.5	11.5	0.5	0.68	0.36
21	1.6	11.5	0.49	0.65	0.36
22	1.3	11.5	0.47	0.65	0.21
23	1.4	11.5	0.47	0.78	0.47
24	1.6	11.7	0.46	0.65	0.47
25	1.5	11.3	0.4	0.75	0.47
26	1.3	11.9	0.48	0.65	0.29
27	1.6	11.5	0.5	0.65	0.32

\* Analog computer trace included

Run 7 - Figure 35  
Run 11 - Figure 36

† Lightly Damped Slosh Oscillations

Run	Frequency (radians/second)	Damping Ratio
4	2.9	0.011
5	2.9	0.014
10	2.6	0.027

Table 8. Tolerance Study Results (t = 79 seconds)

Computer Run Number	$\beta_R$ Maximum, Degrees	$\alpha$ Maximum, Degrees (wind gust input)	Blender Equilibrium Position, K	$\omega$ Rigid Body radians/second	$\zeta$ Rigid Body
2	1.6	9.0	0.53	0.87	0.25
3	1.4	9.8	0.5	0.65	0.16
4†	1.5	9.5	0.5	0.87	0.46
5	1.58	9.5	0.5	0.97	0.38
6	1.5	9.3	0.5	0.97	0.35
7	1.3	9.7	0.5	0.68	0.2
8	1.6	9.0	0.53	0.83	0.21
9	1.6	9.0	0.5	0.83	0.195
10	1.3	9.5	0.485	0.78	0.195
11†	1.45	9.5	0.5	0.87	0.325
12†	1.5	9.5	0.47	0.92	0.31
13	1.36	9.75	0.5	0.78	0.185
14	1.59	9.0	0.5	0.83	0.195
15	1.61	9.0	0.53	0.83	0.235
16	1.38	9.8	0.5	0.75	0.145
17	1.55	9.5	0.53	0.87	0.325
18	1.45	9.4	0.5	0.83	0.325
19	1.3	9.7	0.47	0.7	0.175
20	1.55	8.95	0.5	0.87	0.21
21	1.5	9.0	0.53	0.83	0.275
22*	1.3	9.6	0.51	0.65	0.142
23	1.4	9.5	0.525	0.97	0.38
24	1.5	9.5	0.47	0.92	0.38
25	1.3	9.5	0.45	0.97	0.37
26	1.3	0.75	0.33	0.65	0.145
27	1.58	9.0	0.53	0.83	0.21

\* Analog computer trace included

Run 3 - Figure 37

Run 12 - Figure 38

Run 22 - Figure 39

† Lightly Damped Slosh Oscillations

Run	Frequency (radians/second)	Damping Ratio
4	3.2	0.015
11	2.95	0.006
12	2.95	0.0014



Table 9. Tolerance Study Results (t = 120 seconds)

Computer Run Number	$\beta_R$ Maximum, Degrees	$\alpha$ Maximum, Degrees (wind gust input)	Blender Equilibrium Position, K	$\omega$ Rigid Body radians/second	$\zeta$ Rigid Body
2	1.5	3.0	0.465	1.09	0.34
3	1.4	3.0	0.455	0.92	0.34
4	1.44	3.0	0.465	2.6	0.415
5	1.5	3.0	0.5	2.6	0.38
6	1.6	3.0	0.45	2.2	0.4
7*	1.1	3.0	0.47	0.83	0.285
8	1.4	3.0	0.47	0.97	0.31
9	1.6	3.0	0.43	1.04	0.31
10	1.35	3.0	0.43	0.97	0.335
11†	1.78	3.0	0.43	0.65	0.54
12	1.7	3.0	0.43	0.65	0.5
13	1.35	3.0	0.43	0.97	0.31
14†	1.58	2.8	0.43	0.97	0.36
15	1.43	2.9	0.47	0.97	0.36
16	1.2	3.0	0.455	0.97	0.34
17†	1.4	2.8	0.455	0.87	0.45
18	1.39	2.7	0.43	0.87	0.475
19	1.22	2.95	0.43	0.92	0.34
20	1.4	2.95	0.44	0.97	0.335
21	1.4	2.7	0.47	1.09	0.335
22	1.2	2.8	0.46	0.92	0.34
23	1.39	2.7	0.445	1.57	0.45
24	1.4	2.6	0.47	1.42	0.465
25	1.4	2.95	0.51	1.31	0.5
26	1.32	2.9	0.46	0.97	0.34
27	1.55	2.6	0.47	1.09	0.36

\* Analog computer trace included

Run 7 - Figure 40

Run 11 - Figure 41

† Lightly Damped Slosh Oscillations

Run	Frequency (radians/second)	Damping Ratio
11	3.4	0.0029
14	3.5	0.033
17	3.5	0.029

Table 10. Tolerance Study Results (t = 153 seconds)

Computer Run Number	$\beta_R$ Maximum, Degrees	Blender Equilibrium Position, K	$\omega$ Rigid Body radians/second	$\zeta$ Rigid Body
2	0.8	0.465	1.09	0.32
3	0.8	0.46	0.87	0.26
4	0.8	0.455	1.74	0.335
5	0.82	0.465	1.74	0.32
6	0.8	0.465	1.57	0.31
7	0.8	0.465	0.97	0.26
8	0.9	0.455	0.97	0.275
9	0.8	0.43	1.04	0.295
10	0.7	0.43	0.37	0.295
11	0.8	0.445	1.57	0.36
12	0.8	0.465	1.57	0.36
13	0.78	0.465	0.92	0.31
14	0.8	0.465	1.09	0.31
15	0.9	0.465	0.97	0.325
16	0.8	0.44	0.78	0.31
17	0.8	0.455	1.31	0.415
18	0.8	0.465	1.04	0.405
19	0.64	0.44	0.37	0.255
20	0.64	0.465	0.87	0.305
21	0.71	0.465	0.92	0.305
22*	0.6	0.465	0.78	0.26
23	0.61	0.465	1.31	0.38
24	0.78	0.465	1.57	0.38
25	0.61	0.515	1.31	0.38
26	0.68	0.465	0.87	0.28
27	0.8	0.465	0.92	0.32

\* Analog computer trace included

Run 18 - Figure 42

Run 22 - Figure 43

Slosh oscillations -- Slosh oscillations became highly underdamped for flight times 40, 79, and 120 seconds. It was necessary to increase the nominal slosh damping ratio to 0.06 for system stability at several tolerance combinations. When the damping was increased, the worst case occurred for Run 12,  $t = 79$  seconds, with a closed-loop slosh damping ratio of approximately 0.0014. The magnitude of vehicle attitude oscillations due to slosh for this case did not exceed  $\pm 0.175$  degree. The tolerance combination causing worst-case slosh oscillations included low bending filter frequency, high control and feedback gains, low slosh frequencies, and high bending frequencies. Reference to Figure 13 shows that slosh phase margin is small for these tolerance combinations. (C)

Analog computer traces of eleven tolerance runs are given in Figures 35 through 45. These traces were selected to show worst cases of the tolerance parameters, or any combination which caused poorest relative stability. (C)

In addition to the tolerance results already mentioned, the computer traces show that lightly damped first bending mode oscillations occur for the same tolerance combinations which cause slosh oscillations. These first mode oscillations are present at  $t = 153$  seconds also, when slosh oscillations have disappeared. These first-mode oscillations result in a worst-case vehicle displacement of less than  $\pm 0.07$  meter at the first-mode frequency. (C)

Frequency response plots of the system for four worst-case tolerance combinations are shown in Figures 46 through 49. Gain and phase margins taken from these plots are given in Table 11. (C)

Table 11. Gain and Phase Margins for Four Tolerance Combinations

Flight Time (sec)	Analog Computer Run No.	Slosh		First Bending Mode	
		Gain Margin (db)	Phase Margin (deg)	Gain Margin (db)	Phase Margin (deg)
40	11	3	10	0.5	5
79	12	2.8	40	3.5	40
79	22	9	30	12	40
120	11	1.4	28	0.4	10

(C)

The gain and phase margins for these worst-case combinations show that the system became marginally stable for tolerance Runs 11 at  $t = 40$  and 120 seconds. (C)

The tolerance study showed that the system is particularly sensitive to tolerances at the first bending mode and slosh frequencies. For the particular bending filter chosen, the second and higher bending modes have been heavily attenuated with some resulting reduction of stability margins at the first mode frequencies. The use of a more realistic first bending mode damping ratio than the assumed value of 0.005 would have improved the stability with tolerances as was discussed previously. (C)

VEHICLE AND SYSTEM TOLERANCES:  
 TOLERANCE GROUP 1 - SET B  
 TOLERANCE GROUP 2 - SET A  
 TOLERANCE GROUP 3 - SET A  
 TOLERANCE GROUP 4 - SET A  
 TOLERANCE GROUP 5 - SET A  
 TOLERANCE GROUP 6 - SET A

$K_R = 0.88 \text{ DEG/DEG/SEC}$   
 $K_A = 0 \text{ DEG/SEC/M/SEC}^2$   
 $K_P = 0.99 \text{ DEG/SEC/DEG}$   
 $T_1 = 0.18 \text{ SEC}$   
 $T_A = 1.80 \text{ SEC}$

SLOSH  $\zeta = 0.069$   
 BENDING  $\delta = 0.005$   
 BENDING FILTER = B  
 $X_A = 64 \text{ m}$   
 $X_{RGF} = 85.3 \text{ m}$   
 $X_{RGA} = 5.0 \text{ m}$

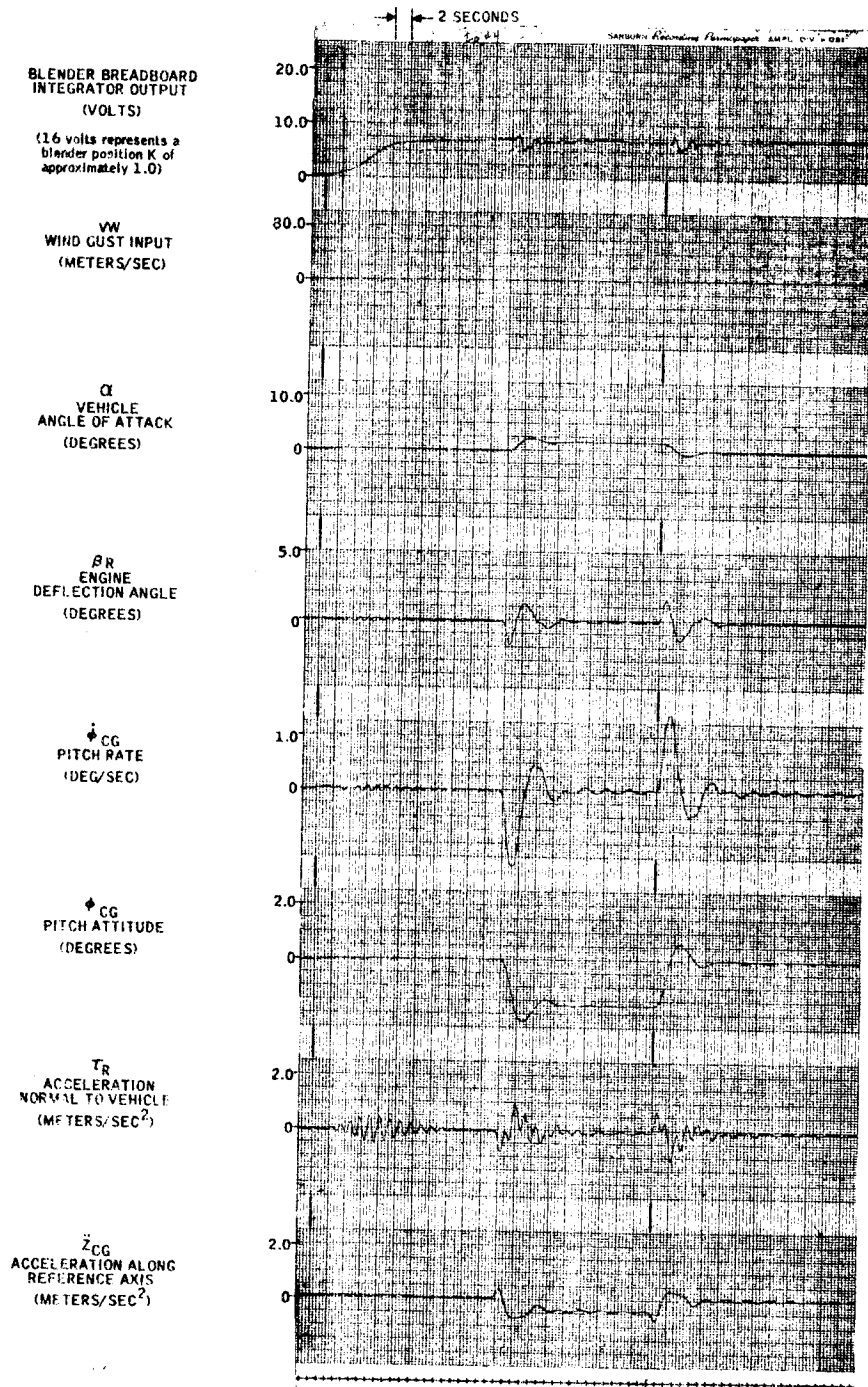


Figure 35. Analog Computer Run 4 (t = 0 seconds) - Step Attitude Command

VEHICLE AND SYSTEM TOLERANCES:  
TOLERANCE GROUP 1 - SET A  
TOLERANCE GROUP 2 - SET A  
TOLERANCE GROUP 3 - SET B  
TOLERANCE GROUP 4 - SET B  
TOLERANCE GROUP 5 - SET A  
TOLERANCE GROUP 6 - SET A

$K_R = 0.72 \text{ DEG/DEG/SEC}$   
 $K_A = 0 \text{ DEG/SEC/M/SEC}^2$   
 $K_P = 0.99 \text{ DEG/SEC/DEG}$   
 $T_1 = 0.22 \text{ SEC}$   
 $T_A = 2.20 \text{ SEC}$

SLOSH  $\zeta = 0.60$   
BENDING FILTER = B  
 $X_A = 64 \text{ m}$   
 $X_{RGF} = 85.3 \text{ m}$   
 $X_{RGA} = 5.0 \text{ m}$

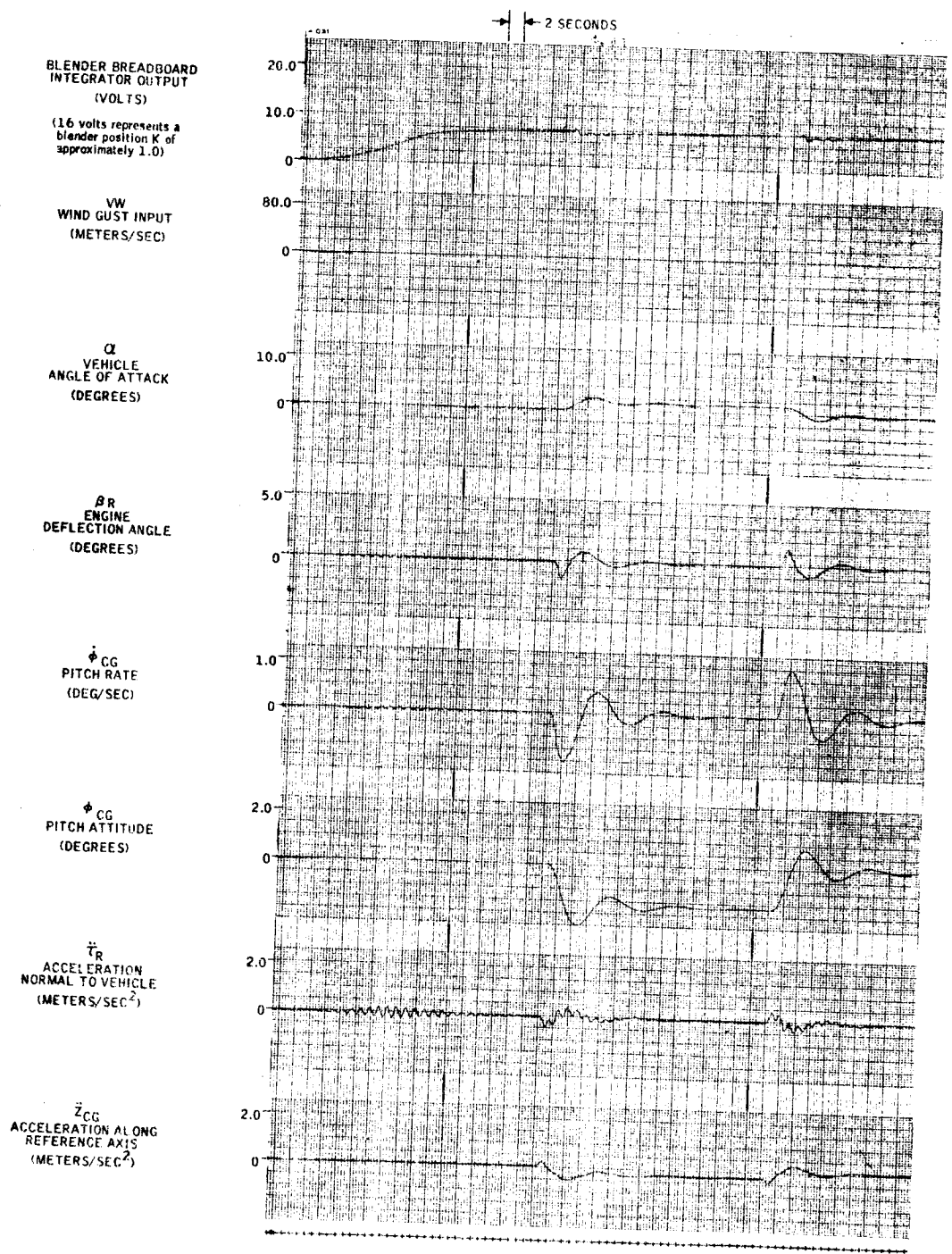


Figure 36. Analog Computer Run 7 (t = 0 seconds) - Step Attitude Command

VEHICLE AND SYSTEM TOLERANCES:

- TOLERANCE GROUP 1 - SET A
- TOLERANCE GROUP 2 - SET A
- TOLERANCE GROUP 3 - SET B
- TOLERANCE GROUP 4 - SET B
- TOLERANCE GROUP 5 - SET A
- TOLERANCE GROUP 6 - SET A

- $K_R = 0.720 \text{ DEG/DEG/SEC}$
- $K_A = 0.045 \text{ DEG/SEC/M/SEC}^2$
- $K_P = 0.990 \text{ DEG/SEC/DEG}$
- $T_I = 0.220 \text{ SEC}$
- $T_A = 2.200 \text{ SEC}$

- SLOSH  $\tau = 0.060$
- BENDING  $\tau = 0.005$
- BENDING FILTER = B
- $X_A = 64 \text{ m}$
- $X_{RCF} = 85.3 \text{ m}$
- $X_{RGA} = 5.0 \text{ m}$

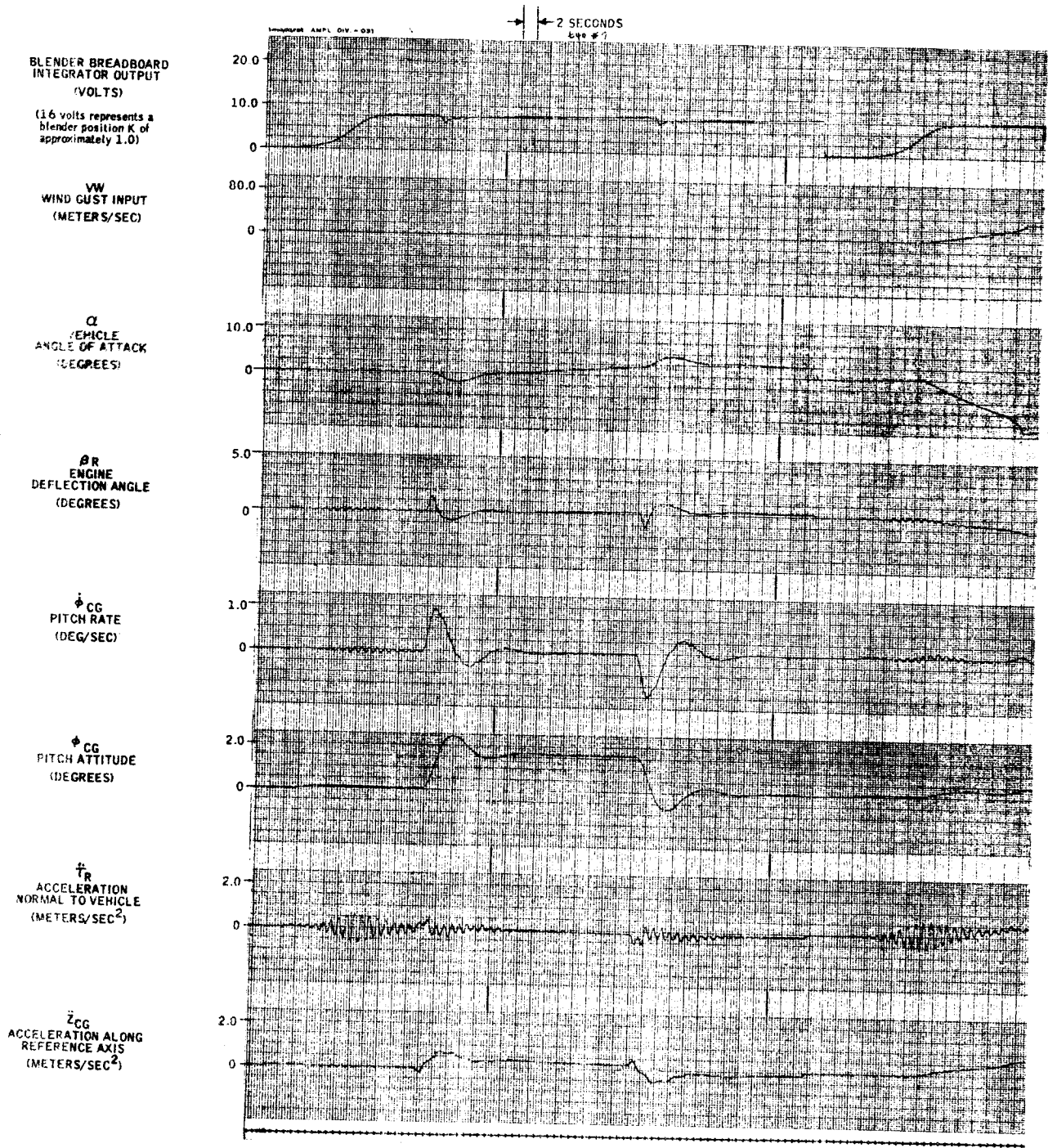


Figure 37. Analog Computer Run 7 (t = 40 seconds) - Step Attitude Command, Synthetic Wind Shear Input

VEHICLE AND SYSTEM TOLERANCES:

TOLERANCE GROUP 1 - SET B	$K_R = 0.880 \text{ DEG/DEG/SEC}$	SLOSH $\zeta = 0.060$
TOLERANCE GROUP 2 - SET B	$K_A = 0.055 \text{ DEG/SEC/M/SEC}^2$	BENDING $\zeta = 0.005$
TOLERANCE GROUP 3 - SET A	$K_P = 0.990 \text{ DEG/SEC/DEG}$	BENDING FILTER = B
TOLERANCE GROUP 4 - SET 9	$T_1 = 0.220 \text{ SEC}$	$X_A = 64 \text{ m}$
TOLERANCE GROUP 5 - SET A	$T_A = 2.200 \text{ SEC}$	$X_{RGF} = 85.3 \text{ m}$
TOLERANCE GROUP 6 - SET A		$X_{RGA} = 5.0 \text{ m}$

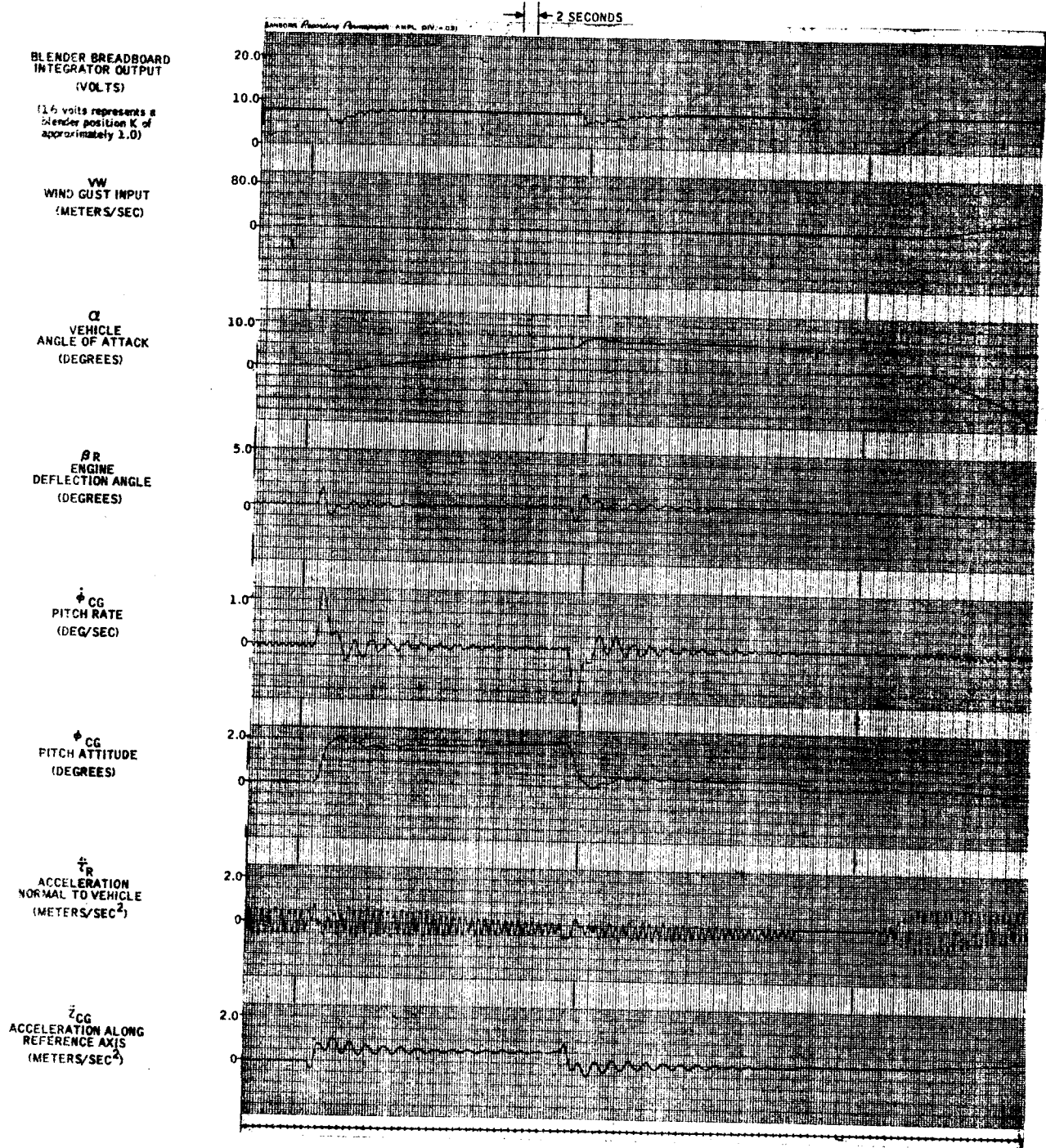


Figure 38. Analog Computer Run 11 (t = 40 seconds) - Step Attitude Command, Synthetic Wind Shear Input



VEHICLE AND SYSTEM TOLERANCES:

TOLERANCE GROUP 1 - SET A	$K_R = 0.720 \text{ DEG/SEC}$	SLOSH = 0.060
TOLERANCE GROUP 2 - SET A	$K_A = 0.045 \text{ DEG/SEC}^2$	BENDING $\tau = 0.005$
TOLERANCE GROUP 3 - SET B	$K_D = 0.390 \text{ DEG/SEC}$	BENDING FILTER = B
TOLERANCE GROUP 4 - SET A	$T_I = 0.180 \text{ SEC}$	$X_A = 64 \text{ m}$
TOLERANCE GROUP 5 - SET A	$T_A = 1.300 \text{ SEC}$	$X_{RGF} = 85.3 \text{ m}$
TOLERANCE GROUP 6 - SET A		$X_{RGA} = 5.0 \text{ m}$

BLENDER BREADBOARD  
INTEGRATOR OUTPUT  
(VOLTS)

(16 volts represents a  
blender position K of  
approximately 1.0)

VW  
WIND GUST INPUT  
(METERS/SEC)

$\alpha$   
VEHICLE  
ANGLE OF ATTACK  
(DEGREES)

$\beta_R$   
ENGINE  
DEFLECTION ANGLE  
(DEGREES)

$\dot{\phi}_{CG}$   
PITCH RATE  
(DEG/SEC)

$\phi_{CG}$   
PITCH ATTITUDE  
(DEGREES)

$\ddot{\tau}_R$   
ACCELERATION  
NORMAL TO VEHICLE  
(METERS/SEC<sup>2</sup>)

$\ddot{z}_{CG}$   
ACCELERATION ALONG  
REFERENCE AXIS  
(METERS/SEC<sup>2</sup>)

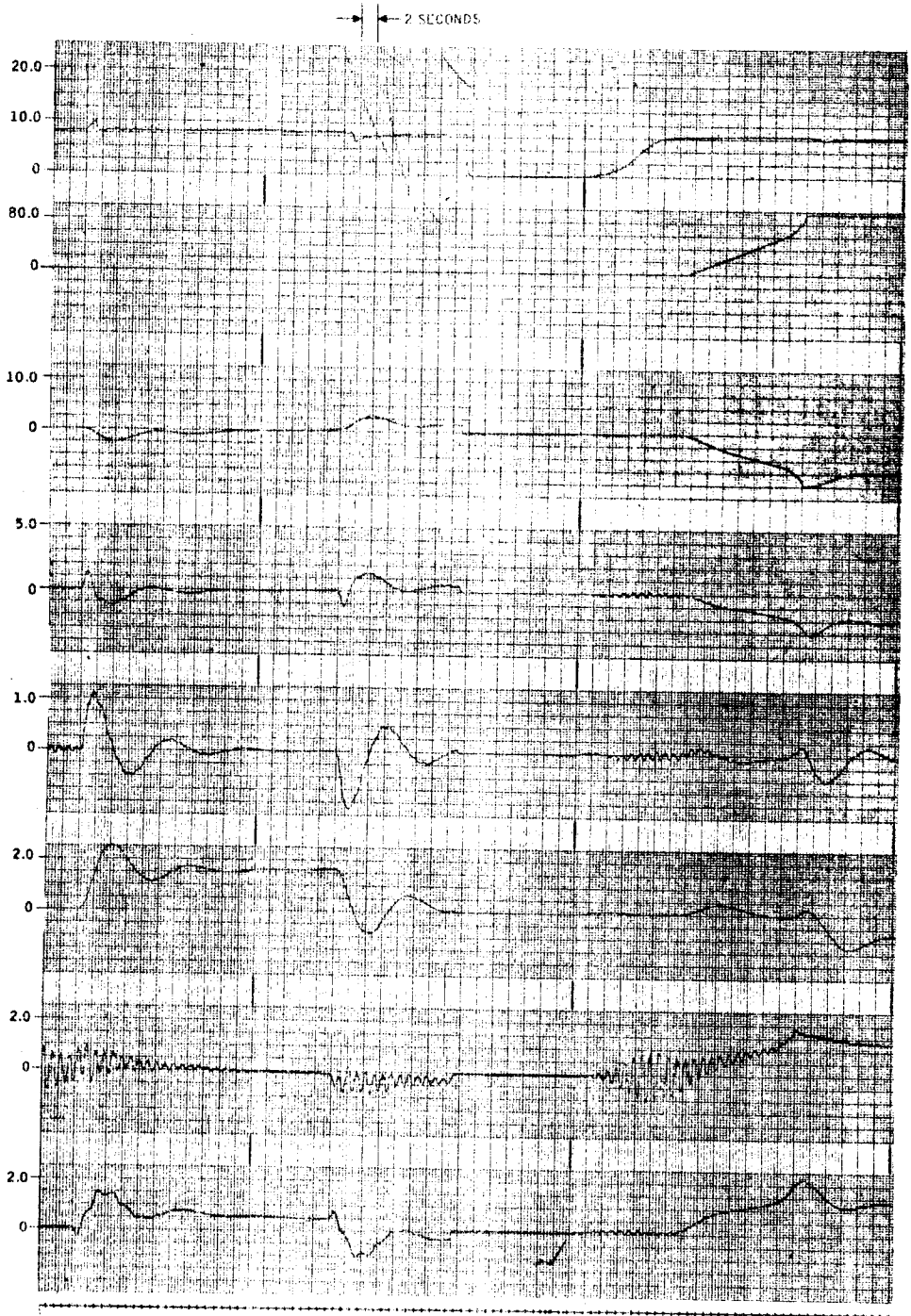


Figure 39. Analog Computer Run 3 (t = 79 seconds) - Step Attitude Command, Synthetic Wind Shear Input

VEHICLE AND SYSTEM PARAMETERS:  
 TOLERANCE GROUP 1 - SET B  
 TOLERANCE GROUP 2 - SET B  
 TOLERANCE GROUP 3 - SET A  
 TOLERANCE GROUP 4 - SET A  
 TOLERANCE GROUP 5 - SET A  
 TOLERANCE GROUP 6 - SET A

$K_0$  1.000 DEG/SEC  
 $K_1$  0.000 M/SEC<sup>2</sup>  
 $K_2$  0.000 M/SEC/DFG  
 $T_1$  0.100 SEC  
 $T_2$  1.000 SEC

SLOSH  $\tau = 0.060$   
 BENDING  $\tau = 0.005$   
 BENDING FILTER = B  
 $X_A = 6.4$  m  
 $X_{RGF} = 85.3$  m  
 $X_{RGA} = 5.0$  m

BLENDER BREADBOARD  
 INTEGRATOR OUTPUT  
 (VOLTS)

(16 volts represents a  
 blender position K of  
 approximately 1.0)

VW  
 WIND GUST INPUT  
 (METERS/SEC)

$\alpha$   
 VEHICLE  
 ANGLE OF ATTACK  
 (DEGREES)

$\beta_R$   
 ENGINE  
 DEFLECTION ANGLE  
 (DEGREES)

$\dot{\phi}_{CG}$   
 PITCH RATE  
 (DEG/SEC)

$\phi_{CG}$   
 PITCH ATTITUDE  
 (DEGREES)

$\ddot{z}_R$   
 ACCELERATION  
 NORMAL TO VEHICLE  
 (METERS/SEC<sup>2</sup>)

$\ddot{z}_{CG}$   
 ACCELERATION ALONG  
 REFERENCE AXIS  
 (METERS/SEC<sup>2</sup>)

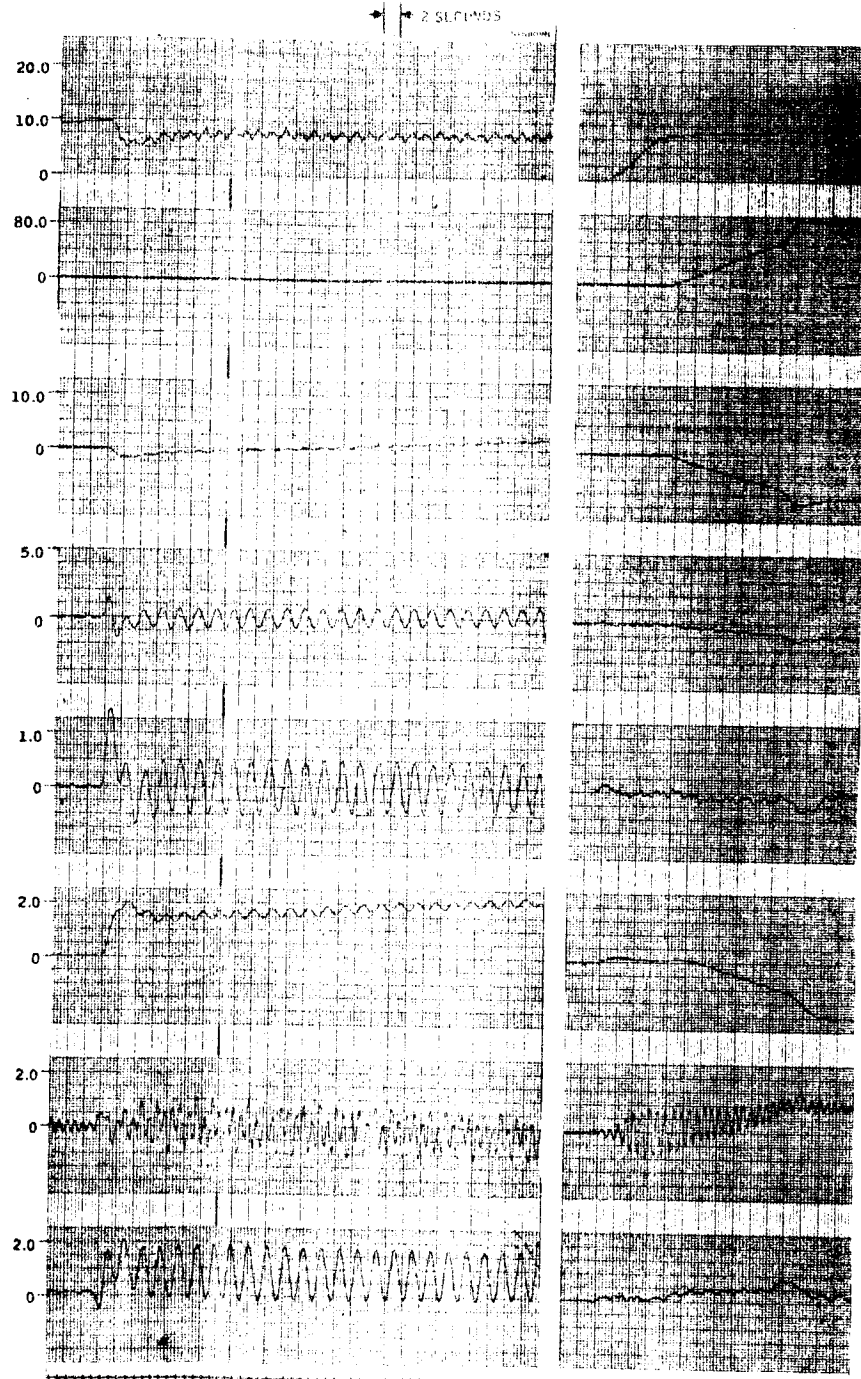


Figure 40. Analog Computer Run 12 ( $t = 79$  seconds) - Step Attitude Command, Synthetic Wind Shear Input

VEHICLE AND SYSTEM TOLERANCES

- TOLERANCE GROUP 1 - SET A
- TOLERANCE GROUP 2 - SET A
- TOLERANCE GROUP 3 - SET B
- TOLERANCE GROUP 4 - SET B
- TOLERANCE GROUP 5 - SET B
- TOLERANCE GROUP 6 - SET A

- $K_W = 0.720 \text{ DEG/SEC/SEC}$
- $K_A = 0.045 \text{ DEG/SEC/M/SEC}^2$
- $K_I = 0.240 \text{ DEG/SEC/DEG}$
- $T_1 = 0.720 \text{ SEC}$
- $I_A = 2.200 \text{ SEC}$

- SLOSH  $\epsilon = 0.060$
- BENDING  $\epsilon = 0.005$
- BENDING FILTER = B
- $X_A = 64 \text{ m}$
- $X_{RGF} = 35.3 \text{ m}$
- $X_{RGA} = 5.0 \text{ m}$

BLENDER BREADBOARD  
INTEGRATOR OUTPUT  
(VOLTS)

(16 volts represents a  
blender position K of  
approximately 1.0)

VW  
WIND GUST INPUT  
(METERS/SEC)

$\alpha$   
VEHICLE  
ANGLE OF ATTACK  
(DEGREES)

$\beta_R$   
ENGINE  
DEFLECTION ANGLE  
(DEGREES)

$\dot{\alpha}_{CG}$   
PITCH RATE  
(DEG/SEC)

$\alpha_{CG}$   
PITCH ATTITUDE  
(DEGREES)

$\ddot{z}_R$   
ACCELERATION  
NORMAL TO VEHICLE  
(METERS/SEC<sup>2</sup>)

$\ddot{z}_{CG}$   
ACCELERATION ALONG  
REFERENCE AXIS  
(METERS/SEC<sup>2</sup>)

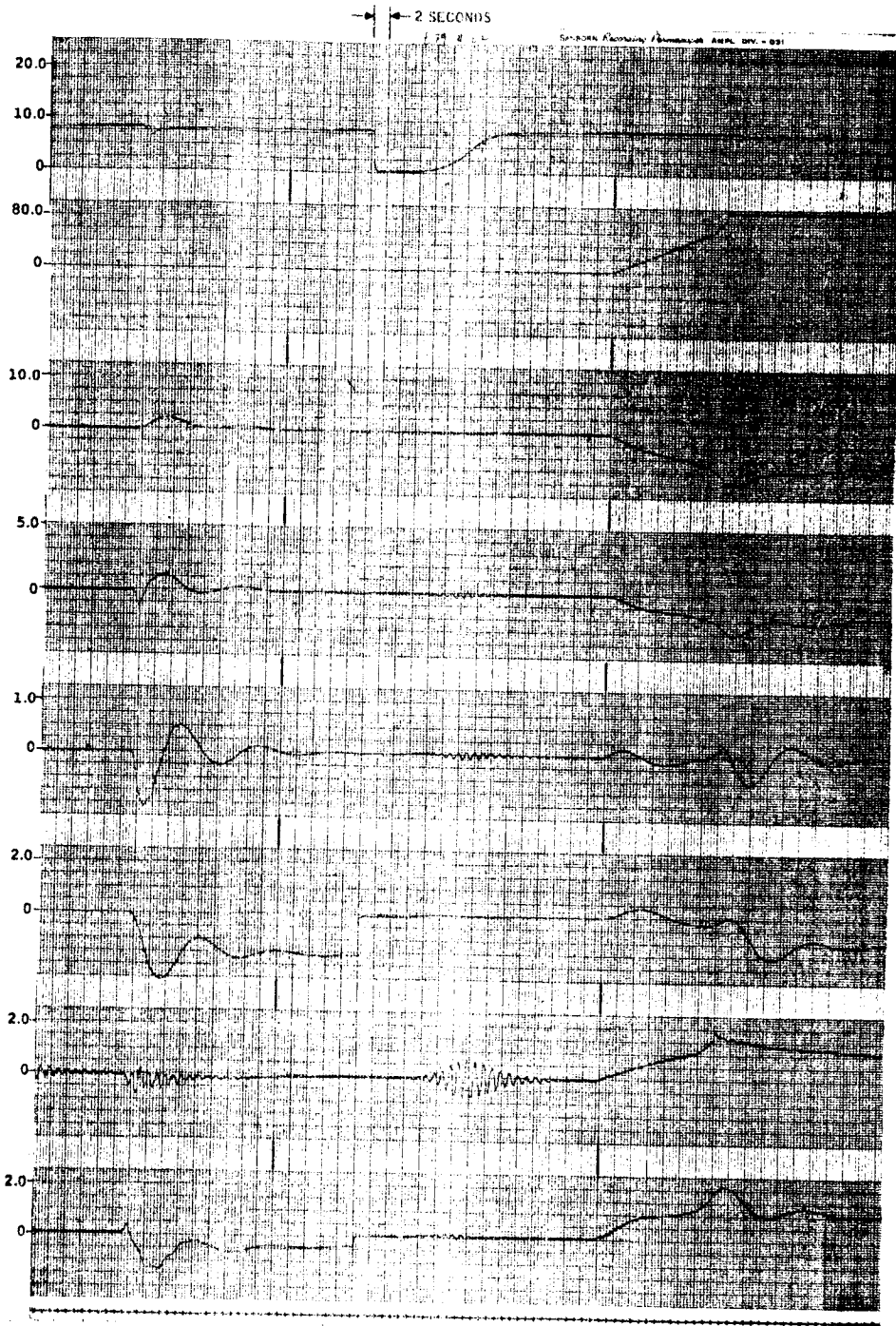


Figure 41. Analog Computer Run 22 (t = 79 seconds) - Step Attitude Command, Synthetic Wind Shear Input

VEHICLE AND SYSTEM TOLERANCES:

- TOLERANCE GROUP 1 - SET A
- TOLERANCE GROUP 2 - SET E
- TOLERANCE GROUP 3 - SET E
- TOLERANCE GROUP 4 - SET B
- TOLERANCE GROUP 5 - SET A
- TOLERANCE GROUP 6 - SET A

$K_R = 0.720 \text{ DEG/DEG/SEC}$   
 $K_A = 0.018 \text{ DEG/SEC/M/SEC}^2$   
 $K_P = 0.990 \text{ DEG/SEC/DEG}$   
 $I_1 = 0.220 \text{ SEC}$   
 $T_A = 2.200 \text{ SEC}$

SLOSH  $\tau = 0.060$   
 BENDING  $\tau = 0.005$   
 BENDING FILTER - B  
 $X_A = 64 \text{ m}$   
 $X_{RGF} = 85.3 \text{ m}$   
 $X_{RGA} = 5.0 \text{ m}$

BLENDER BREADBOARD  
 INTEGRATOR OUTPUT  
 (VOLTS)  
 (16 volts represents a  
 blender position K of  
 approximately 1.0)

$VW$   
 WIND GUST INPUT  
 (METERS/SEC)

$\alpha$   
 VEHICLE  
 ANGLE OF ATTACK  
 (DEGREES)

$\beta_R$   
 ENGINE  
 DEFLECTION ANGLE  
 (DEGREES)

$\dot{\phi}_{CG}$   
 PITCH RATE  
 (DEG/SEC)

$\phi_{CG}$   
 PITCH ATTITUDE  
 (DEGREES)

$\ddot{x}_R$   
 ACCELERATION  
 NORMAL TO VEHICLE  
 (METERS/SEC<sup>2</sup>)

$\ddot{z}_{CG}$   
 ACCELERATION ALONG  
 REFERENCE AXIS  
 (METERS/SEC<sup>2</sup>)

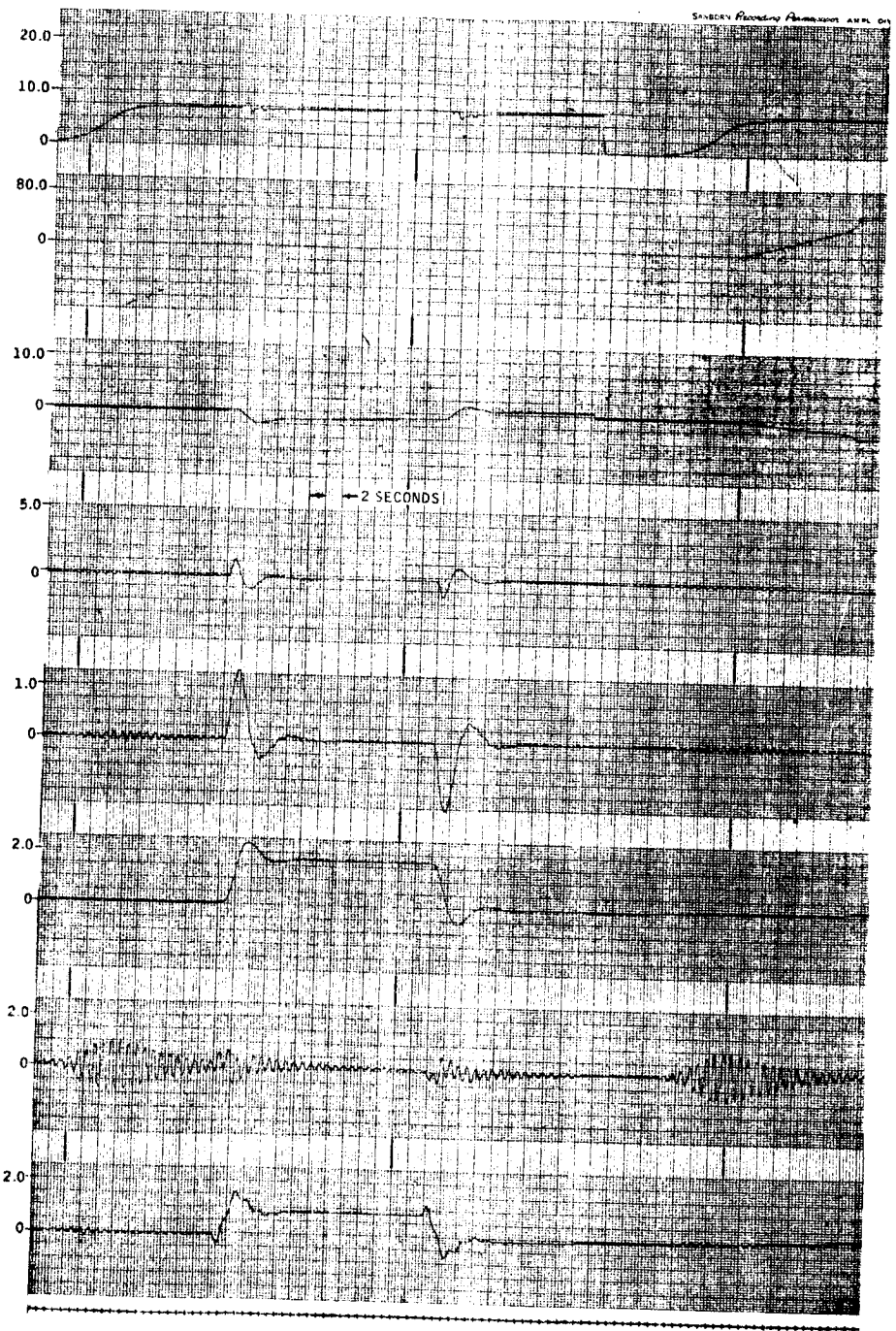


Figure 42. Analog Computer Run 7 (t = 120 seconds) - Step Attitude Command, Synthetic Wind Shear Input

VEHICLE AND SYSTEM TOLERANCES:  
TOLERANCE GROUP 1 - SET B  
TOLERANCE GROUP 2 - SET B  
TOLERANCE GROUP 3 - SET A  
TOLERANCE GROUP 4 - SET B  
TOLERANCE GROUP 5 - SET A  
TOLERANCE GROUP 6 - SET A

$K_R = 0.880 \text{ DEG/DEG/SEC}$   
 $K_A = 0.022 \text{ DEG/SEC/M/SEC}^2$   
 $K_P = 0.990 \text{ DEG/SEC/DEG}$   
 $T_1 = 0.220 \text{ SEC}$   
 $T_A = 2.200 \text{ SEC}$

SLOSH  $\epsilon = 0.060$   
BENDING  $\tau = 0.005$   
BENDING FILTER = B

$X_A = 64 \text{ m}$   
 $X_{RGF} = 85.3 \text{ m}$   
 $X_{RGA} = 5.0 \text{ m}$

BLENDER BREADBOARD  
INTEGRATOR OUTPUT  
(VOLTS)

(16 volts represents a  
blender position  $K$  of  
approximately 1.0)

VW  
WIND GUST INPUT  
(METERS/SEC)

$\alpha$   
VEHICLE  
ANGLE OF ATTACK  
(DEGREES)

$\beta_R$   
ENGINE  
DEFLECTION ANGLE  
(DEGREES)

$\dot{\phi}_{CG}$   
PITCH RATE  
(DEG/SEC)

$\phi_{CG}$   
PITCH ATTITUDE  
(DEGREES)

$\ddot{x}_R$   
ACCELERATION  
NORMAL TO VEHICLE  
(METERS/SEC<sup>2</sup>)

$\ddot{z}_{CG}$   
ACCELERATION ALONG  
REFERENCE AXIS  
(METERS/SEC<sup>2</sup>)

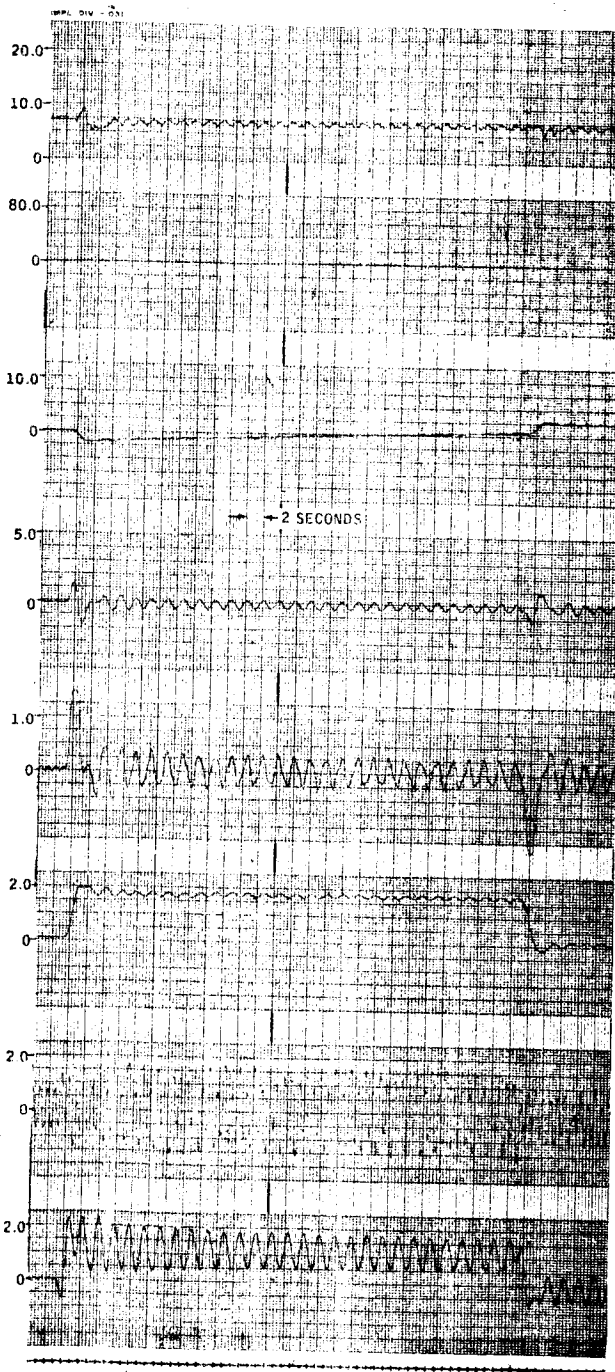


Figure 43. Analog Computer Run 11 (t = 120 seconds) - Step Attitude Command

VEHICLE AND SYSTEM TOLERANCES:

- TOLERANCE GROUP 1 - SET B
- TOLERANCE GROUP 2 - SET B
- TOLERANCE GROUP 3 - SET A
- TOLERANCE GROUP 4 - SET B
- TOLERANCE GROUP 5 - SET B
- TOLERANCE GROUP 6 - SET A

- $K_R = 0.88 \text{ DEG/DEG/SEC}$
- $K_A = 0 \text{ DEG/SEC/M/SEC}^2$
- $K_P = 0.99 \text{ DEG/SEC/DEG}$
- $T_I = 0.22 \text{ SEC}$
- $T_A = 2.20 \text{ SEC}$

- SLOSH  $\tau = 0.060$
- BENDING  $\tau = 0.005$
- BENDING FILTER = B

- $X_A = 64 \text{ m}$
- $X_{RGF} = 85.3 \text{ m}$
- $X_{RGA} = 5.0 \text{ m}$

BLENDER BREADBOARD  
INTEGRATOR OUTPUT  
(VOLTS)

(16 volts represents a  
blender position K of  
approximately 1.0)

VW  
WIND GUST INPUT  
(METERS/SEC)

$\alpha$   
VEHICLE  
ANGLE OF ATTACK  
(DEGREES)

$\theta_R$   
ENGINE  
DEFLECTION ANGLE  
(DEGREES)

$\dot{\phi}_{CG}$   
PITCH RATE  
(DEG/SEC)

$\phi_{CG}$   
PITCH ATTITUDE  
(DEGREES)

$\ddot{z}_R$   
ACCELERATION  
NORMAL TO VEHICLE  
(METERS/SEC<sup>2</sup>)

$\ddot{z}_{CG}$   
ACCELERATION ALONG  
REFERENCE AXIS  
(METERS/SEC<sup>2</sup>)

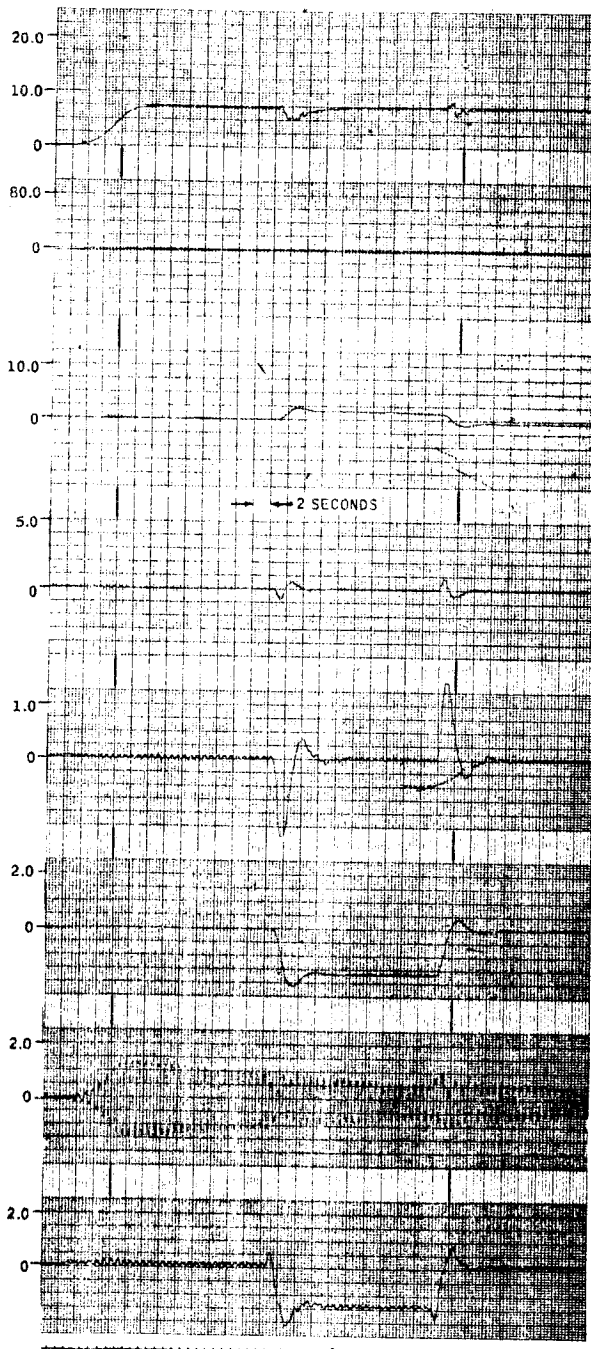


Figure 44. Analog Computer Run 18 (t = 153 seconds) - Step Attitude Command



VEHICLE AND SYSTEM TOLERANCES:  
TOLERANCE GROUP 1 - SET A  
TOLERANCE GROUP 2 - SET A  
TOLERANCE GROUP 3 - SET B  
TOLERANCE GROUP 4 - SET B  
TOLERANCE GROUP 5 - SET B  
TOLERANCE GROUP 6 - SET A

$K_R = 0.77 \text{ DEG/DEG/SEC}$   
 $K_A = 0 \text{ DEG/SEC/M/SEC}^2$   
 $K_P = 0.79 \text{ DEG/SEC/DEG}$   
 $T_I = 0.22 \text{ SEC}$   
 $T_A = 2.20 \text{ SEC}$

SLOSH  $\zeta = 0.060$   
BENDING  $\gamma = 0.005$   
BENDING FILTER = B

$X_A = 64 \text{ m}$   
 $X_{RGF} = 85.3 \text{ m}$   
 $X_{RGA} = 5.0 \text{ m}$

BLENDER BREADBOARD  
INTEGRATOR OUTPUT  
(VOLTS)

(16 volts represents a  
blender position  $K$  of  
approximately 1.0)

VW  
WIND GUST INPUT  
(METERS/SEC)

$\alpha$   
VEHICLE  
ANGLE OF ATTACK  
(DEGREES)

$\beta_R$   
ENGINE  
DEFLECTION ANGLE  
(DEGREES)

$\dot{\phi}_{CG}$   
PITCH RATE  
(DEG/SEC)

$\phi_{CG}$   
PITCH ATTITUDE  
(DEGREES)

$\ddot{z}_R$   
ACCELERATION  
NORMAL TO VEHICLE  
(METERS/SEC<sup>2</sup>)

$\ddot{z}_{CG}$   
ACCELERATION ALONG  
REFERENCE AXIS  
(METERS/SEC<sup>2</sup>)

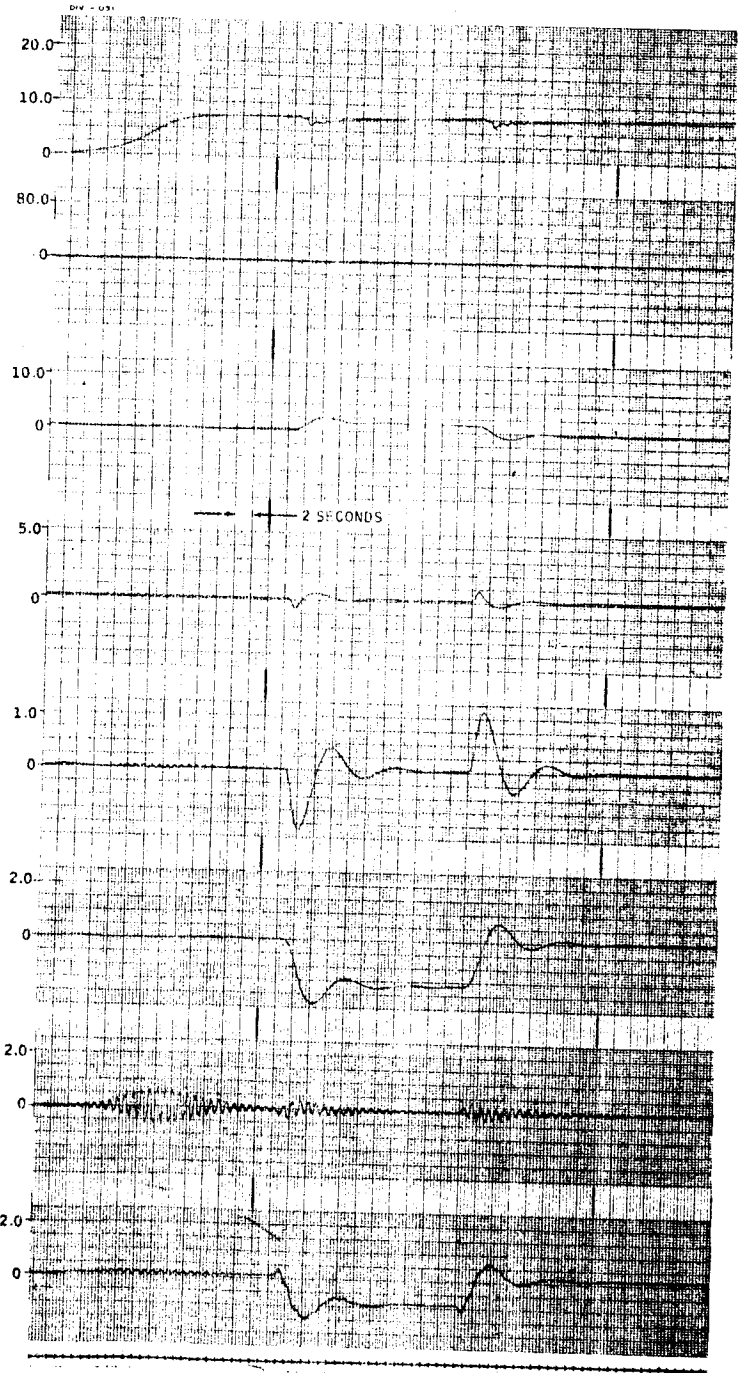


Figure 45. Analog Computer Run 22 (t = 153 seconds) - Step Attitude Command

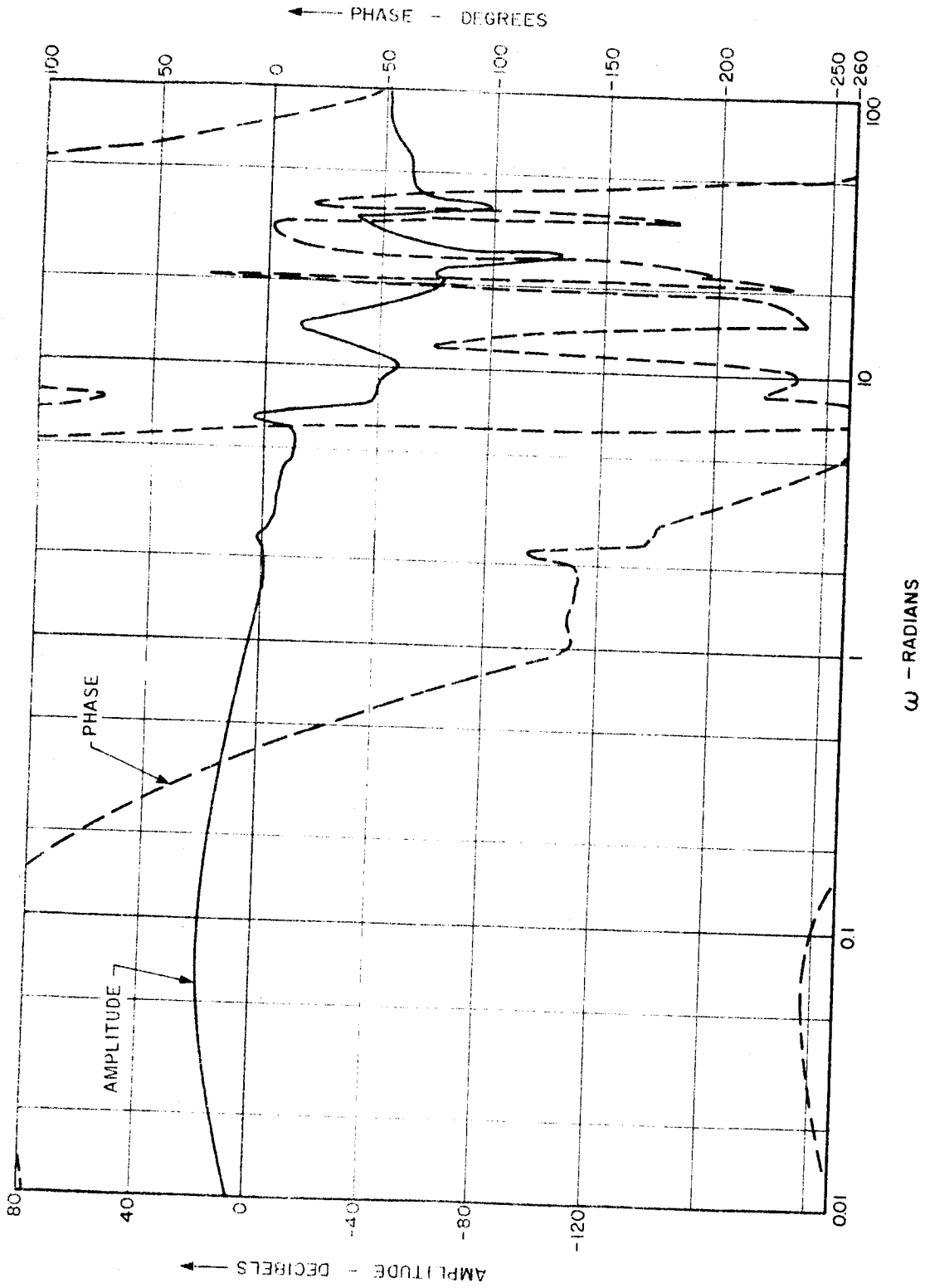


Figure 46. Open-Loop Frequency Response Corresponding to Computer Tolerance Run 11 ( $t = 40$  seconds)



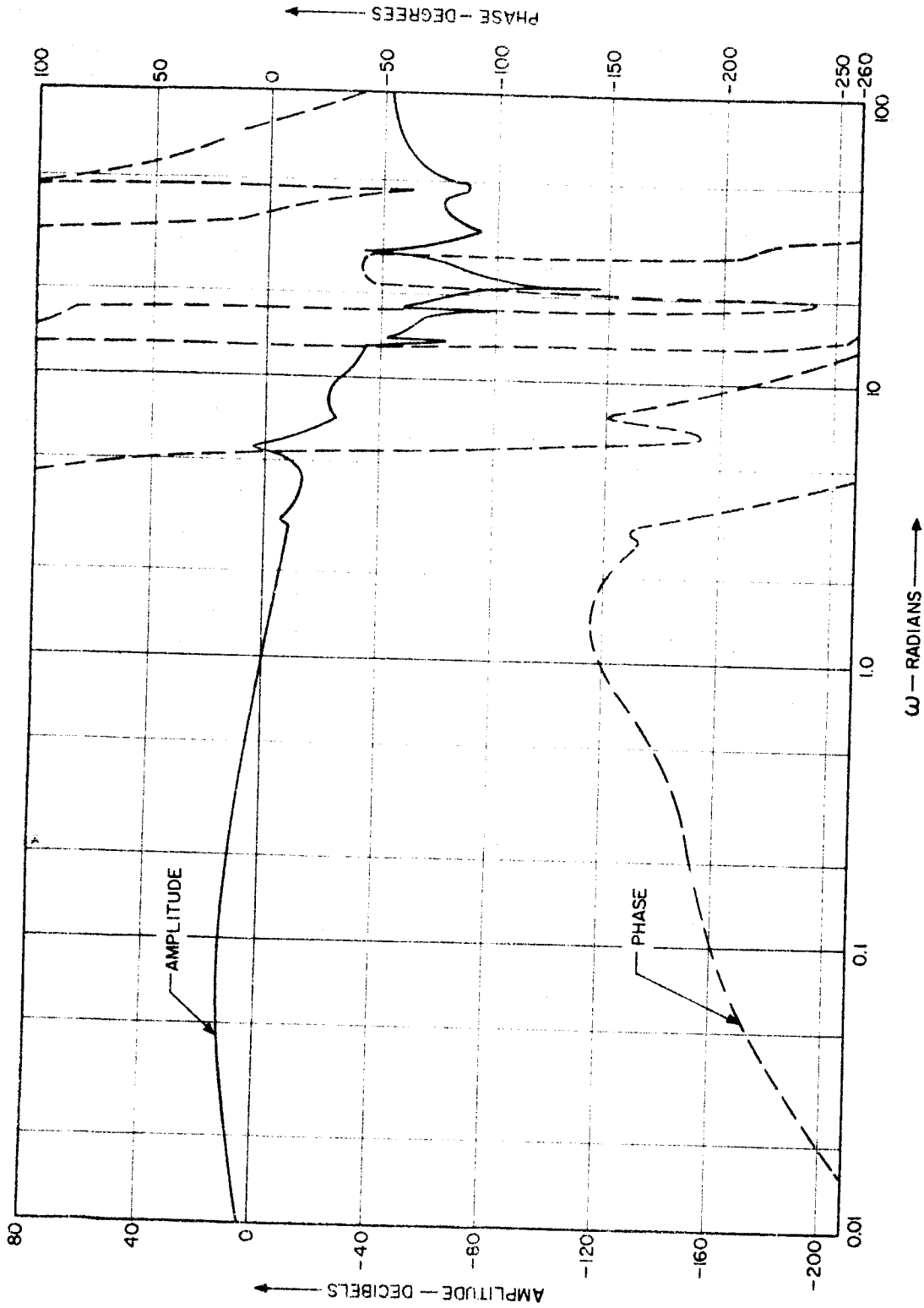


Figure 47. Open-Loop Frequency Response Corresponding to Computer Tolerance Run 12 ( $t = 79$  seconds)

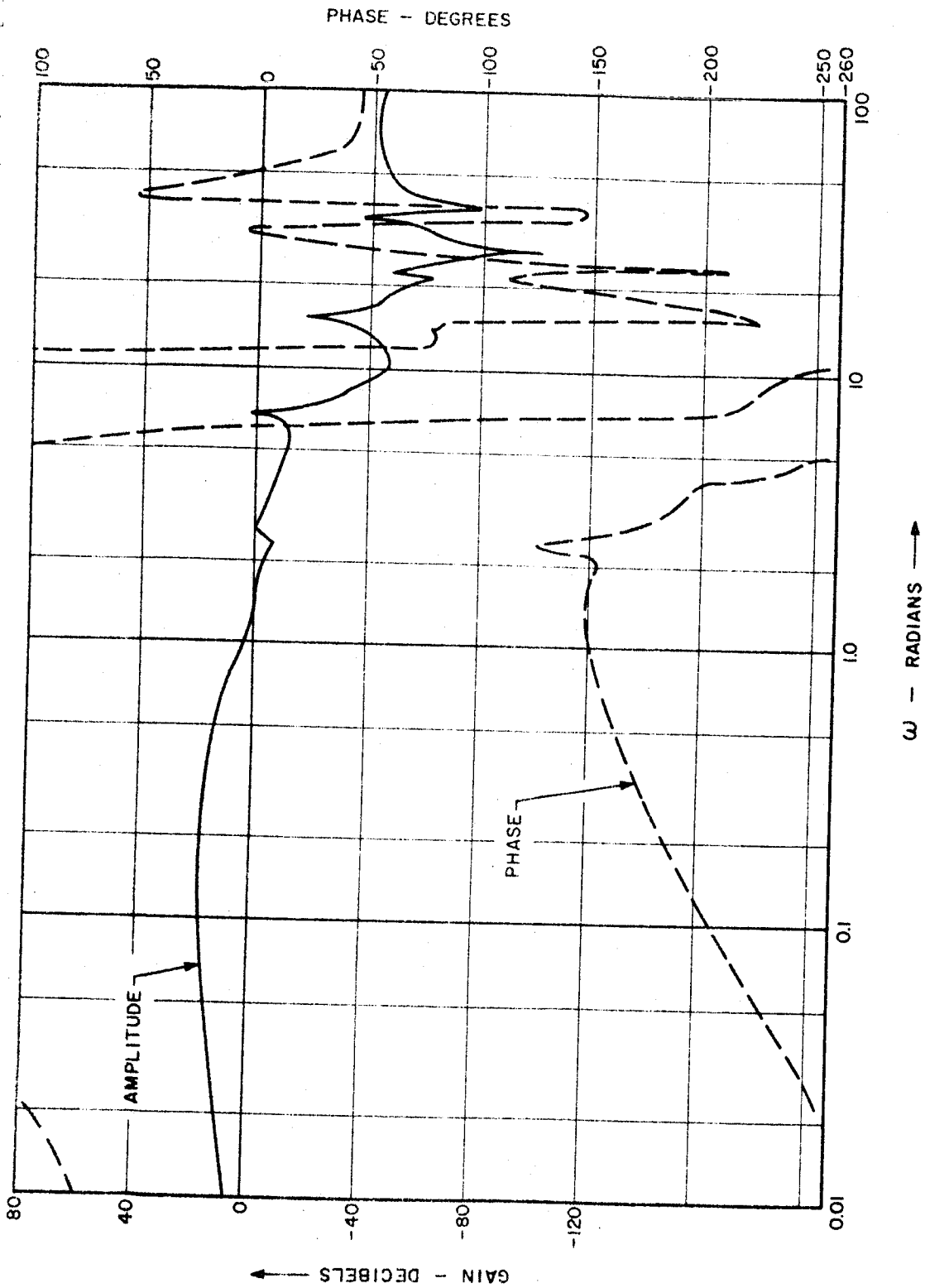


Figure 48. Open-Loop Frequency Response Corresponding to Computer Tolerance Run 22 ( $t = 79$  seconds)

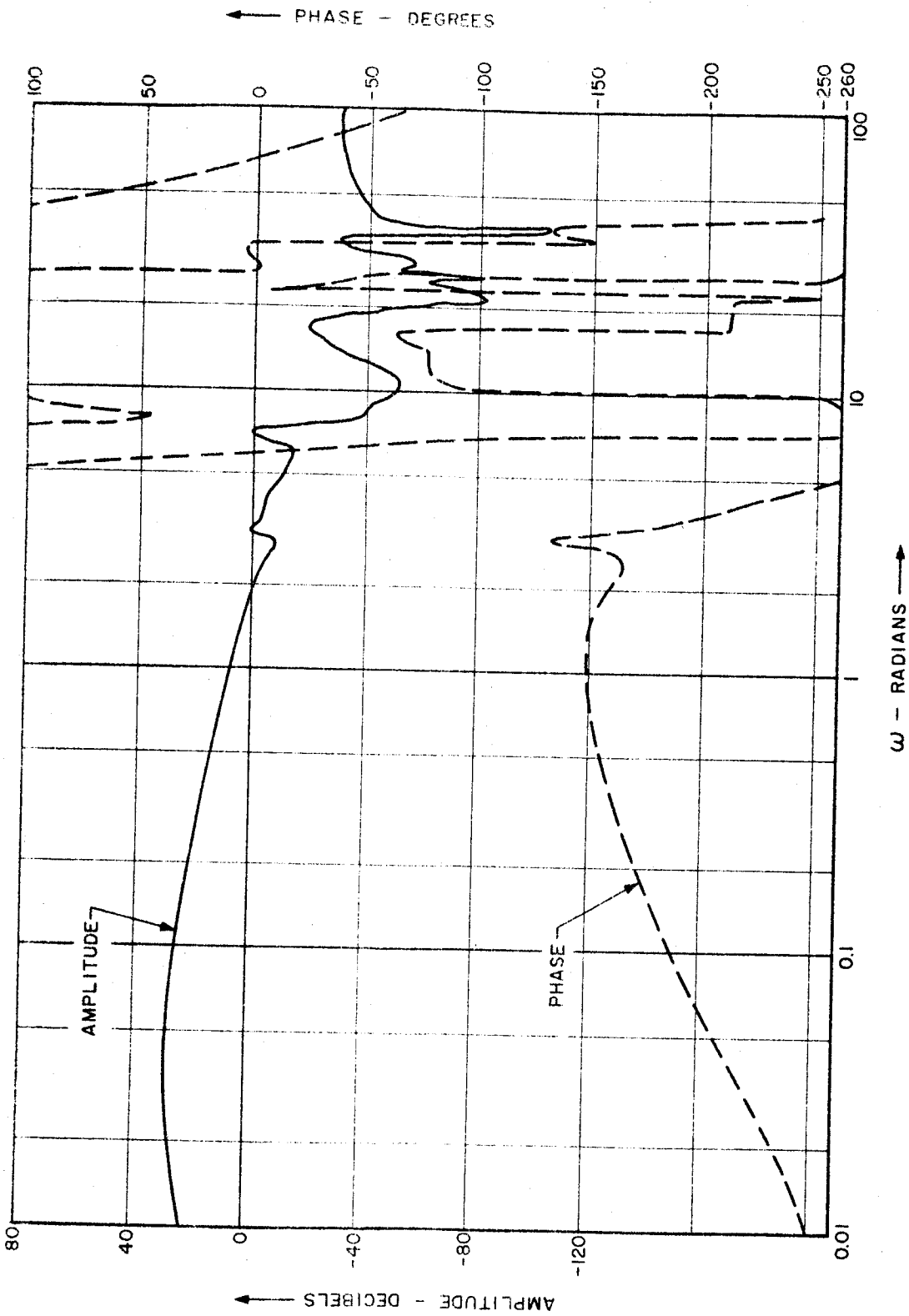


Figure 49. Open-Loop Frequency Response Corresponding to Computer Tolerance Run 11 ( $t = 120$  seconds)

## ANALOG ADAPTABILITY STUDIES

Any system which adapts itself to changes in a given parameter gives rise to the question: What is the largest parameter change for which the system continues to operate satisfactorily? To answer this question, analog computer studies were made in which the first bending mode slope and displacement were varied, and the resulting effect upon blender equilibrium position and critical gain was noted. (U)

The advantage of a gain-stable first bending mode over a phase-stable first mode has been discussed. By the definition of gain stability, the first mode zero has to be so close to the bending pole that first mode stability is independent of phase around the bending pole. This insensitivity to phase angle implies that the bending zeros can have any angular relationship to the poles as long as they stay within a certain radial distance of the poles. Therefore, since the only possible effect of changing first mode bending characteristics is to relocate the bending zero within the radius, it can be concluded that changes in the first mode bending characteristics do not affect the stability of a gain-stabilized blender system. (C)

This insensitivity to changing first mode characteristics is not shared by the phase-stabilized system developed in this study, and it was necessary to establish the adaptability of the phase-stabilized blender system when subjected to variations in the first bending mode pickup. The nine specific combinations of first mode characteristics tested are given in Table 12 together with the corresponding analog computer run number. (C)

The set of nine runs tabulated in Table 12 was made twice for the 79-second flight condition. One set was made for nominal values of all parameters except those first mode parameters listed in the table. Another set of runs was made for parameter values equal to tolerance computer run 12 (see Table 5) except for the first mode parameters. This second set was included because tolerance run 12 (low bending filter frequency, low slosh frequencies, high bending (C)

frequencies, high control moment coefficient, low aerodynamic moment coefficient, high control gains) presented probably the most marginally stable system at the slosh and first mode frequencies. (C)

Table 12. First Mode Tolerance Combinations Used in Analog Computer Adaptability Tests

Computer Run No.	First Mode Slope			First Mode Displacement Accelerometer
	Fwd Rate Gyro	Aft Rate Gyro	Position Sensor	
1	Nominal	Nominal	Nominal	Nominal
2	Nominal	Nominal	Nominal	150%
3	Nominal	Nominal	Nominal	0
4	50%	50%	50%	50%
5	400%	400%	400%	400%
6	400%	Nominal	400%	Nominal
7	Nominal	400%	Nominal	Nominal
8	Nominal	50%	Nominal	Nominal
9	50%	Nominal	50%	50%

(C)

The results of the analog computer adaptability tests are given in Tables 13 and 14. Each adaptability tolerance test was made for three blender positions:  $K = 0.4$  and  $0.6$  with the blender locked, and one run with the blender free to seek its equilibrium position. The critical value of gain at which the system became unstable was recorded for each blender position. Three blender positions were used because of the strong dependence of critical gain upon blender position (see Figure 16). The system was assumed to have failed the adaptability test if the value of  $K_{R_{crit}}$  is less than the nominal value ( $K_R = 0.8$ ). (C)

The two widely separated fixed blender position cases were included in each run to illustrate the difficulty in selecting one fixed position that will be adequate under all tolerance conditions and thus indicate the need for an adaptively changed blender position. (C)

Table 13. Results of Adaptability Studies, First Mode Variations with Other Parameters Nominal

Adaptability Run No.	Fixed Blender K = 0.400		Fixed Blender K = 0.6		Free Blender		
	$K_{R,crit}$	$\omega_{crit}$ (rad/sec)	$K_{R,crit}$	$\omega_{crit}$ (rad/sec)	$K_{R,crit}$	$\omega_{crit}$ (rad/sec)	Blender Equilibrium Position K
1	1.39	3.1	1.11	3.1	1.39	3.1	0.40
2	1.45	3.1	1.11	3.1	1.36	3.1	0.44
3	1.31	3.3	1.09	3.3	1.41	3.3	0.34
4	1.74	3.4	1.55	3.4	1.73	3.4	0.43
5	0.86	2.9	0.48*	3.0	1.15	2.1	0.36
6	0.555*	2.9	0.406*	2.9	1.03	2.9	0.17
7	0.07*	6.4	1.48	3.2	1.38	3.1	0.63
8	1.31	3.1	1.11	3.3	1.38	3.3	0.36
9	0.294*	6.3	1.64	3.3	1.73	3.3	0.525

\*Failed

Table 14. Results of Adaptability Studies, First Mode Variations with All Other Parameters Set to Tolerance Combination No. 12

Adaptability Run No.	Fixed Blender K = 0.4		Fixed Blender K = 0.6		Free Blender		
	$K_{R,crit}$	$\omega_{crit}$ (rad/sec)	$K_{R,crit}$	$\omega_{crit}$ (rad/sec)	$K_{R,crit}$	$\omega_{crit}$ (rad/sec)	Blender Equilibrium Position K
1	0.43*	6.9	1.04	2.7	1.13	2.8	0.48
2	0.26*	6.8	1.07	2.8	1.10	2.8	0.54
3	1.16	2.8	1.01	2.8	1.16	2.8	0.33
4	0.66*	6.8	1.98	3.7	1.21	2.8	0.49
5	0.14*	6.9	0.67*	2.6	0.37*	6.8	0.44
6	0.68*	2.9	0.65*	2.9	0.53*	6.9	0.185
7	0.06*	6.7	0.19*	6.9	1.17	3.1	0.665
8	1.68	3.3	1.01	2.9	1.13	6.9	0.37
9	0.25*	6.9	1.19	2.9	1.24	2.9	0.555

\*Failed

The results obtained in Table 13 (nominal parameters) present a strong case for adaptive action in that three failures occurred with the blender fixed at  $K = 0.40$  and two with the blender fixed at  $K = 0.6$ , while the adaptively changed blender position was never unstable. (C)

The results presented in Table 14 (worst case parameter tolerances) are not as overwhelming since the adaptive blender failed twice. However, this was still fewer failures than obtained with the fixed position of  $K = 0.6$  and a large improvement over the seven failures obtained with the fixed position of  $K = 0.40$ . (C)

Table 13 shows that the blender equilibrium condition varied from  $K = 0.17$  to  $0.64$  for variations in first mode parameters up to 400 per cent. Although only two fixed blender positions were used, the wide range of free blender positions indicates that no fixed blender position would have been adequate for stability with first mode variations of this magnitude. (C)

SECTION VII  
SAMPLE-HOLD FILTER ANALYSIS AND  
BREADBOARD EVALUATION

ANALYSIS

Analysis of the sample-hold filter, which was conceived and breadboarded by MSFC, was an important phase of this study contract. Valid analysis techniques for use with this filter were not available and therefore had to be developed. Upon deriving these analytical methods, it was found that the filter caused low-frequency phase shifts very similar to those obtained with linear second-order filters without appreciably increasing the high-frequency attenuations. Therefore, since the sample-hold filter offered no substantial advantage over simple linear filters, it was not used in conjunction with the gyro blender as originally planned.

The sample-hold filter concept has other possible uses, however. The filter may be mechanized rather easily, although a considerable amount of work on the design of the internal circuitry would be needed. The analytical methods developed during the study have been shown to be valid and may be used in further work.

Concept of the Sample-Hold Filter

The sample-hold filter was originally intended to be a sharp-cutoff low-pass filter. The basic approach was to sample a signal consisting of low and high frequencies in such a way that the output consisted of only the low frequencies.



Thus, the input is of the form

$$e_{in}(t) = f_1(t) + f_2(t) \quad (6)$$

in which  $f_1(t)$  is said to consist of low frequencies and  $f_2(t)$  to consist of high frequencies. The instant of time ( $t_s$ ) at which

$$f_2(t_s) = 0 \quad (7)$$

is defined as the sampling instant. The filter output at this instant is equal to the filter input, and at any time which is not a sampling instant the filter output is equal to the input at the preceding sampling instant. At  $t_s$  then,

$$e_{in}(t_s) = f_1(t_s) + f_2(t_s) \quad (8)$$

$$= f_1(t_s) \quad (9)$$

because  $f_2(t_s)$  is by definition zero.

Also at the sampling instant,

$$e_o(t_s) = e_{in}(t_s) \quad (10)$$

$$= f_1(t_s) \quad (11)$$

and between sampling instants the output is constant at the value of the input at the preceding sampling instant. The output is thus a stepwise approximation of the low frequency component of the input. An exaggerated drawing of the input and output voltages of this filter concept is shown in Figure 50.

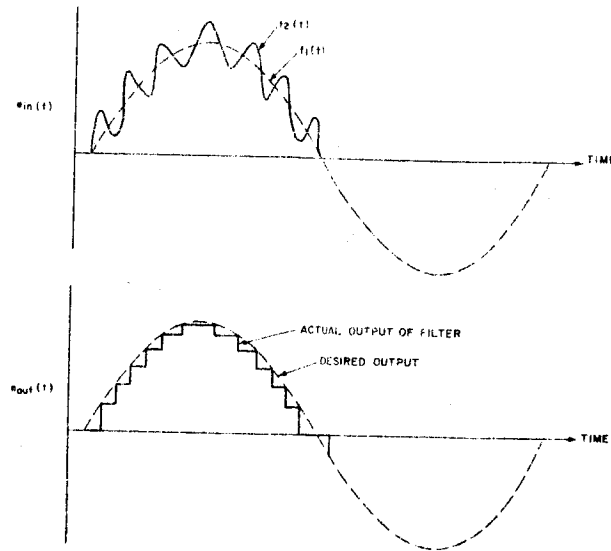


Figure 50. Sample-Hold Filter, Simplified Input-Output Relationship

### Block Diagram and Theory of Operation

A block diagram of the filter circuitry is given in Figure 51. The basic operation is as follows:

- When the high pass output goes through zero, the comparator output changes state.
- When the comparator output changes from positive to negative, the output of one-shot "A" becomes negative and stays negative for 0.5 second or until the comparator output becomes positive, whichever is sooner. When the comparator output changes from negative to positive, the output of one-shot "B" becomes negative and stays negative for 0.5 second or until the comparator output becomes negative, whichever is sooner.

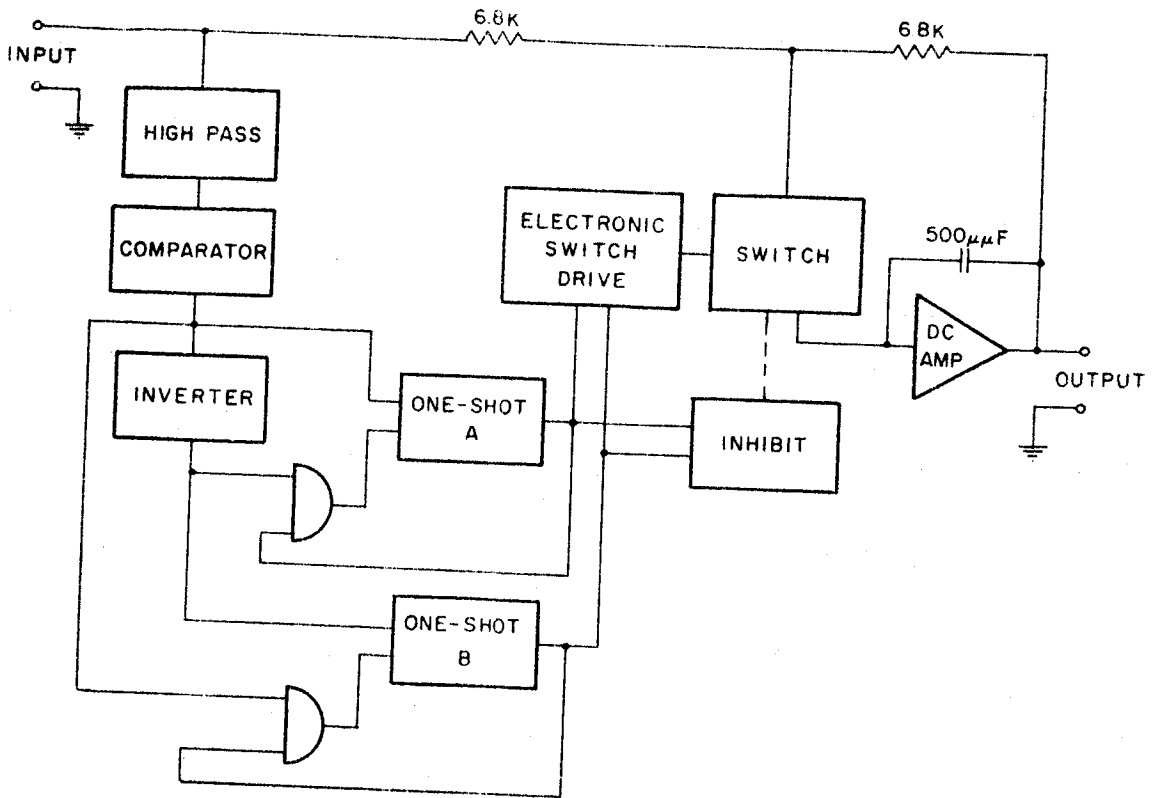


Figure 51. Sample-Hold Filter Block Diagram  
The 0.5-second period mentioned here is arbitrary corresponding to one half-cycle at the inhibit frequency (in this case 1 cps). By adjusting this arbitrary time period, the inhibit frequency may be adjusted at will.

The inhibit frequency is defined as that frequency of operation above which the filter will be in the sampling mode and below which the filter will be in the non-sampling mode.

- At frequencies above 1 cps, the one-shots are always turned off by the comparator, rather than by the built-in 0.5-second limit. This means that at all times there is a negative output from one one-shot or the other, and during switching periods

both have negative outputs. At frequencies below 1 cps, the one-shots are always turned off by the built-in 0.5-second limit, rather than by the comparator. This means that once each half-cycle both comparator outputs are zero and that at no time are they both negative.

- The inhibit circuit is set up so that when both one-shots are negative the switch will be put into the sampling mode if it is not already there. Conversely, when both one-shots are zero the electronic switch will be put into the non-sampling mode if it is not already there. Thus, when the input frequency is above 1 cps the filter is constantly in the sampling mode and when the input frequency is below 1 cps the filter is constantly in the non-sampling mode. Also, when there is a mixed frequency input, the filter will stay in the sampling mode as long as the input goes through zero at least every half-second. If two zero crossings are more than a half-second apart, the filter drops into the non-sampling mode and stays there until two zero crossings occur within a half-second period. It should be noted here that the half-second periods apply only to a 1-cps inhibit frequency, and that by adjusting this period, the inhibit frequency can be changed.

#### Analysis of the Sample-Hold Filter

A frequency response of the sample-hold filter can be determined by assuming single-frequency sine wave inputs and computing the resulting phase and amplitude of the fundamental component of the square-wave output. This analysis should be of value for studying system stability with the sample-hold filter. Consider the filter shown in Figure 52. The filter switching logic closes the sample switch whenever the high-pass output  $H \sin(\omega t + \theta_h)$  passes through zero. Assuming that the sampling duration is very short compared to the period of the input frequency  $\omega$ , and that the hold circuit has zero response

time, the output fundamental  $B \sin(\omega t + \theta_o)$  will either be in phase or 180 degrees out of phase with the high-pass output  $H \sin(\omega t + \theta_h)$ . The presence of the inhibitor circuit in the actual sample-hold filter which prevents sampling for frequencies less than about 1 cps and for small input amplitude will be ignored for the initial portion of this analysis.

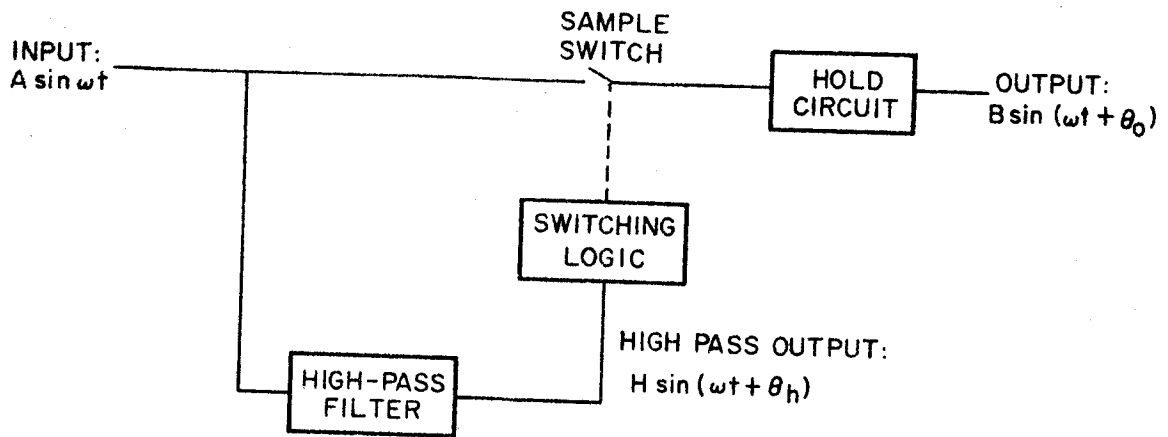


Figure 52. Sample-Hold Filter with Sine-Wave Input

The relationship between the phase angles  $\theta_o$  and  $\theta_h$  is evident from examination of the wave forms shown in Figure 53.

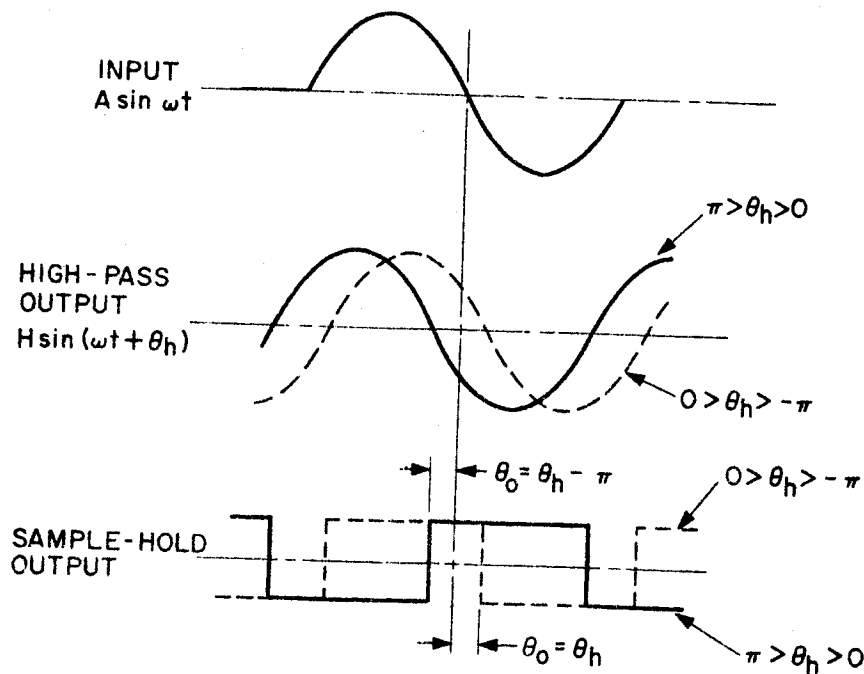


Figure 53. Sample-Hold Filter Phase Relationships

As defined by this figure,

$$\theta_o = \theta_h - \pi \quad (12)$$

where  $0 < \theta_h < +\pi$

$$\theta_o = \theta_h \quad (13)$$

and

where  $0 > \theta_h - \pi$

The fact that  $\theta_o$  is indeterminate at  $\theta_h = 0$  and  $\theta_h = \pi$  is of little consequence since the amplitude of the output signal (B) is zero for these conditions. With the above phase relationships, the sample-and-hold filter phase shift can be computed from the high-pass filter phase characteristics at a given input frequency.

The amplitude of the square-wave output will equal the value of the input at the sampling instant. The sampling instant ( $t_s$ ) occurs when the high-pass output is zero, or

$$\omega t_s + \theta_h = n \quad (14)$$

where  $n$  is any integer or zero.

$$\bar{B} = A |\sin \omega t_s| \quad (15)$$

where  $\bar{B}$  is the amplitude of the square wave output.

Combining Equations (14) and (15)

$$\bar{B} = A |\sin(n\pi - \theta_h)| = A |\sin \theta_h| \quad (16)$$

From Equations (6) and (7), an alternate expression may be derived:

$$\bar{B} = A |\sin \theta_o| \quad (17)$$

The amplitude of the fundamental component (B) of the output square wave is found by Fourier analysis to be:

$$B = \frac{4\bar{B}}{\pi} \quad (18)$$

Hence, the amplitude response of the sample-and-hold filter from Equations (16), (17), and (18) is:

$$\frac{B}{A} = \frac{4}{\pi} |\sin \theta_h| \quad (19)$$

$$= \frac{4}{\pi} |\sin \theta_o| \quad (20)$$

It is evident from the above analysis that the gain and phase of the sample-and-hold filter are completely determined by the phase of the high-pass filter. Hence this phase characteristic is a primary design consideration. Note that the amplitude characteristic of the high pass is important only for multiple frequency inputs and, hence, for transient system performance.

Consider now the application of Equations (18) and (19) to a sample-and-hold filter having a second-order high-pass characteristic with a damping ratio of 0.2. The phase of this high pass decreases from +180 degrees at  $\omega = 0$  to zero degrees at  $\omega = \infty$ . Thus, in accordance with Equation (12), the output phase with respect to the input will vary from zero to -180 degrees. The gain will exhibit a bandpass characteristic in accordance with Equation (19). A frequency response plot of this situation is shown in Figure 54.

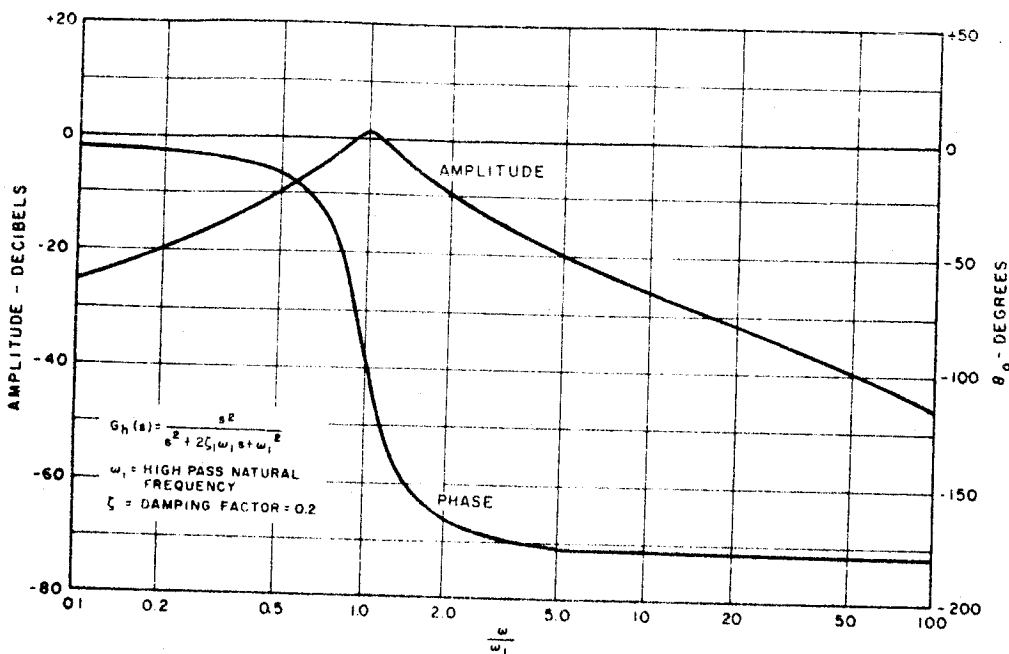


Figure 54. Sample-Hold Filter Frequency Response for Single-Frequency Input, No Inhibit

To obtain the desired low-pass characteristic, the frequency-sensitive inhibitor is added to the sample-and-hold filter, with the sampler activation point set at some selected frequency above the high-pass natural frequency. Since the inhibitor switches the sample-and-hold filter from the sampling mode to a regular amplifier when the period between samples increases beyond a pre-set value, the frequency response will exhibit zero phase shift and unity gain for all frequencies below the inhibit frequency. Above the inhibit frequency the gain and phase will assume the values given by the sample-and-hold analysis. The addition of the inhibitor to the filter response of Figure 54 is shown in Figure 55, where the inhibit frequency is set 40 per cent above the high-pass natural frequency.

The most evident limitation to this type of analysis is the assumption of a single input frequency. However, assuming a multiple frequency input of the form

$$e_{in}(t) = f_1(t) + f_2(t)$$



where

$$f_1(t) = A \sin \gamma t$$

$$f_2(t) = B \sin \lambda t$$

$\gamma <$  the inhibit frequency

$\lambda >$  the inhibit frequency

$\lambda \gg \gamma$

and assuming a high-pass filter with transfer function  $G_h(s)$ , then given

$$E_{in}(s) = F_\gamma(s) + F_\lambda(s) \tag{22}$$

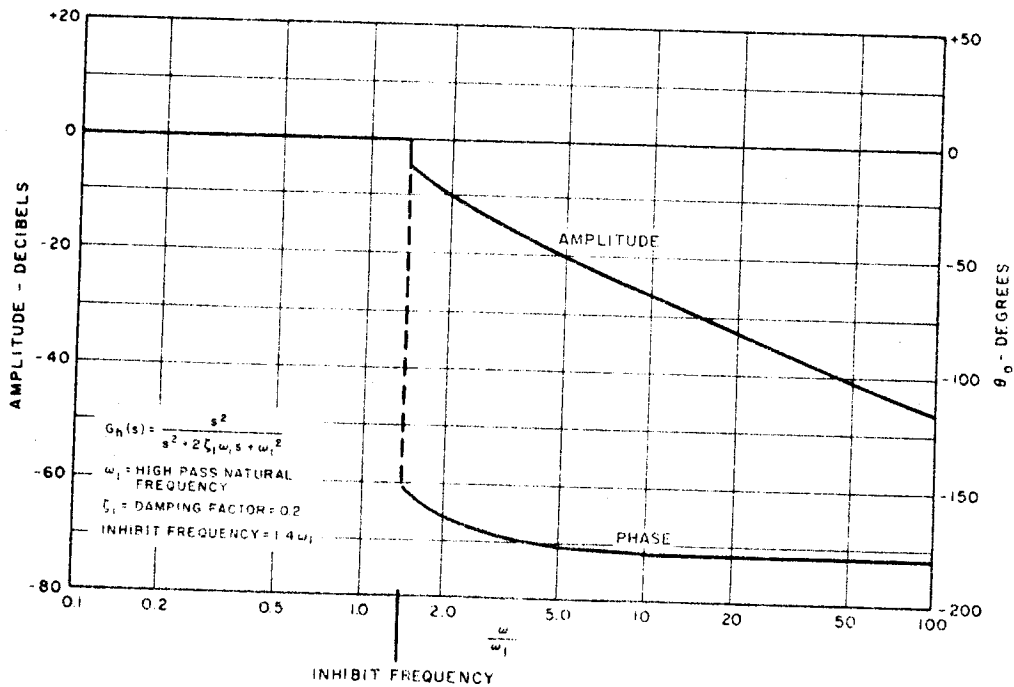


Figure 55. Sample-Hold Filter Frequency Response for Single-Frequency Input Only

The high-pass output is

$$\begin{aligned} E_{oh}(s) &= E_{in}(s) G_h(s) \\ &= F_{\gamma}(s) G_h(s) + F_{\lambda}(s) G_h(s) \\ &= F_{\gamma_1}(s) + F_{\lambda_1}(s) \end{aligned} \tag{23}$$

and

$$e_{oh}(t) = f_{\gamma_1}(t) + f_{\lambda_1}(t) \tag{24}$$

where

$$f_{\gamma_1}(t) = A \sin(\gamma t + \theta_h)$$

$$f_{\lambda_1}(t) = f_{\lambda}(t)$$

because the frequency of  $f_{\lambda}(t)$  is high enough that the high-pass filter has essentially no effect on  $f_{\lambda}(t)$ .

Sampling instant  $t_s$  is defined as the time at which the high-pass output is zero, or

$$e_{oh}(t_s) = 0 \tag{25}$$

so that

$$f_{\gamma_1}(t_s) + f_{\lambda_1}(t_s) = 0 \tag{26}$$

Since  $f_{\lambda_1}(t) = f_{\lambda}(t)$

$$f_{\gamma_1}(t_s) + f_{\lambda}(t_s) = 0 \tag{27}$$

and

$$f_{\lambda}(t_s) = -f_{\gamma_1}(t_s) \tag{28}$$

At the sampling instant then,

$$\begin{aligned} e_{in}(t_s) &= f_{\gamma}(t_s) + f_{\lambda}(t_s) \\ &= f_{\gamma}(t_s) - f_{\gamma_1}(t_s) \end{aligned} \tag{29}$$

and, assuming a perfect sample-and-hold function,

$$\begin{aligned} e_o(t_s) &= e_{in}(t_s) \\ &= f_{\gamma}(t_s) - f_{\gamma_1}(t_s) \end{aligned} \tag{30}$$

With  $\lambda \gg \gamma$ , and assuming that the high-frequency amplitude dominates the high-pass output so that the sampling interval is always small compared to the period of  $\gamma$ , the output can be approximated as linear, rather than step-wise, and equal to  $e_o(t_s)$  at the sampling instants. By this approximation,

$$e_o(t) = f_a(t) - f_{a_1}(t) \tag{31}$$

$$\begin{aligned} E_o(s) &= F_Y(s) - F_{Y_1}(s) \\ &= F_Y(s) - F_Y(s) G_h(s) \\ &= F_Y(s) [1 - G_h(s)] \end{aligned} \tag{32}$$

so that

$$\frac{E_o(s)}{F_Y(s)} = 1 - G_h(s) \tag{33}$$

which indicates that the output wave shape is related to the low-frequency input wave shape by a function of the high-pass transfer function. This function is plotted in Figure 56 for the high pass used for calculating Figure 54. Figure 56 is extended to 100 cps, with the assumption that sampling is always taking place at a much higher frequency than that in question. Combining the portion of Figure 54 above the inhibit and the portion of Figure 56 below the inhibit yields Figure 57. This figure shows filter operation below the inhibit with constant sampling due to a high frequency on the input, and the attenuation of a high frequency input above the inhibit frequency.

The characteristic of Figure 57 indicates that the sample-hold filter, with a second-order high-pass, does not give as good operation as would a linear second-order low-pass filter. A slight delay between the high-pass output and the sampler can result in greater attenuation for some frequencies but has deleterious effects at the higher frequencies, as will be seen later. However, since the attenuation of the filter is dependent on the high pass, a change of high-pass design to give a phase shift which approaches zero more rapidly should give better attenuation characteristics. To obtain this aim, and to give more flexibility in high-pass design, the basic second-order high pass may be changed to

$$G_h(s) = \frac{s(s + \omega_2)}{s^2 + 2\zeta_1 \omega_1 s + \omega_1^2} \tag{34}$$

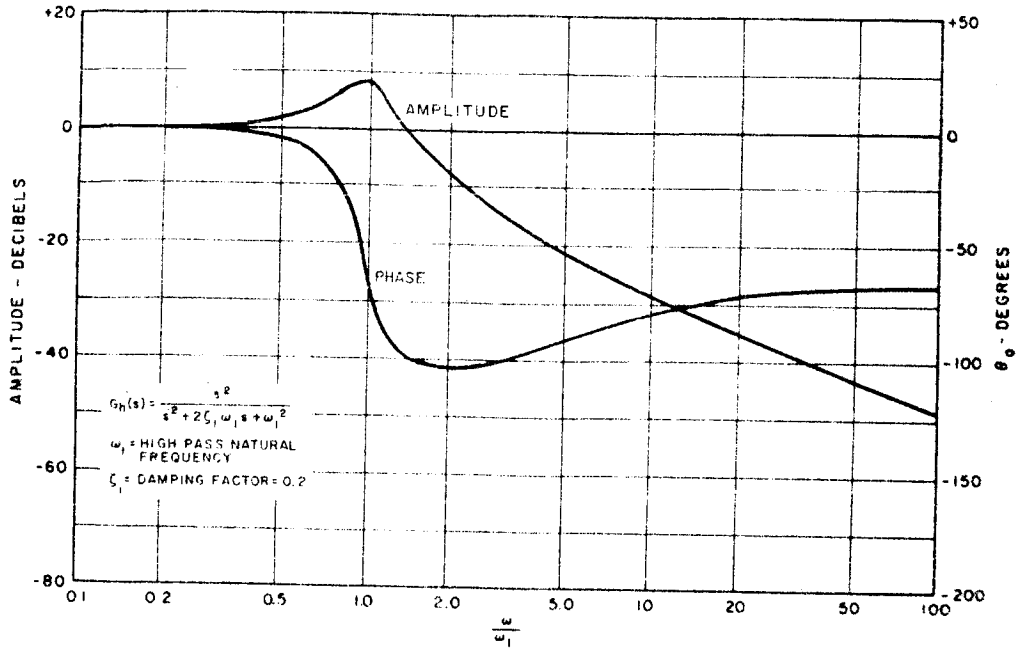


Figure 56. Sample-Hold Filter Frequency Response of Low-Frequency Output to Low-Frequency Input, with Constant High-Frequency Sampling

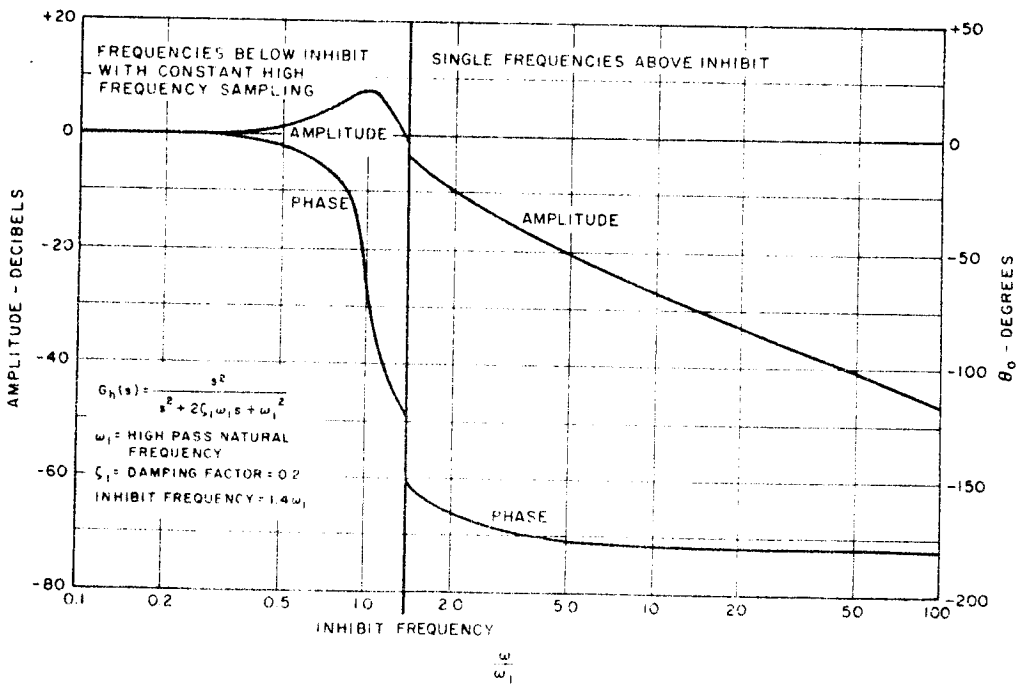


Figure 57. Sample-Hold Filter Composite Frequency Response

which is essentially the second-order high pass with a lag-lead added, as in

$$G_h(s) = \left( \frac{s^2}{s^2 + 2\zeta_1 \omega_1 s + \omega_1^2} \right) \left( \frac{s + \omega_2}{s} \right) \quad (35)$$

By making this addition to the high pass used to construct Figures 54 through 57, and by setting  $\omega_2$  equal to  $0.4 \omega_1$ , the frequency response of Figure 58 may be constructed analogous to Figure 54. Adding the inhibitor to the response of Figure 58 results in Figure 59, a frequency response of the system to single-frequency inputs only, for the given high pass.

If a multiple frequency input is again assumed, with sampling constantly taking place at the higher frequency, the previous analysis resulting in Equation (33) is applicable and the function  $[1 - G_h(s)]$  may be plotted for this high pass, as in Figure 60. Combining Figures 58 and 60 results in Figure 61, which is a composite frequency response of the same type as Figure 57. It can be seen in Figure 61 that with a high pass of this type a good attenuation characteristic can be obtained above the inhibit frequency. However, a slight amount of delay between the high-pass output and the sampler can result in a great amount of change in the frequency response characteristics.

The amplitude expression

$$\frac{B}{A} = \frac{4}{\pi} |\sin \theta_h|$$

as given in Equation (13) assumes sampling immediately when the high-pass output goes through zero. A delay between the high-pass zero crossing and the time the sample was taken would have the same effect as an increase in phase lag in the high pass. For a delay time  $\tau_d$  the amplitude response expression then becomes

$$\frac{B}{A} = \frac{4}{\pi} \sin(\theta_h - \omega \tau_d) \quad (36)$$

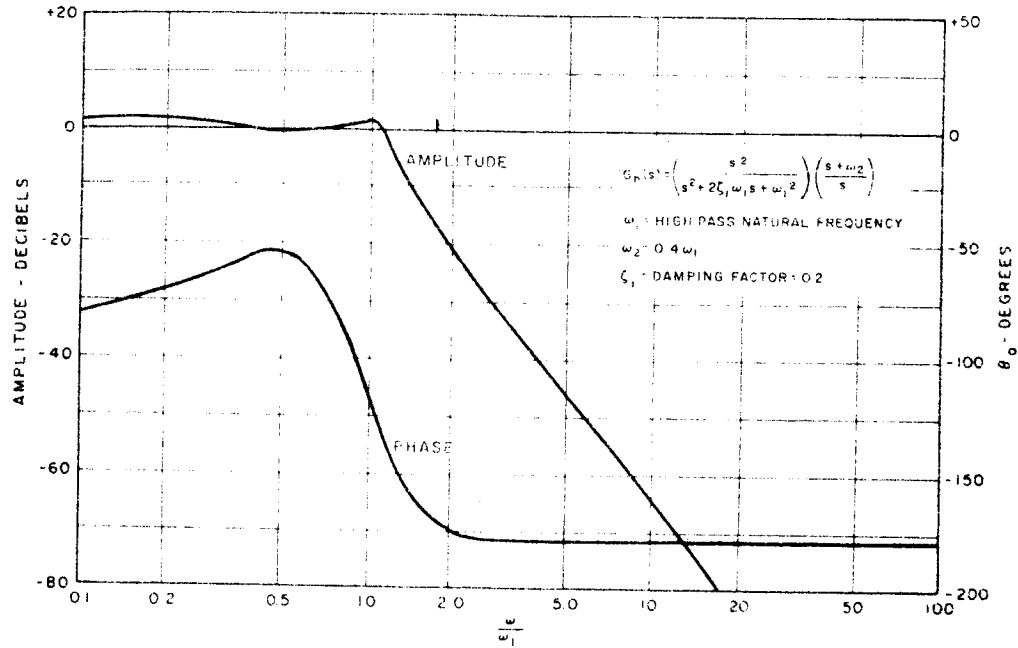


Figure 58. Sample-Hold Filter Frequency Response for Single-Frequency Input, No Inhibit

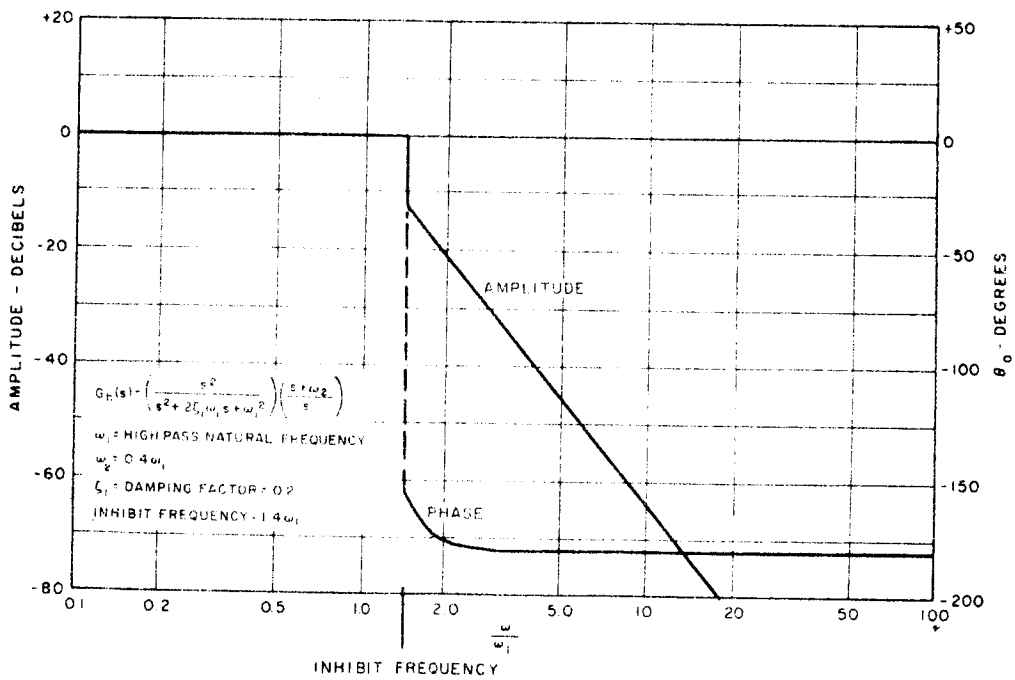


Figure 59. Sample-Hold Filter Frequency Response for Single-Frequency Input Only

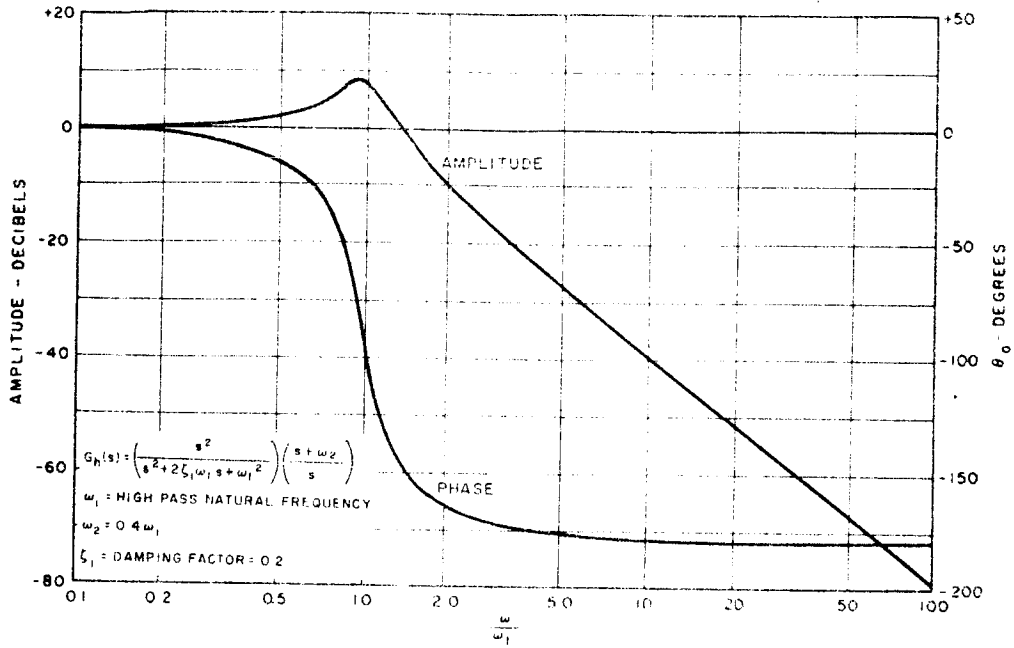


Figure 60. Sample-Hold Filter Frequency Response of Low-Frequency Output to Low-Frequency Input, with Constant High-Frequency Sampling

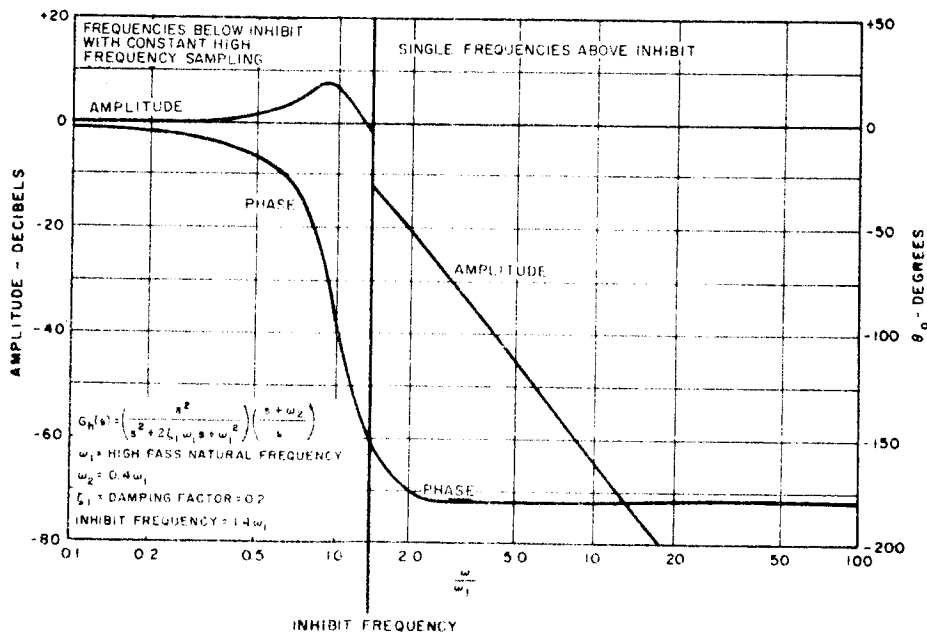


Figure 61. Sample-Hold Filter Composite Frequency Response



for frequency  $\omega$  in radians per second. Figure 62 shows the composite frequency response plot of Figure 60 with the above inhibit portion changed by the addition of a delay time of 0.01 per cent of the period of inhibit frequency. The sharp notch shown here occurs when the effective high-pass phase passes through zero and the output amplitude is zero. The effective high-pass phase is

$$\theta_h = \omega \tau_d$$

as used in the expression above. At the frequency where the leading high-pass phase angle is equal in length of time to the sampling delay time, the sampler takes a sample exactly when the input is zero and thus the output for this frequency is zero. Above this frequency, however, the effective high-pass phase increases with increasing frequency as  $\tau_d$  becomes a larger percentage of the period, and attenuation becomes poorer and poorer. Also at this point the output phase takes a sharp jump of 180 degrees according to Equations (12) and (13). A 100-microsecond delay time is a realistic figure for this device.

If the high pass of Equation (35) is chosen so that the total phase passes through zero to the lagging side and then approaches zero, this problem of a delay causing radical changes in output characteristics can be diminished. In Figure 63 the high pass used is of the form of Equation (35) with  $\omega_2$  set at  $0.247\omega_1$  and a damping factor  $\zeta = 0.1$ . In this case the high-pass phase passes through zero at  $\omega = 2.48\omega_1$ , resulting in an amplitude notch and an output phase jump at that frequency. If the inhibit is then set at  $2.54\omega_1$  the frequency response is as given in Figure 64, for single-frequency inputs. In this case the transfer function below inhibit is unity, and above inhibit the phase shift is almost negligible; attenuation is above 40 decibels for all frequencies. Of course, for multiple-frequency inputs as discussed for the other high-pass configurations, the expression of Equation (33) holds true, resulting in Figure 65. Because of the low damping factor of the high pass, a very high peak is seen at the high-pass natural frequency. If Figures 64 and 65 are combined, the composite frequency response of Figure 66 is the result.

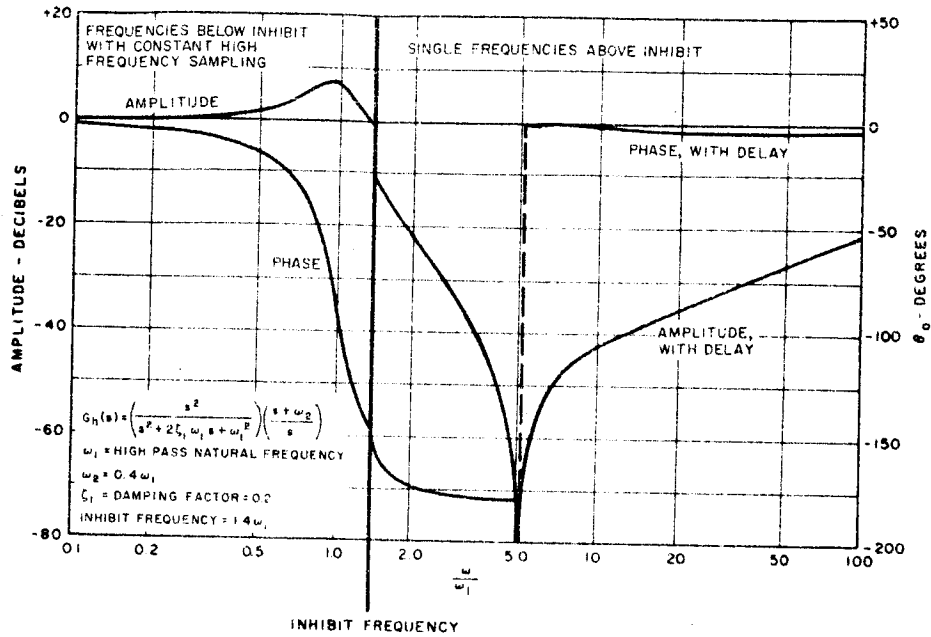


Figure 62. Sample-Hold Filter Composite Frequency Response with Sampling Delay of 0.01 Per Cent of the Period of the Inhibit Frequency

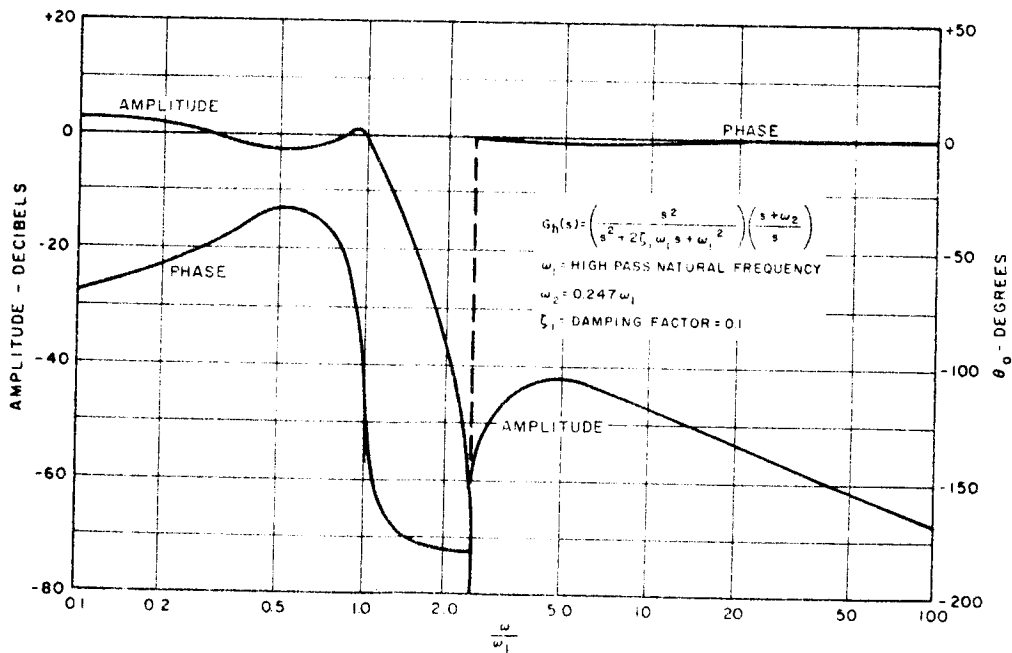


Figure 63. Sample-Hold Filter Frequency Response for Single-Frequency Input, No Inhibit

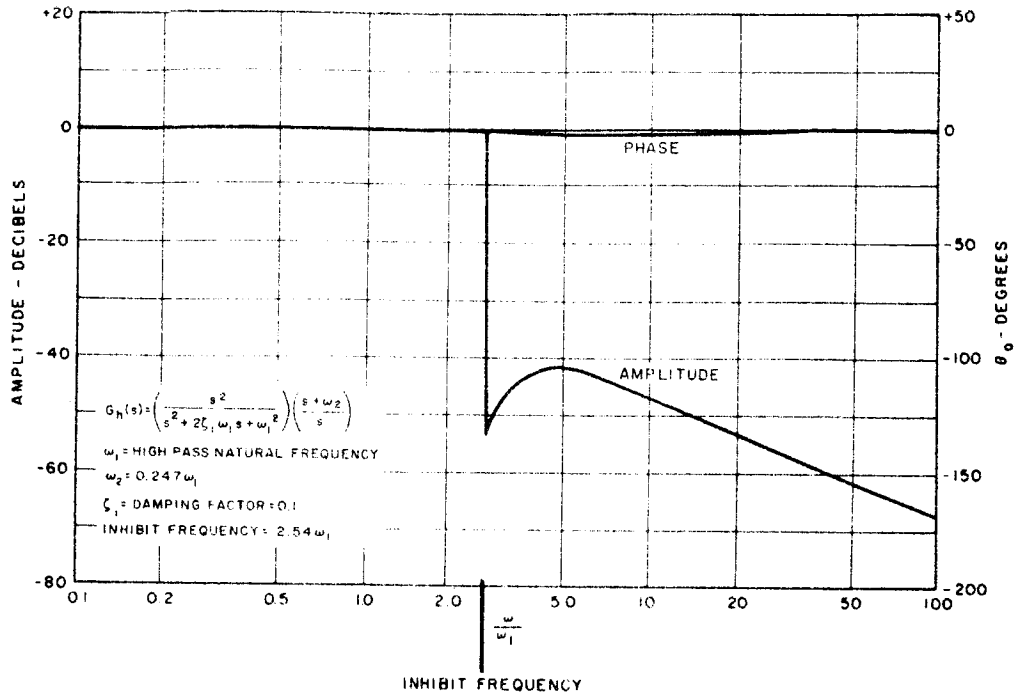


Figure 64. Sample-Hold Filter Frequency Response for Single-Frequency Input Only

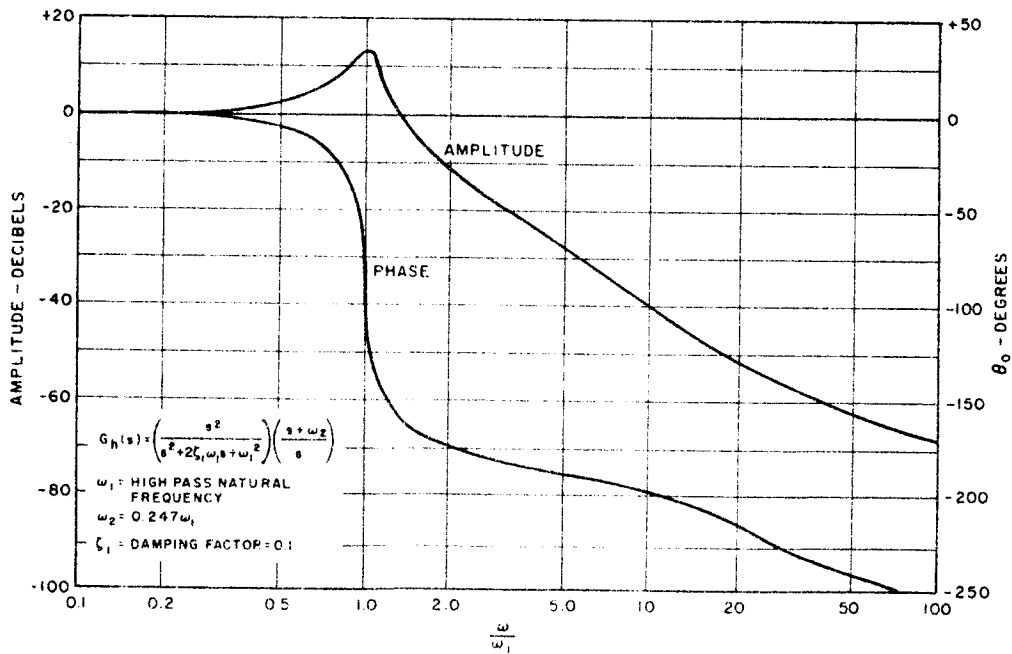


Figure 65. Sample-Hold Filter Frequency Response of Low-Frequency Output to Low-Frequency Input, with Constant High-Frequency Sampling

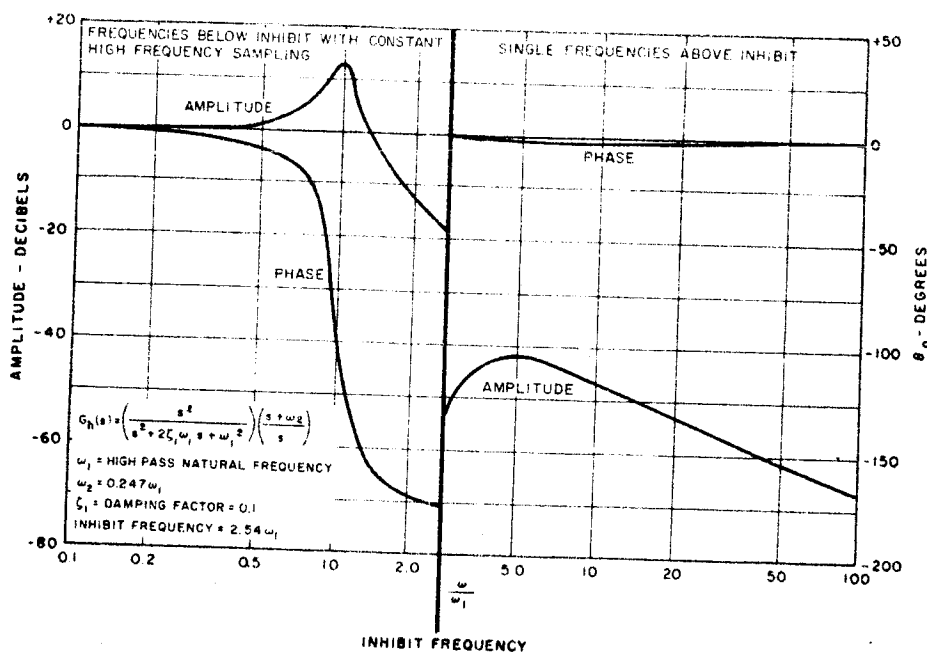


Figure 66. Sample-Hold Filter Composite Frequency Response. The accuracy of this type of analysis can be demonstrated by putting the sample-and-hold filter in a closed loop with a first-order lag. If the input to this system is a frequency high enough to cause sampling, the system should perform according to Figure 67, which is a combination of the composite frequency response of Figure 66, and the frequency response of a first-order lag whose break frequency is 50 per cent above the inhibit frequency. This figure indicates that the system should become unstable at 0.5 cps, and analog studies of the system correspond with this prediction.

If a delay of 0.01 per cent of the period of the inhibit frequency is added to the portion of this figure above inhibit, the result is as shown in Figure 68. The sharp amplitude notch is not seen in this case because the delay is only adding a little more lag to an already lagging phase. This decreases the attenuation somewhat, but does not radically change the shape of the curve.

A comparison of the composite frequency responses include here (Figures 57, 61, and 66) with linear low-pass frequency responses of the same order and with the same damping factor as the particular high passes, shows that little is gained by using a nonlinear instead of a linear filter.

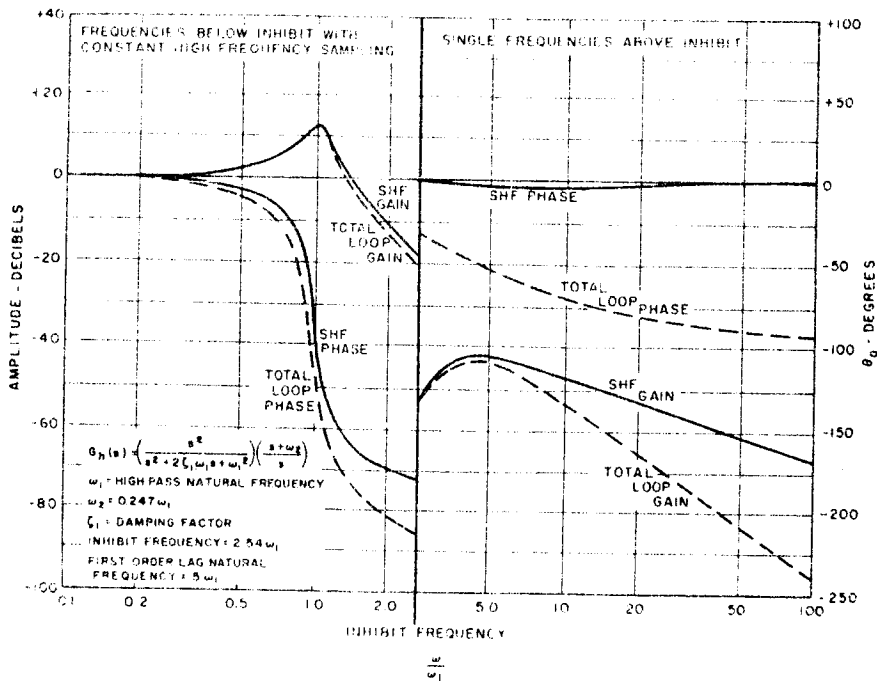


Figure 67. Composite Frequency Response for First-Order Lag Plus Sample-and-Hold Filter with High-Frequency Input to Cause Constant Sampling

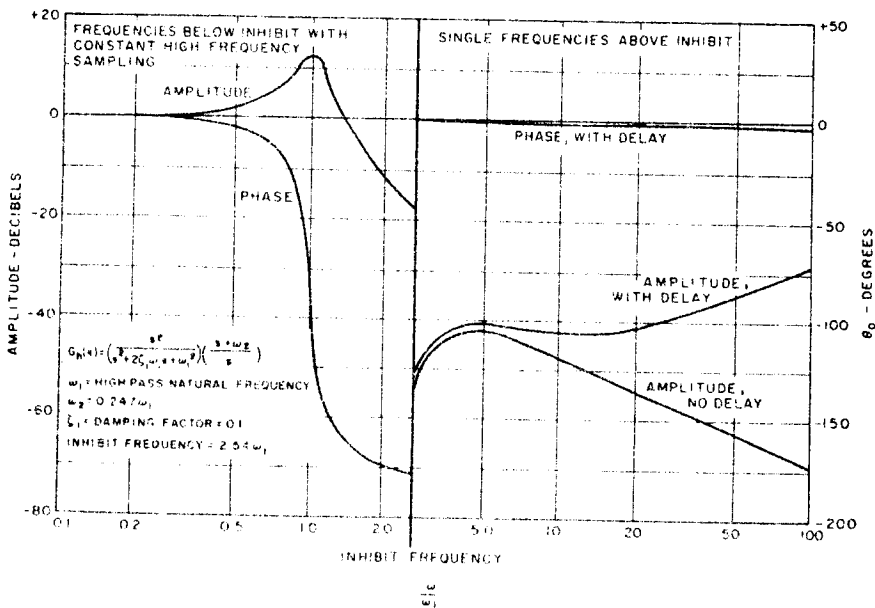


Figure 68. Sample-and-Hold Filter Composite Frequency Response with Sampling Delay of 0.01 Per Cent of the Period of the Inhibit Frequency

An attempt was made to use z-plane analysis on the sample-hold filter, in addition to the above describing function analysis, but no usable way was found to take the high pass into account. Since the above analysis and analog results indicated that performance was critical with respect to the particular high pass being used, the z-plane analysis was discontinued. A description of the z-plane methods tried is included in Section VIII.

### BREADBOARD EVALUATION AND MODIFICATIONS

Several problem areas were discovered during evaluation of the sample-hold filter breadboard: (a) time delay in sampling zero crossings of the high-pass filter output, (b) static and dynamic imbalance in the gate circuit resulting in d-c output bias and sampling errors. Several filter modifications were made for evaluation purposes:

- Bias adjustments and trim potentiometers were added to the comparator input, gating circuit, and reference shifting circuit.
- The differentiation circuit was modified to reduce the sampling time.
- The gating circuit was redesigned to improve operation, mainly by eliminating large changes in output voltage as the inhibit relay operated.
- The comparators were modified to eliminate time delay and minimize transient oscillations.

SECTION VIII  
DESIGN DIFFICULTIES ENCOUNTERED

The purposes of this section are (1) to describe some of the difficulties encountered that required extensive system changes to correct and (2) to describe the "blind-alley" approaches tried so that future study programs can take advantage of the knowledge gained. This section discusses the following items:

- a. Instability caused by blender
- b. First mode gain stability
- c. Sample-hold filter z-plane analytic techniques
- d. Recommendations for conducting future studies (C)

INSTABILITY CAUSED BY BLENDER

The very first attempts to operate the system with a simulated blender gain changer operating adaptively were unsuccessful because the basic control appeared to be too sensitive to gyro blender position. This situation had an undesirable effect on the gyro blender gain-changing intelligence because blender gain changes affected the bending content of the feedback signals more by the change in oscillation frequency than by the change in signal magnitude provided by the blender gains ( $K$  and  $1-K$ ). A frequency response test was run on the analog simulation by inserting a sinusoidal engine angle ( $\beta$ ) signal into the closed-loop system (rigid body, tail-wag-dog zeros, first bending mode) operating at nominal gains, and with the gyro blender gain fixed at 0.5. The output signals observed corresponded to forward and aft sensor signals,  $|\varphi_{FF}| / |\varphi_{FA}|$ , is shown in Figure 69, where the critical frequencies for blender gains of 0.5 and 0.6 are also noted. (C)

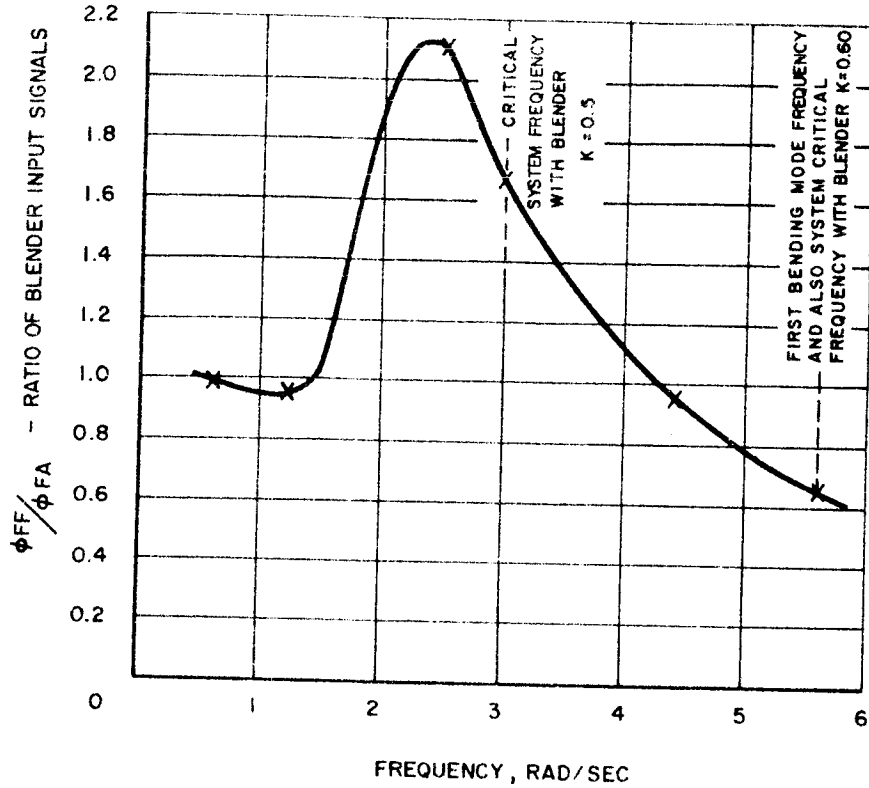


Figure 69. Frequency Response Results for Engine Angle Disturbances in a System Containing Rigid Body with Second-Order Model, Tail-Wag-Dog Zeros, and First Bending Mode at Maximum Dynamic Pressure

Assuming that K is at equilibrium at a value of 0.60 and that  $|\phi_{FA}|$  is equal to 1 so that  $|\phi_{FF}|$  is equal to the ratio  $|\phi_{FF}| / |\phi_{FA}|$ , then (from Figure 69)  $|\phi_{FF}|$  is equal to 0.67. Thus, the gain-changing logic equation,

$$\text{Error signal} = |\phi_{FF}| (K) - |\phi_{FA}| (1 - K)$$

gives

$$\text{Error signal} = (0.67)(0.60) - (1.0)(0.40) = 0.40 - 0.40 = 0 \quad (C)$$

Now if the blender were transiently displaced to 0.5 and if, as is normally the case, the ratio  $|\phi_{FF}| / |\phi_{FA}|$  were not a function of blender position, the error signal would be

$$\text{Error signal} = (0.67)(0.5) - (1.0)(0.5) = 0.335 - 0.500 = -0.165 \quad (C)$$



In this case, however, the ratio  $|\varphi_{FF}| / |\varphi_{FA}|$  is a function of blender position. The specific value for a blender position of 0.5 can be determined from Figure 69 by first determining the system crossover frequency using a root-locus plot made with a blender position of 0.5. This frequency was 3.0 radians per second as indicated on Figure 69, and therefore  $|\varphi_{FF}| / |\varphi_{FA}|$  at this frequency is 1.65. (C)

Substituting this value into the error signal equation gives the following result:

$$\text{Error signal} = (1.65)(0.5) - (1.0)(0.5) = 0.825 - 0.500 = +0.325 \quad (C)$$

Thus, in the normally expected case for this example, the error signal is negative and tends to drive the blender in one direction; but in the given case it is positive and tends to drive the blender in the opposite direction. Obviously, both cannot be correct. Since the fault was that the ratio  $|\varphi_{FF}| / |\varphi_{FA}|$  was a function of blender position, the remedy lay in making the basic system stability points less sensitive to blender position. This sensitivity to blender position was found to be a function of the phase near the first mode frequency (neglecting any phase variations due to the first mode itself). A lead network, providing about 40 degrees of phase lead at the first mode frequency, was added to the forward loop and the problem disappeared. (C)

While in this instance the phase field was such that the blender position was "statically unstable", the same reasoning process could be applied to a system to show how this sensitivity to blender position is beneficial because it is forcing the blender position to go to its equilibrium gain faster than it normally would. This would have happened if in Figure 69 the ratio of  $|\varphi_{FF}| / |\varphi_{FA}|$  at 3.0 radians had been lower than at 5.6 radians. (C)

No firm design guideline can be formulated to circumvent this situation. The system apparently should be designed without regard to it, as suggested previously; and then if a problem exists, the phase field about the first mode can be altered either by changes in system filtering or by sensor relocations. (C)

## FIRST MODE GAIN STABILITY

First bending mode gain stability is very desirable in that the range of allowable first mode slopes and deflections is increased as the bending pole is more nearly cancelled. It can readily be seen that if the first mode poles are completely cancelled, the control system will be unaffected by infinite changes in first mode bending characteristics. (C)

The present study indicated that the mechanization problems involved in converting the blender into a device which could reliably gain-stabilize the first mode were too formidable to permit such conversion at this time. (C)

The specific problem areas are summarized below. Gain stability can be obtained only if both of these problem areas are resolved:

1. The bandpass amplifier must have a tracking gain accuracy of between 0.5 and 1.0 per cent, which must be maintained over the entire environmental range. This degree of accuracy is presently unobtainable in practical hardware designs.
2. An equally stringent requirement is placed on the phase alignment between the feedback signals being blended. Examination of System I indicated that the phase angle between the blender signals could not be greater than  $\pm 22$  arc-minutes. This value is the total range, meaning that measurement and phase changing device accuracies must be considerably better. The practical difficulties involved in measuring and changing phase angles of this magnitude are beyond the present state of the art. (C)

The phase accuracy requirement is strongly dependent on the control system used; e. g., if no attitude or accelerometer signals were used, no strong out-of-phase bending components would be present. Therefore, no universally applicable accuracy requirement can be formulated, although it is felt that the problem would not be changed significantly even if an order-of-magnitude increase in phase angle tolerance were obtained. (C)

## Z-PLANE ANALYSIS

Initial analytical efforts to describe the sample-hold filter were directed toward z-plane techniques used in sampled-data stability studies. This method of analysis was discontinued for the following reasons:

- The variable-sampling-rate approach was too complicated and indeterminate.
- The constant-sampling-rate approach did not correspond to actual filter operation; i. e., it did not take into account high-pass effects or the special relationship of sampling instant to input phase, which is the main point of the sample-hold filter. (U)

These attempted approaches are described below.

### Variable Rate Investigation

The sample-hold filter is a variable sampling rate device because each sample period may be of a different length. However, even though consecutive periods may differ in length, the arrangement of different length periods may in itself be periodic. Therefore, if the output of the high-pass filter is assumed to be periodic with period  $T$ , and to be zero at times  $0, \tau_1, \tau_2, \dots, \tau_k, \tau_{k+1}, \dots, \tau_n; T, T+\tau_1, \dots, T+\tau_n$ , then the filter can be represented as a group of samplers, holds, advances, and delays as shown in Figure 70. (U)

In this figure, the filter is represented by a group of samplers, one for each zero crossing during one period. The advances and delays are analytical devices used to make the samplers operate in synchronism. As an example, take the  $k^{\text{th}}$  sampler, which is preceded by a fictitious advance  $e^{s\tau_k}$  and corresponds to the  $k^{\text{th}}$  zero crossing, which occurs  $\tau_k$  seconds after the start of (U)

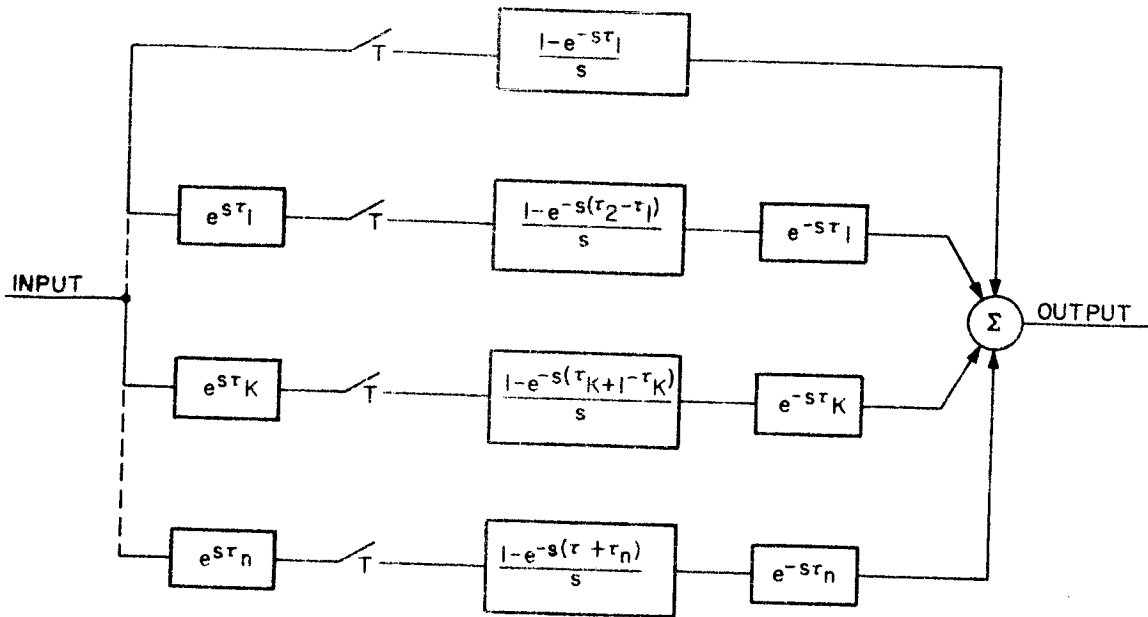


Figure 70. Sample-and-Hold Filter Representation

the period. In this case, when the sampler operates (at the start of the period), the sample it takes is equal to the value of the input  $k$  seconds after the start of the period, because of the advance  $e^{s\tau_k}$ . The value of this sample is held for  $(\tau_{k+1} - \tau_k)$  seconds, delayed  $\tau_k$  seconds, and then added into the output. In this way the output consists of a succession of pulses, the first representing the value of the input at the first zero crossing of the high pass and lasting until time  $\tau_1$ ; the second representing the value of the input at time  $\tau_1$ , when the high-pass output goes through zero again, and lasting from  $\tau_1$  to  $\tau_2$ ; the third representing the input value at time  $\tau_2$ , etc. (U)

This model would accurately represent the filter if the times  $\tau_1, \tau_2, \tau_3, \dots$  could be accurately determined. However, these times depend on input frequencies, amplitudes, phase relationships, and the high-pass transfer function, and are hence indeterminable in general form. Even if these times were determinable, the expressions for the system would be so involved as to be practically unusable. For these reasons it was decided to assume that the system would be dominated by one frequency at a time and the filter would therefore be sampling at a constant rate. (U)

Constant Rate Investigation

Using the assumption that the filter is operating at a constant rate, a simplified approach to the analysis and testing of the sample-hold filter was advantageous for several reasons:

1. The basic operation of the filter, attenuating high-frequency signals in a closed-loop situation, could be analyzed and evaluated without the additional complexities inherent in the actual vehicle simulation.
2. Comparisons between linear filters and the sample-hold filter could be more readily made, with less chance of ambiguity.
3. Analytical methods are easier to use and verify. (U)

The simplified vehicle used had a transfer function of

$$\left( \frac{s^2 + 2\zeta_1 \omega_1 s + \omega_1^2}{s^2 + 2\zeta_2 \omega_2 s + \omega_2^2} \right) \left( \frac{1}{s+1} \right)$$

(U)

Figure 71 is a block diagram of this vehicle in a closed-loop situation. (U)

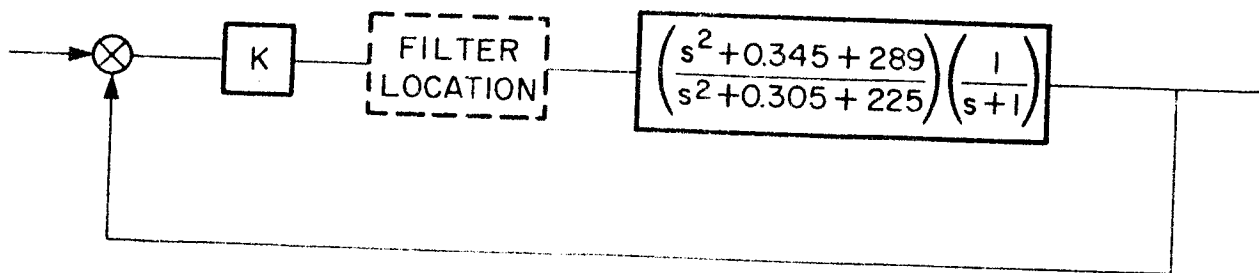


Figure 71. Simplified Vehicle in a Closed-Loop Configuration

A general root-locus of this system, without a filter, is shown in Figure 72. As can be seen from this figure, the dipoles closely resemble the dipoles due to bending while the first-order pole can be thought of as representing the rigid-body response. The damping ratio of the dipoles was selected so the system became unstable at a relatively low gain. (U)

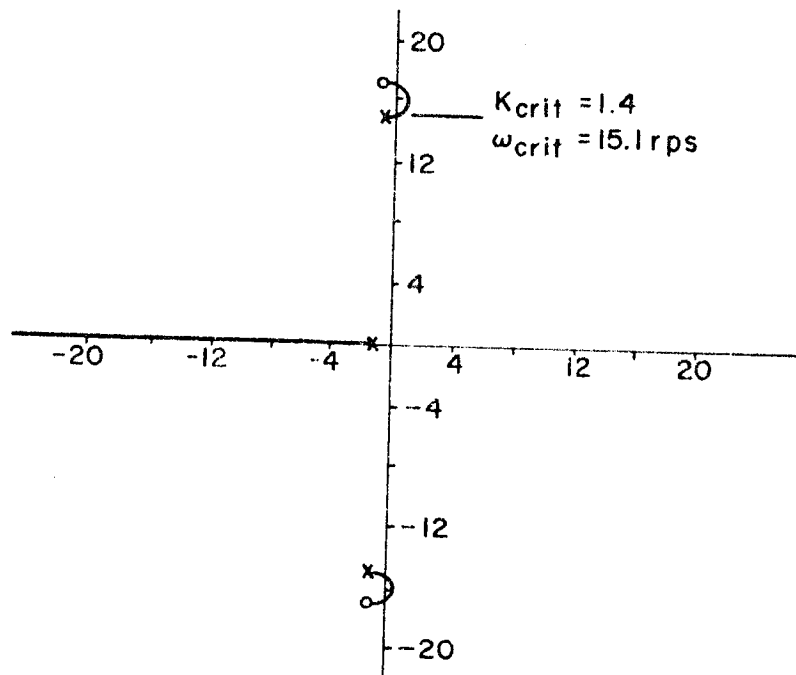


Figure 72. Root-Locus of System of Figure 71

The constant rate studies were made in an effort to determine what effect a change in sampling frequency would have on system critical gain and frequency. The sample-hold filter was assumed to be a constant rate sampler plus a zero-order hold. The z-transform of the system transfer function plus the sampler and zero-order hold was determined for varying values of the sampling period. It was determined that when half the sampling frequency was close to the natural frequency of the high-frequency pole, a slight change in the sampling period would produce a noticeable change in the system critical gain. This indicates that if this approach is to be used in analyzing a system in which the sample-hold filter is to be placed, the assumed sampling frequency must be very accurately picked or the results will not be accurate. All of the above accuracy (U)

assumptions are in addition to the original assumption that this is a valid and accurate representation of the sample-and-hold filter. (This assumption was subsequently shown to be false by the describing function analysis performed.) (U)

When this system was tested on the analog computer, the frequency of divergence seemed to be a combination of the linear system critical frequency and a frequency of about 0.5 cps. The operation was one in which the filter dropped in and out of sampling due to the inherent amplitude thresholds and therefore did not meet the provisions of the constant rate assumption. Thus, system operation did not correlate well with the z-plane studies because it did not correspond well with the imposed conditions. (U)

#### RECOMMENDATIONS FOR CONDUCTING FUTURE STUDIES

At the beginning of the study program, considerable effort was expended on defining a control system for the rigid body only because the basic control configuration, sensor locations, and gain ranges could be optimized more easily with this simple problem. It was anticipated that the addition of the slosh and bending modes would detract appreciably from system performance, but it was reasoned that a given loss in performance would leave the greatest operating margin if it started from an optimized system. Unfortunately, this is not the case; the inclusion of additional degrees of freedom so alters the control problem that the optimum conditions no longer have any relationship to those selected as optimum for rigid body alone. This effect is probably caused mainly from the low bending and slosh frequencies, which result in a tighter coupling of rigid, bending, and slosh modes merely because of their proximity to each other. (U)

The suggested future procedure with similar problems is to:

1. Conduct rigid-body studies, but direct them toward obtaining an understanding of the basic problems and determining the

(U)

effects of various system parameter changes. It is also extremely important to include an appropriate bending mode filter, even though the bending modes themselves are not included. The low-frequency phase introduced by this filter is a very important consideration.

2. Include the additional degrees of freedom, such as bending and slosh, into the analysis program as quickly as possible. This does not imply, however, that they should be included all at once. Adding one degree of freedom at a time and examining the effects of the variable system parameter on this added mode seems to be a satisfactory method. The gains, dynamics, and sensor locations should then be determined, taking into account all the effects previously studied. (U)



REFERENCES

1. "A Model Vehicle for Adaptive Control Studies", George C. Marshall Space Flight Center.
2. "Natural Environmental Design Criteria for the C-5 Vehicle", MSFC Memorandum M-Aero-G-10-62 dated 22 May 1962.
3. "Operational Manual for the Gyro Blender Breadboard", Honeywell R-ED 5184, 15 October 1963.

APPENDIX A  
GLOSSARY

		<u>Unit</u>
A	Amplitude of sample-hold filter input signal	volts
$A_A$	Accelerometer output	$m/sec^2$
$A_x$	Vehicle longitudinal acceleration, including g effects	$m/sec^2$
$a_{LA}$	Vehicle longitudinal acceleration, $\frac{F-X}{m}$	$m/sec^2$
$\bar{B}$	Amplitude of sample-hold filter square wave output	volts
$B_1, B_2$	Band-pass amplifier gain of channels 1 and 2, respectively	volts/volt
$C_1$	Aerodynamic moment coefficient	$1/sec^2$
$C_2$	Control moment coefficient	$1/sec^2$
$C_{z\alpha}$	Aerodynamic force coefficient	1/rad
$e^{s\tau n}$	Time advance of $\tau n$ seconds	sec
$e^{-s\tau n}$	Time delay of $\tau n$ seconds	sec
F	Total thrust of the vehicle booster	kg
$f_i$	Bending frequency	cps
$f_{s,j}$	Slosh frequency	cps
G	Side force due to wind	kg
G(s)	General representation of a Laplace transfer function	-
H	Amplitude of sample-hold filter high-pass filter output	volts

		<u>Unit</u>
$I_k$	Moment of inertia	$\text{kg-m-sec}^2$
$I_{xx}$	Pitch plane moment of inertia about the CG	$\text{kg-m-sec}^2$
$K$	Blender position	Unitless
$K_A$	Accelerometer gain	$\frac{\text{rad/sec}}{\text{m/sec}^2}$
$K_P$	Position (altitude) gain	$\frac{\text{rad/sec}}{\text{rad}}$
$K_R$	Rate gain	$\frac{\text{rad}}{\text{rad/sec}}$
$K_i$	Blender integrator gain	$\frac{\text{volts/sec}}{\text{volt}}$
$\ell_A = x_{CG} - x_A$	Distance from vehicle CG to accelerometer	m
$\ell_{CP} = x_{CG} - x_{CP}$	Distance from vehicle CG to the CP	m
$\ell_{CG} = x_{CG} - x_P$	Distance from engine gimbal to vehicle CG	m
$\ell_E = x_\beta - x_E$	Distance from engine gimbal to engine mass CG	m
$\ell_k$	Distance between vehicle CG and vehicle station K	m
$\ell_{sj} = x_{CG} - x_{sj}$	Distance from vehicle CG to slosh mass CG	m
$M_i$	Generalized mass	$\text{kg-sec}^2/\text{m}$
$m$	Total mass of the vehicle	$\text{kg-sec}^2/\text{m}$
$m_k$	Mass	$\text{kg-sec}^2/\text{m}$
$m_{sj}$	Slosh mass	$\text{kg-sec}^2/\text{m}$
$m_x$	Concentrated mass at station x	$\text{kg-sec}^2/\text{m}$
$N$	Aerodynamic force	kg
$Q_i$	Generalized force for the $i^{\text{th}}$ mode	kg

		<u>Unit</u>
$q$	Dynamic pressure	$\text{kg/m}^2$
$R'$	Thrust of control engines	$\text{kg}$
$S_E$	First moment of engine swivel	$\text{kg-sec}^2$
$T$	Period of periodic sample	$\text{sec}$
$T_A$	Time constant of lag on acceleration feedback filter	$\text{sec}$
$T_B$	Blender time constant This is the time constant of the long lag representing the blender integrator	$\text{sec}$
$T_1$	Time constant of lag on attitude feedback filter	$\text{sec}$
$t_s$	Sampling instant	$\text{sec}$
$U$	Blender imbalance - value of attenuator in one channel of band-pass amplifiers	unitless
$V$	Velocity	$\text{m/sec}$
$V_i$	Reference potential energy of the $i^{\text{th}}$ mode	$\text{kg-m}$
$V_w$	Wind velocity	$\text{m/sec}$
$W_{(x,t)}$	Force distribution over the length of the vehicle for all forces acting upon the vehicle	$\text{kg/m}$
$X$	Displacement of the vehicle centerline	$\text{m}$
$x_k$	Distance from tip of engine to vehicle station $k$	$\text{m}$
$x_k - x_\beta$	Distance to the vehicle station $x_k$ as measured from the vehicle gimbal point	$\text{m}$
$x_{sj} - x_\beta$	Distance from engine gimbal to slosh mass CG	$\text{m}$
$Y_i(X)$	Normalized* displacement at station $x$	unitless
$Y'_i(X)$	Normalized* slope = $\frac{d}{dx} [Y_i(X)]$	$1/\text{m}$

\*The bending displacement is normalized to "1" at the vehicle gimbal point. The slope is a function of the normalized displacement.

		<u>Unit</u>
$Y_i(x) \eta_i$	Displacement at station x to the $i^{\text{th}}$ mode	m
$Y_i'(x) \eta_i$	Angular displacement at station x due to the $i^{\text{th}}$ mode	rad
$Y_i''(x) \eta_i$	Angular rate at station x due to the $i^{\text{th}}$ mode	rad/sec
$Y_i'''(x) \eta_i$	Angular acceleration at station x due to the $i^{\text{th}}$ mode	rad/sec <sup>2</sup>
$Z_{CG}$	Displacement normal to reference	m
$\ddot{Z}_{CG}$	Linear acceleration of the undeformed vehicle along the reference axes at the vehicle station corresponding to the steady state CG of the entire vehicle, due to all forces (including forces due to bending at the engine gimbal)	m/sec <sup>2</sup>
$Z_{sj}$	Slosh mass displacement, normal to reference	m
$\alpha$	Angle of attack	rad
$\beta$	Control deflection angle	rad
$\beta_c$	Commanded engine angle after bending filter	deg
$\beta_c'$	Commanded engine angle before bending filter	deg
$\epsilon$	Error signal - blender or control system	
$\zeta$	General damping ratio term	unitless
$\zeta_{Bi}$	Bending mode damping ratio	unitless
$\zeta_k$	Damping	unitless
$\zeta_{sj}$	Slosh damping	unitless
$\eta_i$	Generalized displacement of the $i^{\text{th}}$ mode (usually denoted as "normal coordinates")	m

		<u>Unit</u>
$\theta$	Angle between reference and inertial velocity vector	rad
$\theta_h$	Phase angle of sample-hold filter high-passed signal	deg
$\theta_o$	Phase angle of sample-hold filter output signal	deg
$\tau$	Displacement normal to vehicle centerline	m
$\tau_D$	Sample-hold filter delay time	sec
$\tau_K$	Approximate open-loop time constant of blender response to step change in the ratio $\phi_{FA}/\phi_{FF}$	sec
$\phi_{CG}$	Attitude angle	rad
$\ddot{\phi}_{CG}$	Angular acceleration of the undeformed vehicle centerline, at the vehicle station corresponding to the steady-state CG of the entire vehicle, due to all moments (including moments due to bending at the engine gimbal)	rad/sec <sup>2</sup>
$\phi_{FA}$	Sum of aft signals to be blended	} Depends upon particular signals being summed
$\phi_{FF}$	Sum of forward signals to be blended	
$X$	Drag force	kg
$\psi$	Angle between local vertical and vehicle X axis	rad
$\omega$	General frequency term	rad/sec
$\omega_{Bi}$	Bending frequency	rad/sec
$\omega_k$	Angular frequency	rad/sec
$\omega_o$	Center frequency of first notch of multiple-notch filter	rad/sec
$\omega_{sj}$	Slosh frequency	rad/sec

Subscripts "k"

A	Accelerometer
B	Bending body
CG	Center of gravity
CP	Center of pressure
crit	Critical
E	Engine
i	$i^{\text{th}}$ bending mode, $i = 1, 2, 3, 4$
IR	Instantaneous rotation
j	$j^{\text{th}}$ slosh tank, $j = 1, 2, 3$
LA	Longitudinal acceleration
P	Platform
R	Rigid body
RGF	Forward rate gyro
RGA	Aft rate gyro
s	Slosh
W	Wind
x	Vehicle station
$\alpha$	Angle of attack
$\beta$	Engine gimbal
$\downarrow$	Position gyro

Superscripts

" . "	Derivative with respect to time
"   "	Derivative with respect to X, the vehicle longitudinal axis

APPENDIX B  
SATURN V EQUATIONS OF MOTION



APPENDIX B  
SATURN V EQUATIONS OF MOTION

Angle of Attack Relationship

$$\alpha = \alpha_W + \phi_{CG} - \theta; \quad \alpha_W = \frac{V_W}{V_o}; \quad \theta = \frac{\dot{Z}}{V_o}$$

Rotation of the Vehicle About Station X<sub>CG</sub>

$$\ddot{\phi}_{CG} = \ddot{\phi}_R + \ddot{\phi}_B + \ddot{\phi}_s + \ddot{\phi}_E$$

$$\ddot{\phi}_R = -C_1 \alpha - C_2 \beta_R$$

$$\ddot{\phi}_B = \frac{F l_{CG}}{I_{xx}} \sum_i \left( Y'_{i(x\beta)} \eta_i \right) - \frac{F}{I_{xx}} \sum_i \left( Y_{i(x\beta)} \eta_i \right)$$

$$\ddot{\phi}_s = \frac{1}{I_{xx}} \sum_j \left[ l_{sj} \ddot{Z}_{sj} + \left( \frac{F - \chi}{m} \right) Z_{sj} \right] m_{sj}$$

$$\ddot{\phi}_E = - \left[ \frac{l_{CG}}{I_{xx}} S_E + \frac{I_E}{I_{xx}} \right] \ddot{\beta} - \left( \frac{F - \chi}{m} \right) \frac{S_E}{I_{xx}} \beta$$

Acceleration Normal to Vehicle Reference At Station X<sub>CG</sub>

$$\ddot{Z}_{CG} = \ddot{Z}_R + \ddot{Z}_B + \ddot{Z}_s + \ddot{Z}_E$$

$$\ddot{Z}_R = \left( \frac{F - \gamma}{m} \right) \phi_{CG} + \frac{R'}{m} \beta_R + \frac{N'}{m} \alpha$$

$$\ddot{Z}_B = - \sum \left( \frac{F}{m} Y'_{i(x\beta)} \right) \eta_i$$

$$\ddot{Z}_s = - \sum_j \frac{m_{sj} \ddot{Z}_{sj}}{m}$$

$$\ddot{Z}_E = \frac{\beta S_E}{m}$$

Accelerometer Equation at Station X<sub>a</sub>

$$\left[ \frac{s^2}{\omega_A^2} + \frac{2\zeta_A}{\omega_A} s + 1 \right] A_A = \ddot{\tau}_R + \ddot{\tau}_B + \ddot{\tau}_s + \ddot{\tau}_E$$

$$\ddot{\tau}_R = \frac{R'}{m} \beta_R + \frac{N'}{m} \alpha - l_A \ddot{\phi}_{CG}$$

$$\ddot{\tau}_B = \sum_i \left[ Y_{i(x_A)} \ddot{\eta}_i \right] - \sum \left[ \frac{F}{m} Y'_{i(x\beta)} - \frac{F - \gamma}{m} Y'_{i(x_A)} \right] \eta_i$$

$$\ddot{\tau}_s = - \sum_j \frac{m_{sj} \ddot{Z}_{sj}}{m}$$

$$\ddot{\tau}_E = \frac{S_E \beta}{m}$$

Rate Gyro Equation at Station X<sub>RG</sub>

$$\dot{\phi}_{CG} = \dot{\phi}_R + \dot{\phi}_B + \dot{\phi}_S + \dot{\phi}_E$$

$$\left[ \frac{s^2}{(\omega_{RG})^2} + \frac{2\zeta_{RG}}{\omega_{RG}} s + 1 \right] \dot{\phi}_{RG} = \dot{\phi}_{CG} - \sum_i \left[ Y'_{i(x_{RG})} \eta_i \right]$$

Bending Equation

$$\ddot{\eta}_i + 2\zeta_i \omega_i \dot{\eta}_i + \omega_i^2 \eta_i = \frac{\sum Q_i}{M_i}$$

$$\sum Q_i = Q_{i\beta} + Q_{i s_j}$$

$$Q_{i\beta} = R'_{\beta} Y_{i(x_{\beta})} + \left[ S_E Y_{i(x_{\beta})} + I_E Y'_{i(x_{\beta})} \right] \ddot{\beta}$$

$$Q_{i s_j} = - \sum_j m_{s_j} \left[ \ddot{Z}_{s_j} Y_{i(x_{s_j})} + \left( \frac{F - \chi}{m} \right) Z_{s_j} Y'_{i(x_{s_j})} \right]$$

Sloshing Propellant Acceleration Normal to Vehicle Centerline

$$\begin{aligned} \ddot{Z}_{s_j} + 2\zeta_{s_j} \omega_{s_j} \dot{Z}_{s_j} + \omega_{s_j}^2 Z_{s_j} &= \ell_{s_j} \ddot{\phi}_{CG} + \left( \frac{F - \chi}{m} \right) \phi_{CG} \\ &- \ddot{Z}_{CG} - \sum_i \left[ Y_{i(x_{s_j})} \ddot{\eta}_i + \left( \frac{F - \chi}{m} \right) Y'_{i(x_{s_j})} \eta_i \right] \\ &= - \left( \ddot{\gamma}_{R(x_{s_j})} + \ddot{\gamma}_{B(x_{s_j})} + \ddot{\gamma}_S + \ddot{\gamma}_E \right) \end{aligned}$$

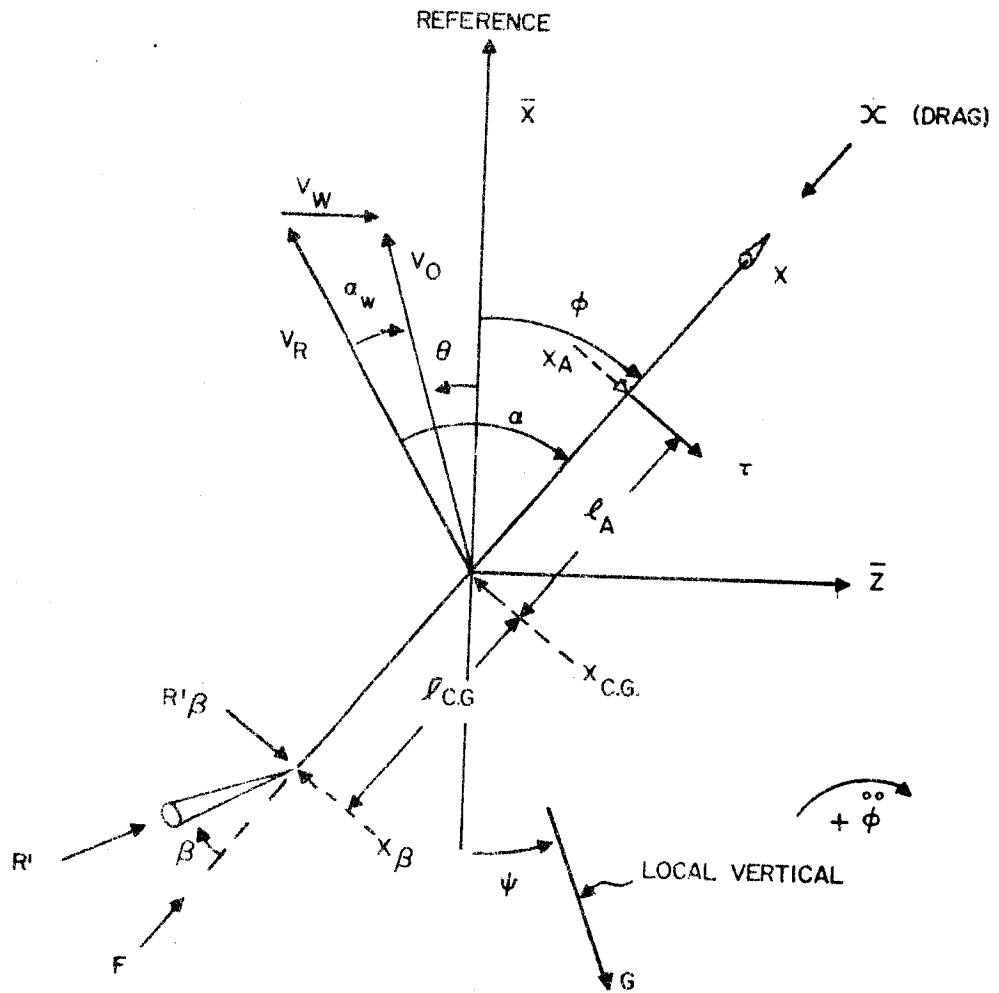
Engine Angular Relationship

$$\beta = \beta_R - \sum_i \left( Y_{i(x\beta)}' \eta_i \right)$$

$$\beta_R = \frac{\beta_c \omega_E^2}{(1 + T_E s) (s^2 + 2\zeta_E \omega_E s + \omega_E^2)}$$

APPENDIX C  
COORDINATE SYSTEMS

Rigid-Body Coordinate System

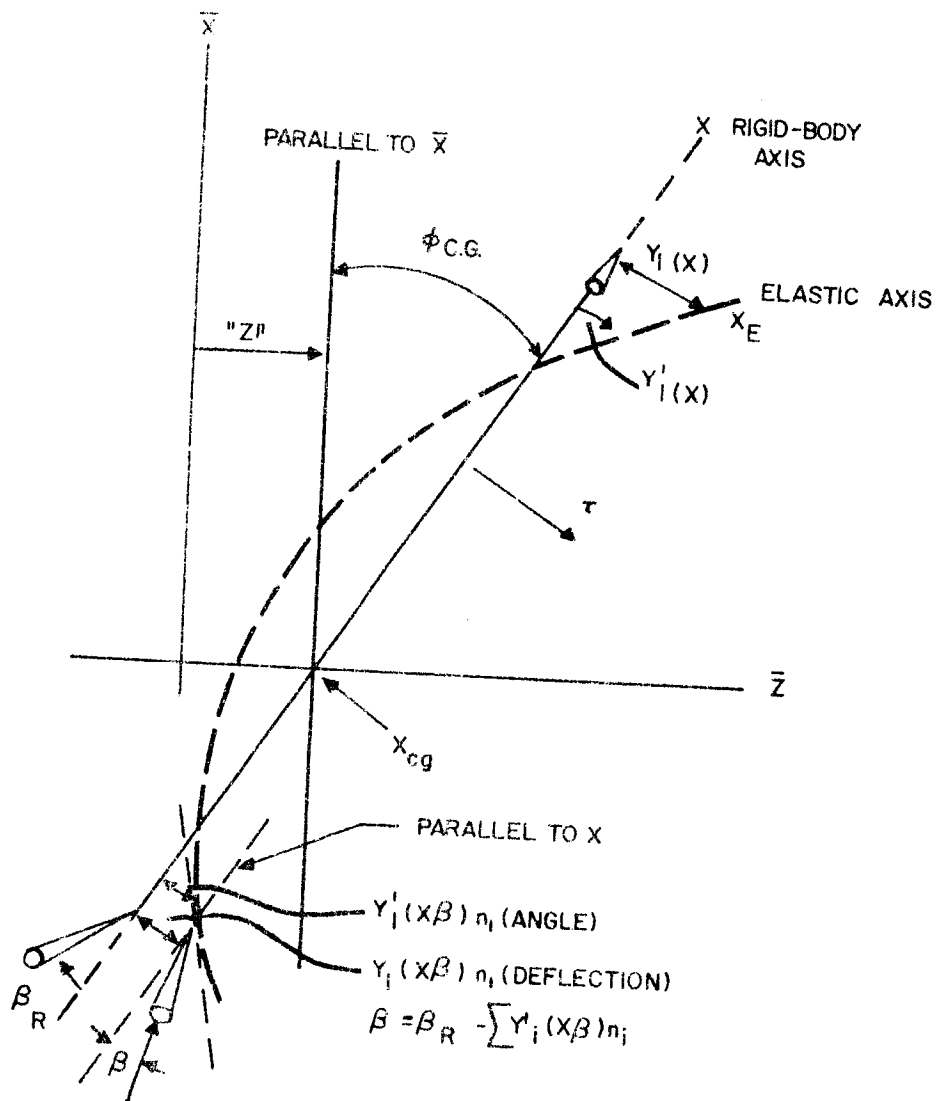


$$\alpha = \alpha_w + \phi - \theta$$

$$\alpha_w = \frac{v_w}{V}$$

$$\theta = \frac{\dot{Z}}{V}$$

First Bending Mode Geometry



$\phi_{CG}$  = rotation of the undeformed vehicle center line, at the vehicle station corresponding to the steady-state center of gravity of the entire vehicle, due to all moments (including moments due to bending at the engine gimbal)

"Z" = normal deviation from  $\bar{X}$

APPENDIX D  
FREE-FREE BENDING MODE DATA



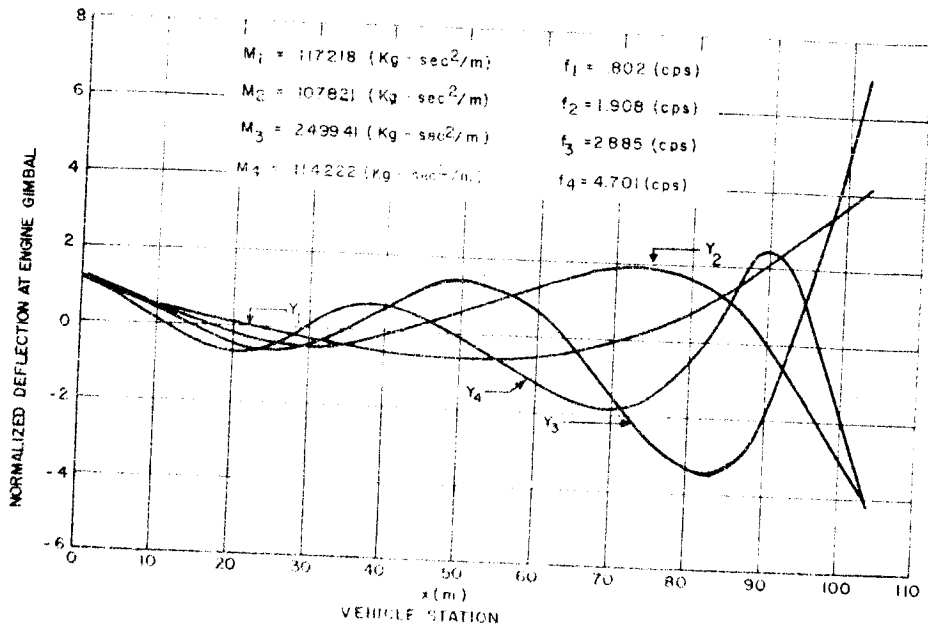


Figure D1. Free-Free Bending Mode Data (t = 0 seconds)

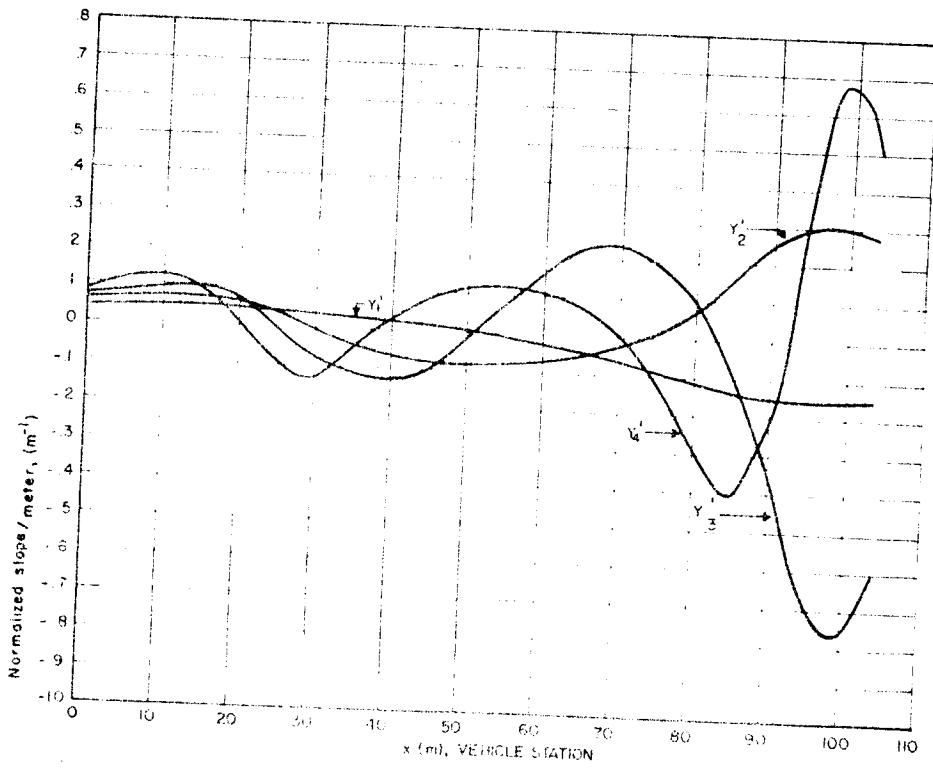


Figure D2. Bending Mode Slope Data (t = 0 seconds)

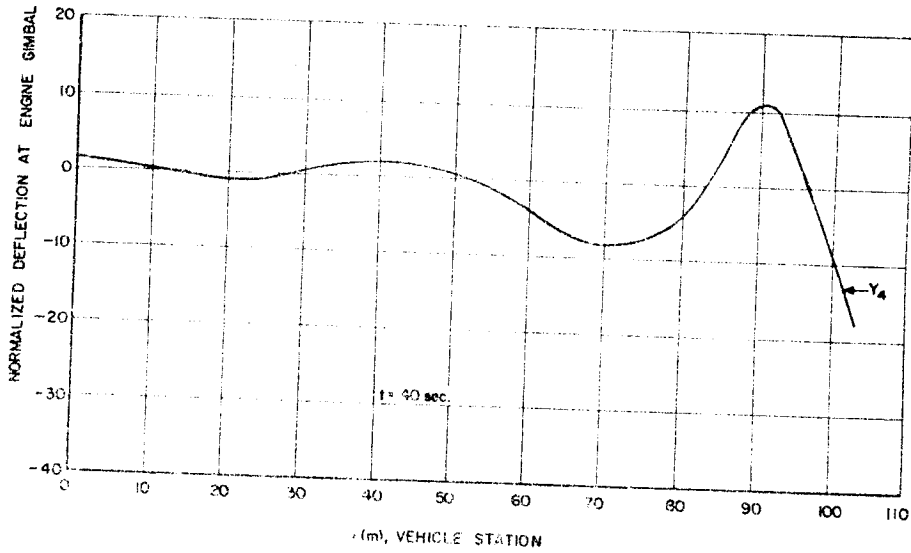
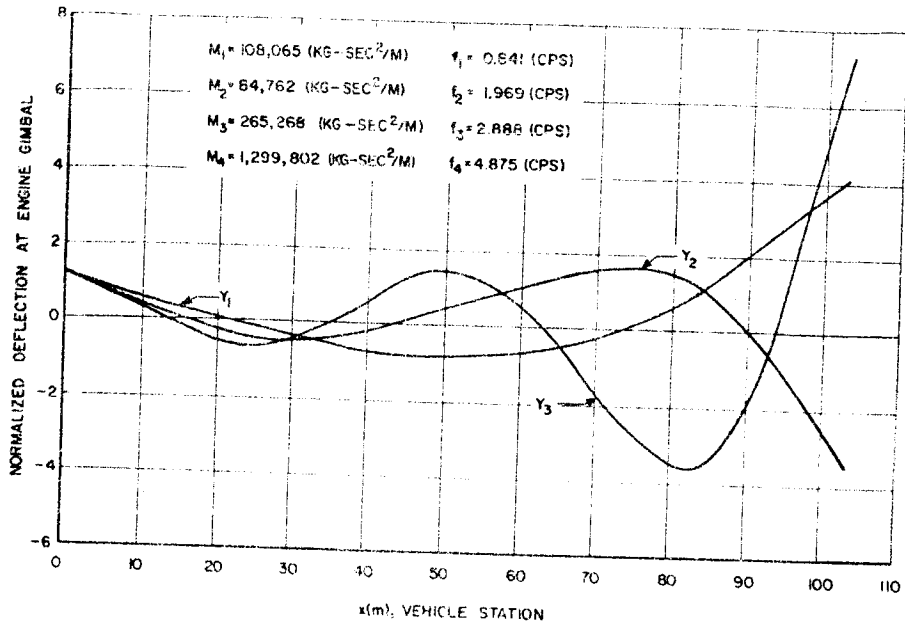


Figure D3. Free-Free Bending Mode Data (t = 40 seconds)

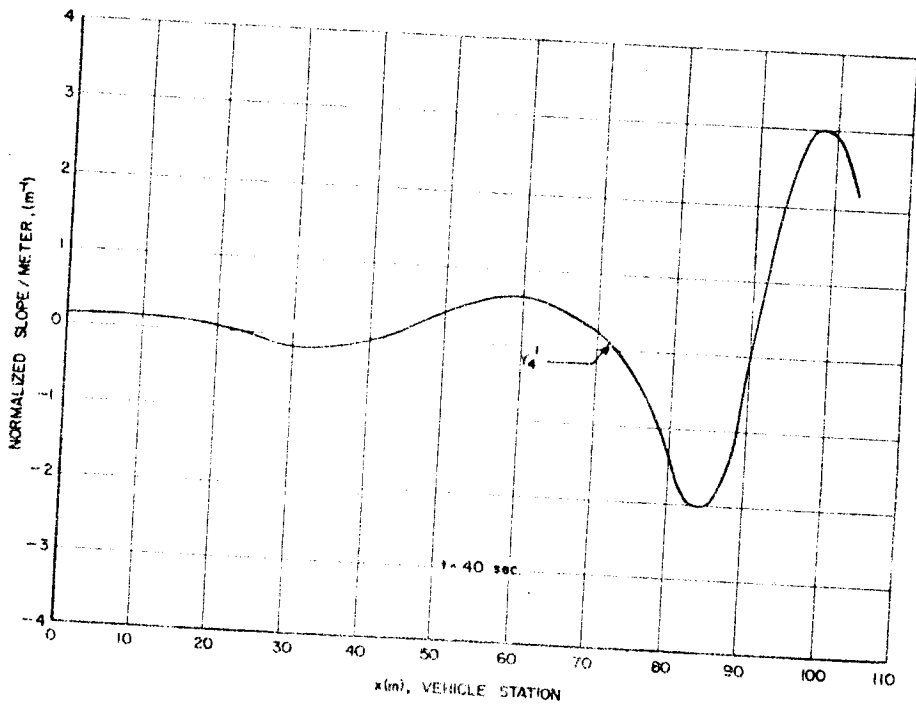
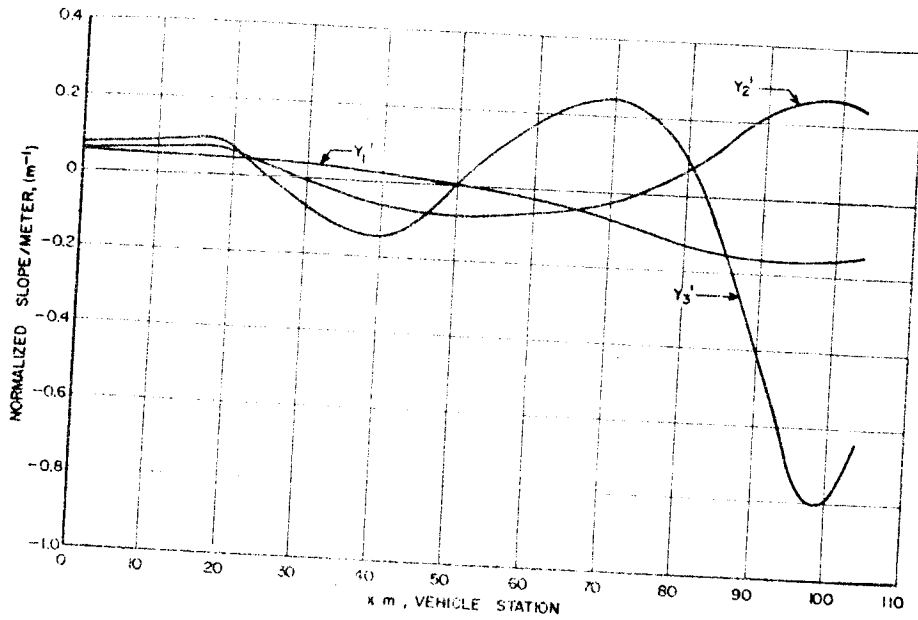


Figure D4. Bending Mode Slope Data (t = 40 seconds)

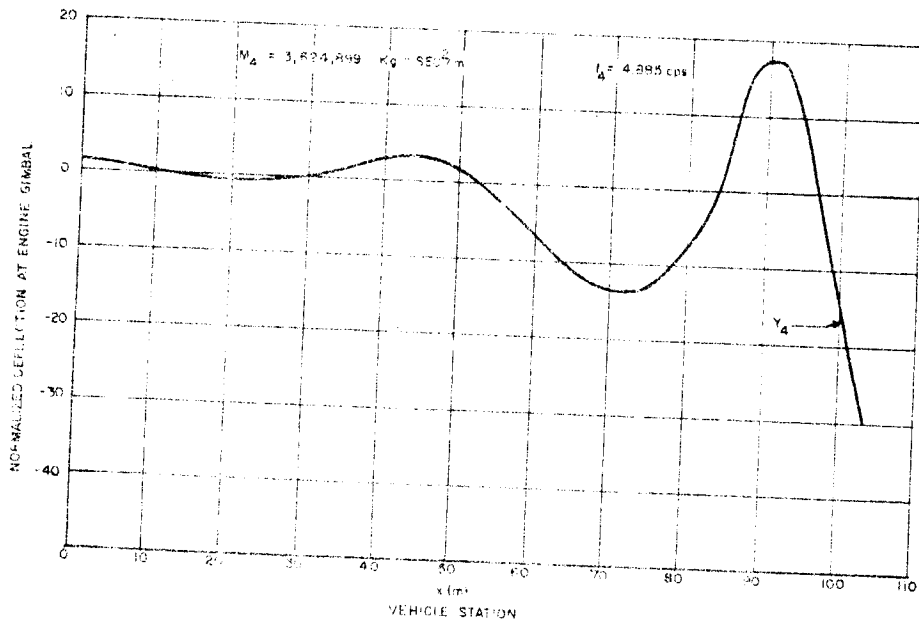
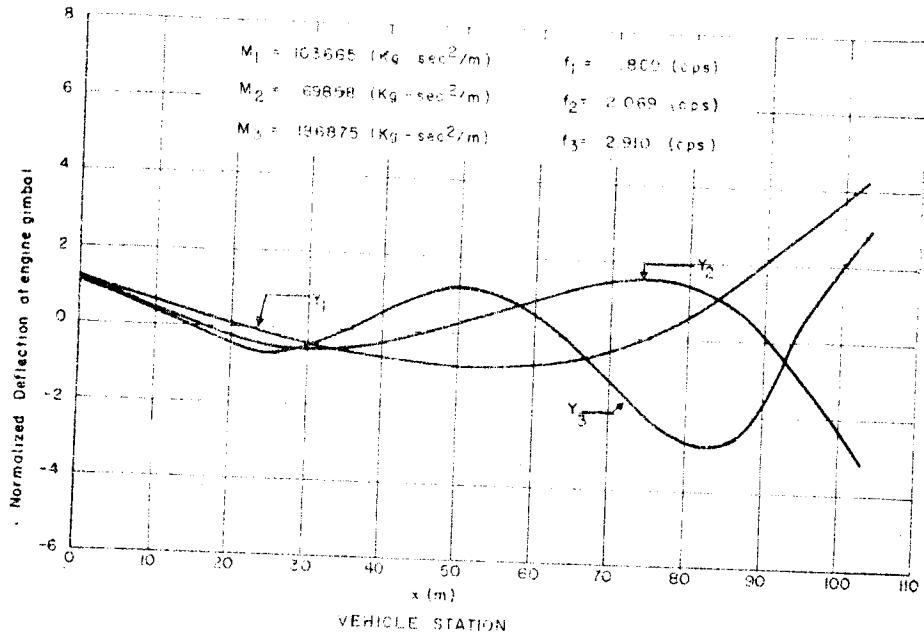


Figure D5. Free-Free Bending Mode Data (t = 79 seconds)

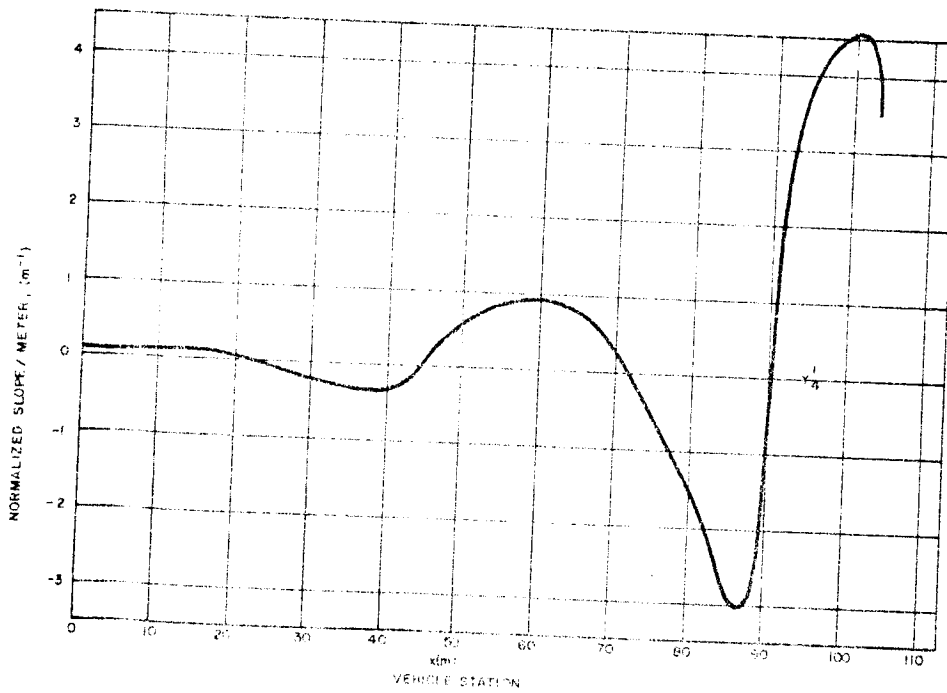
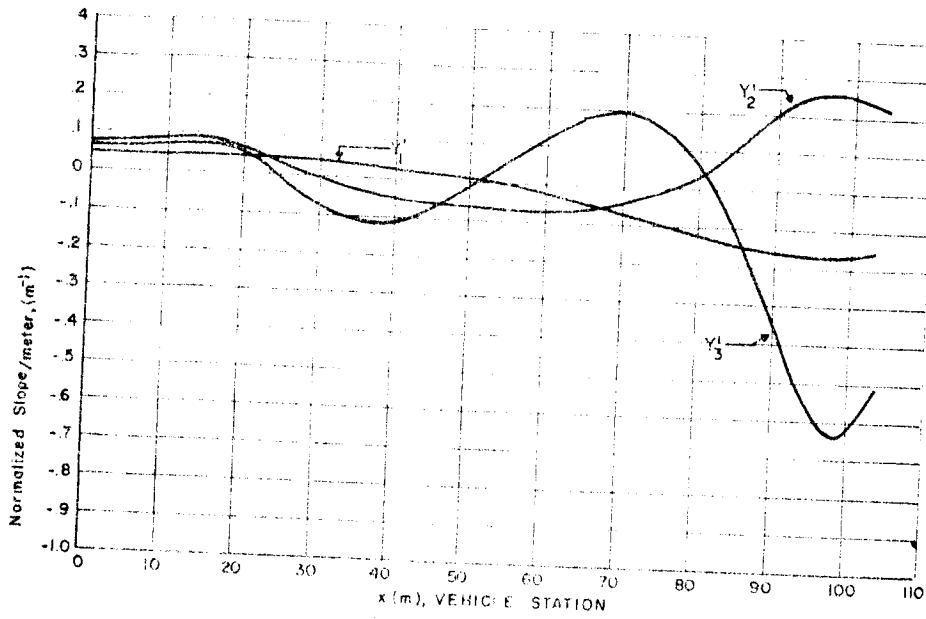


Figure D6. Bending Mode Slope Data (t = 79 seconds)

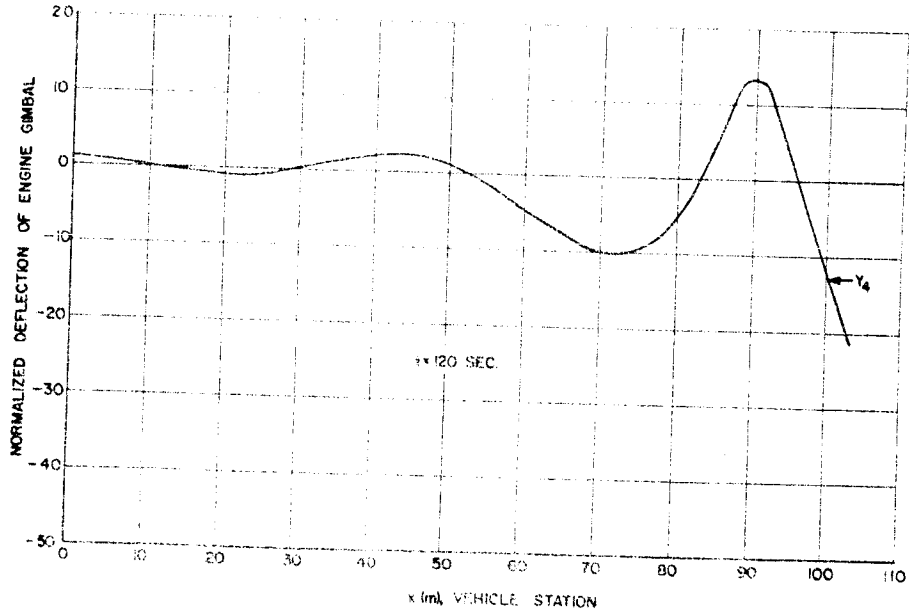
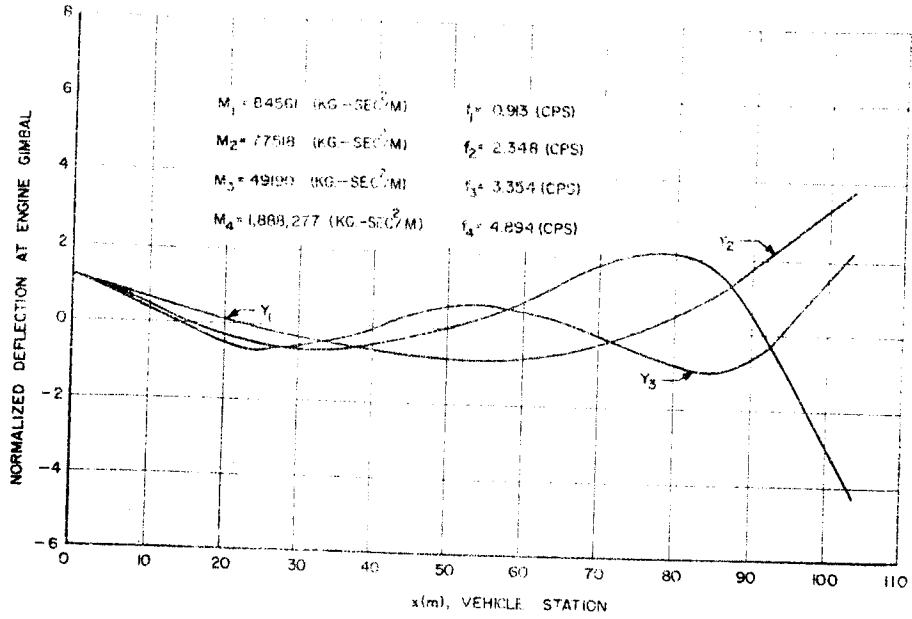


Figure D7. Free-Free Bending Mode Data (t = 120 seconds)

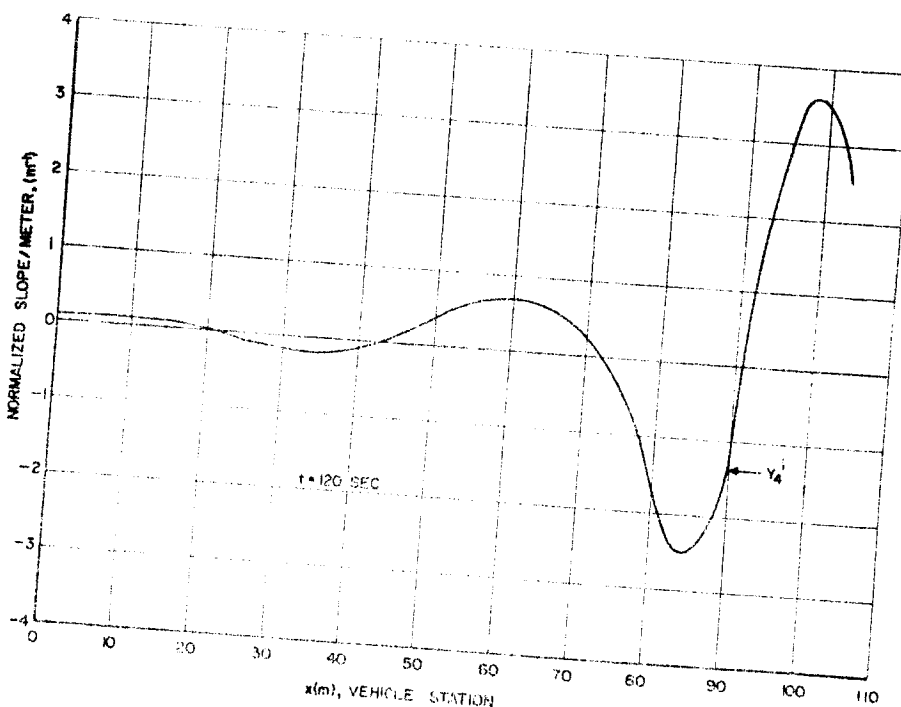
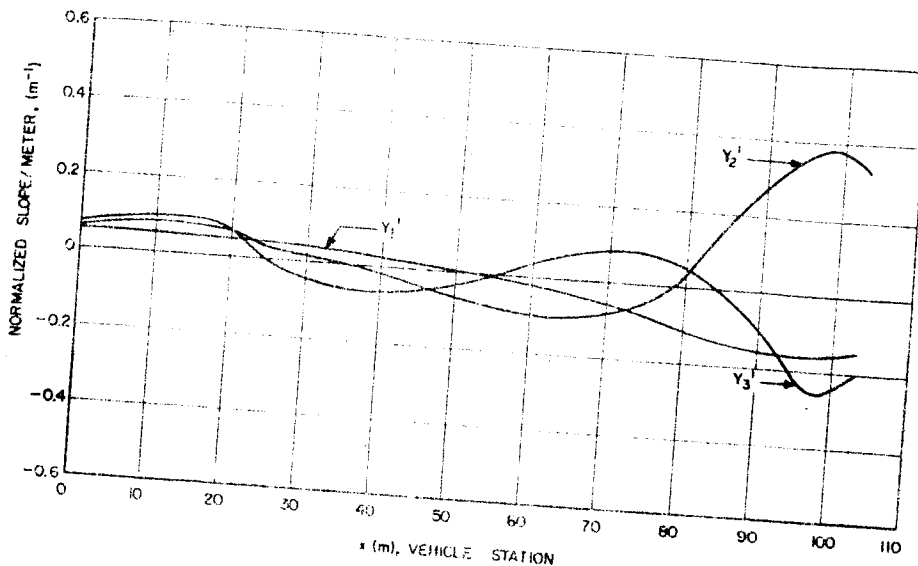


Figure D8. Bending Mode Slope Data (t = 120 seconds)

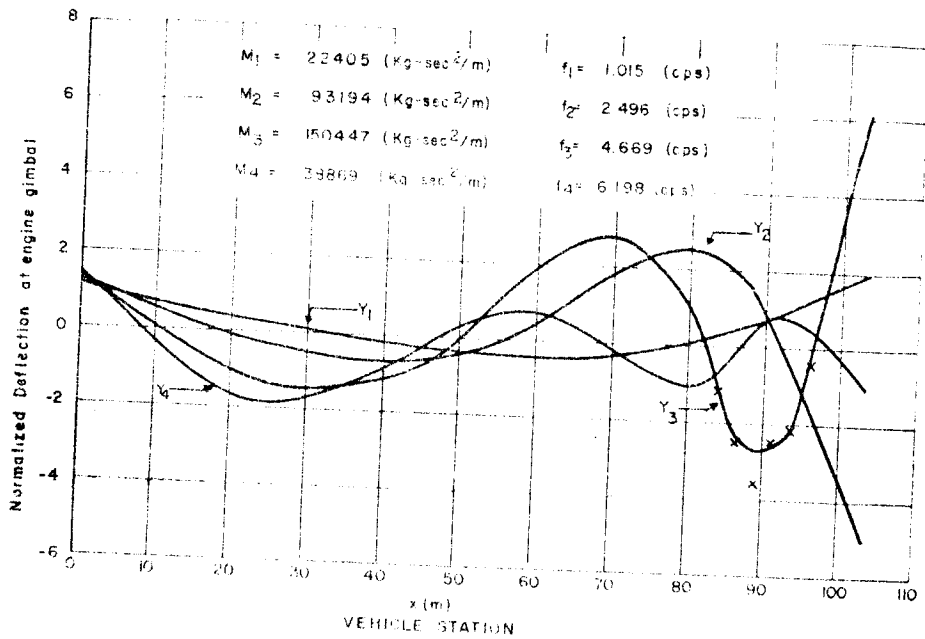


Figure D9. Free-Free Bending Mode Data (t = 153 seconds)

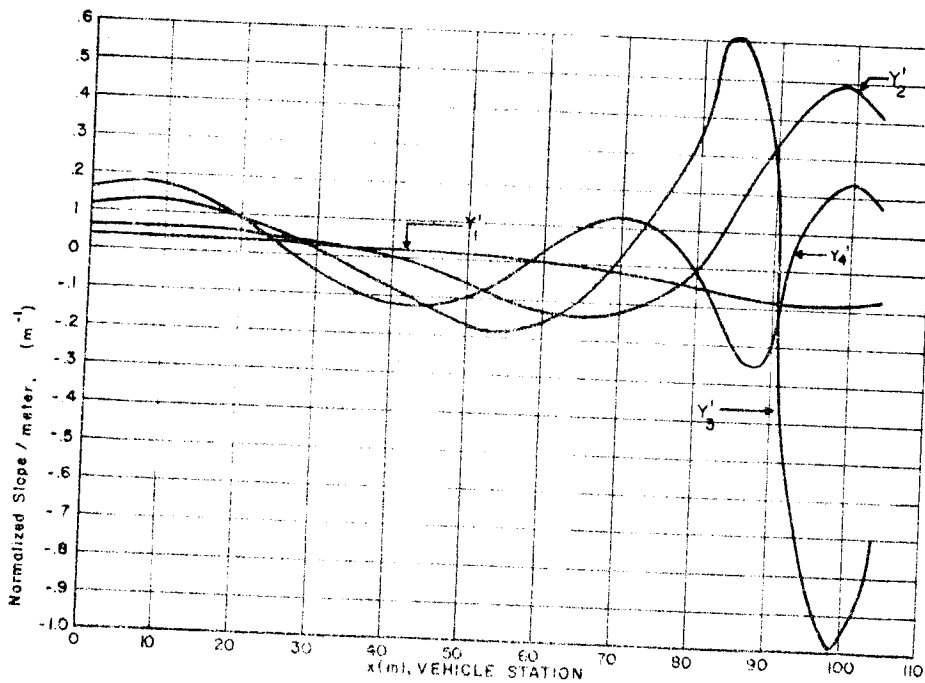


Figure D10. Bending Mode Slope Data (t = 153 seconds)



APPENDIX E  
SYSTEM PARAMETER VALUES (Revision 5)

Symbol	1 x 10 <sup>6</sup>	1 x 10 <sup>5</sup>	1 x 10 <sup>4</sup>	1 x 10 <sup>3</sup>	1 x 10 <sup>2</sup>	Units	Description
$N^* = C_{Z_0}$ gA	0	1.1556	1.1734 x 10 <sup>4</sup>	120.741	1.9766 x 10 <sup>4</sup>		
$C_{Z_0}$	3.35	1.15	4.52	5.02	5.02	Kg	Aerodynamic force term
G	0	-1947.32	156.17	177.24	82.37	1/mal	Aerodynamic force coefficient
A	78.46	78.46	78.46	78.46	78.46	Kg/m <sup>2</sup>	Dynamic pressure
m	277,423.4	274,809.8	173,640.7	118,387.5	75,430.7	m <sup>2</sup>	Area
F	5,541,550	5,541,517	3,840,844	3,840,844	3,173,281	Kg-sec <sup>2</sup> /m	Vehicle mass
$R = \frac{1}{6} F$	2,734,570	2,838,977.6	1,994,877	3,173,281	2,806,621	kg	Total thrust
X	0.00	61.532	2,119.53	15,713	984	Kg	Control engine thrust
V	0	19,958	507,898	1931,492	2522,118	Kg	Drag
$I_{xx}$	8.5138 x 10 <sup>7</sup>	8.23 x 10 <sup>7</sup>	7.621 x 10 <sup>7</sup>	6.85 x 10 <sup>7</sup>	4.4427 x 10 <sup>7</sup>	m <sup>2</sup> /sec	Velocity
$\psi$	0	0.0	0	0.3	0.8	Kg-sec <sup>2</sup> /m	Moment of inertia
Altitude	0	2,700	19,348	76,100	62,904	deg	Angle between vehicle and local vertical
$X_{CG}$	29,245	-1,658	31,105	31,331	43,287	m	Altitude
$X_{CP}$	44,181	44,28	50,267	59,395	51,322	m	CG location
$X_P$	2.54	2.54	2.54	2.54	2.54	m	CP location
$X_A$	64.0	64.0	64.0	64.0	64.0	m	Gimbal location
$X_P$	85.317	85.317	85.317	85.317	85.317	m	Accelerometer location
$X_{RCF}$	85.317	85.317	85.317	85.317	85.317	m	Position gyro location
$X_{RGA}$	5.00	5.00	5.00	5.00	5.00	m	Forward rate gyro location
$X_{CO}$	26.858	27.150	29.865	32.789	42.748	m	Aft rate gyro location
$X_{CP}$	-14.986	-14.986	-14.182	-18.581	-8.035	m	Dist. CG to gimbal
$X_A$	-34.604	-34.604	-32.887	-38.47	-18.714	m	Dist. CG to CP
$X_P$	-55.921	-55.921	-41.212	-49.982	40.029	m	Dist. CG to accel.
$X_{RCF}$	-55.921	-55.921	-41.212	-49.982	40.029	m	Dist. CA to position gyro
$X_{RGA}$	24.898	24.898	26.105	30.34	40.388	m	Dist. CG to forward rate gyro
$X_{CO}$	24.898	24.898	26.105	30.34	40.388	m	Dist. CG to aft rate gyro
$I_E$ per engine	1111.4	1111.4	1111.4	1111.4	1111.4	Kg-sec <sup>2</sup>	First moment of swivel
$I_E$ per engine	14.54	14.54	14.54	14.54	14.54	Kg-sec <sup>2</sup> /m	Engine moment of inertia
$C_1 = \frac{N^*}{V} (CF)$	0	-0.0121	-0.2103	-0.1801	-0.00268	1/sec <sup>2</sup>	Aerodynamic moment coefficient
$C_2 = \frac{R}{V} (CG)$	0.0033	0.0033	1.1481	1.587	2.1119	1/sec <sup>2</sup>	Control moment coefficient
$M_1$	117,218	105,053	105,805	84,881	24,405	Kg-sec <sup>2</sup> /m	Mode generalized bending mass
$M_2$	137,421	84,762	60,508	77,518	89,194	Kg-sec <sup>2</sup> /m	
$M_3$	24,141	205,998	186,821	43,750	150,447	Kg-sec <sup>2</sup> /m	
$M_4$	114,022	1,098,892	1,024,107	1,803,175	83,486	Kg-sec <sup>2</sup> /m	
$\zeta_1$	0.000	0.000	1.000	0.000	0.000	Unitless	Bending mode damping factor
$\zeta_2$	0.000	0.000	0.000	0.000	0.000	Unitless	
$\zeta_3$	0.000	0.000	0.000	0.000	0.000	Unitless	
$\zeta_4$	0.000	0.000	0.000	0.000	0.000	Unitless	

Symbol	1st	2nd	3rd	4th	5th	Units	Description
$f_1$	1.400	1.311	1.222	1.133	1.044	Hz	Bending mode frequency
$f_2$	1.995	1.92	1.841	1.762	1.683	Hz	
$f_3$	2.626	2.565	2.504	2.443	2.382	Hz	
$f_4$	3.293	3.24	3.181	3.122	3.063	Hz	
$\omega_1$	9.429	9.292	9.155	9.018	8.881	rad/sec	Bending mode frequency
$\omega_2$	12.488	12.36	12.233	12.106	11.979	rad/sec	
$\omega_3$	16.463	16.345	16.227	16.109	15.991	rad/sec	
$\omega_4$	20.437	20.322	20.204	20.086	19.968	rad/sec	
$Y_1(\sigma_1)$	0.155	0.157	0.160	0.163	0.166	Unitless	Normalized bending deflection at first slosh tank
$Y_2(\sigma_1)$	-0.27	-0.26	-0.25	-0.24	-0.23	Unitless	
$Y_3(\sigma_1)$	0.27	0.26	0.25	0.24	0.23	Unitless	
$Y_4(\sigma_1)$	-0.27	-0.26	-0.25	-0.24	-0.23	Unitless	
$Y_1(\sigma_2)$	0.115	0.117	0.119	0.121	0.123	1/m	Normalized bending slope at first slosh tank
$Y_2(\sigma_2)$	0.113	0.115	0.117	0.119	0.121	1/m	
$Y_3(\sigma_2)$	0.112	0.114	0.116	0.118	0.12	1/m	
$Y_4(\sigma_2)$	0.112	0.114	0.116	0.118	0.12	1/m	
$Y_1(\sigma_2)$	-0.170	-0.172	-0.174	-0.176	-0.178	Unitless	Normalized bending deflection at second slosh tank
$Y_2(\sigma_2)$	-0.170	-0.172	-0.174	-0.176	-0.178	Unitless	
$Y_3(\sigma_2)$	-0.170	-0.172	-0.174	-0.176	-0.178	Unitless	
$Y_4(\sigma_2)$	0.170	0.172	0.174	0.176	0.178	Unitless	
$Y_1(\sigma_2)$	0.055	0.056	0.057	0.058	0.059	1/m	Normalized bending slope at second slosh tank
$Y_2(\sigma_2)$	-0.054	-0.055	-0.056	-0.057	-0.058	1/m	
$Y_3(\sigma_2)$	-0.055	-0.056	-0.057	-0.058	-0.059	1/m	
$Y_4(\sigma_2)$	-0.055	-0.056	-0.057	-0.058	-0.059	1/m	
$Y_1(\sigma_3)$	-0.08	-0.08	-0.08	-0.08	-0.08	Unitless	Normalized bending deflection at third slosh tank
$Y_2(\sigma_3)$	0.10	0.10	0.10	0.10	0.10	Unitless	
$Y_3(\sigma_3)$	1.40	1.40	1.40	1.40	1.40	Unitless	
$Y_4(\sigma_3)$	0.10	0.10	0.10	0.10	0.10	Unitless	
$Y_1(\sigma_3)$	0.112	0.113	0.114	0.115	0.116	1/m	Normalized bending slope at third slosh tank
$Y_2(\sigma_3)$	0.112	0.113	0.114	0.115	0.116	1/m	
$Y_3(\sigma_3)$	-0.112	-0.113	-0.114	-0.115	-0.116	1/m	
$Y_4(\sigma_3)$	0.112	0.113	0.114	0.115	0.116	1/m	
$Y_1(\sigma)$	-0.07	-0.07	-0.07	-0.07	-0.07	Unitless	Normalized bending deflection at accelerometer
$Y_2(\sigma)$	1.01	1.01	1.01	1.01	1.01	Unitless	
$Y_3(\sigma)$	-0.10	-0.10	-0.10	-0.10	-0.10	Unitless	
$Y_4(\sigma)$	-1.10	-1.10	-1.10	-1.10	-1.10	Unitless	

Symbol	1 x 9	1 x 40	1 x 75	1 x 120	1 x 151.17	Units	Description
$Y_1(A)$	-0.041	-0.041	-0.043	-0.043	-0.009	1/m	Normalized bending slope at accelerometer
$Y_2(A)$	-0.056	-0.056	-0.062	-0.102	0.141	1/m	
$Y_3(A)$	0.222	0.22	0.165	0.09	-0.100	1/m	
$Y_4(A)$	0.077	0.50	0.510	0.63	0.090	1/m	
$Y_1(G)$	1.00	1.00	1.00	1.00	1.00	Unitless	Normalized bending deflection of gimbal
$Y_2(G)$	1.00	1.00	1.00	1.00	1.00	Unitless	
$Y_3(G)$	1.00	1.00	1.00	1.00	1.00	Unitless	
$Y_4(G)$	1.00	1.00	1.00	1.00	1.00	Unitless	
$Y_1(G)$	0.045	0.05	0.049	0.05	0.037	1/m	Normalized bending slope at gimbal
$Y_2(G)$	0.064	0.062	0.064	0.072	0.062	1/m	
$Y_3(G)$	0.072	0.073	0.074	0.005	0.127	1/m	
$Y_4(G)$	0.100	0.100	0.100	0.100	0.172	1/m	
$Y_1(p)$	-0.140	-0.140	-0.150	-0.198	-0.070	1/m	Normalized bending slope at position gyro
$Y_2(p)$	0.170	0.154	0.120	0.100	0.175	1/m	
$Y_3(p)$	-0.118	-0.105	-0.120	-0.015	0.600	1/m	
$Y_4(p)$	-0.407	-2.05	-2.95	-2.43	-0.247	1/m	
$Y_1(RGF)$	-0.140	-0.148	-0.150	-0.198	-0.070	1/m	Normalized bending slope at forward rate gyro
$Y_2(RGF)$	0.170	0.154	0.120	0.100	0.175	1/m	
$Y_3(RGF)$	-0.118	-0.105	-0.120	-0.015	0.600	1/m	
$Y_4(RGF)$	-0.407	-2.05	-2.95	-2.43	-0.247	1/m	
$Y_1(RGA)$	0.050	0.050	0.048	0.05	0.039	1/m	Normalized bending slope at aft rate gyro
$Y_2(RGA)$	0.089	0.066	0.089	0.078	0.062	1/m	
$Y_3(RGA)$	0.060	0.029	0.080	0.080	0.130	1/m	
$Y_4(RGA)$	0.130	0.100	0.100	0.100	0.160	1/m	
$m_{s1}/m$	0.040	0.0575	0.067	0.020	0.0031	Unitless	Slosh mass to vehicle mass ratio
$m_{s2}/m$	0.062	0.093	0.100	0.090	0.014	Unitless	
$m_{s3}/m$	0.040	0.0908	0.0810	0.030	0.105	Unitless	
$x_{s1}$	11.703	10.024	9.776	6.156	5.850	m	Slosh mass locations
$x_{s2}$	21.703	20.062	21.600	23.104	20.710	m	
$x_{s3}$	31.693	47.001	47.801	42.005	47.001	m	
$l_{s1}$	11.9023	11.642	22.907	20.064	19.020	m	Distance, CG to slosh masses
$l_{s2}$	21.322	2.714	0.435	13.020	24.543	m	
$l_{s3}$	31.000	10.197	-10.001	-12.473	-2.513	m	
$c_{s1}$	0.000	0.000	0.000	0.000	0.000	Unitless	1st } Slosh mass damping factor
$c_{s2}$	0.000	0.000	0.000	0.000	0.000	Unitless	
$c_{s3}$	0.000	0.000	0.000	0.000	0.000	Unitless	
$f_{s1}$	0.340	0.387	0.425	0.501	0.57	cps	1st } Slosh mass frequency
$f_{s2}$	0.340	0.387	0.427	0.501	0.568	cps	
$f_{s3}$	0.340	0.387	0.440	0.503	0.507	cps	
$\%s1$	2.130	2.43	2.070	2.149	2.233	rad/sec	1st } Slosh mass frequency
$\%s2$	0.120	2.43	2.607	3.204	4.000	rad/sec	
$\%s3$	0.100	2.43	2.700	0.100	1.220	rad/sec	

APPENDIX F  
MOTION AND CONTROL EQUATIONS MATRIX AND COEFFICIENTS



Matrix Coefficients (Revision 5)

Coefficient	Definition	t = 0	t = 40	t = 79	t = 120	t = 150.00
A <sub>11</sub>	Y <sub>1</sub> (s <sub>1</sub> )	0.500	0.615	0.680	0.790	0.900
A <sub>12</sub>	$\frac{F-X}{m} [Y_1'(s_1)]$	0.6127	0.8047	1.0026	1.630	1.6282
A <sub>13</sub>	Y <sub>1</sub> (s <sub>2</sub> )	-0.370	-0.220	-0.140	0	0.320
A <sub>14</sub>	$\frac{F-X}{m} [Y_1'(s_2)]$	0.4289	0.619	0.8564	1.532	1.2234
A <sub>15</sub>	Y <sub>1</sub> (s <sub>3</sub> )	-0.660	-0.810	-0.690	-0.630	-0.380
A <sub>16</sub>	$\frac{F-X}{m} [Y_1'(s_3)]$	0.0735	0.07737	0.2715	0.4563	0.6966
A <sub>17</sub>	Y <sub>1</sub> (RGP)	-0.190	-0.148	-0.150	-0.138	-0.070
A <sub>18</sub>	Y <sub>1</sub> (RGA)	0.050	0.050	0.048	0.050	0.039
A <sub>19</sub>	Y <sub>1</sub> (p)	-0.140	0.148	-0.150	-0.138	-0.070
A <sub>21</sub>	Y <sub>2</sub> (s <sub>1</sub> )	0.370	0.500	0.530	0.600	0.780
A <sub>22</sub>	$\frac{F-X}{m} [Y_2'(s_1)]$	0.8045	1.080	1.4621	2.575	2.4007
A <sub>23</sub>	Y <sub>2</sub> (s <sub>2</sub> )	-0.490	-0.490	-0.470	-0.470	-0.170
A <sub>24</sub>	$\frac{F-X}{m} [Y_2'(s_2)]$	-0.2841	0.283	0.5848	1.605	2.0420
A <sub>25</sub>	Y <sub>2</sub> (s <sub>3</sub> )	0.500	0.300	0.130	-0.280	-0.550
A <sub>26</sub>	$\frac{F-X}{m} [Y_2'(s_3)]$	-0.9802	-1.008	-1.2552	-1.728	-1.8350
A <sub>27</sub>	Y <sub>2</sub> (RGP)	0.170	0.104	0.120	0.168	0.175
A <sub>28</sub>	Y <sub>2</sub> (RGA)	0.060	0.066	0.060	0.078	0.050
A <sub>29</sub>	Y <sub>2</sub> (p)	0.170	0.154	0.120	0.168	0.175
A <sub>31</sub>	Y <sub>3</sub> (s <sub>1</sub> )	0.270	0.400	0.480	0.590	0.570
A <sub>32</sub>	$\frac{F-X}{m} [Y_3'(s_1)]$	1.1273	1.362	1.7127	3.031	5.3273
A <sub>33</sub>	Y <sub>3</sub> (s <sub>2</sub> )	-0.290	-0.600	-0.680	-0.680	-1.100
A <sub>34</sub>	$\frac{F-X}{m} [Y_3'(s_2)]$	-1.2120	0.619	-0.2089	0.890	3.4013
A <sub>35</sub>	Y <sub>3</sub> (s <sub>3</sub> )	1.400	1.43	1.130	0.480	-0.280
A <sub>36</sub>	$\frac{F-X}{m} [Y_3'(s_3)]$	-0.5091	-0.5410	-0.9817	-1.369	-6.5157
A <sub>37</sub>	Y <sub>3</sub> (RGP)	-0.118	-0.155	-0.120	-0.015	0.500
A <sub>38</sub>	Y <sub>3</sub> (RGA)	0.080	0.079	0.080	0.090	0.120
A <sub>39</sub>	Y <sub>3</sub> (p)	-0.118	-0.155	-0.120	-0.015	0.600
A <sub>41</sub>	Y <sub>4</sub> (s <sub>1</sub> )	-0.030	0.200	0.500	0.500	0.400
A <sub>42</sub>	$\frac{F-X}{m} [Y_4'(s_1)]$	1.4704	1.5870	2.2976	3.2595	7.5702
A <sub>43</sub>	Y <sub>4</sub> (s <sub>2</sub> )	0.400	-0.460	-0.500	-1.00	-1.800
A <sub>44</sub>	$\frac{F-X}{m} [Y_4'(s_2)]$	-1.4704	-2.167	-1.9621	-0.9778	3.1144
A <sub>45</sub>	Y <sub>4</sub> (s <sub>3</sub> )	0.100	1.500	2.600	1.900	0.100
A <sub>46</sub>	$\frac{F-X}{m} [Y_4'(s_3)]$	1.2866	3.095	8.1548	8.149	-4.6356
A <sub>47</sub>	Y <sub>4</sub> (RGP)	-0.407	-2.050	-2.950	-2.480	-0.247
A <sub>48</sub>	Y <sub>4</sub> (RGA)	0.110	0.100	0.100	0.100	0.100
A <sub>49</sub>	Y <sub>4</sub> (p)	-0.407	-2.050	-2.950	-2.480	-0.247

Coefficient	Definition	t = 0	t = 40	t = 79	t = 120	t = 153.58
A <sub>51</sub>	Y <sub>1</sub> (A)	-0.39	-0.61	-0.66	-0.71	-0.42
A <sub>52</sub>	$\frac{F}{m} [Y_1(\beta)] - \frac{F-X}{m} [Y_1(A)]$	1.057	1.4219	2.005	2.7116	1.885
A <sub>55</sub>	$\frac{F}{m} [Y_1(\beta)]$	0.5516	0.7874	1.0596	1.656	1.5187
A <sub>56</sub>	$\frac{F I_{CG}}{I_{xx}} [Y_1(\beta)] - \frac{F}{I_{xx}} [Y_1(\beta)]$	0.60833	0.01557	0.01848	0.0382	0.04102
A <sub>57</sub>	Y <sub>1</sub> (β)	0.045	0.050	0.048	0.050	0.037
A <sub>61</sub>	Y <sub>2</sub> (A)	1.61	1.300	1.20	1.090	0.93
A <sub>62</sub>	$\frac{F}{m} [Y_2(\beta)] - \frac{F-X}{m} [Y_2(A)]$	1.486	1.8730	2.7108	5.6807	8.52
A <sub>65</sub>	$\frac{F}{m} [Y_2(\beta)]$	0.7723	0.8764	1.4120	2.356	2.5414
A <sub>66</sub>	$\frac{F I_{CG}}{I_{xx}} [Y_2(\beta)] - \frac{F}{I_{xx}} [Y_2(\beta)]$	0.02764	0.02875	0.04125	0.08125	0.11839
A <sub>67</sub>	Y <sub>2</sub> (β)	0.065	0.062	0.064	0.072	0.062
A <sub>71</sub>	Y <sub>3</sub> (A)	-0.18	-0.100	-0.10	0.270	2.40
A <sub>72</sub>	$\frac{F}{m} [Y_3(\beta)] - \frac{F-X}{m} [Y_3(A)]$	-1.85	-2.2549	-1.8344	0.8263	9.64
A <sub>75</sub>	$\frac{F}{m} [Y_3(\beta)]$	0.88258	1.1496	1.6335	2.782	5.2059
A <sub>76</sub>	$\frac{F I_{CG}}{I_{xx}} [Y_3(\beta)] - \frac{F}{I_{xx}} [Y_3(\beta)]$	0.03730	0.04274	0.05547	0.10675	0.31236
A <sub>77</sub>	Y <sub>3</sub> (β)	0.072	0.073	0.074	0.085	0.127
A <sub>81</sub>	Y <sub>4</sub> (A)	-1.68	-0.100	-10.6	-7.480	3.45
A <sub>82</sub>	$\frac{F}{m} [Y_4(\beta)] - \frac{F-X}{m} [Y_4(A)]$	0.285	-6.1627	-14.719	-17.2618	3.28
A <sub>85</sub>	$\frac{F}{m} [Y_4(\beta)]$	1.2258	1.5748	2.2074	3.373	7.0504
A <sub>86</sub>	$\frac{F I_{CG}}{I_{xx}} [Y_4(\beta)] - \frac{F}{I_{xx}} [Y_4(\beta)]$	0.08734	0.07464	0.09246	0.13615	0.44303
A <sub>87</sub>	Y <sub>4</sub> (β)	0.100	0.100	0.100	0.100	0.173
B <sub>1</sub>	$\frac{m_{s1}}{m}$	0.040	0.0573	0.067	0.0528	0.0027
B <sub>2</sub>	$\frac{m_{s2}}{m}$	0.062	0.0903	0.106	0.0943	0.034
B <sub>3</sub>	$\frac{m_{s3}}{m}$	0.040	0.0508	0.0618	0.0930	0.145
B <sub>11</sub>	$\frac{m_{s1}}{I_{xx}} (s_1)$	0.002394	0.31026 x 10 <sup>-2</sup>	0.003375	0.2735 x 10 <sup>-2</sup>	0.000590
B <sub>12</sub>	$\frac{m_{s1}}{I_{xx}} \left( \frac{F-X}{m} \right)$	0.001105	0.2448 x 10 <sup>-2</sup>	0.003157	0.3084 x 10 <sup>-2</sup>	0.000613
B <sub>13</sub>	$\frac{m_{s1}}{M_1} Y_1(s_1)$	0.04715	0.07331	0.07828	0.0589	0.02871
B <sub>14</sub>	$\frac{m_{s1}}{M_1} \left( \frac{F-X}{m} \right) Y_1(s_1)$	0.05602	0.09592	0.11246	0.1217	0.04745
B <sub>15</sub>	$\frac{m_{s1}}{M_2} Y_2(s_1)$	0.03610	0.0780	0.08622	0.0562	0.00557
B <sub>16</sub>	$\frac{m_{s1}}{M_2} \left( \frac{F-X}{m} \right) Y_2(s_1)$	0.09219	0.1646	0.24337	0.1097	0.01785
B <sub>17</sub>	$\frac{m_{s1}}{M_1} Y_3(s_1)$	0.01189	0.01943	0.02987	0.07578	0.00252



Coefficient	Definition	t = 3	t = 40	t = 70	t = 120	t = 180
B <sub>18</sub>	$\frac{m_{s1}}{M_3} \left( \frac{F-X}{m} \right) Y_3'(s_1)$	0.05905	0.06617	0.10856	0.3892	0.00353
B <sub>19</sub>	$\frac{m_{s1}}{M_4} Y_4(s_1)$	-0.00292	$0.1983 \times 10^{-2}$	0.00161	$0.1672 \times 10^{-2}$	0.00884
B <sub>20</sub>	$\frac{m_{s1}}{M_3} \left( \frac{F-X}{m} \right) Y_4'(s_1)$	0.14291	0.61534	0.00738	0.01090	0.12821
B <sub>21</sub>	$\frac{m_{s2}}{I_{xx}} t_{s2}$	-0.0004672	$0.8769 \times 10^{-3}$	0.0015394	$0.2278 \times 10^{-2}$	0.005910
B <sub>22</sub>	$\frac{m_{s2}}{I_{xx}} \left( \frac{F-X}{m} \right)$	0.0024757	$0.365 \times 10^{-2}$	0.004951	$0.5613 \times 10^{-2}$	0.009366
B <sub>23</sub>	$\frac{m_{s2}}{M_1} Y_1(s_2)$	-0.05431	-0.04134	-0.02484	0	0.31323
B <sub>24</sub>	$\frac{m_{s2}}{M_1} \left( \frac{F-X}{m} \right) Y_1'(s_2)$	0.06296	0.1163	0.15194	0.2044	0.35872
B <sub>25</sub>	$\frac{m_{s2}}{M_2} Y_2(s_2)$	-0.07819	-0.1124	-0.12377	-0.0638	-0.00156
B <sub>26</sub>	$\frac{m_{s2}}{M_2} \left( \frac{F-X}{m} \right) Y_2'(s_2)$	-0.04694	0.06304	0.15400	0.2466	0.2752
B <sub>27</sub>	$\frac{m_{s2}}{M_3} Y_3(s_2)$	-0.01996	-0.04593	-0.06694	-0.1556	-0.01762
B <sub>28</sub>	$\frac{m_{s2}}{M_3} \left( \frac{F-X}{m} \right) Y_3'(s_2)$	-0.08350	-0.0474	-0.02056	0.2018	-0.02438
B <sub>29</sub>	$\frac{m_{s2}}{M_4} Y_4(s_2)$	0.06026	$-0.6248 \times 10^{-2}$	-0.00254	$-0.5972 \times 10^{-2}$	-0.04953
B <sub>30</sub>	$\frac{m_{s2}}{M_4} \left( \frac{F-X}{m} \right) Y_4'(s_2)$	-0.22150	-0.03383	-0.00741	$-0.5839 \times 10^{-2}$	0.08574
B <sub>31</sub>	$\frac{m_{s3}}{I_{xx}} t_{s3}$	-0.002399	$-0.254 \times 10^{-2}$	-0.002328	$-0.2118 \times 10^{-2}$	-0.000627
B <sub>32</sub>	$\frac{m_{s3}}{I_{xx}} \left( \frac{F-X}{m} \right)$	0.001597	$0.2171 \times 10^{-2}$	0.002912	$0.5533 \times 10^{-2}$	0.01022
B <sub>33</sub>	$\frac{m_{s3}}{M_1} Y_1(s_3)$	-0.06250	-0.08562	-0.09207	-0.1091	-0.18723
B <sub>34</sub>	$\frac{m_{s3}}{M_1} \left( \frac{F-X}{m} \right) Y_1'(s_3)$	0.00651	$0.3178 \times 10^{-2}$	0.02209	0.060	0.04460
B <sub>35</sub>	$\frac{m_{s3}}{M_2} Y_2(s_3)$	0.05144	0.04044	0.01996	-0.03731	-0.06393
B <sub>36</sub>	$\frac{m_{s3}}{M_2} \left( \frac{F-X}{m} \right) Y_2'(s_3)$	-0.10092	-0.1401	-0.10240	-0.2480	-0.22418
B <sub>37</sub>	$\frac{m_{s3}}{M_3} Y_3(s_3)$	0.06217	0.06159	0.06485	0.1085	-0.02136
B <sub>38</sub>	$\frac{m_{s3}}{M_3} \left( \frac{F-X}{m} \right) Y_3'(s_3)$	-0.02394	-0.02371	-0.05634	-0.3095	-0.48001
B <sub>39</sub>	$\frac{m_{s3}}{M_4} Y_4(s_3)$	0.00972	0.01338	0.00770	0.01119	0.02462
B <sub>40</sub>	$\frac{m_{s3}}{M_4} \left( \frac{F-X}{m} \right) Y_4'(s_3)$	0.12504	0.0272	0.02473	0.04799	-1.37884
C <sub>1</sub>	$\frac{N'}{I_{xx}} t_{CG}$	0	-0.0629	-0.2165	-0.0506	-0.003865
C <sub>2</sub>	$\frac{R'}{I_{xx}} t_{CG}$	0.8583	0.945	1.1701	1.567	2.410

Coefficient	Definition	t = 0	t = 30	t = 79	t = 120	t = 150.58
C <sub>3</sub>	$\frac{N'}{M}$	0	1.561	6.7670	1.846	0.2589
C <sub>4</sub>	$\frac{R'}{M}$	9.8067	22.598	17.6889	26.182	32.7826
D <sub>1</sub>	$\frac{S_E I_{CG} + I_E}{I_{xx}}$	0.0015644	$0.4132 \times 10^{-3}$	0.0018306	$0.6092 \times 10^{-3}$	0.0045687
D <sub>2</sub>	$\frac{F-X}{m} \left( \frac{S_E}{I_{xx}} \right)$	0.000638	$0.2112 \times 10^{-3}$	0.0012072	$0.5532 \times 10^{-3}$	0.0041
D <sub>3</sub>	$\frac{S_E Y_1(\beta) + I_E Y_1'(\beta)}{M_1}$	0.043236	0.01188	0.049284	0.01622	0.221252
D <sub>4</sub>	$\frac{R'}{M_1} Y_1(\beta)$	23.2181	26.31	29.5633	37.04	111.8780
D <sub>5</sub>	$\frac{S_E Y_2(\beta) + I_E Y_2'(\beta)}{M_2}$	0.049312	0.01588	0.076304	0.01758	0.057052
D <sub>6</sub>	$\frac{R'}{M_2} Y_2(\beta)$	25.2416	33.429	43.8701	40.39	26.8969
D <sub>7</sub>	$\frac{S_E Y_3(\beta) + I_E Y_3'(\beta)}{M_3}$	0.021772	$0.515 \times 10^{-2}$	0.028264	0.02862	0.041218
D <sub>8</sub>	$\frac{R'}{M_3} Y_3(\beta)$	10.8889	10.578	16.3996	63.65	16.6613
D <sub>9</sub>	$\frac{S_E Y_4(\beta) + I_E Y_4'(\beta)}{M_4}$	0.051024	$0.1123 \times 10^{-3}$	0.001608	$0.773 \times 10^{-3}$	0.175548
D <sub>10</sub>	$\frac{R'}{M_4} Y_4(\beta)$	23.8271	2.179	0.8435	1.658	64.4691
D <sub>11</sub>	$\frac{S_E}{M}$	0.016	$0.4042 \times 10^{-2}$	0.0256	$0.9294 \times 10^{-2}$	0.05616
E <sub>1</sub>	$f_{s1}$	17.6026	19.632	22.329	26.364	39.428
E <sub>2</sub>	$f_{s2}$	-2.3122	2.714	5.437	13.226	24.543
E <sub>3</sub>	$f_{s3}$	-18.465	-18.107	-18.846	-12.473	-2.513
E <sub>4</sub>	$\frac{F-X}{m}$	12.253	15.475	20.887	32.595	40.979
E <sub>5</sub>	$f_A$	-34.6	-34.304	-32.9	-28.67	-18.715
F <sub>1</sub>	$\frac{1}{V_0}$	$\infty$	$0.0372 \times 10^{-2}$	0.001970	$0.7493 \times 10^{-3}$	0.000396
G <sub>1</sub>	$2\zeta_1 \omega_1$	0.0252	0.0521	0.0546	0.05734	0.06372
G <sub>2</sub>	$2\zeta_2 \omega_2$	0.11988	0.1237	0.1300	0.14745	0.15683
G <sub>3</sub>	$2\zeta_3 \omega_3$	0.18127	0.1813	0.18284	0.2106	0.29336
G <sub>4</sub>	$2\zeta_4 \omega_4$	0.20537	0.2062	0.20693	0.2073	0.20943
G <sub>5</sub>	$2\zeta_{s1} \omega_{s1}$	0.2562	0.2916	0.3204	0.3780	0.4500
G <sub>6</sub>	$2\zeta_{s2} \omega_{s2}$	0.2562	0.2916	0.322	0.3840	0.4640
G <sub>7</sub>	$2\zeta_{s3} \omega_{s3}$	0.2562	0.2916	0.3244	0.4082	0.5200
G <sub>8</sub>	$1/\omega_A^2$	0.00031328	$0.31328 \times 10^{-3}$	0.00031328	$0.31328 \times 10^{-3}$	0.00031225
G <sub>9</sub>	$1/\omega_{RC}^2$	0.0002817	$0.2817 \times 10^{-4}$	0.0002817	$0.2817 \times 10^{-4}$	0.0002817
G <sub>10</sub>	$1/\omega_{I}^2$	0.0002817	$0.2817 \times 10^{-4}$	0.0002817	$0.2817 \times 10^{-4}$	0.0002817

Coefficient	Definition	t = 0	t = 40	t = 70	t = 100	t = 150.05
G <sub>11</sub>	1/ω <sub>E</sub> <sup>2</sup>	0.0005299	0.5299 x 10 <sup>-3</sup>	0.0005299	0.5299 x 10 <sup>-3</sup>	0.0005299
G <sub>12</sub>	2ξ <sub>F</sub> /ω <sub>F</sub>	0.004788	0.4788 x 10 <sup>-2</sup>	0.004788	0.4788 x 10 <sup>-2</sup>	0.004788
G <sub>13</sub>	T <sub>E</sub>	0.068	0.068	0.068	0.068	0.068
H <sub>1</sub>	ω <sub>1</sub> <sup>2</sup>	25.3915	27.629	29.8116	32.8738	40.8024
H <sub>2</sub>	ω <sub>2</sub> <sup>2</sup>	143.7121	152.89	169.0000	217.415	245.9565
H <sub>3</sub>	ω <sub>3</sub> <sup>2</sup>	328.5881	328.78	334.3046	443.65	860.8009
H <sub>4</sub>	ω <sub>4</sub> <sup>2</sup>	872.4344	937.58	942.0602	944.33	1518.5312
H <sub>5</sub>	ω <sub>n1</sub> <sup>2</sup>	4.3625	5.305	7.1289	9.910	12.8236
H <sub>6</sub>	ω <sub>s2</sub> <sup>2</sup>	4.3625	5.305	7.1935	10.266	3.6530
H <sub>7</sub>	ω <sub>s3</sub> <sup>2</sup>	4.3625	5.305	7.301	11.642	18.6887
H <sub>8</sub>	2ξ <sub>A</sub> /ω <sub>A</sub>	0.024778	0.024778	0.024778	0.024778	0.024778
H <sub>9</sub>	2ξ <sub>RG</sub> /ω <sub>RG</sub>	0.007431	0.7431 x 10 <sup>-2</sup>	0.007431	0.7431 x 10 <sup>-2</sup>	0.007431
H <sub>10</sub>	2ξ <sub>RG</sub> /ω <sub>RG</sub>	0.007431	0.7431 x 10 <sup>-2</sup>	0.007431	0.7431 x 10 <sup>-2</sup>	0.007431



APR 19 1964  
U.S. DEPARTMENT OF THE ARMY  
WASHINGTON, D.C.

~~CONFIDENTIAL~~

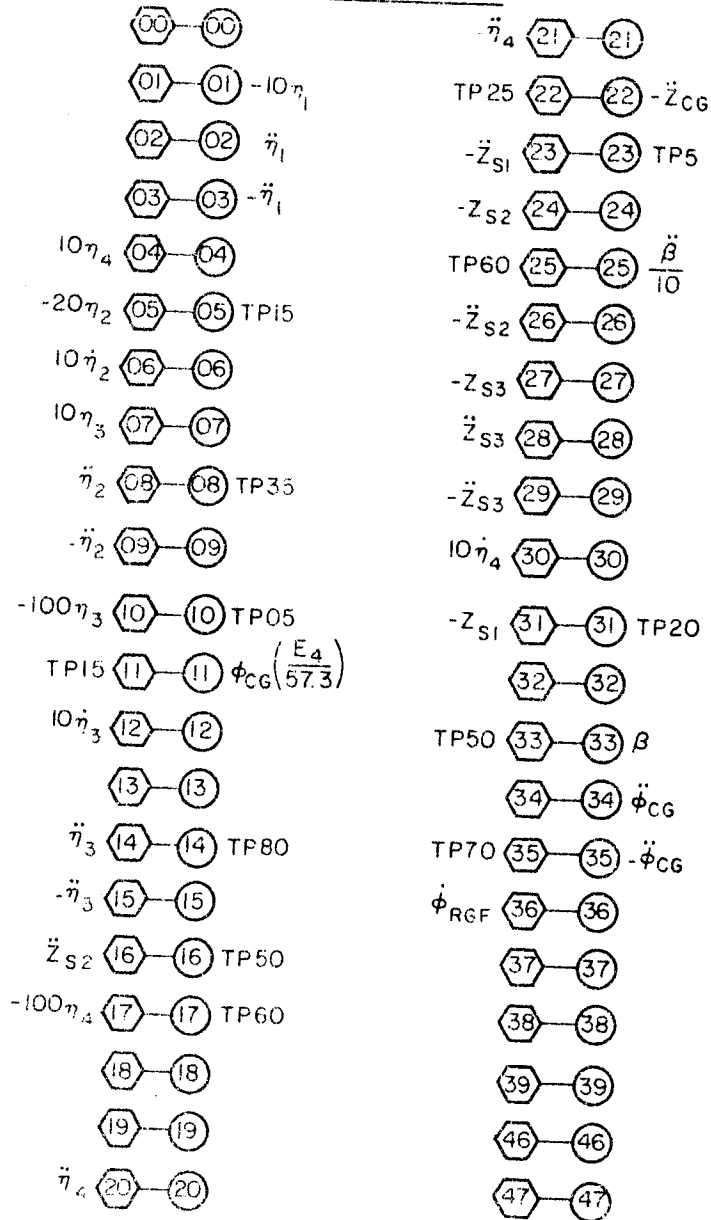
- G1 -



ANALOG SIMULATION - LIMITER SETTINGS

Limited Amplifier	Limit, Volts	Limit, System
10	60	15 sec
15	5	$5^\circ, \beta$
19	3.7	$700^\circ/\text{sec}^2, \ddot{\beta}$
20	4.8	$10^\circ/\text{sec}, \dot{\beta}$
21	75	75 m/sec, $V_W$

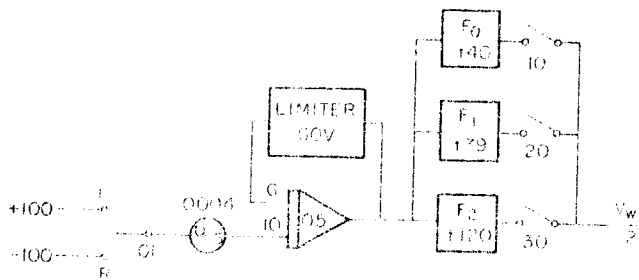
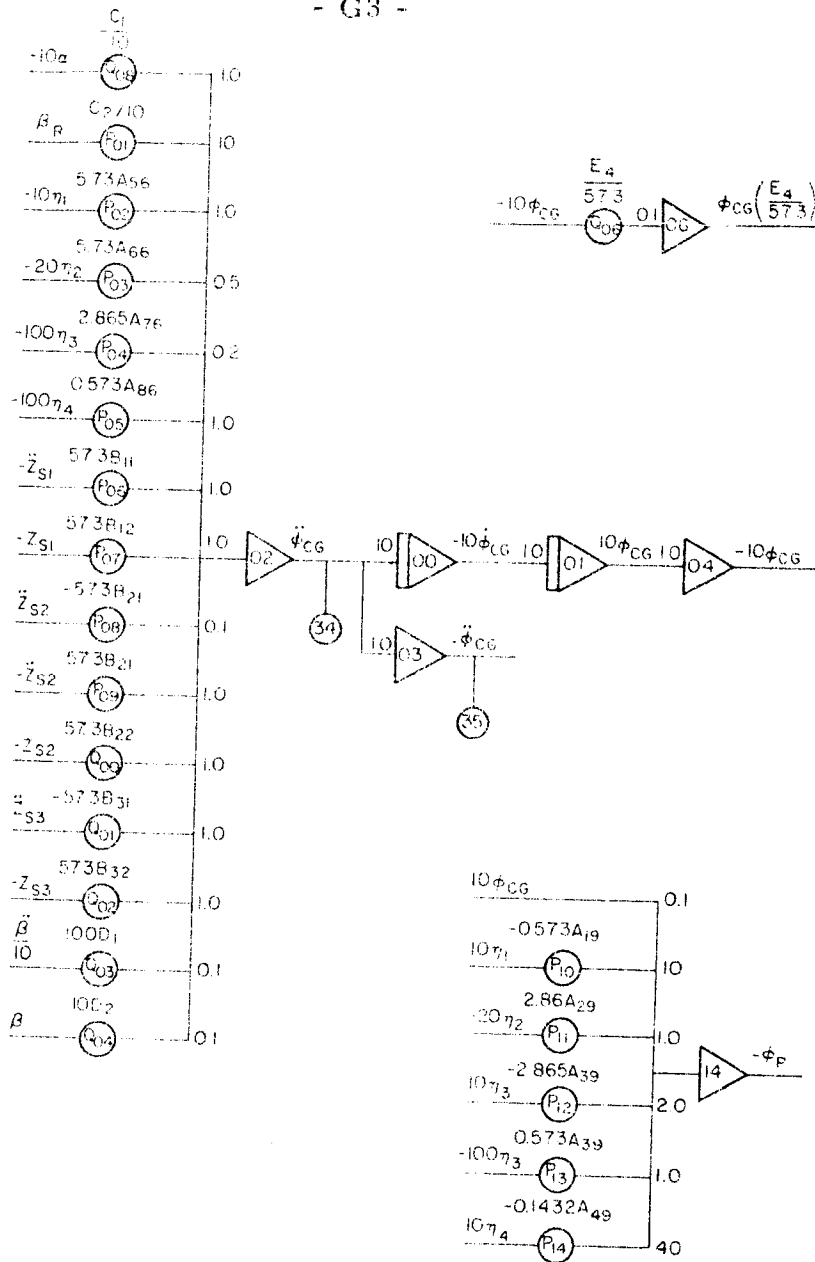
~~CONFIDENTIAL~~

INTERCONNECTS



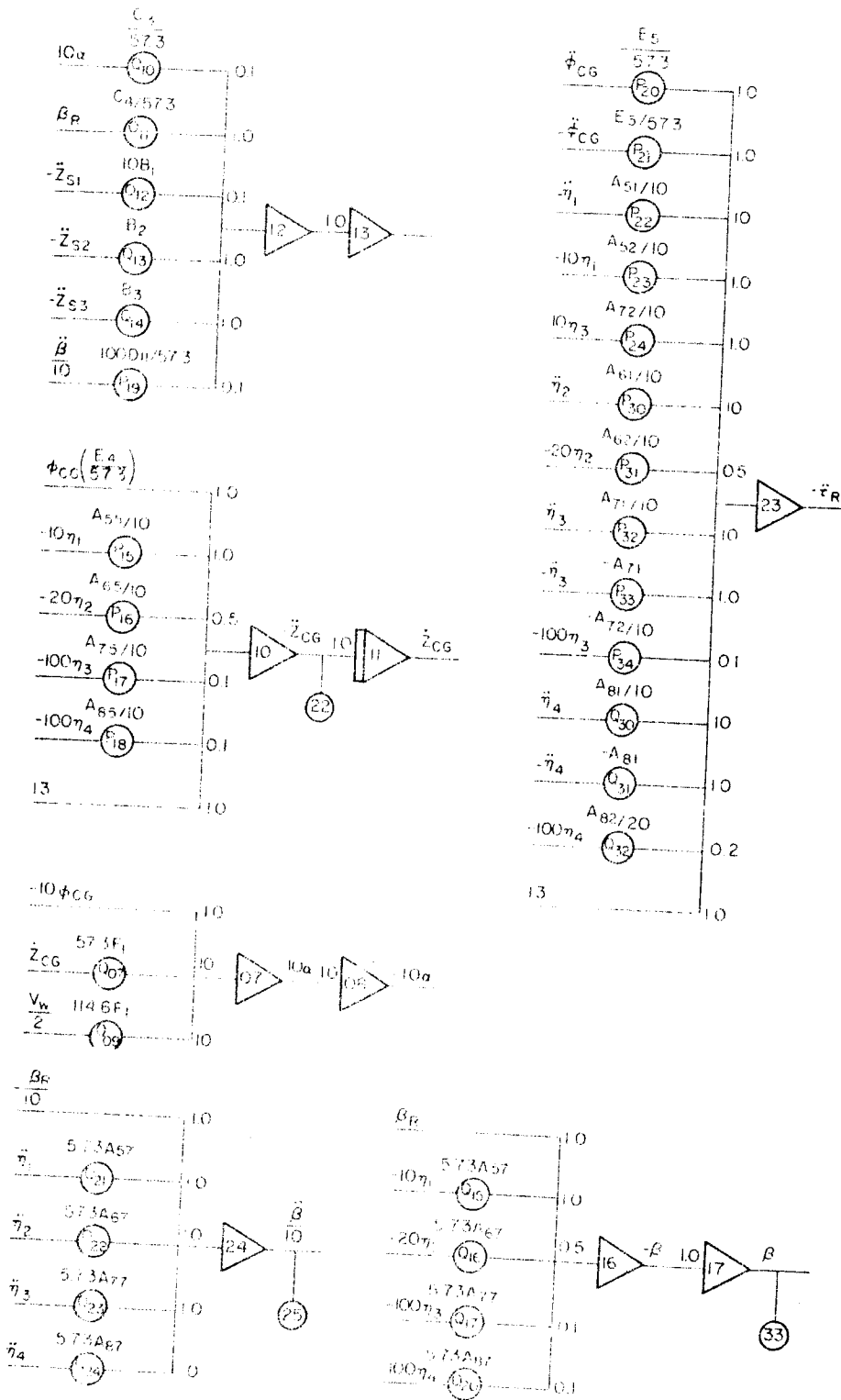
 - BOARD #15  
 - BOARD #3

- G3 -



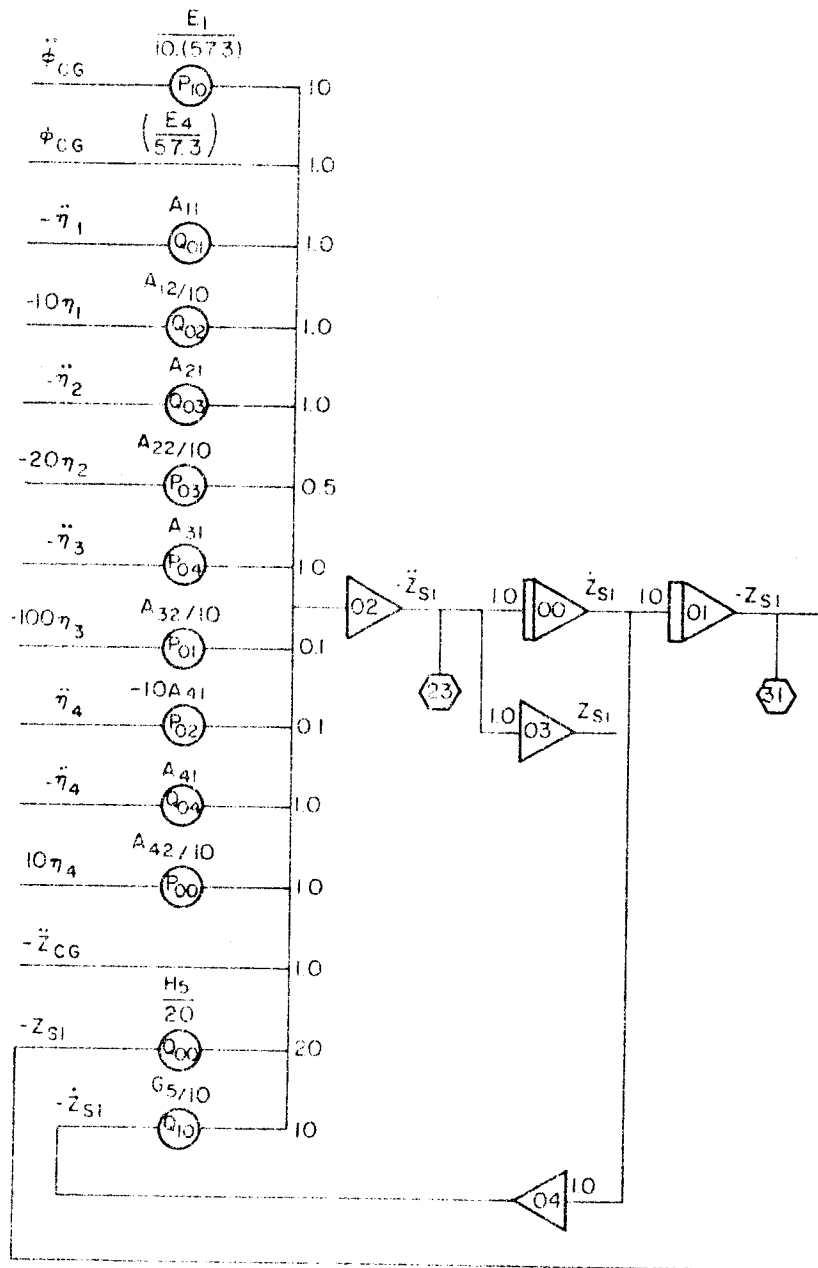
Board 3





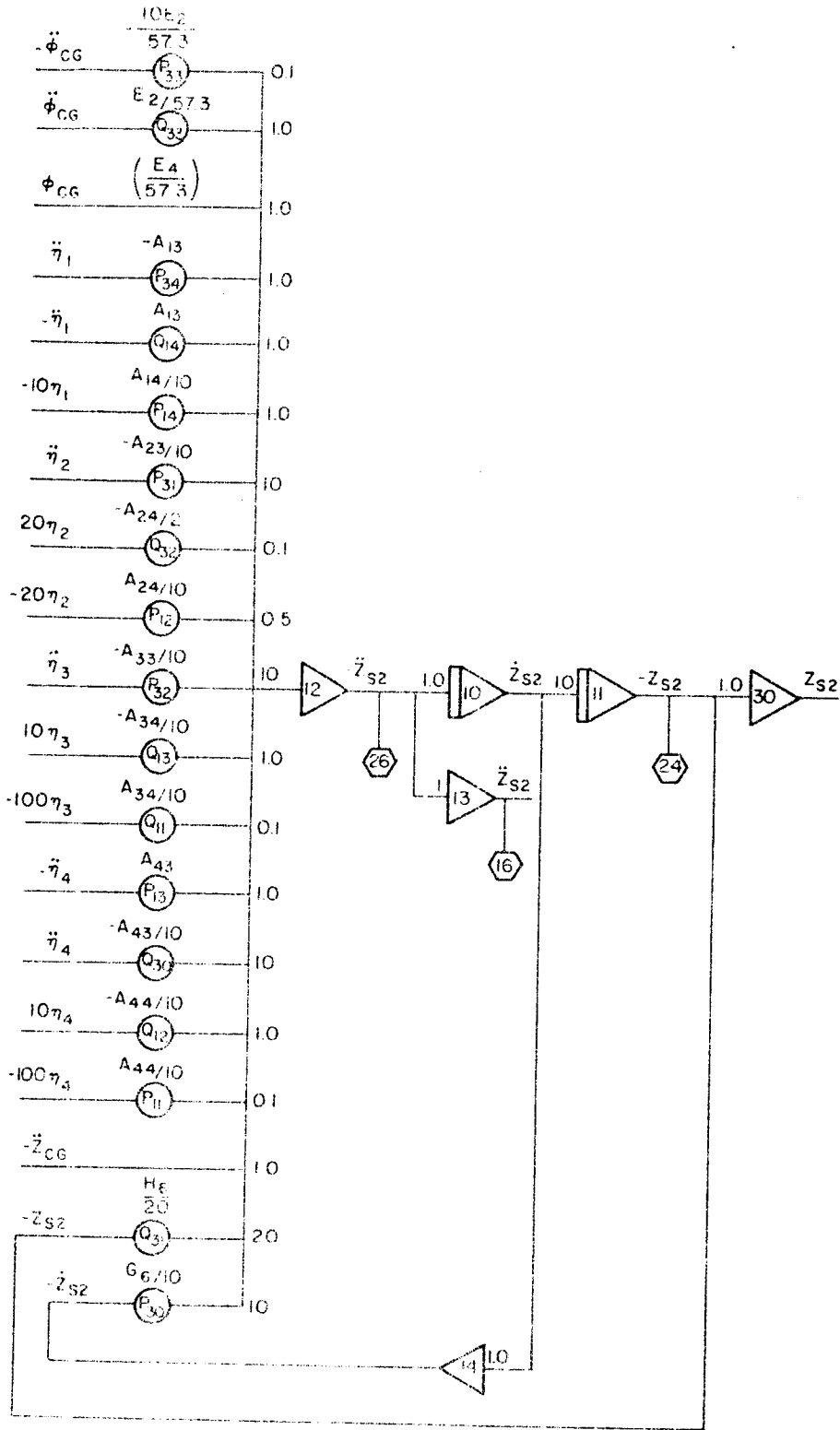
Board 3





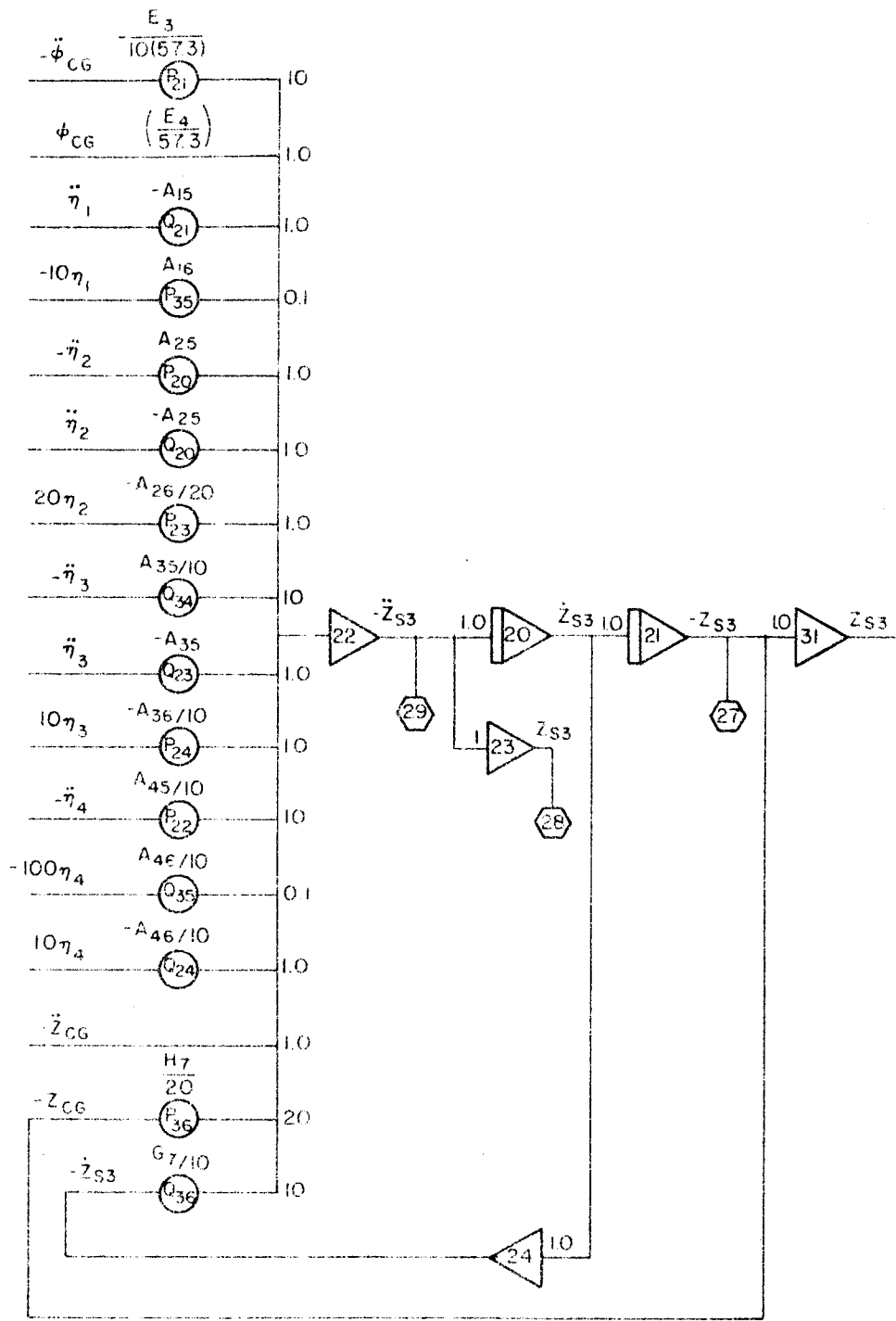
Board 15

- G7 -

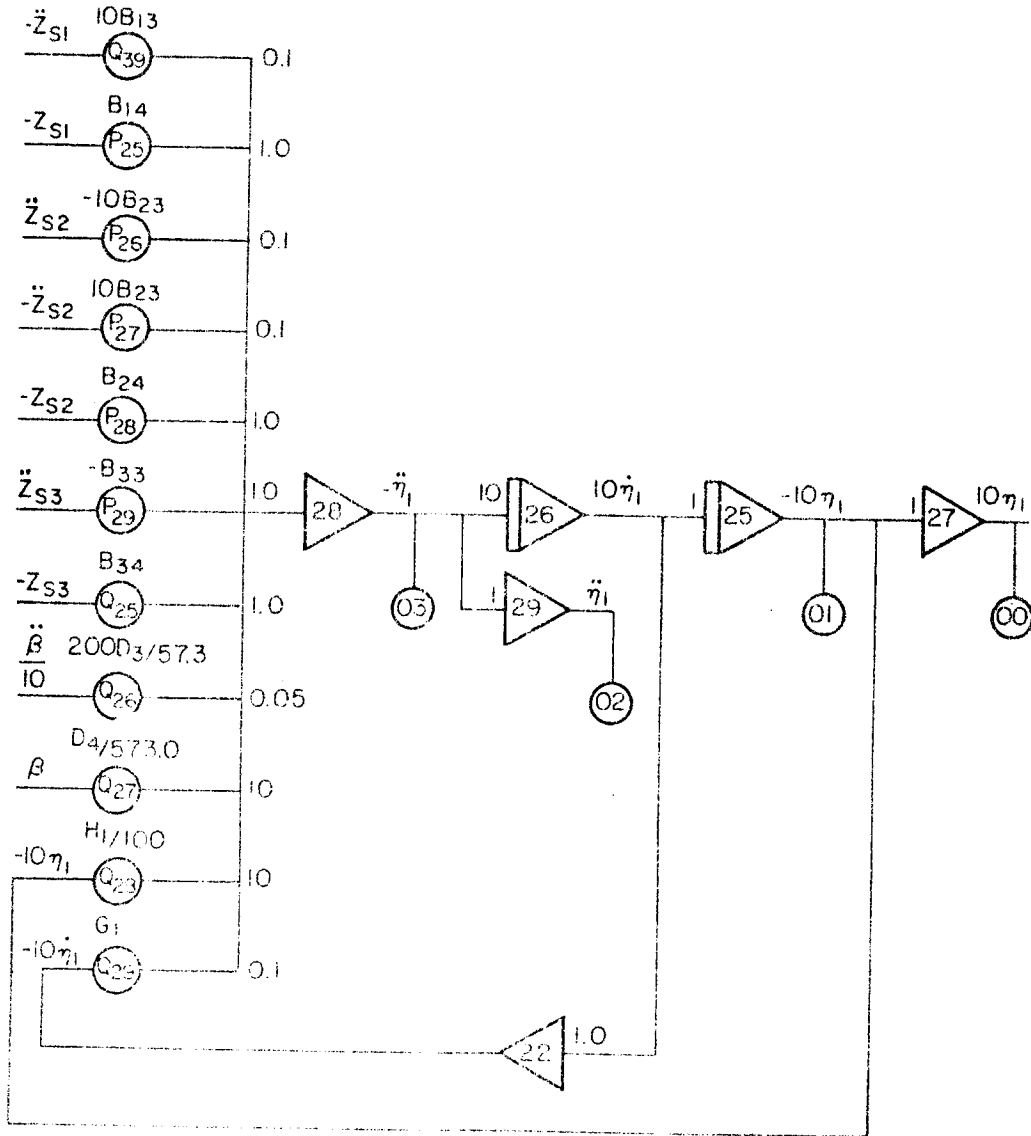


Board 15

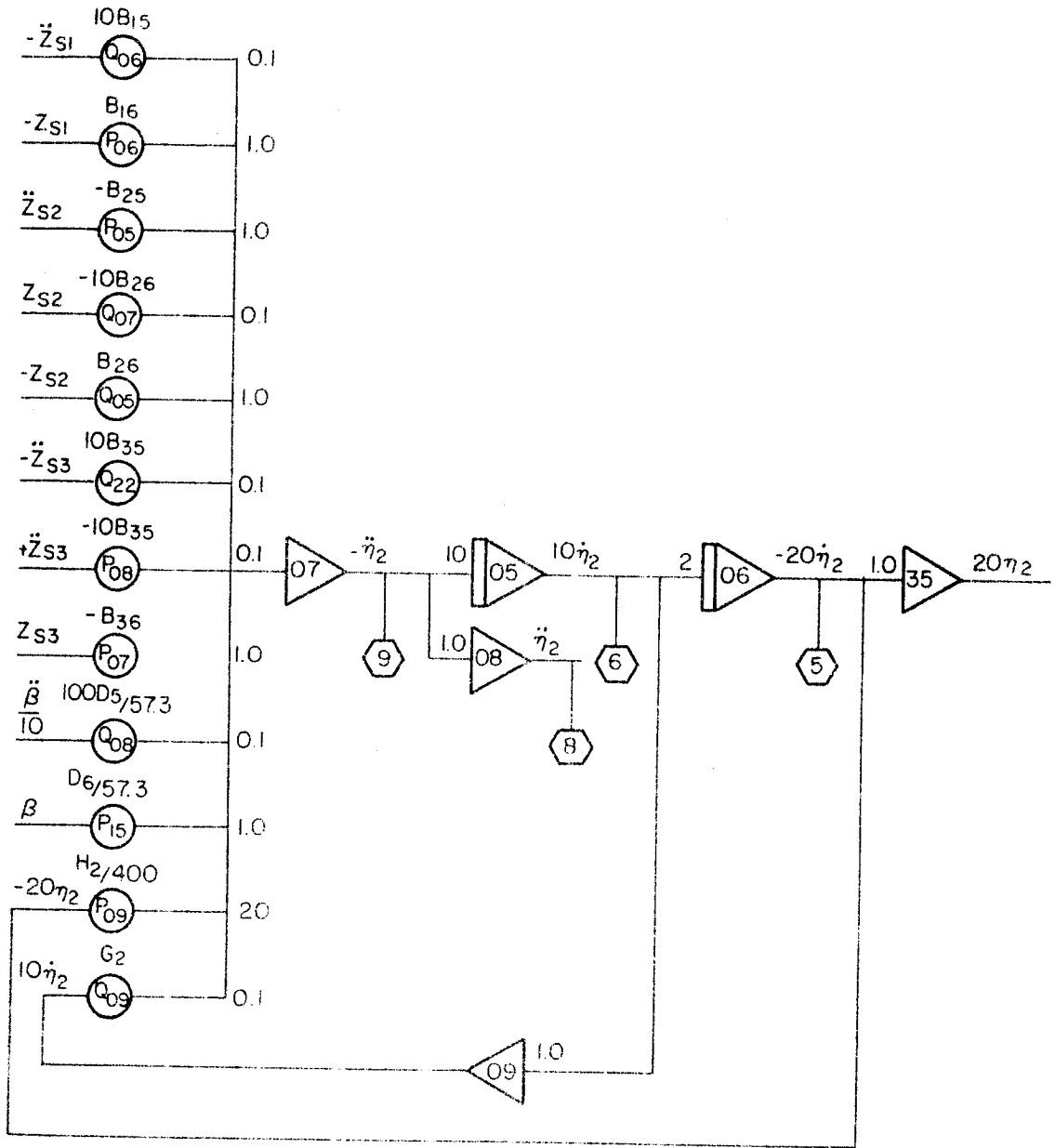
1300-TR1



Board 15

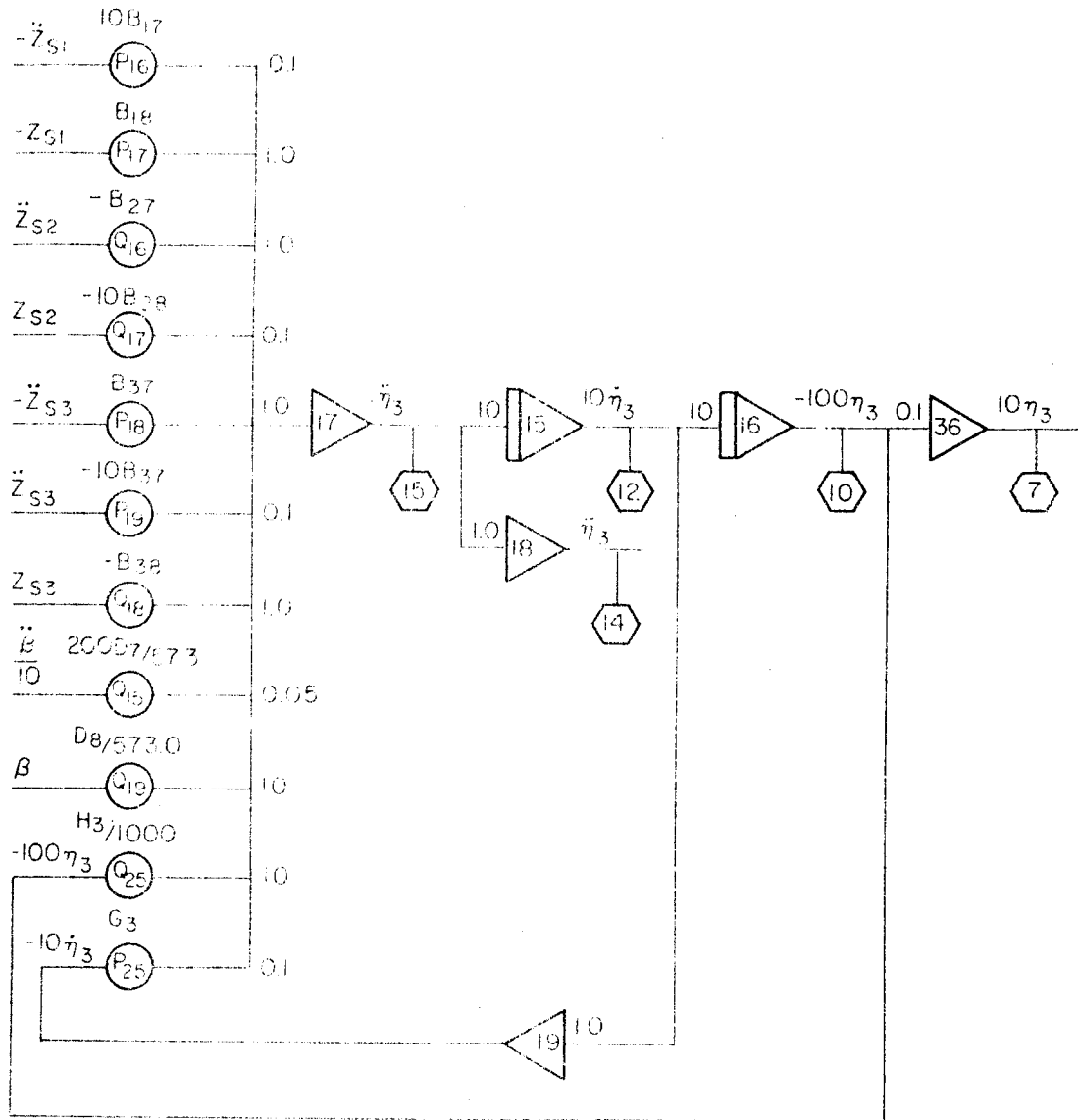


Board 3



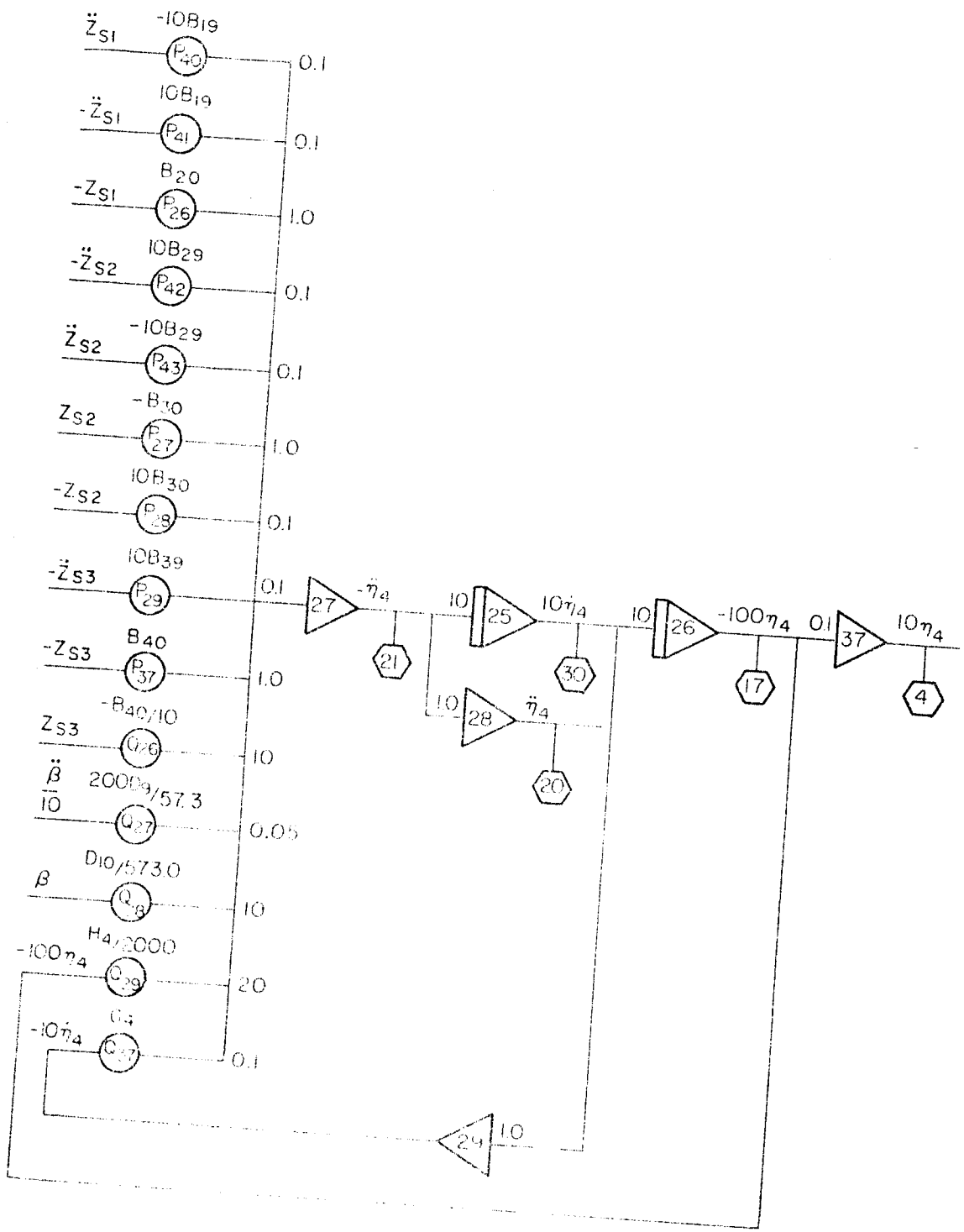
Board 15

- G11 -



Board 15





Board 15



APPENDIX II  
ANALOG SIMULATION POTENTIOMETER SETTINGS

- HI -

$X_A = 64.0$

$X_{RGA} = 5.0$

$X_{RGF} = 85.3$

$K_P = 0.9$

$K_A = 0$

Pot	Quantity	Nominal	Pot	Quantity	Nominal
P00	KR/10	0.210 <sup>*</sup>	Q20	5.73A87	0.5730
P01	C2/10	0.0800**	Q21	5.73A57	0.2579
P02	5.73A56	0.0858	Q22	5.73A67	0.3610
P03	5.73A66	0.0477	Q23	5.73A77	0.4126
P04	2.865A76	0.1584	Q24	5.73A87	0.5730
P05	0.573A86	0.1069	Q30	A81/10	0.0540
P06	57.3B11	0.0386	Q31	-A81	0
P07	57.3B12	0.1314	Q32	A82/20	0.0245
P08	-573B21	0.0914	Q33	5.73A38	0.4584
P09	57.3B21	0.2677	Q34	0.573A48	0.0630
Q00	+57.3B22	0	P15	A55/10	0.0552
Q01	-57.3B31	0.1418	P16	A65/10	0.0772
Q02	57.3B32	0.1374	P17	A75/10	0.0883
Q03	100D1	0.0915	P18	A85/10	0.1226
Q04	100D2	0.1564	P19	100D11/573	0.0279
Q05		0.0064	P25	B14	0.0580
Q06	E4/57.3	0	P26	-10B23	0.05431
Q07	57.3F1	0.2138	P27	10B23	0
Q08	-C1/10	0	P28	B24	0.0630
Q09	114.6F1	0	P29	-B33	0.0625
P10	-0.573A19	0.0802	P35	-0.573A17	0.0802
P11	2.865A29	0.4871	P36	0.573A18	0.0287
P12	-2.865A39	0.3330	P37	5.73A28	0.3954
P13	0.573A39	0	P38	5.73KA	0
P14	-0.1432A49	0.0583	P39	ω E2/10,000	0.1887
P20	-E5/57.3	0.6030	Q15	5.73A57	0.2579
P21	E5/57.3	0	Q16	5.73A67	0.3610
P22	-A51/10	0.0390	Q17	5.73A77	0.4126
P23	A52/10	0.1057	Q18	K1	0.020
P24	-A73/10	0.1350	Q19	Blender	0.80
P30	A61/10	0.1610	Q25	Balance	0.0070
P31	A62/10	0.1486	Q26	B34	0.1509
P32	A71/10	0	Q27	200D3/57.3	0.0405
P33	-A71	0.1800	Q28	D4/573	0.2539
P34	A72/10	0	Q29	H1/100	0.0252
Q10	C3/57.3	0	Q35	G1	0.1628
Q11	C4/57.3	0.1311	Q36	φ c/10	0.0900
Q12	10B1	0.4900	Q37	KP/10	0.9036
Q13	B2	0.0620	Q38	2ζ E3E/10	0.2088
Q14	B3	0.0400	Q39	ω E/2000ζ E	0.4735
				10B13	

\* Breadboard Blender

\*\* Simulated Blender

Board 3, t = 0 Seconds

$N_A = 64.0$

$N_{RGA} = 5.0$

$N_{RGE} = 85.3$

$K_P = 0.9$

$K_A = 0$

Pot	Quantity	Nominal	Pot	Quantity	Nominal
P00	A42/10	0.1470	Q22	10B35	0.3148
P01	A32/10	0.1127	Q23	-A35	0
P02	-10A41	0.3000	Q24	-A46/10	0
P03	A22/10	0.0895	Q30	-A43/10	0
P04	A31	0.2700	Q31	H6/20	0.2281
P05	-B25	0.0732	Q32	-A24/2	0.1470
P06	B16	0.0921	Q33	E2/57.3	0
P07	-B36	0.1009	Q34	A35/10	0.1400
P08	-10B35	0	P15	D6/57.3	0.4405
P09	H2/400	0.3593	P16	10B17	0.1199
Q00	H5/20	0.2281	P17	B18	0.0501
Q01	A11	0.5000	P18	B37	0.0622
Q02	A12/10	0.0613	P19	-10B37	0
Q03	A21	0.3700	P25	G3	0.1813
Q04	A41	0	P26	B20	0.1429
Q05	B26	0	P27	-B30	0.2215
Q06	10B15	0.3810	P28	10B30	0
Q07	-19B26	0.4693	P29	10B39	0.0972
Q08	100D5/57.3	0.0861	P35	A16	0.0735
Q09	G2	0.1199	P36	H7/20	0.2281
P10	E1/573	0.0307	P37	B40	0.1250
P11	A44/10	0	P38	2.865A27	0.4871
P12	A24/10	0	P39	-2.865	0.3380
P13	A43	0.4000	Q15	200D7/57.3	0.0760
P14	A14/10	0.0429	Q16	-B27	0.0199
P20	A25	0.5000	Q17	-10B28	0.8350
P21	-E3/573	0.0321	Q18	-B38	0.0239
P22	A35/10	0.0300	Q19	D3/573	0.0190
P23	-A26/20	0.0490	Q25	H3/1000	0.3286
P24	-A36/10	0.0539	Q26	-B40/10	0
P30	G6/10	0.0252	Q27	200D9/57.3	0.1781
P31	-A23/10	0.0490	Q28	D10/573	0.0416
P32	-A33/10	0.0290	Q29	H4/2000	0.4362
P33	-10E2/57.3	0.4035	Q35	A46/10	0.1287
P34	-A13	0.3700	Q36	G7/10	0.0252
Q10	G5/10	0.0252	Q37	G4	0.2954
Q11	A34/10	0	Q38	0.573A37	0
Q12	-A44/10	0.1470	Q39	-0.1432A47	0.0583
Q13	-A34/10	0.1213	P40	-10B19	0.0281
Q14	A13	0	P41	10B19	0
Q20	-A25	0	P42	10B29	0.6026
Q21	-A15	0.6600	P43	-10B29	0

$\xi_s = 0.000$

Board 15, t = 0 Seconds

$X_A = 64.0$  $X_{RGA} = 5.0$  $X_{RGP} = 55.3$  $K_P = 0.9$  $K_A = 0.05$ 

Pot	Quantity	Nominal	Pot	Quantity	Nominal
P00	KR	0.210	Q20	5.73A87	0.5730
P01	C2/10	0.0860**	Q21	5.73A57	0.2865
P02	5.73A56	0.0945	Q22	5.73A67	0.3553
P03	5.73A66	0.0892	Q23	5.73A77	0.4183
P04	2.865A76	0.1705	Q24	5.73A87	0.5730
P05	0.573A86	0.1225	Q30	A81/10	0.1800
P06	57.3B11	0.0428	Q31	-A81	0
P07	57.3B12	0.1778	Q32	A82/20	0.1251
P08	-573B4	0.1403	Q33	5.73A38	0.4527
P09	57.3B21	0	Q34	0.573A48	0.0573
Q00	57.3B22	0.0388	P15	A55/10	0.0787
Q01	57.3B22	0.2206	P16	A65/10	0.0976
Q02	-57.3B31	0.1455	P17	A75/10	0.1150
Q03	57.3B32	0.1244	P18	A85/10	0.1575
Q04	100D1	0.1653	P19	100D11/57.3	0.0345
Q05	10D2	0.0084	P25	B14	0.0959
Q06	E4/57.3	0.0040	P26	-10B23	0.4134
Q07	57.3F1	0.2701	P27	10B23.	0
Q08	-C1/10	0.3651	P28	B24	0.1163
Q09	114.6F1	0.0063	P29	-B33	0.0856
P10	-0.573A19	0.7302	P35	-0.573A17	0.08480
P11	2.865A29	0.0848	P36	0.573A18	0.02865
P12	-2.865A39	0.4412	P37	5.73A28	0.3782
P13	-2.865A39	0.4441	P38	5.73KA	0.2865
P14	0.573A39	0	P39	ωE2/10,000	0.1887
P20	-0.1432A49	0.2936	Q15	5.73A57	0.2865
P21	-E5/57.3	0.5990	Q16	5.73A67	0.3553
P22	E5/57.3	0	Q17	5.73A77	0.4183
P23	-A51/10	0.0520	Q18	Ki	0.020
P24	A52/10	0.1408	Q19	Blender	0.800
P30	-A72/10	0.2245	Q25	Balance	0.0082
P31	A61/10	0.1300	Q26	B34	0.1661
P32	A62/10	0.1862	Q27	200D3/57.3	0.0457
P33	A71/10	0	Q28	D4/573	0.2789
P34	-A71	0.1000	Q29	H1/100	0.05210
Q10	A72/10	0	Q35	G1	0.1628
Q11	C3/57.3	0.0272	Q36	φC/10	0.090
Q12	C4/57.3	0.2199	Q37	KP/10	0.9036
Q13	10B1	0.5730	Q38	2φEωE/10	0.2089
Q14	B2	0.0903	Q39	ωE/2000φE	0.7331
	B3	0.0508		10B13	

\* Breadboard blender

\*\* Simulated blender

Board 3, t = 40 Seconds

1300-TR1

~~CONFIDENTIAL~~

- H4 -

$X_A = 64.0$      $X_{RGA} = 5.0$      $X_{RGE} = 85.3$      $K_P = 0.9$      $K_A = 0.05$

Pot	Quantity	Nominal	Pot	Quantity	Nominal
P00	A42/10	0.1548	Q22	10B35	0.4044
P01	A32/10	0.1362	Q23	-A35	0
P02	-10A41	0	Q24	-A46/10	0
P03	A22/10	0.1083	Q30	-A43/10	0.0400
P04	A31	0.4000	Q31	H6/20	0.2953
P05	-B25	0.1174	Q32	-A24/2	0
P06	B16	0.1646	Q33	E2/57.3	0.0474
P07	-B36	0.1481	Q34	A35/10	0.1430
P08	-10B35	0	P15	D6/57.3	0.5834
P09	H2/400	0.3822	P16	10B17	0.1943
Q00	H5/20	0.2953	P17	B18	0.0662
Q01	A11	0.6150	P18	B37	0.0616
Q02	A12/10	0.0805	P19	-10B37	0
Q03	A21	0.5000	P25	G3	0.1813
Q04	A41	0.2000	P26	B20	0.0153
Q05	B26	0.0630	P27	-B30	0.0338
Q06	10B15	0.7600	P28	10B30	0
Q07	-10B26	0	P29	10B39	0.1318
Q08	100D5/57.3	0.1095	P35	A16	0.0774
Q09	G2	0.1237	P36	H7/20	0.2953
P10	E1/573	0.0342	P37	B40	0.0272
P11	A44/10	0	P38	2.865A27	0.4412
P12	A24/10	0.0263	P39	-2.865A37	0.4441
P13	A43	0	Q15	200D7/57.3	0.0719
P14	A14/10	0.0619	Q16	-B27	0.0459
P20	A25	0.3000	Q17	-10B28	0.4740
P21	-E3/573	0.0316	Q18	-B38	0.0233
P22	A45/10	0.1500	Q19	D8/573	0.0186
P23	-A26/20	0.0550	Q25	H3/1000	0.3287
P24	-A36/10	0.0542	Q26	-B40/10	0
P30	G6/10	0.0288	Q27	200D9/57.3	0.0039
P31	-A23/10	0.0490	Q28	D10/573	0.0038
P32	-A33/10	0.0600	Q29	H4/2000	0.4688
P33	-10E2/57.3	0	Q35	A46/10	0.3095
P34	-A13	0.2200	Q36	G7/10	0.0288*
Q10	G5/10	0.0288	Q37	G4	0.3062
Q11	A34/10	0	Q38	0.573A37	0
Q12	-A44/10	0.2167	Q39	-0.1432A47	0.2936
Q13	-A34/10	0.0619	P40	-10B19	0
Q14	A13	0	P41	10B19	0.0198
Q20	-A25	0	P42	10B29	0
Q21	-A15	0.3100	P43	-10B29	0.0625

\*  $\zeta_s = 0.000$

Board 15, t = 40 Seconds

$X_A = 64.0$      $X_{RGA} = 5.0$      $X_{RGE} = 85.3$      $K_P = 0.9$      $K_A = 0.05$

Pot	Quantity	Nominal	Pot	Quantity	Nominal
P00	KR/100	0.210*	Q20	5.73A87	0.5730
P01	C2/10	0.0300**	Q21	5.73A57	0.2750
P02	5.73A56	0.1138	Q22	5.73A67	0.3667
P03	5.73A66	0.1059	Q23	5.73A77	0.4240
P04	2.865A76	0.2364	Q24	5.73A87	0.5730
P05	0.573A86	0.1589	Q30	A81/10	0.3300
P06	57.3B11	0.0530	Q31	-A81	0
P07	57.3B12	0.1934	Q32	A82/20	0.3715
P08	-573.B21	0.1809	Q33	A82/20	0.3715
P09	57.3B21	0	Q34	5.73A38	0.4584
Q00	57.3B22	0.0882	P15	0.573A48	0.0573
Q01	57.3B22	0.2836	P16	A55/10	0.1060
Q02	-57.3B31	0.1333	P17	A65/10	0.1413
Q03	57.3B32	0.1668	P18	A75/10	0.1634
Q04	100D1	0.1831	P19	A85/10	0.2207
Q05	10D2	0.0121	P25	100D11/57.3	0.0447
Q06	E4/57.3	0.0040	B14	B14	0.1125
Q07	57.3F1	0.3645	P26	-10B23	0.2484
Q08	-C1/10	0.1129	P27	10B23	0
Q09	114.6F1	0.0217	P28	B24	0.1520
P10	-0.573A19	0.2258	P29	-B33	0.0921
P11	2.86A29	0.0860	P35	-0.573A17	0.0860
P12	-2.865A29	0.3438	P36	0.573A18	0.0275
P13	-2.865A39	0.3438	P37	5.73A28	0.3954
P14	0.573A39	0	P38	5.73KA	0.2865
P20	-0.1432A49	0.4226	P39	ωE2/10,000	0.1887
P21	-E5/57.3	0.5742	Q15	5.73A57	0.2750
P22	E5/57.3	0	Q16	5.73A67	0.3667
P23	-A51/10	0.0660	Q17	5.73A77	0.4240
P24	A52/10	0.2005	Q18	Ki	0.020
P30	-A72/10	0.1834	Q19	Blender	0.800
P31	A61/10	0.1200	Q25	Balance	0.0281
P32	A62/10	0.2711	B34	B34	0.1720
P33	A71/10	0	Q26	200D3/57.3	0.0516
P34	-A71	0.1000	Q27	D4/573	0.2981
Q10	A72/10	0	Q28	H1/100	0.0546
Q11	C3/57.3	0.1181	Q29	G1	0.1628
Q12	C4/57.3	0.3082	Q35	φC/10	0.0900
Q13	10B1	0.6700	Q36	KP/10	0.9036
Q14	B2	0.1060	Q37	2φEωE/10	0.2088
	B3	0.0618	Q38	ωE/2000φE	0.7628
			Q39	10B13	

\* Breadboard blender

\*\* Simulated blender

Board 3, t = 79 Seconds



- H6 -

$X_A = 64.0$     $X_{PGA} = 5.0$     $X_{RGP} = 85.3$     $K_P = 0.9$     $K_A = 0.05$

Pot	Quantity	Nominal	Pot	Quantity	Nominal
P00	A42/10	0.2298	Q22	10B35	0.1996
P01	A32/10	0.1713	Q23	-A35	0
P02	-10A41	0	Q24	-A46/10	0
P03	A22/10	0.1462	Q30	-A43/10	0.0500
P04	A31	0.4800	Q31	H6/20	0.3599
P05	-B25	0.1238	Q32	-A24/2	0
P06	B16	0.2434	Q33	E2/57.3	0.1123
P07	-B36	0.1924	Q34	A35/10	0.1130
P08	-10B35	0	P15	D6/57.3	0.7656
P09	H2/400	0.4225	P16	10B17	0.2987
Q00	H5/20	0.3564	P17	B18	0.1066
Q01	A11	0.6800	P18	1B37	0.0648
Q02	A12/10	0.1003	P19	-10B37	0
Q03	A21	0.5300	P25	G3	0.1828
Q04	A41	0.5000	P26	B20	0.0074
Q05	B26	0.1540	P27	-B30	0.0074
Q06	10B15	0.8822	P28	10B30	0
Q07	-10B26	0	P29	10B39	0.0770
Q08	100D5/57.3	0.1332	P35	A16	0.2715
Q09	G2	0.1300	P36	H7/20	0.3651
P10	E1/573	0.0389	P37	B40	0.0249
P11	A44/10	0	P38	2.865A27	0.3438
P12	A24/10	0.0585	P39	-2.865A37	0.3438
P13	A43	0	Q15	200D7/57.3	0.1020
P14	A14/10	0.0856	Q16	-B27	0.0669
P20	A25	0.1300	Q17	-10B28	0.2056
P21	-E3/573	0.0290	Q18	-B38	0.0563
P22	A45/10	0.2600	Q19	D8/573	0.0286
P23	-A26/20	0.0626	Q25	H3/1000	0.3343
P24	-A36/10	0.0982	Q26	-B40/10	0
P30	G6/10	0.0324*	Q27	200D9/57.3	0.0056
P31	-A23/10	0.0470	Q28	D10/573	0.0015
P32	-A33/10	0.0680	Q29	H4/2000	0.4710
P33	-10E2/57.3	0	Q35	A46/10	0.8355
P34	-A13	0.1400	Q36	G7/10	0.0324*
Q10	G5/10	0.0324*	Q37	G4	0.3069
Q11	A34/10	0	Q38	0.573A37	0
Q12	-A44/10	0.1462	Q39	-0.1432A47	0.4226
Q13	-A34/10	0.0209	P40	-10B19	0
Q14	A13	0	P41	10B19	0.0161
Q20	-A25	0	P42	10B29	0
Q21	-A15	0.8900	P43	-10B29	0.0254

\*  $\zeta_s = 0.060$

Board 15, t = 79 Seconds

$X_A = 64.0$      $X_{RGA} = 5.0$      $X_{RGE} = 85.3$      $K_P = 0.9$      $K_A = 0.02$

Pot	Quantity	Nominal	Pot	Quantity	Nominal
P00	KR/100	0.210	Q20	5.73A87	0.5730
P01	C2/10	0.0300**	Q21	5.73A57	0.2865
P02	5.73A56	0.1567	Q22	5.73A67	0.4126
P03	5.73A66	0.2189	Q23	5.73A77	0.4871
P04	2.865A76	0.4656	Q24	5.73A87	0.5730
P05	0.573A86	0.3058	Q30	A81/10	0.1800
P06	57.3B11	0.0780	Q31	-A81	0
P07	57.3B12	0.1567	Q32	A82/20	0.2615
P08	-573B21	0.1767	Q33	5.73A38	0.5157
P09	57.3B21	0	σ34	0.573A48	0.0573
Q00	57.3B22	0.1305	P15	A55/10	0.1636
Q01	-57.3B31	0.3216	P16	A65/10	0.2356
Q02	57.3B32	0.1214	P17	A75/10	0.2782
Q03	100D1	0.3172	P18	A85/10	0.3273
Q04	10D2	0.2436	P19	100D11/57.3	0.0648
Q05		0.0221	P25	B14	0.1217
Q06	E4/57.3	0.0040	P26	-10B23	0
Q07	57.3F1	0.5688	P27	10B23	0
Q08	-C1/10	0.0429	P28	B24	0.2044
Q09	114.6F1	0.0061	P29	-B33	0.1091
P10	-0.573A19	0.0859	P35	-0.573A17	0.07907
P11	2.865A29	0.0791	P36	0.573A18	0.02865
P12	-2.865A39	0.4813	P37	5.73A28	0.4469
P13	0.573A39	0.0430	P38	5.73KA	0.1146
P14	-0.1432A49	0	P39	ωE2/10,000	0.1887
P20	-E5/57.3	0.3552	Q15	5.73A57	0.2865
P21	E5/57.3	0.5010	Q16	5.73A67	0.4126
P22	-A51/10	0	Q17	5.73A77	0.4871
P23	A52/10	0.07200	Q18	K <sub>1</sub>	0.020
P24	-A72/10	0.2613	Q19	Blender	0.800
P30	A61/10	0		Balance	
P31	A62/10	0.1070	Q25	B34	0.0600
P32	A71/10	0.5715	Q26	200D3/57.3	0.2260
P33	-A71	0.0260	Q27	D4/573	0.0646
P34	A72/10	0	Q28	H1/100	0.3288
Q10	C3/57.3	0.0825	Q29	G1	0.05734
Q11	C4/57.3	0.0322	Q35	φC/10	0.1628
Q12	10B1	0.4569	Q36	KP/10	0.090
Q13	B2	0.5280	Q37	2ζEωE/10	0.9036
Q14	B3	0.0943	Q38	ωE/200ζE	0.2089
		0.0930	Q39	10B13	0.5890

Breadboard blender

\*\* Simulated blender

Board 3, t = 120 Seconds

~~CONFIDENTIAL~~

- H10 -

XA = 64.0    XRGa = 5.0    XRCF = 85.3    KP = 0.9    KA = 0

Pot	Quantity	Nominal	Pot	Quantity	Nominal
P00	A42/10	0.7376	Q22	10B35	0
P01	A32/10	0.5327	Q23	-A35	0.2900
P02	-10A41	0	Q24	-A46/10	0.4836
P03	A22/10	0.2500	Q30	-A43/10	0.1800
P04	A31	0.5700	Q31	H6/20	0.6827
P05	-B25	0.0020	Q32	-A24/2	0
P06	B16	0.0179	Q33	E2/57.3	0.4283
P07	-B36	0.2242	Q34	A35/10	0
P08	-10B35	0.6303	P15	D6/57.3	0.4694
P09	H2/400	0.6149	P16	10B17	0.0252
QC0	H5/20	0.6412	P17	B18	0.0236
Q01	A11	0.9000	P18	B37	0
Q02	A12/10	0.1598	P19	-10B37	0.2136
Q03	A21	0.7800	P25	G3	0.2934
Q04	A41	0.4000	P26	B20	0.1262
Q05	B26	0.0235	P27	-B30	0
Q06	10B15	0.0557	P28	10B30	0.8574
Q07	-10B26	0	P29	10B39	0.2852
Q08	100D5/57.3	0.0996	P35	A16	0.6966
Q09	G2	0.1568	P36	H7/20	0.9344
P10	E1/573	0.0688	P37	B40	0
P11	A44/10	0.3114	P38	2.865A27	0.5014
P12	A24/10	0.2049	P39	-2.865A37	0
P13	A43	0	Q15	200D7/57.3	0.1439
P14	A14/10	0.1229	Q16	-10B27	0.0078
P20	A25	0	Q17	-10B28	0.2418
P21	-E3/573	0.0044	Q18	-B38	0.4800
P22	A45/10	0.0100	Q19	D8/573	0.0291
P23	-A26/20	0.0942	Q25	H3/1000	0.8606
P24	-A36/10	0.6516	Q26	-B40/10	0.1379
P30	G6/10	0.0444*	Q27	200D9/57.3	0.6127
P31	-A23/10	0.0170	Q28	D10/573	0.1125
P32	-A33/10	0.1100	Q29	H4/2000	0.7583
P33	-10E2/57.3	0	Q35	A46/10	0
P34	-A13	0	Q36	1/10G7	0.0258
Q10	G5/10	0.0444*	Q37	G4	0.3894
Q11	A34/10	0.3401	Q38	0.573A37	0.3438
Q12	-A44/10	0	Q39	-0.1432A47	0.0354
Q13	-A34/10	0	P40	-10B19	0
Q14	A13	0.3200	P41	10B19	0.0684
Q20	-A25	0.5300	P42	10B29	0
Q21	-A15	0.3800	P43	-10B29	0.4955

\* $\zeta_s$  = 0.060

Board 15, t = 153 Seconds

1300-TR1

~~CONFIDENTIAL~~

APPENDIX J  
SYNTHETIC WIND SHEAR PROFILES

~~CONFIDENTIAL~~

- J1 -

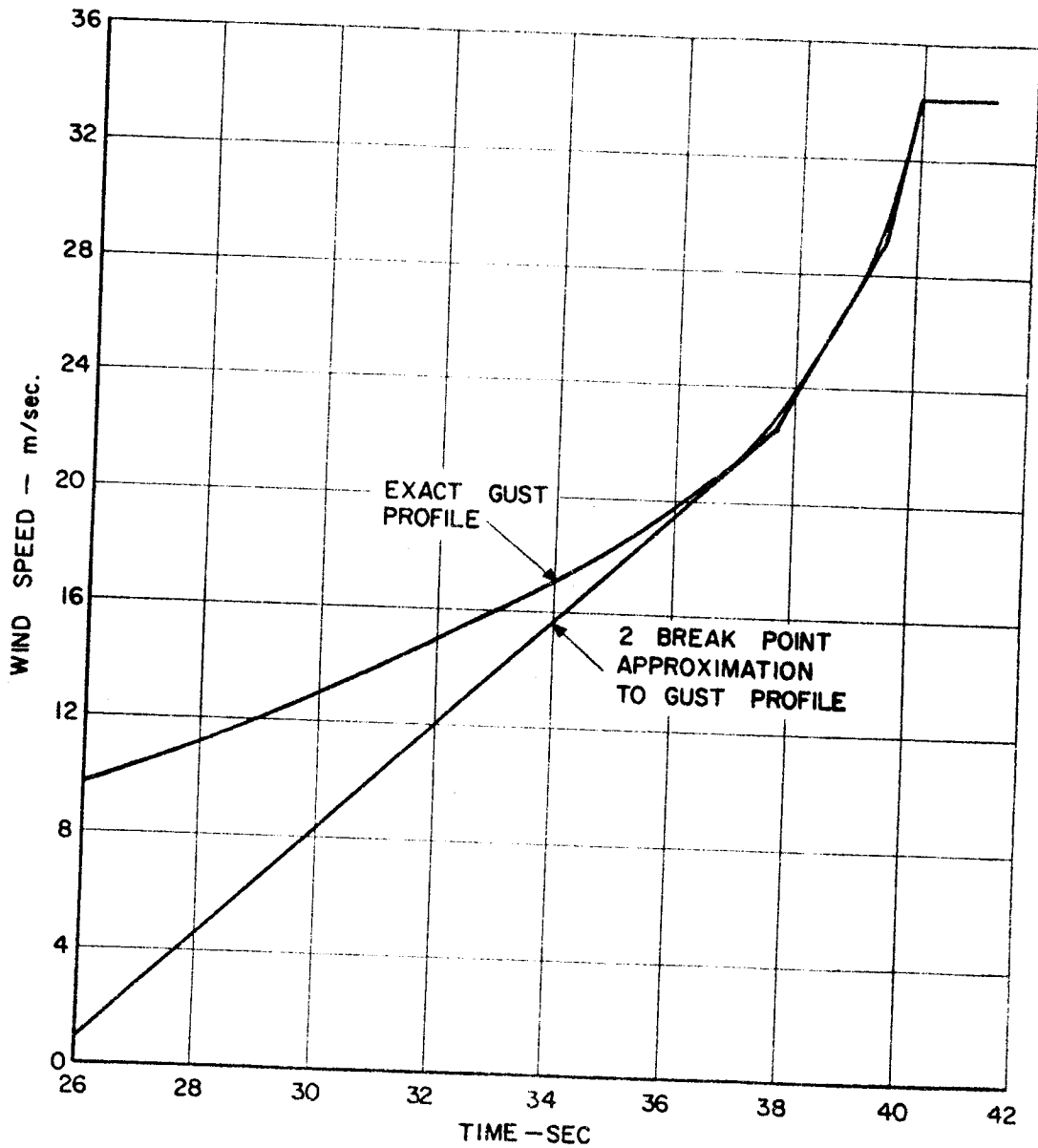


Figure J1. Synthetic Wind Shear Profile - Maximum Dynamic Pressure (t = 40 seconds)

1300-TR1

~~CONFIDENTIAL~~

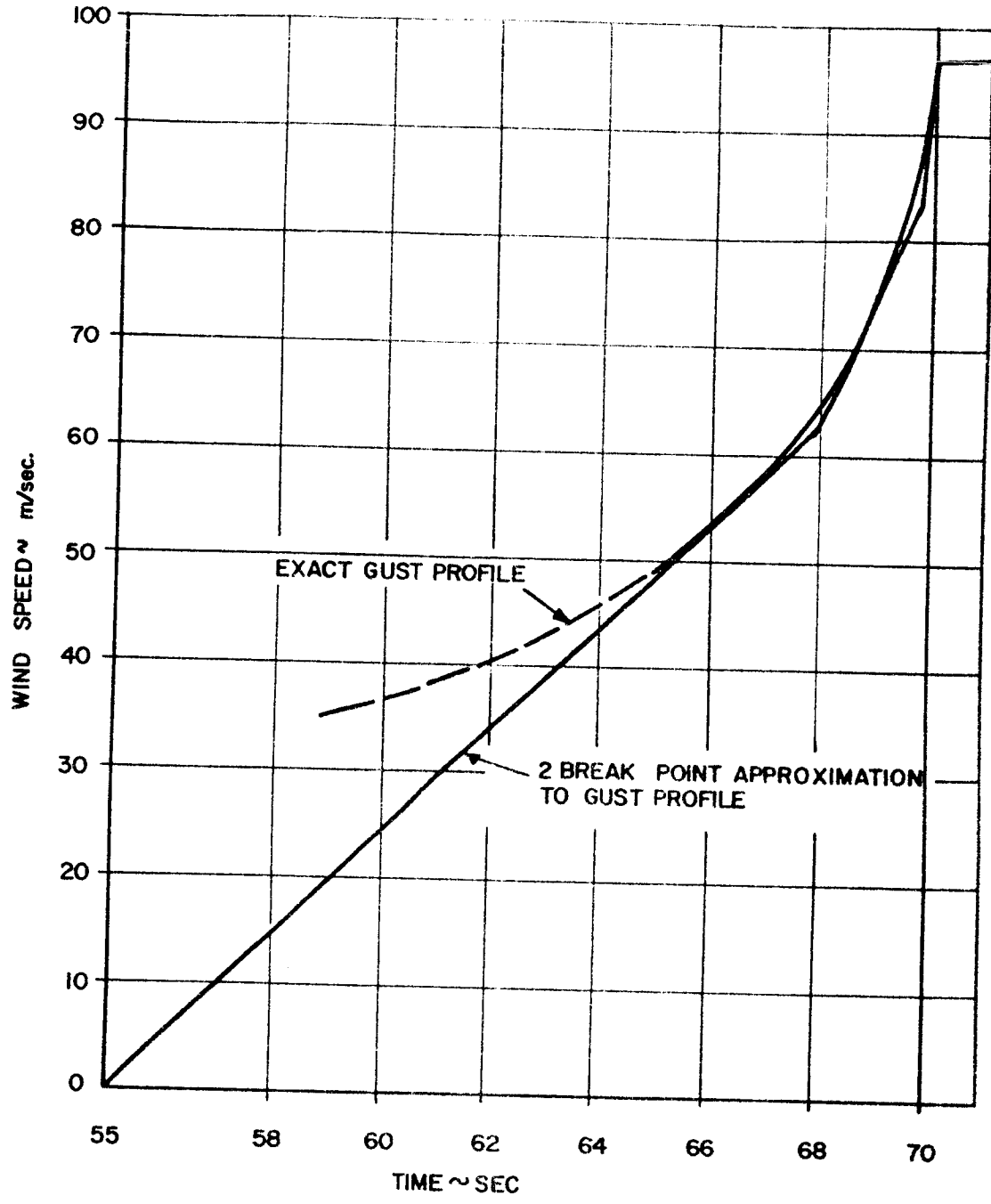


Figure J2. Synthetic Wind Shear Profile - Maximum Dynamic Pressure (t = 79 seconds)

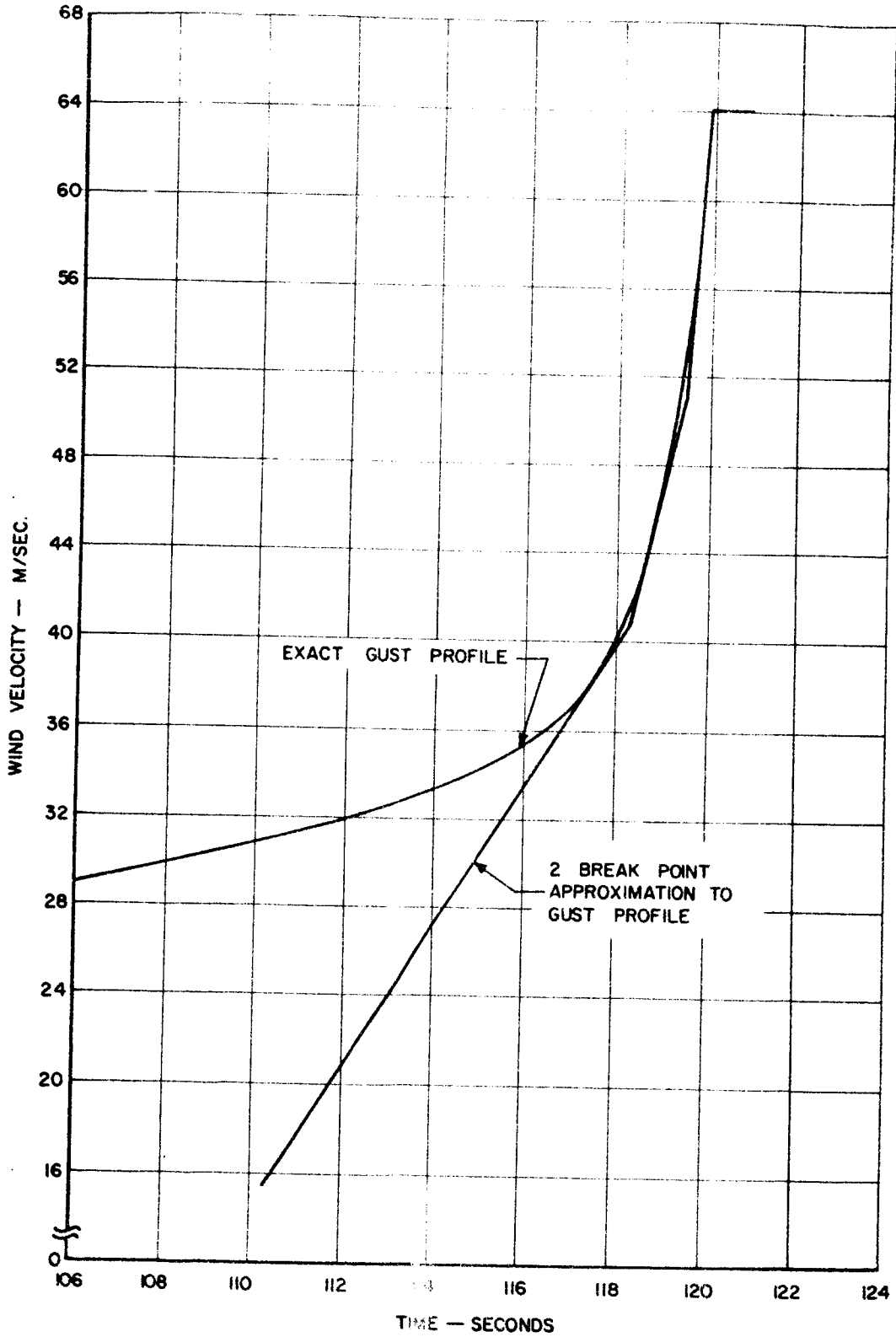


Figure J3. Synthetic Wind Shear Profile - Maximum Dynamic Pressure (t = 120 seconds)